

Automatic Detection and Classification of Neural Signals in Epilepsy

Rajeev Yadav

A Thesis

in

The Department

of

Electrical and Computer Engineering

Presented in Partial Fulfillment of the Requirements
for the Degree of Doctor of Philosophy at
Concordia University,
Montreal, Quebec, Canada

April 2012

© Rajeev Yadav, 2012

CONCORDIA UNIVERSITY
School of Graduate Studies

This is to certify that the thesis prepared

By: : **Rajeev Yadav**

Entitled: **Automatic Detection and Classification of Neural Signals
in Epilepsy**

and submitted in partial fulfilment of the requirements for the degree of

Doctor of Philosophy (Electrical Engineering)

complies with the regulations of this University and meets the accepted standards
with respect to originality and quality.

Signed by the final examining committee :

_____ Chair
Dr. D. Dysart-Gale

_____ External Examiner
Dr. J. Gotman

_____ External to Program
Dr. C. Y. Su

_____ Examiner
Dr. M. O. Ahmad

_____ Examiner
Dr. W-P. Zhu

_____ Thesis Supervisor
Dr. M. N. S. Swamy

_____ Thesis Supervisor
Dr. R. Agarwal

Approved by _____
Dr. J. X. Zhang, Graduate Program Director

April 10, 2012.

Dr. Robin A. L. Drew, Dean of Faculty
(Engineering and Computer Science)

ABSTRACT

Automatic Detection and Classification of Neural Signals in Epilepsy

Rajeev Yadav, Ph.D.
Concordia University, 2012

The success of an epilepsy treatment, such as resective surgery, relies heavily on the accurate identification and localization of the brain regions involved in epilepsy for which patients undergo continuous intracranial electroencephalogram (EEG) monitoring. The prolonged EEG recordings are screened for two main biomarkers of epilepsy: seizures and interictal spikes. Visual screening and quantitation of these two biomarkers in voluminous EEG recordings is highly subjective, labor-intensive, tiresome and expensive. This thesis focuses on developing new techniques to detect and classify these events in the EEG to aid the review of prolonged intracranial EEG recordings.

It has been observed in the literature that reliable seizure detection can be made by quantifying the evolution of seizure EEG waveforms. This thesis presents three new computationally simple non-patient-specific (NPS) seizure detection systems that quantify the temporal evolution of seizure EEG. The first method is based on the frequency-weighted-energy, the second method on quantifying the EEG waveform sharpness, while the third method mimics EEG experts. The performance of these new methods is compared with that of three state-of-the-art NPS seizure detection systems. The results show that the proposed systems outperform these state-of-the-art systems.

Epilepsy therapies are individualized for numerous reasons, and patient-specific (PS) seizure detection techniques are needed not only in the pre-surgical evaluation of prolonged EEG recordings, but also in the emerging neuro-responsive therapies. This thesis proposes a new model-based PS seizure detection system that requires only

the knowledge of a template seizure pattern to derive the seizure model consisting of a set of basis functions necessary to utilize the statistically optimal null filters (SONF) for the detection of the subsequent seizures. The results of the performance evaluation show that the proposed system provides improved results compared to the clinically-used PS system.

Quantitative analysis of the second biomarker, interictal spikes, may help in the understanding of epileptogenesis, and to identify new epileptic biomarkers and new therapies. However, such an analysis is still done manually in most of the epilepsy centers. This thesis presents an unsupervised spike sorting system that does not require *a priori* knowledge of the complete spike data.

*I dedicate this work to people suffering from epilepsy,
and to great mentors who enlightened my career and life.*

Acknowledgements

I would like to express deepest gratitude to my phenomenal advisers Drs. R. Agarwal and M. N. S. Swamy for their meticulous guidance, unflagging support and encouragement, persistent drive towards excellence, and the freedom to pursue ideas in my own way. I am indebted to my advisers for everything that I have achieved in these many years.

I sincerely thank Drs. M. Omair Ahmad and Weiping Zhu for their guidance and feedback as members of my thesis committee.

I gratefully acknowledge the support of Concordia University through bursaries and graduate teaching assistantships; and the Natural Sciences and Engineering Research Council (NSERC), Regroupement Stratégique en Microsystèmes du Québec (ReSMiQ), and the National Institutes of Health (NIH) and National Institute of Neurological Disorders and Stroke (NINDS) through grants awarded to Drs. R. Agarwal and M. N. S. Swamy.

I thank Stellate Systems Inc. for providing the MNI database and the Harmonie EEG software. I wish to thank the University of Freiburg and the University Hospital Freiburg for the FSP database, the Department of Neurology and the Center for Molecular Medicine and Genetics, Wayne State University for the WSU database, and the Free/Libre/Open Source Software (FLOSS) for a variety of tools, namely, BioSig, MikTeX, LyX, and JabRef.

Thanks en masse to my colleagues at the Centre for Signal Processing and Communication, and friends I have come to know during my PhD years, including Drs. Saad Bouguezel, Gui Xie, Yong Zeng, Sreeraman Rajan, Aashit K. Shah, Jeffrey A. Loeb, and Fabiano Pandozzi; and Yves McDonald, Ralph Pollard and Victor Lanzo. A very special thanks go to Tarun Madan for his helping hands during my entry into Canada.

I am grateful for God's provision of joys, challenges, and grace for growth. My achievements up to this moment would not have been possible without the support from my family members. First of all, I would like to thank my late grandparents (Shri Balram and Smt. Kulwanti Devi Yadav), and my parents (Shri Jagan Nath and Smt. Sneh Lata Yadav) for providing the encouragement and confidence that sustained me throughout the tough times. I am grateful to my supportive parents-in-law (Shri Gauri Shankar and Smt. Luxmi Yadav), maternal uncles, especially Shri Arun Kumar Yadav and his family, brothers (Sanjeev, Jeetendra, Amit and Ankit), sisters-in-law (Reeta and Indu) and sisters (Sonia and Vidisha).

Last, but not the least, I eternally thank my wife, Kanak, for her unconditional love, constant encouragement, support, understanding and patience throughout the completion of this research.

Contents

List of Figures	xiii
List of Tables	xxvi
List of Acronyms	xxvii
1 Introduction	1
1.1 Epileptic Seizure	1
1.2 Electroencephalography	2
1.3 EEG Classification	4
1.4 Motivation	8
1.5 Scope of the Thesis	12
1.6 Organization of the Thesis	13
2 Literature Review	14
2.1 Introduction	14
2.2 Automatic Seizure Detection	14
2.2.1 Non-Patient-Specific Seizure Detection	17
2.2.2 Patient-Specific Seizure Detection	24
2.3 Spike Sorting Techniques	28
2.4 Summary	31

3	Data Description	35
3.1	Introduction	35
3.2	Data Description	35
3.2.1	MNI Database	36
3.2.2	FSP Database	37
3.2.3	WSU Database	37
3.2.4	Data Conversion	38
3.2.5	Data Selection	41
3.3	Performance Evaluation Methodology	42
3.3.1	Seizure Detection	42
3.3.2	Spike Sorting	45
4	New Non-Patient-Specific Seizure Detection Systems	46
4.1	Introduction	46
4.2	Time-evolution of Seizure	47
4.3	Relative Frequency-Weighted Energy System	48
4.3.1	Pre-processing and Artifact Rejection	49
4.3.2	Feature Extraction	51
4.3.3	Classification	54
4.3.4	Performance Evaluation	58
4.3.5	Results	60
4.3.6	Discussion	60
4.4	Morphology System	67
4.4.1	Pre-processing and Artifact Rejection	69
4.4.2	Feature Extraction	71
4.4.3	Classification	73
4.4.4	Performance Evaluation	76
4.4.5	Results	77

4.4.6	Discussion	77
4.5	Evolution Seizure Detection System	82
4.5.1	Pre-processing and Artifact Rejection	84
4.5.2	Feature Extraction	84
4.5.3	Identification of Candidate Seizure Event	89
4.5.4	Validation of Candidate Seizure Event	91
4.5.5	Performance Evaluation	93
4.5.6	Results	95
4.5.7	Discussion	95
4.6	Summary	100
5	Performance Evaluation and Rapid EEG Review Tool	104
5.1	Introduction	104
5.2	MNI Database Results	104
5.3	Discussion	106
5.4	FSP Database Results	111
5.5	Discussion	115
5.6	Rapid Review of Prolonged EEG Recordings	124
5.6.1	Background	124
5.6.2	Method	125
5.6.3	Results and Discussion	127
5.7	Summary	133
6	A New Model-Based Patient-Specific Seizure Detection System	135
6.1	Introduction	135
6.2	Problem Formulation	136
6.3	Model-Based Seizure Detection	139
6.4	Pre-processing and Artifact Rejection	141

6.5	Seizure Model	143
6.5.1	STFT-based Segmentation	144
6.5.2	Rejection of Artifacts and Redundant Epochs in T_{PAT}	145
6.5.3	Modeling of T_{PAT} Epochs	147
6.6	Statistically Optimal Null Filter	148
6.6.1	Classifier Training	151
6.6.2	Model Selection	151
6.6.3	Evolution-based Classification	153
6.7	Performance Evaluation	154
6.8	Results	157
6.9	Discussion	157
6.10	Summary	164
7	Unsupervised Spike Sorting	165
7.1	Introduction	165
7.2	Challenges in Spike Sorting	166
7.3	Automatic Spike Classification	168
7.3.1	Spike Data (Spike Detection)	170
7.3.2	Spike Alignment	171
7.3.3	Morphological Correlator	172
7.3.4	Principal Component Analysis	173
7.3.5	Codebook-based Template-Matching	175
7.3.6	Hierarchical Clustering and Post-classification	176
7.3.7	Graphical User Interface and Result Display	177
7.4	Performance Evaluation	178
7.4.1	Geometric Technique	179
7.4.2	Dendrogram Analysis	180
7.5	Results	181

7.6	Discussion	183
7.7	Summary	191
8	Conclusion	193
8.1	Concluding Remarks	193
8.2	Contributions	197
8.3	Future Perspectives	199
8.3.1	Non-Patient-Specific System	199
8.3.2	Patient-Specific System	201
8.3.3	Spike Sorting System	202
	References	204

List of Figures

1.1	Classification of EEG-based on the electrode placement. Images obtained from (a) www.erwinadr.blogspot.com , and (b-c) www.uwhealth.org .	3
1.2	An example of 20 seconds of multi-channel intracerebral EEG of a patient.	4
1.3	Schematic for classification of EEG in epilepsy by the EEGer. Adapted from <i>Self-adapting algorithms for seizure detection during EEG monitoring</i> by H. Qu, 1995, McGill University, Canada [20].	6
1.4	An example 20 seconds of SEEG representing ictal (seizure) and interictal activity for a patient	6
1.5	Graphical illustration of behavioral changes during seizure in epileptic children. Images obtained from the website of WHO/UNESCO, and from http://wikinoticia.com	7
1.6	Architecture of a fully automatic patient-specific seizure detection system.	11
3.1	Protocol for analysis of the EEG signals.	39
3.2	Section-based technique of performance evaluation. Numbered events represent the algorithm detections, EEGer section is a multi-channel duration event and the 'red' rectangular box represents the detection section on channel of interest (LH1-LH3).	44

4.1	Encoding the time evolution of seizure by tracking the EEG characteristics. The example parametrizes temporal changes in EEG amplitude. Seizure onset is at the point 'A'. Seizure is segmented into three sections representing monotonic increase (AB), stable (BC) and monotonic decrease (CD) in the amplitude.	48
4.2	Flow chart of the RFWE seizure detection system.	49
4.3	(A): Single channel EEG contaminated by the two common artifacts present in the intracranial EEG. (B) represents the time instances of IEAs, and (C) represents the time instances of HAs in (A).	51
4.4	Feature extraction techniques: (A) single sliding window, and (B) two sliding window feature extraction.	52
4.5	The example represents 160 s of EEG activity that includes normal (background) and seizure activity. The RFWE describes the changes seen in the EEG as it progresses from inter-ictal (background) to ictal (seizure) state, and back to inter-ictal state.	54
4.6	Tracking the continual increase of the RFWE trajectory at the seizure onset.	56
4.7	Effect of filter length on the feature trajectory.	57
4.8	ROC analysis for Grewal-Gotman system and Reveal algorithm. The detection threshold of the Grewal-Gotman system and Reveal algorithm is varied from 1 to 10. The selected thresholds for Grewal-Gotman system (detection threshold = 3) and Reveal algorithm (perception value = 5) are selected.	59
4.9	Seizure classification-based on duration.	62
4.10	Comparison of sensitivity against comparison systems. The error bars represent standard error.	63

4.11	Missed 30 s long seizure in Channel LH1-LH3 in Patient 1. The seizure was missed by the RFWE system as well as all three comparison systems.	64
4.12	An example of low amplitude, mixed frequency seizure in Patient 5 that was missed by the RFWE and Gotman systems, but detected by the Reveal algorithm and Grewal-Gotman system.	64
4.13	Good detection in Patient 2 (channel: RC1-RC3) of the MNI training dataset. The multichannel EEG (15 s) containing a seizure that was detected by RFWE system and Grewal-Gotman system but missed by Gotman system and Reveal algorithm. The detection time instance is shown by vertical line.	65
4.14	Multichannel EEG (30 s) with an example of false detection in Patient 5 (channel: LP1-LP2) of the MNI training dataset that was detected by the RFWE system and the three comparison systems. The detection time instance is shown by the vertical line.	66
4.15	An example of false detection in Patient 2 (channel: RC1-RC3) of the MNI training dataset. The multichannel EEG (15 s) containing a seizure-like event that was detected by RFWE system and Reveal algorithm, but missed by Gotman and Grewal-Gotman systems. The detection time instance is shown by the vertical line.	67
4.16	Comparison of specificity against comparison systems. The error bars represent standard error.	67
4.17	Illustration of gradually increasing number of sharp components (sharp wave complexes and spike-like activities) as the seizure evolves. The number of sharp components prior to seizure onset is non-existent compared to post-onset.	69
4.18	Flow chart of the morphology system.	70

4.19	A section of EEG is zoomed in to illustrate half-wave decomposition and estimation of sharpness of the half-wave. The slope of the best-fit line between the local extrema (thick-black line) is the sharpness feature.	72
4.20	Evolution of SHW as the seizure progresses. (A) Seizure with background. (B) SHW corresponding to the EEG in (A).	73
4.21	Threshold estimation using the receiver operating characteristics (ROC) analysis. The threshold m_{th} is varied from 5 to 50 and for each m_{th} , the average sensitivity and false detection rate is computed to generate the ROC curve. The default threshold ($m_{th} = 25$) which we use for morphology system is shown encircled.	75
4.22	Epileptic seizure recognized by the morphology system. (A) Detected seizure event. (B) Raw EEG in A is decomposed into half-waves as modeled by the best-fit straight line. (C) represents bar graph of the absolute slope ($ m $) for each half-wave after processing by the activation function, and (D) is median filtered $g(n)$. The horizontal line represents the detection threshold.	76
4.23	Comparison of sensitivity of the proposed morphology system against other systems. Error bars represent the standard error.	79
4.24	An example of good detection in Patient 2 of the MNI training dataset. Multichannel EEG (20 s) containing a seizure that was detected by both the new NPS systems but missed by all three comparison systems. The channel of interest is RC1-RC3 and detection time instance is shown by vertical line.	80
4.25	An example of good detection in Patient 3 of the MNI training dataset. Multichannel EEG (30 s) containing a seizure that was detected by all NPS systems. The channel of interest is LH1-LH3 and detection time instance is shown by the vertical line.	80

4.26	Detections by the morphology system in Patient 2 (channel: RC1-RC3). All examples are 30 s in duration and the detection time intervals are shown by downward pointing arrows. The 'red' rectangle in (C) denotes six seconds of electrographic event that we considered as false event.	82
4.27	Comparison of specificity of the morphology system with the other systems on the MNI training dataset. Error bars represent standard error.	83
4.28	Flowchart of the eSD system.	86
4.29	Time evolution of coefficient of variation of amplitude superimposed on the EEG.	88
4.30	Time evolution of relative amplitude superimposed on the EEG.	89
4.31	Illustration of dynamically setting a local detection threshold. (A) A 30-seconds EEG obtained from one patient with a short seizure (~ 40 s), and the three features: (B) relative frequency-weighted-energy (C) relative amplitude and (D) coefficient of variation of amplitude (CV). The dots represent the feature at every m -point. The 'thick' and 'dashed' vertical line encloses the learning phase.	92
4.32	Illustration of the quantification of evolution of SWC density. (A) is 10-second candidate seizure (CSZ) pattern, (B) transformation of the CSZ pattern into elementary waveform obtained by fitting straight line on the half-waves, (C) the slope of the half-wave (m) shown as bar graph and slope threshold m_{th} by horizontal 'dashed' horizontal line. (D) The total number of SHW ($m > m_{th}$) N_k , in 2-second bins is shown by vertical lines. The minimum number of sharp component (N_{th}^T) in a candidate seizure event is represented by horizontal 'dashed' line. The continual increase of the sharp components is estimated by the slope of the regression line μ fitted on the five SHW density data point.	94

4.33	Comparison of sensitivity of the eSD system with morphology system, RFWWE system and comparison systems on the MNI training data. Error bars represent standard error.	98
4.34	Seizure embedded in the 60 s EEG section in Patient 5 (channel: LP1-LP2) missed by the eSD system, Gotman System and Reveal algorithm. The vertical downward arrow represents the detection time instances.	99
4.35	Seizure embedded in the 30 s EEG section in Patient 6 (channel: LS4-LS5) missed by the eSD system, and also by all three comparison systems. The vertical downward arrow represents the detection time instances.	100
4.36	Comparison of specificity of the eSD system with morphology system, RFWWE system and comparison systems on the MNI training data. Error bars represent standard error.	101
4.37	An example of false detection in Patient 1 (channel: LH-Lh3) of the MNI training dataset. The multichannel EEG (30 s) containing a false event detected by the morphology, eSD and Grewal-Gotman system. The detection time instance is shown by the vertical line.	102
5.1	Comparison of the sensitivity and specificity on the MNI test dataset. Error bars represents the standard error. Specificity bar plots are in 'GREEN' background color for each system. The 'up' arrow represents improved results on the test data while 'down' arrow represents improved results on the training data. No change or similar results on both the training and test data is represented by 'dash'.	107

5.2	An example of low amplitude seizure in Patient 9 of the MNI test dataset. The example contains 30 s of multichannel EEG (channel: RH1-RH3) containing a seizure that was detected by the morphology and RFWE systems, but missed by the eSD, Gotman, Reveal, and Grewal-Gotman systems. The detection time instances are shown by the vertical line.	108
5.3	An example of seizure in Patient 10 of the MNI database. The example contains 30 s of multichannel EEG (channel: RH1-RH2) containing a seizure that was detected by all systems except the Gotman system and Reveal algorithm. The detection time instances are shown by the vertical lines.	109
5.4	An example of short length seizure in Patient 14 of the MNI database. The example contains 30 s of multichannel EEG (channel: RE3-RE4) containing a seizure that was detected by Gotman system and Reveal algorithm, and missed by all other systems. The detection time instances are shown by the vertical lines.	110
5.5	An example of false detection in Patient 9 of the MNI test data. The example contains 30 s of multichannel EEG (channel: RH1-RH3) detected by RFWE system and morphology system, but not by other NPS systems. The detection time instances are shown by the vertical lines.	111
5.6	Comparison of sensitivity and specificity of the morphology system with Grewal-Gotman system on the MNI and FSP database. Error bars represent standard errors. Specificity results for FSP database are after re-classification of false detections by the EEGer A and B using 'Assessment I' technique.	116

5.7	An example of good detection in Patient 7 of FSP database. Multichannel EEG (20 s) containing a seizure that was detected by both systems. The detection time instance is shown by vertical line.	117
5.8	An example of missed event in Patient 5 of FSP database. Multichannel EEG (20 s) containing a seizure that was missed by both systems. The detection time instance by EEGer is shown by the dotted vertical line.	118
5.9	A 20 s example for false detections in the Patient 9 and 11 belonging to the test dataset from the MNI database. The channel of interest is enclosed in the rounded rectangle box with detection made by the proposed system shown by solid vertical line.	120
5.10	An example of false event detected in Patient 9 of FSP database. Multichannel EEG (20 s) with detection by our system (represented by solid vertical line) and Grewal-Gotman system (represented by dashed vertical line). The detection time instance is shown by vertical line. . .	121
5.11	An example of false event detected in Patient 18 of FSP database. A 20 s of multichannel EEG with detection by our system (represented by solid vertical line) and Grewal-Gotman system (represented by dashed vertical line). The detection time instance is shown by vertical line. . .	121
5.12	Re-assessment of false detections in the FSP database.	123
5.13	Identification of seizure in the compressed EEG display. The example represents 10 min single channel RSI and CDSA displays. Seizure detected by the EEGer is annotated with 'horizontal bar' on both the displays.	127

5.14	Example of multichannel compressed EEG display. The display represents 30 channel 4 h EEG section of Patient 1 for the three schemes (RSI, CDSA and aEEG). The section contains three seizure identified by the EEGer and is annotated by 'downward pointing (blue)' arrows on top of each display. Three events are selected from the RSI display (A, B, and C) with corresponding EEG shown in Fig. 5.15. Location of the selected event is shown by enumerated arrows on the RSI display.	129
5.15	EEG corresponding to the events selected from the RSI display in Fig. 5.14. (A) represents a seizure around the time point '1', (B) represents the pre-ictal rhythmic discharge of sharp waves around the time point '2', and (C) represents discharges of sharp wave complexes around the time point '3' in Fig. 5.13, respectively. Each segment represents 30 s of 10 channel EEG.	130
5.16	Example of 18 channel RSI display for Patient 2. The RSI display represents 16 h of data in three segments (1, 2, and 3), and contains a total of six seizures. Downward pointing 'blue' arrows denote EEGer identified seizures. EEG review panel displays 30 s of an event selected from RSI display for segment #1.	132
6.1	The example illustrates temporal evolution of a seizure which is observed as piecewise stationary rhythms. This example encapsulates a 90 s single channel EEG (channel: RH1-RH2) of a patient, which is considered as the template pattern in this patient. The piecewise stationary rhythms (template epochs) in the template pattern are enumerated and is obtained by the proposed STFT-based adaptive segmentation algorithm.	137

6.2	Model-based PS seizure detection scheme. $x(n)$ = observed EEG, T_{PAT} = template seizure pattern, Φ = seizure model (basis functions) derived from template seizure pattern, $\hat{s}(n)$ =estimated seizure waveform, γ = detection metric	140
6.3	Instantaneous matched filter	142
6.4	An illustration of impact of high-amplitude transients on the tracking ability of the SONF. (A) depicts the input signal $x(n)$ containing two sharp transients labeled as 1 and 2 (enclosed by the ellipse) along with its estimate $\hat{s}(n)$ using SONF, and (B) represents the corresponding IMF output ($v_i(n)$). (C) represents the sharp transients attenuated input signal $x(n)$ along with the its estimate $\hat{s}(n)$ using SONF, and (D) represents the corresponding IMF output ($v_i(n)$).	144
6.5	STFT-based segmentation of T_{PAT} . The 60 s long template seizure pattern (T_{PAT}) is shown in (A) along with evolution of dominant (peak) frequency F_m obtained from Fourier transform in (B). The dashed-boxes represent the stationary epochs identified by the adaptive segmentation algorithm in the T_{PAT} , and are labeled $E_1, E_2, \dots E_7$	146
6.6	Estimation of signal using statistically optimal null filter (SONF). (A) represents block diagram of k -branches of SONF utilized to track the temporal evolution of seizures. Model (basis function) for the template epoch, represented by Φ_k is employed in the SONF to the estimate seizure waveform ($\hat{s}(n) = \sum_{i=1}^k \hat{s}_i(n)$) in the input signal $x(n)$. (B) represents the estimation counterpart of the k th discrete SONF. . . .	152

6.7	Evolution-based classification. (A) represents two disjoint ($k = 2$) template epochs of T_{PAT} along with their power spectral density plot. A candidate seizure pattern C_{PAT} similar to T_{PAT} detected using the seizure model is shown in (B). (C) represents the C_{PAT} and (D) the energy ratios γ_k for the k -SONF branches (one model for each template epochs), and (E) depicts detection by the individual SONF branches. The 'number' represents time-order in which the template epochs constitute the $T_{PAT}, = \{E_1, E_2\}$ that are examined by the evolution-based classifier to make a detection. The vertical 'dashed' line denotes the final detection of an event similar to T_{PAT}	155
6.8	Examples of T_{PAT} and a missed seizure by the proposed model-based seizure detection system. Plot represents 60 s of the template seizure and a missed seizure in Patient 3 (channel: RC1-RC3) shown in 20 s segments.	160
6.9	Examples of T_{PAT} and a missed seizure by the proposed PS system. Plot represents 60 s of the template seizure and a missed seizure in Patient 4 (channel: LH1-LH3) broken in segments of 30 s. The missed seizure did not evolve similar to T_{PAT} , therefore, did not satisfy the detection criterion.	162
6.10	Examples of a template seizure and a missed seizure by the comparison system in Patient 7. Data represents 20 s of the training data and 20 s of a missed seizure.	163
7.1	Block diagram of the proposed unsupervised sorting algorithm (enclosed in blue box).	169

7.2	Multichannel spike and spike-waveform complex event. (A) represents multichannel EEG event extracted around the vertex of the reference (detected) spike. Vertical line represents the vertex of the detected spike. (B) represents 100 ms of multichannel spike data (\mathbf{X}), and (C) represents example of multichannel spike-waveform complex (\mathbf{Y}), both aligned to the reference spike vertex.	171
7.3	Identification of channels with spikes similar to the reference spike using morphological correlator.	173
7.4	Principal component analysis of the multi-channel SWC.	175
7.5	Events lost in the insignificant clusters on thresholding relative to the most significant cluster.	177
7.6	Visual analysis of the cluster quality	180
7.7	Percentage of events lost by the proposed ASC and WAVE_CLUS methods. Error bar represents standard error.	181
7.8	Codebook generated using AutoSpike and ManuSpike events for Patient 5 using the proposed spike sorting algorithm.	187
7.9	Illustration of cluster validation in terms of inter- and intra- cluster distance for the two codebooks of Patient 5.	188
7.10	Visual comparison of the AutoSpike and ManuSpike codebooks using dendrogram for Patient 5.	188
7.11	Sorting results for Patient 4 using the AutoSpike SWC events. (A) contains three most significant clusters obtained with the proposed sorting algorithm. (B) contains results obtained from the WAVE_CLUS sorting algorithm.	189
7.12	Sorting results for Patient 9 using the AutoSpike SWC events. (A) represents three most significant clusters obtained with the ASC algorithm, and (B) depicts results obtained using the WAVE_CLUS sorting algorithm.	190

7.13 Graphic user interface of the ASC software. 191

List of Tables

2.1	Summary of seizure detection systems	18
4.1	Detection results for the proposed RFWE system on the MNI training dataset	60
4.2	Detection results for the three comparison systems on the MNI training dataset	61
4.3	Single channel evaluation of the MNI training dataset	77
4.4	Comparison results of the MNI training dataset	78
4.5	Single channel analysis of eSD system on the MNI training dataset.	95
4.6	Single channel evaluation of eSD system on the MNI training dataset in comparison with the two new systems and comparison systems.	96
5.1	MNI database results.	105
5.2	Multichannel evaluation of the FSP database	113
5.3	Re-assessment of false detections in the FSP Database	115
6.1	Detections of the Proposed and Qu-Gotman Systems	158
7.1	Quantitative analysis of the proposed sorting results.	182
7.2	Quantitative analysis of the WAVE_CLUS sorting results.	184

List of Acronyms

AED	Anti-Epileptic Drug
aEEG	Amplitude Integrated EEG
ASC	Automatic Spike Classification
ASD	Automatic Seizure Detection
CDSA	Color Density Spectral Array
CEPA	Compressed EEG Pattern Analysis
CSA	Compressed Spectral Array
CSZ	Candidate Seizure Event
CT	Computerized Tomography
CVA	Coefficient of Variation of the Amplitude
DFT	Discrete Fourier Transform
EEG	Electroencephalograph
EEGer	EEG Expert
EMU	Epilepsy Monitoring Unit
FDR	False Detection Rate

FIR	Finite Impulse Response
fMRI	Functional Magnetic Resonance Imaging
FWE	Frequency-Weighted-Energy
GMM	Gaussian Mixture Model
GUI	Graphical User Interface
HA	High-Amplitude Artifact
HW	Half-Wave
IEA	Iso-Electric Artifact
IED	Interictal Epileptic Discharge
IIR	Infinite Impulse Response
IMF	Instantaneous Matched Filter
IS	Interictal Spike
LTM	Long-Term Monitoring
MA	Moving Average
MF	Matched Filter
NICU	Neurological Intensive Care Unit
NLEO	Non-linear Energy Operator
NPS	Non-Patient-Specific
NRT	Neuro-Responsive Therapy
PCA	Pincipal Component Analysis

PET	Positron Emission Tomography
PNN	Probablistic Neural Network
PPV	Positive Percentage Agreement Value
PS	Patient-Specific
RA	Relative Amplitude
RFWE	Relative Frequency-weighted Energy
ROC	Receiver Operating Characteristic
RSI	Relative Sharpness Index
SBR	Signal-to-Background Ratio
SEEG	Stereoencephalogram
SHW	Sharpness of the Half-Wave
SOM	Self-Organizing Map
SONF	Statistically Optimal Null Filter
STL	Short-term Lyapunov Exponent
SUDEP	Sudden Unexplained Death in Epilepsy
SWC	Sharp-Wave Complex
SWCD	Sharp-Wave Complex Density

Chapter 1

Introduction

Epilepsy is a name given to a collection of neurological disorders. It is usually defined as a tendency to have recurrent seizures. It is an ancient disorder found in all civilizations, and it can be traced back as far as medical records exist. In fact, epilepsy is a disorder that can occur in all mammalian species, probably more frequently as brains become more complex. Remarkably, epilepsy is also uniformly distributed around the world. There are no racial, geographical or social class boundaries. It occurs in both genders at all ages, especially in neonates and in aging population. The clinical features of seizures are often dramatic and alarming and frequently elicit fear and misunderstanding. This in turn has led to profound social consequences for sufferers and has greatly added to the burden of this disease [1].

In this chapter, we introduce some basic concepts in recognition and management of epilepsy, and motivation for this research. Finally, we will give an outline of the thesis.

1.1 Epileptic Seizure

Epilepsy is one of the most common and the oldest chronic neurological disorder known to mankind. It is not a singular disease entity, but a variety of disorders

reflecting underlying brain dysfunction that may result from many different causes [2]. Approximately, 2% of the world population exhibit symptoms of epilepsy characterized by the existence of abnormal synchronous discharges in large ensembles of neurons in the brain structure [3]. This results in one or more clinical symptoms such as loss of consciousness, behavioral changes, loss of motor activity, loss of senses. At times, it can lead to death due to unexplained reasons, known as sudden unexplained death in epilepsy (SUDEP). It is characterized by a tendency to have recurrent seizures. A person is diagnosed epileptic on the occurrence of two or more unprovoked seizures, and every year more than 2 million new cases of epilepsy are diagnosed [1, 4-9]. Seizure prevalence increases with age resulting in severe neurological damage that often becomes medically intractable, a condition in which seizure cannot be controlled by the administration of two or more anti-epileptic drugs (AEDs). Patients with medically intractable seizures are often candidates for surgical resection (removal of the epileptic foci in the brain), which requires accurate localization. Because of the unknown time of occurrence of seizures, these patients undergo prolonged monitoring during which a variety of clinical examinations are performed. These include electrophysiological assessment and neuroimaging evaluation to accurately identify and localize epileptic foci. Unfortunately, not all patients with intractable seizure can benefit from resective surgery because of the associated severe systemic consequences. Alternatively, these patients may benefit by the recent emergence of novel electroconvulsive and neuromodulation therapies.

1.2 Electroencephalography

Electrophysiological assessment of epileptic patients involves mainly the electroencephalography, which is the primary tool for the clinical recognition and management of various neurological disorders, including epilepsy. It represents neurophysiologic

activity of the brain measured electrographically using electrodes placed on the scalp or in special cases, subdurally on the cerebral cortex or deeper brain tissues. The resulting traces are known as an electroencephalogram (EEG) and are sometimes called brainwaves. Depending on how the electrodes are used for recording the EEG, it can be specified as the scalp EEG (electrodes placed on the scalp), or intracerebral EEG (electrodes implanted on the surface or deep brain). Subdural EEG electrodes are those electrodes which sit over the surface of the brain while depth EEG electrodes are inserted in the brain. The placement of these electrodes is confirmed with co-registration on the MRI scan image. Figure 1.1 illustrates the three modes of electrode placement in patients undergoing EEG monitoring.

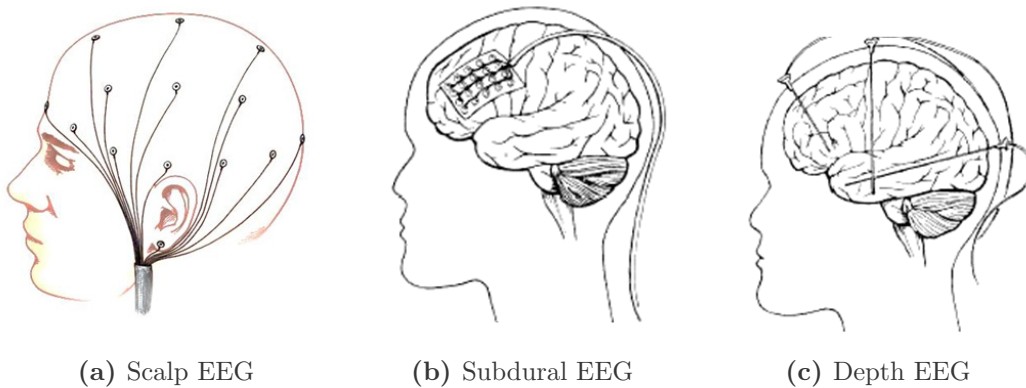


Figure 1.1: Classification of EEG-based on the electrode placement. Images obtained from (a) www.erwinadr.blogspot.com, and (b-c) www.uwhealth.org.

Intracerebral EEG is often called stereoencephalogram (SEEG) and an example of multi-channel SEEG is shown in Fig. 1.2. The EEG becomes a very informative tool to monitor activities observed during epilepsy and provides exact information about the time of occurrence, nature and the focus of these neuronal discharges in the brain.

Advanced imaging tools, such as functional magnetic resonance imaging (fMRI), positron emission tomography (PET) or computerized tomography (CT) scans can provide anatomical information about an abnormal growth or detectable lesion if present in the brain. These methods are discontinuous and cannot scan a patient during

an on-going seizure where the time of occurrence is unknown. That is, continuously scanning a patient is not possible. Thus, EEG is the only practical approach for functional long-term continuous monitoring of the brain with a high temporal and spatial resolution. Recent advances in the new neurostimulating system for epilepsy rely on the EEG to detect seizures and subsequently abort their progression by triggering focal treatment (electrical stimulation, focal cooling or drug release) [10-18]. Clearly, EEG plays a significant role from diagnosis to treatment of epileptic patients. However, interpretation of EEG is notoriously difficult and requires EEG experts (EEGer) consensus for its recognition.

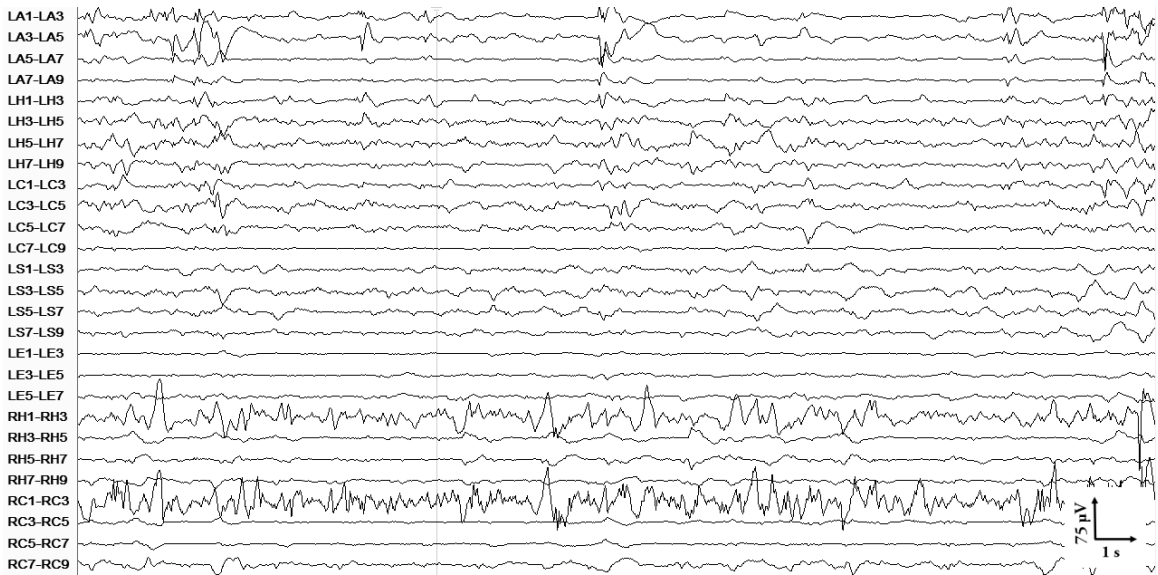


Figure 1.2: An example of 20 seconds of multi-channel intracerebral EEG of a patient.

1.3 EEG Classification

The EEG consists of signals from both the cerebral and non-cerebral origins. Depending on the recording technique, the contribution from each may vary. Abnormal EEG patterns are specific to the type of study being performed. It is the task of the EEGer to recognize the waveform of interest from the observed EEG and to identify the likely locations of their generators. Since intracerebral or subdural electrodes are usually

closer to neurons than the scalp electrodes, the amplitude of EEGs recorded by the depth electrodes is usually larger than that from scalp electrodes [19-21]. When EEG is recorded with scalp electrodes, the amplitude is of the order of $20\mu V$ to $100\mu V$, and of the order of $100\mu V$ to $2mV$ when recorded using depth electrodes. The spectral bandwidth of the EEG (normal and abnormal) is from under 0.5 Hz to about 500 Hz.

The EEG experts visually inspect the prolonged recordings to identify epileptiform activities. The common approach utilized to classify EEG is shown in Fig. 1.3. Interictal EEG is defined as the non-seizure activity or the background EEG. The interictal EEG comprises of normal patterns as well as abnormal patterns (such as spikes, high frequency oscillations, etc) along with normal rhythmic discharges such as alpha rhythm and sleep spindles [5, 22-27].

Generally, most of the seizures have some common characteristics, such as rhythmic discharge of large amplitude or a low amplitude desynchronized EEG at the onset, and repetitive spikes and irregular slow waves. No two patients have identical ictal pattern. Even within the same patient, the two ictal patterns are never identical though similar. Thus, the definition of a seizure still remains vague. However, the most widely accepted definition for seizure states that *during an epileptic seizure, a new type of EEG rhythm appears, hesitantly, and then more distinctly, and soon it boldly dominates the EEG tracing. It tends to become slower with increasing amplitude and the more distinct spiky phases of the rhythmical waves observed in an EEG recording* [5]. An example of such a seizure is shown in Fig. 1.4.

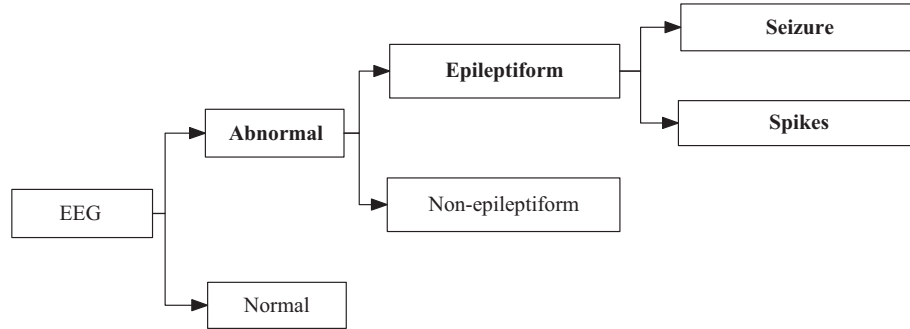


Figure 1.3: Schematic for classification of EEG in epilepsy by the EEGer. Adapted from *Self-adapting algorithms for seizure detection during EEG monitoring* by H. Qu, 1995, McGill University, Canada [20].

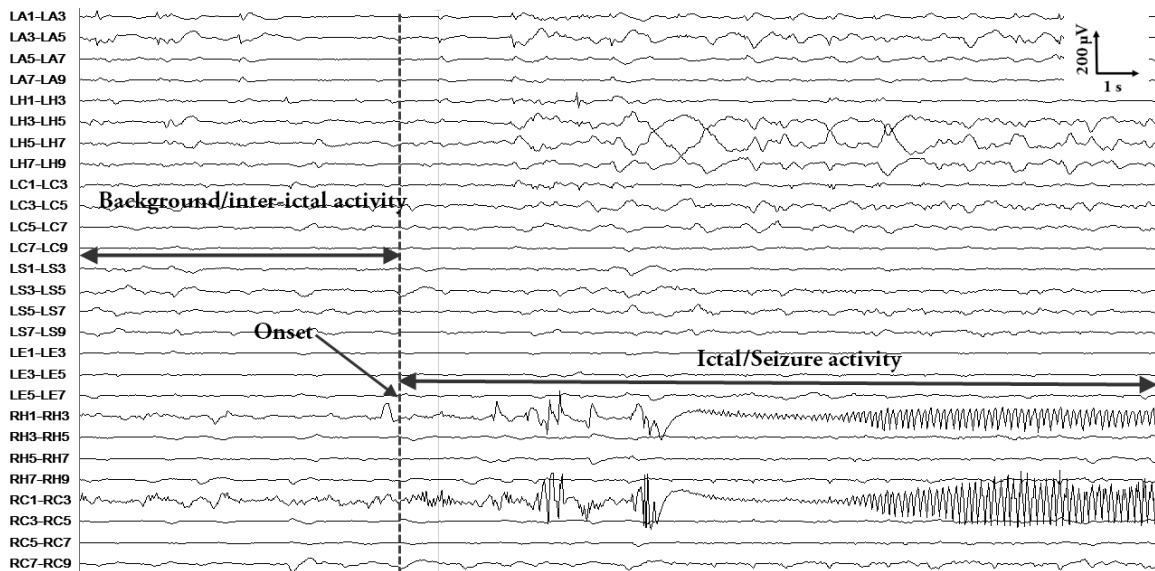


Figure 1.4: An example 20 seconds of SIEG representing ictal (seizure) and interictal activity for a patient

Early stages of an epileptic seizure provide information about the seizure focus, type and various characteristics of clinical significance. Seizures can be divided into two distinct categories: (a) clinical and (b) sub-clinical. Clinical seizures are recognized by certain behavioral changes associated with the seizure. Behavioral symptoms in epileptic children are illustrated in Fig. 1.5. In some patients, there is minimal or no behavioral changes during an epileptic seizure. Such seizures are known as electrographic or sub-clinical seizures. EEG captures the abnormal activity in both

types of seizure. To prevent irreversible secondary brain damages and to maintain patient safety, therapeutic intervention must be made during the initial stages of the epileptic seizure which requires constant observation of patient by medical or nursing staff. Monitoring an epileptic patient continuously over a long period of time by simultaneously observing the behavioral manifestations in video along with the EEG patterns is one way to capture all of the seizures. The continuous long-term monitoring (LTM) is performed in a time frame ranging from days to weeks in the epilepsy monitoring unit (EMU), and during this period, whenever an epileptic event occurs, the observer simply tags relevant areas of the video and the EEG recording for a later review by neurologists. However, this procedure is very labor intensive, expensive, and not a practical solution.



Figure 1.5: Graphical illustration of behavioral changes during seizure in epileptic children. Images obtained from the website of WHO/UNESCO, and from <http://wikinoticia.com>.

Alternatively, an EEGer can review the voluminous long-term EEG recordings once the monitoring has been completed. Typically, an EEGer reviews these records in a page/window of 10-20 seconds in search of an epileptic event that can last from several seconds to several minutes. However, much of the data is uninteresting in these voluminous recordings except the sections corresponding to epileptic spikes and seizures, and such sections are highlighted for a subsequent review by the experts.

This review process is again highly subjective, labor intensive, and tiresome.

Automatic seizure and spike detection methods can assist the nursing staff as well as the EEGer to rapidly review the prolonged EEG recordings to retain sections from recordings of clinical significance. Therefore, there arises a need for automatic detection and classification of seizures and interictal spikes.

1.4 Motivation

The following provides the role of seizures and spikes in the management of epilepsy in the EMUs, highlighting the clinical needs and challenges encountered that builds the foundation for this research.

Seizure Detection

Automatic seizure detection techniques have received intense attention in the recent past. Such methods are used in the EMU as a seizure warning system and aid in the rapid review of the prolonged EEG recordings. Majority of the existing seizure detection systems are designed for the scalp EEG. Patients who are candidate for resective surgery or neurostimulating therapies undergo prolonged intracranial EEG recording. Intracranial EEG contains a wide variety of seizure patterns that are minimally contaminated by artifacts. Seizure detection methods designed for intracranial EEG often require very high sensitivity and with minimal number of false detections. In spite of high sensitivity, several electrographic seizures go undetected. Additionally, majority of the existing seizure detection methods report difficulty in detecting short-duration seizures or those with non-rhythmic mixed frequency characteristics or low amplitude seizures.

In order to maintain high sensitivity and specificity, majority of the existing methods employ strategies by combining a number of neighboring channels. Such

methods often fail to detect seizures occurring on a few channels, i.e., focal seizures that occur on spatially separated channels. To improve sensitivity and specificity, a handful of patient-specific seizure detection methods, that are based on the recurring nature of epileptic seizures, have been proposed. Isolating precisely reproducible phenomena in EEG signals still remains a difficult task that can highlight the neurophysiological mechanisms to characterize an epileptic brain. Patient-specific seizure detection systems thus become an indispensable tool aimed at better defining and understanding epileptogenic areas to improve surgical treatments [28, 29].

Even though patient-specific seizure detectors demonstrate improved performance over the generic methods, they are not practical. The main limiting factors in all patient-specific detectors are (a) supervised selection of the seizure EEG, (b) supervised selection of the non-seizure EEG (or a set of non-seizure EEG patterns), and (c) supervised training of the classifier. Another fundamental problem in all seizure detection methods is the detection of seizures with subtle changes in the amplitude [30-37]. This is a problem that persists even in the visual detection of seizures. Addressing some of these limitations will lead to a more practical patient-specific detector.

In addition to the seizure detection, one of the primary aims of the review of prolonged intracranial EEG monitoring is to map channel-by-channel timeline of seizures and epileptiform activities that can provide visualization of seizure onset and spread (both temporally and spatially), which is pivotal when planning resective surgery. This type of 2D visualization is unavailable for the review of intracranial EEG. Automatic seizure detection can aid in the rapid identification of seizures. However, it does not allow for a quantitative seizure analysis, which is still done manually by experts. Therefore, adjunctive methods that allow quick identification of seizures, provide a view of seizure activity over prolonged durations, seizure recurrence frequency, and sites involved in the seizure generation for therapeutic interventions, and management are much needed in the EMUs [5, 38-42].

Prolonged intracranial EEG recording is also performed prior to the implantation of a neurostimulating device to identify the seizure foci and neural areas for stimulation therapy for patients who may not benefit from the resective surgery. The idea behind neurostimulation devices is to deliver focal treatment to inhibit the epileptic activity. Electrical stimulation of the epileptogenic foci to inhibit the progression of seizure is one such method that is gaining popularity [13-16, 18, 43, 44]. The success of such devices rely heavily on the seizure detection capabilities. Computationally light, low-power, robust and patient-specific seizure detectors are prerequisite to maintain the longevity of the device (battery) and patient safety. However, seizure detection system for application in the neurostimulating device is still in its infancy.

A fully automatic patient-adaptive seizure detection system is much needed, but the clinical requirements of the seizure detection system and the existing challenges in the non-patient specific (NPS) and patient-specific (PS) approaches of seizure detection do not allow the existence of such a system. However, a fully automated patient-adaptive seizure detection system is feasible by combining NPS and PS systems to capture the advantages of the two approaches. The architecture of such a system is shown in Fig. 1.6. Automatic patient-adaptation in such a system may be possible by addressing the limitations in the PS systems, that is, by removing the need for a large background EEG, automating the selection of the template seizure pattern and training of the classifier. In such a system, the NPS system bootstraps the PS system with template seizure patterns, and the PS system leverages on the event it detects to optimize itself. It may be possible that seizures that are difficult to be detected by the NPS system are easily identifiable by the PS system. Conversely, seizure patterns that are difficult to be detected by the PS system are detected by the NPS system. The patient-specific pattern database is updated on subsequent detections. Then, the patterns in the database, ranked based on their recurrence frequency via the PS system, may allow the experts to perform rapid qualitative and quantitative analysis.

Thus, the time involved in the manual qualitative analysis of the detected patterns, quantification of reproducible seizure patterns, and correlation with the clinical data, reduces significantly. However, realization of such a system demands that both the NPS and PS systems are computationally light and robust.

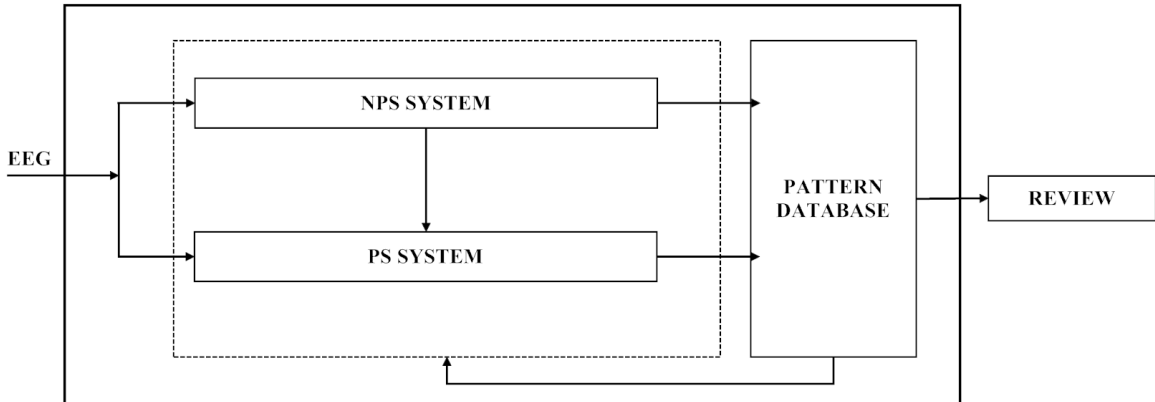


Figure 1.6: Architecture of a fully automatic patient-specific seizure detection system.

In this thesis, we aim to develop new NPS and PS systems that can be used in the fully automatic PS seizure detection system of Fig. 1.6.

Spike Classification

In addition to seizures, epileptic spikes also play an important role in the diagnosis of seizure onset zones. They tend to occur more frequently than seizures and are linked to the seizure onset zones. Detection and classification of spikes thus can improve the epilepsy management. Furthermore, several studies have reported a better surgical outcome when regions of frequent spikes (interictal) are also removed [45]. However, it is still unclear as to exactly how interictal spikes develop, and how they propagate and contribute to the generation of seizures [46-48]. A recent study examined human brain tissues at regions of seizure onset and found a small group of genes highly correlated with the interictal spike frequency [49, 50]. Quantitative analysis of interictal spiking thus becomes inevitable, and may help to identify epileptic biomarkers for drug therapy.

Automatic spike detection has received intense attention in the literature. On the other hand, to date, spike classification is still done manually by the experts in most of the EMUs, which is extremely subjective, challenging, tiresome, and expensive. There exist a large number of automatic spike classification systems for neurophysiological experiments but not for the intracranial EEG recording that can handle a large number of electrodes and massive amount of data. Unavailability of a system for quantitative analysis of interictal spikes in the intracranial EEG motivated us to develop a new spike classification system.

1.5 Scope of the Thesis

The first objective of this research is to devise robust computationally-light techniques for seizure detection that find widespread application in the EMU as a seizure warning system, aid in the rapid review of the prolonged intracranial EEG recordings, and provide quantitative and qualitative seizure related information towards rapid identification of epileptogenic sites. New NPS and PS seizure detection methods are developed to overcome some of the existing challenges present in the seizure detection literature. The proposed methods are compared against the popular seizure detection techniques in the literature. These systems are also explored from the point of view of generation of a new multi-channel 2D visualization of epileptiform activities that allows easy and rapid quantitation of intracranial EEG recordings in the EMU.

The second objective of this research is to devise a robust spike sorting technique for intracranial EEG recordings. Towards this goal, we develop an unsupervised spike sorting algorithm that does not require *a priori* knowledge of spike classes, is computationally simple and overcomes some of the existing challenges in spike sorting. A graphical user interface (GUI) for spike sorting is developed to facilitate easy integration of the algorithm in the clinical settings.

1.6 Organization of the Thesis

The thesis is organized as follows.

Chapter 2 reviews popular seizure detection and spike sorting methods.

Chapter 3 describes the EEG data used to develop and evaluate the performance of the methods proposed in this thesis.

Chapter 4 describes three new, computationally simple, data driven NPS systems. The NPS systems quantify the continual increase (temporal evolution) in the seizure-related EEG characteristics to make detections. This chapter presents results obtained on the training dataset.

Chapter 5 presents performance evaluation results on the test data for the new NPS methods compared against three popular comparison systems (Gotman system [51], Reveal algorithm [52], and Grewal-Gotman system [32]). This chapter also describes a new digital trending tool aimed to facilitate rapid review of prolonged EEG recordings in the EMU.

Chapter 6 describes a new model-based PS system suitable for the development of a fully automatic PS system. The PS system is developed in the framework of statistically optimal null filters, which is a novel approach for solving the problem of enhancement/suppression of narrowband signals of short-record length. The performance of the new model-based PS system is compared with that of the popular PS system of Qu-Gotman [21]).

Chapter 7 describes a new graphical user interface (GUI) software package for automatic classification of epileptic spikes in the intracranial EEG recordings. The chapter describes the data utilized in the development, validation strategy and the spike classification algorithm. An easy-to-use GUI is developed that facilitates easy integration of the method in the clinical settings.

Finally, in Chapter 8, concluding remarks highlighting the contributions of the thesis and suggestions for further investigation are provided.

Chapter 2

Literature Review

2.1 Introduction

This chapter provides an overview of published research on seizure detection and spike sorting. A plethora of seizure detection and spike sorting algorithms¹ exists in the literature. We limit our discussion to some of the recent and landmark approaches of seizure detection and spike sorting methods, with particular attention to the algorithms that are relevant to this research work.

2.2 Automatic Seizure Detection

The topic of seizure detection has gained much attention in recent years due to its evidence in prognosis, diagnosis and as a therapeutic tool in the epilepsy care along with the availability of low-cost, fast computation tools. Chapter 1 introduced the role of EEG in epilepsy care and management and discussed some of the existing challenges in the design of the automatic seizure detection (ASD) systems. The study of Ives and Woods [53] on 100 patients reported 30% of seizures as only electrographic

¹It is important to note that the spike sorting algorithms reviewed in this chapter are designed specifically for the action potentials that are also called spikes and not for the epileptic spikes. Nonetheless, the process in these methods can be employed for epileptic spike classification.

changes with no observable behavioral manifestations. This study demonstrated the importance of EEG monitoring and the role of ASD systems without which it would have been virtually impossible to detect purely electrographic seizures. Majority of ASD systems are designed to facilitate the review of prolonged EEG recordings, whereas only a few ASD systems are designed to perform online detection during the monitoring session. Care and management of an epileptic patient are dependent on the ASD system. Therefore, automatic seizure detectors must have a very high sensitivity (proportion of seizures that are detected) and a very low false detection rate (FDR). In the EMU settings, the detection sensitivity is of more importance than the FDR, since missed seizures may never be reviewed by the EEGer, and are therefore of more serious consequence [22, 54]. Both sensitivity and FDR are equally important in neurological intensive care unit (NICU) applications, as large number of false detections are annoying and require additional staff vigilance in a very busy and stressful environment [55-59]. In certain applications of ASD systems, the time lag associated in a seizure detection is also important. For example, neuroresponsive therapy (NRT) application requires the ASD system to predict/detect seizure as early as possible to initiate preventive measures.

The first automatic seizure detection method designed to detect seizures with sustained paroxysmal rhythmic activity is the pioneering work of Gotman [51, 54] and is an industry standard in seizure detection. Since then, there has been a marked increase in seizure-related research. ASD systems are available (a) as seizure onset detectors, (b) as seizure pattern detectors or (c) as seizure prediction systems. A seizure onset detector aims to detect seizures at the onset, which inherently results in a higher rate of false detection. Some methods aim to detect the seizure patterns, improving FDR rate at the cost of increased detection delay, while a few methods predict seizures minutes or even hours in advance. However, such systems report none to minimal success in predicting seizures.

In general, an ASD system comprises of three main stages, pre-processing, feature extraction, and decision-making (classifier). The two popular approaches of feature extraction considered in the design of the ASD systems are based on (a) waveform or morphology and (b) EEG statistics in short segments, which we define as segment-based features for the sake of simplicity. In the first approach, the EEG waveform characteristics or morphology include, such as the height/width of the wave complexes, and area of the positive/negative half-waves. In the second approach, the more popular ones are the segment-based features such as average amplitude, energy, variance, and power spectral density. The classifier is designed using features to discriminate the EEG into two classes: seizure or non-seizure. A number of classifiers are available in the literature that can be broadly categorized as linear classifiers, statistical classifiers, non-linear classifiers, or artificial neural networks.

Based on the number of channels used in the EEG classification, ASD systems are further sub-divided into single channel or multi-channel system. It should be noted that a majority of the multi-channel ASD systems are, in fact, single channel detectors that combine the individual channel detections to include spatial information from several channels towards the final decision. Furthermore, based on the patient age group, ASD systems are grouped into newborn (neonate) or adult seizure detection systems, and according to the method of EEG acquisition into scalp (surface) or depth (intracranial) ASD systems.

In addition to the above, ASD systems are available as generic or specific to each patient. Generic ASD systems can be termed as non-patient-specific (NPS) systems, and those that are optimized for each patient as the patient-specific (PS) systems. Majority of the ASD systems in the literature belongs to the former category. This is because seizure-pattern information for a given patient is usually unavailable in advance. On the contrary, there exist only a few PS systems, which rely on *a priori* information of seizure and non-seizure data for each patient to train the detector

prior to usage. Table 2.1 provides a summary of the ASD systems according to the categories described above.

Clearly, the challenges facing the designer of an automatic seizure detector are significant. No one detector can easily satisfy the varying requirements, and is the reason for the existence of many seizure detection methods in the literature. In this thesis, we broadly categorize automatic seizure detection into two groups:

- NPS seizure detection
- PS seizure detection

2.2.1 Non-Patient-Specific Seizure Detection

Gotman [54] designed a seizure detection system, which detected seizures based on decomposing EEG signals into half-wave components and analyzing them in 2-second epochs. The features selected to characterize seizures were the zero-crossings, half-wave amplitude, and rhythmicity. Relative to a background that trails the test epoch, a seizure detection occurs in the test epoch when the features exceed the pre-defined detection thresholds. Detections in individual channels are combined in some spatio-temporal context for final detection. Numerous types of seizures were detected by this method in 22 scalp EEG recordings (mean duration 12.4 h) and 44 depth EEG recordings (mean duration 18.7 h). The method was subsequently improved by increasing the distance between the background and test epoch to account for seizures with a gradual onset [51]. By altering the amplitude parameters, the method was capable of detecting low amplitude seizure discharges. Additionally, enhanced temporal context further reduced the false detections caused by short rhythmic bursts. A patient alarm was introduced to automatically record ictal event when either the patient or nurse became aware of a seizure onset. These modifications on 293 h of EEG of 49 patients resulted in an overall sensitivity ranging between 70-80% with a

Table 2.1: Summary of seizure detection systems

Waveform/Morphology-based NPS systems			Segment-based NPS systems		
Author	Classifier	Application	Author	Classifier	Application
Gotman [54]	LC	adult, scalp, depth	lasemidis <i>et al.</i> [103]	NLC	adult, depth
Gotman [31]	LC	adult, scalp, depth	Murro <i>et al.</i> [62]	SC	adult, depth
Harding [97]	LC	adult, depth	Hilfiker [63]	LC	adult, scalp
Webber <i>et al.</i> [113]	ANN	adult, scalp	Liu <i>et al.</i> [112]	SC	neonate, scalp
Navakatikyan <i>et al.</i> [110]	LC	neonate, scalp	Schiff <i>et al.</i> [64]	NLC	adult, scalp
PS systems			Gabor <i>et al.</i> [98]	ANN	adult, scalp
Author	Classifier	Application	Pradhan <i>et al.</i> [65]	ANN	adult, scalp
Qu and Gotman [21]	SC	adult, scalp, depth	Gotman <i>et al.</i> [111]	LC	neonate, scalp
Wendling <i>et al.</i> [28]	SC	adult, depth	Hofmann <i>et al.</i> [66]	LC	adult, scalp
D'Alessandro <i>et al.</i> [60]	NLC	adult, depth	Klatchko <i>et al.</i> [67]	LC	adult, scalp
Shoeb <i>et al.</i> [124]	ANN	neonate, scalp	Osorio <i>et al.</i> [100]	LC	adult, depth
Shi <i>et al.</i> [132]	LC	adult, depth	Park <i>et al.</i> [68]	ANN	adult, scalp
Osario <i>et al.</i> [100]	LC	adult, depth	Lehnertz [69]	NLC	adult, depth
Wilson <i>et al.</i> [130]	ANN	adult, scalp, depth	Sartoretto <i>et al.</i> [70]	NLC	adult, scalp
Zandi <i>et al.</i> [35]	LC	adult, scalp	Boarshash <i>et al.</i> [71]	SC	neonate, scalp
Minasyan <i>et al.</i> [61]	ANN	adult, scalp	Liu <i>et al.</i> [72]	ANN	adult, scalp
Salam <i>et al.</i> [133]	LC	adult, depth	McSharry <i>et al.</i> [73]	SC	adult, scalp
			Altenburg <i>et al.</i> [74]	SC	neonate, scalp
			lasemidis <i>et al.</i> [72]	NLC	adult, scalp
			Khan <i>et al.</i> [101]	LC	adult, depth
			Kiyamik <i>et al.</i> [75]	ANN	adult, scalp
			Nigam <i>et al.</i> [76]	ANN	adult, scalp
			Wilson <i>et al.</i> [52]	ANN	adult, scalp, depth
			Acir <i>et al.</i> [77]	ANN	adult, scalp
			Alkan <i>et al.</i> [78]	ANN	adult, scalp
			Grewal <i>et al.</i> [79]	SC	adult, depth
			Saab <i>et al.</i> [102]	SC	adult, scalp
			Subasi [79]	ANN	adult, scalp
			Lommen <i>et al.</i> [80]	LC	neonate, scalp
			Aarabi <i>et al.</i> [81]	ANN	neonate, scalp
			Gardner <i>et al.</i> [82]	ANN	adult, scalp
			Adeli <i>et al.</i> [83]	NLC	adult, scalp
			Ghosh-Dastidar <i>et al.</i> [84]	ANN	adult, scalp
			Srinivasan <i>et al.</i> [115]	ANN	adult, scalp
			Subasi <i>et al.</i> [85]	ANN	adult, scalp
			Tzallas <i>et al.</i> [86]	ANN	adult, scalp
			Greene <i>et al.</i> [87]	ANN	neonate, scalp
			Harrison <i>et al.</i> [88]	NLC	adult, depth
			Aarabi <i>et al.</i> [114]	ANN	adult, depth
			Kuhlmann <i>et al.</i> [89]	SC	adult, scalp
			Abibullaev <i>et al.</i> [90]	LC	adult, scalp
			Guo <i>et al.</i> [91]	ANN	adult, scalp
			Thomas <i>et al.</i> [92]	SC	neonate, scalp
			Polychronaki <i>et al.</i> [93]	SC	adult, scalp
			Temko <i>et al.</i> [94]	SC	neonate, scalp
			Chiu <i>et al.</i> [95]	SC	animal, <i>in vitro</i>
			Majumdar and Vardhan [96]	SC	adult, depth

LC: linear classifiers, NLC: non-linear classifiers, SC: statistical classifiers, ANN: artificial neural network

FDR of 0.84/h in scalp EEG and a FDR of 1.35/h in depth EEG [51]. Many of the concepts introduced by Gotman continue to be pervasive in seizure detection research.

Pauri *et al.* [96] evaluated the method of [51] in a clinical setting. The EEG data of twelve patients with medically intractable partial seizure, who had undergone video-EEG monitoring over 1-15 days (mean 10.5 days), were marked with the help of the Gotman ASD system and fast video review. Detections in individual channels were rated from 1 to 4 according to their likelihood of being genuine. The method was tested with several settings. A total of 461 hours of EEG having 216 seizures from twelve patients were analyzed. The two best performing settings showed a sensitivity of 81.4% with a FDR of 5.38/h and a sensitivity of 73.1% with a FDR of 5.01/h. The study demonstrated the need for tunable detection thresholds in ASD systems.

Harding [97] proposed a system to detect seizures (temporal lobe epilepsy) by detecting spiking phases using two main features: (1) magnitude of the sample-to-sample difference, and (2) the time difference between large magnitude spikes to determine the spiking rate. In this method, the number of large magnitude spikes are counted in a 5 s epoch and when the counter value exceeds a pre-defined threshold, a detection is made. The magnitude of a spike is considered large if it is greater than the running average of the background spikes scaled by a signal-to-background ratio (SBR). Spiking rate and rhythmicity are used to differentiate between the seizure activity and the spike bursts or artifacts. The method was tested on 40 patient EEG data with a total of 416 seizures over 1578 hours, and resulted in a sensitivity of 92.6% and a FDR of 1.94/h. The detection threshold was adjusted for individual patients on observation of the first seizure.

Gabor *et al.* [98] proposed a self-organizing map (SOM) neural network-based seizure detector named as CNet. In this method, the individual channels are filtered using a wavelet transform-based matched filter followed by 256-point FFT. Input to the SOM were the 256 coefficients that constituted the feature vector. The method

detected seizures with a sensitivity of 90% and a FDR of 0.79/h. The weak aspects in this study are the use of a high-dimensional feature vector, pre-selection of the seizure type (frontal and temporal lobe) and tuning of the detection parameters to optimize the performance. In a subsequent study [99], the authors validated the performance of their method against two commercial seizure detection algorithms, namely, Monitor (Stellate Systems Inc.) and audio-transformation (Oxford Medilog). The methods were evaluated on 4553.8 h of EEG data of 65 patients. CNet resulted in a sensitivity of 92.8% with a FDR of 1.35/h, Monitor resulted in a sensitivity of 74.4% sensitivity with a FDR of 3.02/h, and audio-transformation method reported a sensitivity of 98.3% (false detection was not reported because of the subjective nature of the method). The authors demonstrated variation in the performance of the algorithm on data previously unseen by the algorithm.

Osorio *et al.* [100] proposed a real-time seizure detection system with short detection delay. The EEG is filtered in the frequency range of 5-40 Hz using a wavelet finite impulse response (FIR) filter. The filtered EEG is squared, median filtered and compared to a background signal. The method was tested on 125 seizures reporting 100% sensitivity and zero false positives. The authors claim the method to be generic, but on close inspection, it seems to be specific to a group of patients (mesial temporal seizures). Furthermore, the method has neither been validated on continuous data nor on previously unseen data, thus contributing to overestimated performance.

Khan and Gotman [101] proposed a seizure onset method to improve the performance of [51] for depth EEG recordings. The method requires a minimum of two channels for detection and employs wavelet decomposition to separate the EEG into frequency scales. A number of features are calculated for each scale and applied to empirical decision thresholds. The method was evaluated on 229 hours of depth EEG from 11 patients that resulted in a sensitivity of 85.6% with a FDR of 0.3/h. Note that the wavelet decomposition into different scales hinders the clinical use of

the method, since different clinical settings record EEG at different sampling rates. This research was extended in [102] for scalp EEG and in [32] for depth EEG. The limitation introduced by wavelet decomposition is addressed by the use of filter-banks and the limitations of the empirical thresholds with an approximate Bayesian classifier. The method included a user tunable threshold, which allows for trade-off between sensitivity, detection delay, and FDR. The data is processed in 4 s epoch and is filtered by a filter-bank similar to wavelet decomposition. Relative energy, relative amplitude, and coefficient of variance of the amplitude were adapted from the previous work of [101]. Once the EEG data is separated into frequency bands, each frequency band has a combination of five features to create a feature vector. Using Bayes theorem, the classifier is trained to separate the two classes. The method was evaluated on 360 h of EEG and resulted in a sensitivity of 77.9% with a FDR of 0.85/h for scalp EEG and a sensitivity of 86.4% with a FDR of 0.47/h for depth EEG without any tuning.

Iasemidis *et al.* [103] proposed a short-term maximum Lyapunov exponent (STL_{max})-based seizure prediction and detection system to assist in easy review of EEG recordings. The authors in subsequent studies [68-73] demonstrated a progressive dynamical entrainment of electrode sites as seizure onset approaches. The method has been validated on single as well as on the multi-channel EEG recording from 2-5 patients that resulted in prediction sensitivity ranging between 82-91% and FDR between 0.16-0.19/h. The method has not been validated on a large data set and is designed for a specific type of seizure (TLE). However, the method is promising for therapeutic application.

Wilson *et al.* [52] proposed the *Reveal* algorithm based on Matching Pursuit (MP), small neural-network-rules and connected-object hierarchical clustering based seizure detection system for clinical application in the EMU. The EEG is decomposed into a set of 'atoms' each localized in time and frequency using the MP algorithm. From the resulting set of atoms, temporal features are extracted relative to a background

and combined with spatial information to develop a set of rules, which authors have referred to as neural network-rules. The detections are clustered together towards the final detection. The algorithm has been validated on a large dataset and compared with two other methods CNet and Sensa (Stellate Systems). The method included 676 seizures from 1046 hours of EEG recording and resulted in a sensitivity of 76% with a FDR of 0.11/h, whereas CNet and Sensa reported sensitivities of 48.2 and 38.5% with FDR of 0.75 and 0.11/h respectively. The method is another widely accepted clinical seizure detection tool used in the EMU.

Navakatikyan *et al.* [110] proposed a waveform-based (morphology) neonatal seizure detection algorithm to detect heightened regularity in EEG wave sequences using wave intervals, amplitudes and shapes. The algorithm involves several steps mimicking human experts. It includes filtering the EEG signal, parallel fragmentation of EEG signal into waves, wave-feature extraction and averaging, and elementary, preliminary and final detection. The EEG trace is fragmented into waves using a moving average technique to determine the points of intersection with the EEG signal. Then, each wave is partitioned into two halves based on the local maxima and minima of the wave. The positive half of the wave is defined as peak-wave and negative half of the wave as the trough wave. To quantify increased regularity in the EEG waveforms during seizure, the peak- and trough- waves are matched with the peak- and trough- waves of previous two consecutive waves. The average of the previous four matching parameters (correlation coefficient) is compared to a threshold to detect seizure. The performance of the algorithm was assessed against Gotman [111] and Liu [112] algorithms and resulted in sensitivity ranging between 83-95% when tested on 55 neonate EEG data. The method of Gotman [111] and Liu [112] resulted in sensitivities ranging between 45-88% and 96-99% respectively. This study (along with the study of [51, 97, 113]) suggests that methods based on morphological features tend to perform better over the ASD techniques that employ the more popular segment-based features

for classification.

Aarabi *et al.* [114] proposed an adaptive neuro-fuzzy inference-based seizure detection system for depth EEG recordings. In this method, the measures employed to quantify seizure were adapted from [32] and [115]. The measures are input to a rule-based classifier which detects seizure on individual channels. The individual channel detections are combined in some spatio-temporal context to make a multichannel final detection. The study reported a sensitivity of 98.7% and a FDR of 0.27/h for depth EEG from 21 patients. The study considered only clinical seizures with an average duration of 102 s and excluded all subclinical and short seizures from their analysis.

Kelly *et al.* [116] proposed the *IdentEvent* seizure detection method for scalp EEG that has recently received FDA approval for clinical use in review of EEG recordings. The method employs three descriptors: pattern-match regularity statistic, local maximum frequency, and amplitude variation, in order to identify seizures. The *IdentEvent* algorithm performance has been evaluated on 1208.24 hours of the scalp EEG of 55 patients that resulted in positive percentage agreement value (PPV) of 79.5% and a FDR of 2/h and is compared against the *Reveal* algorithm [52]. *Reveal* algorithm was evaluated at three different detection settings that resulted in PPV ranging between of 74-80% with FDR ranging between 6-13/h.

Duun-Henriksen *et al.* [117] have investigated the performance of automatic seizure detection using only a few recording channels. The method operates in two stages: first, it selects the channels used for analysis based on a simple feature, and then it performs seizure detection using a support vector machine-based classifier with wavelet domain features. Data from 10 patients undergoing presurgical invasive monitoring with 48-64 channels sampled at 239.75 Hz were considered to train and test the ASD system. The data contains a total of 59 clinical seizure in 1419 h of recordings. The study reports minimal improvement in the sensitivity by the algorithm over the EEGer on a set of preselected channels having highest variance and entropy between the two

groups. Note that the selected channel may not always remain the highest variance channel at all times during the monitoring session. Furthermore, the study did not include sub-clinical and focal seizures in the performance evaluation. Therefore, the claims may not hold true for all types of epileptic seizures.

Recently, Majumdar and Vardhan [118] have proposed a differential operator and windowed variance based seizure detection system that yielded 91.5% sensitivity and a FDR of 0.12/h on 15 patients depth EEG recording. It is interesting to note that the method quantifies abnormally sharp activities to make a seizure detection similar to our work in [33, 34, 119, 120], but using different features. Authors excluded six patients on which their method did not perform satisfactorily. Furthermore, this method did not detect subclinical seizures in this data.

2.2.2 Patient-Specific Seizure Detection

Qu and Gotman [21] introduced the concept of patient-specific seizure detection using a template matching approach. During LTM, once a seizure occurs in a patient, its onset is manually selected and stored. A large background preceding the seizure is also selected. This information about the seizure and the background is utilized to train a classifier. During subsequent monitoring sessions for the given patient, the EEG is scanned for a good match to the template seizure using the trained classifier; when one is found, it is reported immediately as the onset of a similar seizure. The classifier used in the method is a modified nearest-neighbor classifier. The method is not automatic and its applicability in clinical setting is limited because of the requirement of manual selection of the template seizure pattern and manual selection of a large background EEG. Additionally, the training of the classifier is complex. However, this study opened new avenues towards building new PS seizure detection schemes.

Wendling *et al.* [28] proposed a method to quantify similar seizures using a modified Wagner and Fischer’s algorithm . The process involves (i) segmentation of depth EEG

signals, (ii) characterization and labeling of the EEG segments, and (iii) comparison of observations coded as sequences of symbol vectors. The third step is based on a vectorial extension of the Wagner and Fischer’s algorithm [121] to first quantify the similarities between observations and then to extract invariant information, referred to as spatio-temporal signatures. The study reported reproducible mechanisms occurring during seizures for a given patient. In subsequent studies on medically refractory partial seizures, the authors demonstrated reproducible propagation schemes that may help in the understanding of epileptogenic networks [122, 123].

Shoeb *et al.* [124] proposed a multichannel seizure onset detector system using wavelet decomposition to capture morphological and spatial information that constituted feature vector as an input to a support vector machine (SVM) classifier for the presence of seizure. The method requires prior knowledge of at least 2-4 seizures, and non-seizure background EEG. The trained classifier is used to detect subsequent seizures in the record. The method was evaluated on 36 pediatric scalp EEGs resulting in a sensitivity of 94% with a FDR of 0.25/h. In contrast to other PS methods, where only a single seizure pattern is used for training, this method requires more than one template seizure pattern. The method has been considered in a neuroresponsive therapy [125], where the EEG features were computed within the implantable device. The features were then transmitted to a high performance remote computer for classification. Authors suggest that remote classification reduces the computational cost and is aimed at extending the implant’s battery life. However, a centralized remote system for seizure classification is not a practical solution.

Osario *et al.* [64, 90-93] extended their originally proposed NPS method [100] in the design of PS system to prevent propagation of a seizure using electrical stimulation. A set of candidate filter banks based on the power in the different spectral bands are designed using *a priori* known seizure and non-seizure patterns. The filter that maximally separates the seizure and non-seizure is selected to train the classifier. The

trained classifier is used to detect remaining seizures in the data. The authors selected short segments of seizure and non-seizure to demonstrate their method. However, the scheme has not been validated on prolonged and continuous EEG recordings.

Wilson *et al.* [130, 131] presented a neural network architecture to design a PS method (known as *MagicMarker*) similar to their *Reveal* algorithm. It trains the PS classifier rapidly without human intervention, requires minimal sample data, and employs a supervised learning algorithm to improve classification errors. The probabilistic neural network (PNN) is trained on a single seizure event and the corresponding background activity that extends from the end of the previous seizure event (or the beginning of the record) to the start of the current seizure event. Although the method requires a single seizure pattern, it needs extensively long background EEG, thus limiting its practical application.

Shi *et al.* [132] proposed a model-based seizure detection using statistically optimal null filter (SONF) which requires only the *a priori* knowledge of a single seizure pattern. The authors proposed sinusoidal wavelet basis function to model the template seizure. The approach provided 100% sensitivity and no false detection on single channel study of two patients. However, the method has several drawbacks: (1) it is not automatic, (2) involves visual segmentation of the template pattern, (3) employs wavelet domain-based modeling of the template pattern, and (4) has not been validated on large dataset. Addressing the limitation to this method may lead to the development of an automatic, robust and more practical PS system.

Zandi *et al.* [35] proposed a patient-specific seizure detection method for scalp EEG recording based on wavelet packet transform. The method requires *a priori* knowledge of the seizure and a large background EEG (~ 30 min.). The seizure and background EEG is analyzed in a 2 s moving window with 50% overlap. Each epoch is decomposed into a wavelet-packet tree. Energy in each sub-band is used to estimate the probability density function of each sub band relative to a reference, to estimate

the distance between seizure and non-seizure. In addition, regularity index is also computed from the decomposed wavelet packets to train the classifier. The combined seizure index which measures increased regularity and energy index on the individual channels are combined with multichannel information to identify seizures similar to the template seizure. The method has been validated on 14 patients resulting in a sensitivity of 90.5% with a false detection rate of 0.51/h. The PS scheme has several drawbacks: not automatic, selection of very large non-seizure reference, wavelet-packet based analysis, manual tuning of the detection thresholds, and selection of specific type of seizure dataset (temporal lobe epilepsy).

Salam *et al.* [133] recently proposed a low-power patient-specific seizure onset detector for implantable devices. The method is based on the concept of detecting progressive increase in the amplitude and frequency at the seizure onset to make accurate seizure detection proposed in [33, 34, 36, 98-100]. Based on this concept, the authors devised an algorithm that consists of a set of voltage and frequency detectors to identify a progressive increase in the amplitude and frequency at the seizure onset in multiple frequency bands. The detection thresholds are customized for each individual patient to maximize specificity and to prevent unwarranted neural stimulation. The algorithm is validated on seven medically refractory epileptic patients with a report of 100% specificity and average onset delay of 13.5 seconds. The method is designed specifically for seizure that progressively increases with low-voltage fast-activity. Note that specificity can be maximized to 100%, but at the cost of sensitivity, which has not been reported in this study. Further, the method has also not been validated on varied and large intracranial EEG recordings.

2.3 Spike Sorting Techniques

Patients with medically refractory seizures are candidates for surgical resection of the seizure onset area or for deep brain stimulation therapies that can lead to significant reduction or cessation of seizures. Several studies report a better surgical outcome when regions of frequent interictal spikes are also removed [45, 101-106]. However, as to how exactly the interictal spikes develop and as to how they propagate and contribute to the generation of seizures is not well understood [107-109]. Automatic spike detection techniques have received intense attention to aid rapid identification of spikes in the voluminous EEG recordings. However, quantitative analysis of epileptiform spikes is still done manually which is a very labor-intensive and time consuming task.

On the other hand, spike² classification is the first step in experimental neurophysiological studies aimed to better understand the brain functions. Classification of spikes is studied since (1) spikes are highly stereotypical, permitting the modeling of their shapes to facilitate classification of the associated neurons, (2) spike trains carry an affluent amount of information permitting modeling of brain functions at very high temporal and spatial resolutions, and (3) spike occurrences mediate plasticity such as learning and memory formations [110-112]. However, spike classification schemes mainly focus on the timing of their individual occurrences (spike train analysis) and not on their actual shapes [146, 147]. A relatively large number of spike classification methods have been proposed for neuro-physiological experiments. The following presents some of the popular spike classification methods.

Willming and Wheeler [149] proposed a four channel extracellular spike sorting algorithm based on spike amplitude. The classification routine considered a spike to belong to the same class when the peak amplitude fell within a user specified interval.

²It must be noted that spikes in the EEG and in the basic neurophysiological experiments are two different entities. The use of the term 'spike' in experimental neurophysiological studies refer to action potentials, recorded using microelectrodes (1 ms events) that represent the normal and abnormal functions of single/multi-cell neurons. The epileptic spikes in the EEG are recorded with macroelectrodes that typically last 35 to 200 milliseconds.

The authors proposed two more approaches that compared the RMS error between the stored templates of each unit’s spike waveform and the spike most recently detected. The new spike was classified according to the minimum of the RMS errors computed. The third algorithm utilized principal component analysis (PCA) for classification. Peak amplitude windowing-based algorithm outperformed the principal component and template matching algorithm. The signal-to-noise ratio of the spikes and large variation in the spike waveforms justifies the poor classification by template matching approach compared to peak-amplitude and principal component approaches.

Chandra and Optican [150] proposed a connectionist neural network for sorting extracellular spike recordings. Spikes were detected when the amplitude of the recorded signal exceeded a positive or negative threshold. Detected spikes were clustered together to form noise-free templates using the *simultaneous clustering algorithm*, which first finds the best clusters around each waveform, groups these initial clusters together and then selects the best and final clusters. Each detected waveform is initially a potential initiator waveform for a cluster. The waveforms are clustered with the initiator waveform based on the best alignment and Euclidean distance, resulting in M clusters for M waveforms. The clusters are selected based on inter-cluster distance, cluster density and a cluster-scatter measure. Centroids of the selected clusters are the templates. A fully connected feed-forward, three layer trained neural network examines the template and spikes. The performance was determined on simulated data.

Quiroga *et al.* [151] proposed a method for detecting and sorting spikes from multi-unit extracellular recordings. The method combines wavelet transform and super-paramagnetic clustering and encompasses three principal stages. Spikes are detected with an automatic amplitude threshold on the high-pass filtered data and a small set of wavelet coefficients from each spike is chosen as input for the clustering algorithm. Clustering algorithm is based on simulated interaction between each

data point and its k -nearest neighbors, which is implemented as a Monte Carlo iteration of a Potts model. The complete clustering algorithm is known as superparamagnetic clustering algorithm. The algorithm outperformed when compared to other conventional methods using several simulated data sets whose characteristics closely resemble those of *in vivo* recordings. The unsupervised and fast implementation of the sorting technique is commonly known as WAVE_CLUS.

Wood *et al.* [152] studied variability in manual spike sorting and its implications in the neural prosthetics. The study highlighted the challenges encountered in manually sorting a large number of multi-channel data and the need for a robust spike sorting algorithm.

Kaneko *et al.* [153] proposed tracking spike-amplitude changes to improve the sorting results. Their sorting algorithm included spike detection, spike vectorization, burst detection, and spike classification. A spike was detected by matching the recorded waveforms with a set of spike templates with different durations (spike detection). The amplitudes of these waveforms constituted a spike-amplitude vector (spike vectorization). Spike bursts were detected based on attenuation of the spike amplitude and inter-spike intervals (ISIs) (burst detection). Finally, clusters of spike-amplitude vectors in the six-dimensional vector space were statistically classified by bottom-up hierarchical clustering in which every spike-amplitude vector was first assigned to a cluster, and then the nearest clusters were repeatedly combined into a new cluster until clustering ended by Mahalanobis generalized distance. The study reports that cluster tracking improves the quality of multi-neuronal data analysis resulting in compact clusters.

Wolf *et al.* [154] proposed an unsupervised algorithm for sorting and tracking action potentials of individual neurons in multi-unit extracellular recordings. This approach assumes that each neuron produces spikes whose waveform features vary according to a probability distribution, and thus, each generating neuron may be

represented as a component in a mixture model. Additionally, the method incorporates the knowledge of available information over time to re-identify previously identified neurons despite possible changes in the amplitude, phase, and numbers of neuronal signals. This is achieved by dividing the long recordings into short time intervals followed by temporal alignment of spike events. The detected spike waveform is then projected onto a d -dimensional feature space, and are clustered by optimizing the Gaussian mixture models (GMM) via expectation–maximization (EM). Validation of the sorting algorithm on the recordings from macaque parietal cortex showed significantly more consistent clustering and tracking results than traditional methods based on EM optimization of the mixture models.

Chan *et al.* [155] proposed an unsupervised spike sorting method for extracellular recordings. It is based on wavelet coefficients, spike alignment and template-matching. The method uses significant wavelet coefficients near the alignment point to improve the sorting results. Herein, once a spike is detected, its selected wavelet coefficients are used as a vector to find a match in the codebook. The method does not require *a priori* knowledge of complete recording to derive the templates.

2.4 Summary

Seizure detection

In the first part of this chapter, we have reviewed seizure detection to identify the drawbacks, limitations and scope for improvements in existing methods. A large number of seizure detectors exists in the literature that are designed based on the patient age group (neonatal and adult), type of EEG recording (scalp, ECoG, or depth), and clinical use (prediction or detection). The seizure detection techniques can be broadly classified according to the detection approach: non-patient-specific and patient-specific.

It is noted that the literature is abundant with NPS seizure detection methods and there exist relatively few PS seizure detection methods. In the development of NPS seizure detection methods, a large training dataset is employed, whereas in the PS detection methods, the patient's own seizure and non-seizure EEG data constitute the training data. The NPS/PS methods derive features using the training data to build a classifier for an accurate detection of seizure events.

Some NPS algorithms use a simple threshold-based classifier (rule-based), where the detection threshold is generally fixed and only a few of these provide a facility to tune the detection threshold. The study of Pauri *et al.* [96] showed that sensitivity is inversely proportional to the detection threshold. Low detection threshold results in high sensitivity, but at the cost of increased false detections, whereas a high threshold setting causes an increased number of missed detections. Unpredictable and dynamic behavior of the epileptic seizure increases the complexity in selecting the detection threshold. In order to reduce this trade off, a multitude of features are extracted from the short EEG segment. The linearly separable dichotomy problem of the EEG into seizure and non-seizure becomes hyper-dimensional with the increase in the numbers of features. ANN-based classifiers are often considered in the seizure detection systems, which requires a complex supervised training of the classifier. The large number of features in the ANN-based methods typecast such methods to some specific type of seizures, and also increases the algorithm's complexity.

In contrast to the non-patient-specific seizure detection systems, there exists no patient-specific method that is fully automatic. PS methods rely on the manual selection of one or more seizure and non-seizure sections by the EEGer to train the classifier. Manual selection of the EEG sections is time-consuming and very subjective. To some extent, the model-based seizure detection using SONF of Shi *et al.* [132] reduces the dependence of the classifier on both the template seizure and the background EEG. This approach still needs the *a priori* known template pattern

that is provided by an EEGer. The performance of PS methods are superior to that of the NPS methods, but they are generally not practical.

Spike classification

The second part of the chapter reviewed spike sorting techniques to identify drawbacks, limitations and scope of improvements in the existing methods. Spike classification is of immense importance in basic sciences, experimental and clinical neurophysiology to better understand the dynamic brain functions. Analyzing neural signals allows a better understanding of the mechanism underlying complex functions such as perception, learning, and motor processing that lead to accurate diagnosis and development of new bio-markers, drug therapies and prosthetic devices. This is one of the reasons as to why spike sorting literature primarily dominates intra- and extra-cellular spikes (action potentials). Furthermore, literature review depicts why spike sorting still remains as one of the most challenging problems despite decades of effort. The difficulties (intra- and extracellular recordings) are well-known and include issues of nonstationarity, non-Gaussianity, temporal dependencies between spikes and overlapping spike shapes due to synchronous activity in nearby neurons. Several unsupervised methods for spike sorting have been proposed in the recent past with varying degree of success. Most methods are offline classification, which employ principal component analysis, wavelet transform and/or neural networks. Some online spike sorting approaches based on template-matching have been proposed that dynamically derive templates, which are susceptible to noise interferences leading to misclassification, and often employ computationally demanding techniques such as hierarchical clustering.

Epileptiform spikes which tend to occur more frequently compared to seizures are stereotyped and linked to specific neurons involved in their generation. Removing the sites of frequent epileptic spikes has been shown to improve surgical outcome. Recently, it has been shown that a small group of genes to be highly correlated with the interictal

spike frequency demanding a need for qualitative and quantitative analysis of epileptic spikes. While immense attention is given to automatic detection of epileptic spikes, only a handful spike sorting algorithms are available for the EEG recordings. Note that spike sorting methods designed for extracellular recordings (local field potentials or action potentials) cannot be applied to classify spikes in the EEG for several reasons. Typically, epileptic patients undergo prolonged monitoring period for several days to weeks making it nearly impossible to have *a priori* knowledge of the spike waveforms, which is required in most of the sorting algorithms. The number of electrodes also varies across patients and generally ranges between 32-256 channels. A large number of channels introduce computational complexity in online spike sorting. Additionally, the EEG is digitized at different sampling rates (200 to 5000 Hz) within the same centre and across laboratories. Sorting methods based on multi-resolution analysis, such as wavelet transform, are limited by the sampling rate which ultimately limits their widespread application.

Chapter 3

Data Description

3.1 Introduction

In this chapter, we provide the details of the data used in the development and testing of the new systems described in this thesis along with the techniques of performance evaluation.

3.2 Data Description

The International League Against Epilepsy (ILAE) commission [156] provides a guideline for the use of long-term monitoring in epilepsy. We have selected EEG data as per this recommendation to train and test the new seizure detection methods. The data for the seizure detection methods are obtained from two different sources - (1) Montreal Neurological Institute, McGill University (MNI), and (2) Freiburg University Hospital (FSP), while the data for spike classification method is obtained from Wayne State University (WSU). The databases from these sites are as described in this section.

3.2.1 MNI Database

The first dataset referred to as the MNI database consists of intracerebral EEG data acquired with the Harmonie System (Stellate System Inc., Montreal, Canada) from the Epilepsy Telemetry Unit at the Montreal Neurological Institute and Hospital (MNI/MNH). The database contains fifteen patients' data collected for another study [32]. One patient data was rejected because it was not possible to define unambiguous start and end of seizures. Thus, data from 14 patients with over 304 h of EEG constitutes the MNI database.

MNI data were bandpass filtered between 0.5 and 70 Hz prior to digitization at the sampling rate of 200 Hz. All patients had stainless steel nine contact depth EEG electrodes that were surgically placed inside the brain with contacts located 5 mm apart. Some patients also had epidural peg electrodes that were typically labeled using the letter 'E'. Depth electrodes were most commonly placed in the amygdala, hippocampus, frontal or occipital lobes labeled as 'AM', 'H', 'F', and 'O' with deepest contact labeled as 1. Normally, electrodes placed in the left and right hemispheres were labeled with either an 'L' or an 'R', for example, electrode in the left amygdala was labeled 'LAM'. There was no pre-screening of the patients other than the requirement that they had at least three electrographic seizures during the monitoring sessions. For each patient, five sections of recordings, approximately 4-7 h each, were extracted in such a way that the three sections had at least one seizure each, one section during wakefulness without seizures, and one without seizures during sleep. This ensured that no patient biased the overall performance. Prior to sectioning, a trained EEG specialist using a bipolar montage scored all data for seizures.

In our initial assessment of the MNI database, we observed that some seizures are present only on a single channel. Therefore, we considered analyzing MNI database in single channel configuration. We selected the channel in which seizure is visually clearest or obvious in the first seizure section of each patient of the MNI database.

The same channel is used in the remaining data for each patient in all the methods.

3.2.2 FSP Database

The second dataset of intracerebral EEG, referred to as the FSP database, consists of a subset of data from the Freiburg seizure prediction (FSP) database which is a subset of European epilepsy database [30, 157]. The FSP database contains invasive EEG recordings of 21 patients suffering from medically intractable focal epilepsy. The data were recorded from patients undergoing presurgical epilepsy monitoring at the Epilepsy Center of the University Hospital of Freiburg, Germany. The EEG data were acquired using Neurofile NT digital video EEG system with 128 channels sampled at 256 Hz sampling rate, and digitized using a 16-bit analogue-to-digital converter. The database contains EEG recordings obtained using grids, strips and depth-electrodes. The six contacts from the implanted grids, strips and depth-electrodes were selected by visual inspection of the raw data by the EEGer. Three of these contacts were selected from the seizure onset zone, specifically from the areas involved in early ictal activity. The remaining three electrode contacts were selected as *not involved* or *involved* last in the seizure spread [157].

FSP database data were filtered using a 5th order digital Butterworth bandpass filter between 0.5 and 70 Hz, and notched to remove 50 Hz power line noise. Four bipolar channels were constructed by subtracting the signals of consecutive intracerebral contacts, two for the epileptogenic zone and two for the associated remote locations [114].

3.2.3 WSU Database

The third dataset of intracerebral EEG, referred to as the WSU database, consists of a subset of data of nine medically intractable epilepsy patients who underwent presurgical evaluation between January, 2002 and August, 2008 at the Comprehensive

Epilepsy Program at Wayne State University, Detroit, USA. The EEG in the WSU database were obtained with Stellate Harmonie digital recorder (Stellate Inc., Montreal, PQ, Canada) with a sampling rate of 200 Hz. For each patient, three distinct 10 minute segments of the continuous awake EEG were selected based on the criteria: (a) at least a 3 h interval between each segment, and (b) ≥ 2 h after a partial seizure and ≥ 8 h after a secondarily generalized tonic-clonic seizure as described in [49, 50]. One of the three randomly selected 10 minute segment for each patient is considered in the design and evaluation of the spike sorting algorithm. The study was designed to elucidate activity-dependent molecular pathways in human epileptic foci using functional genomic methods and to quantify interictal patterns linked with specific genes in epilepsy.

3.2.4 Data Conversion

In this dissertation, algorithm development, data processing and performance evaluations are carried out using the MATLAB (Mathwork Inc., USA), while the review of the EEG signals and detected events are performed in the Stellate Harmonie software. Figure 3.1 illustrates the various steps involved in the data conversion, analysis and review. The EEG signals in the two databases were acquired using two different EEG machines that store the data in a format that is incompatible with the MATLAB environment. Therefore, the data must be converted to a format that is recognized by MATLAB in order to process the EEG signals.

The signal files in the MNI and WSU database are imported into MATLAB environment using the Stellate’s MATLAB interface toolbox. The signal files in the FSP database were only available in the ASCII format. Neurofile NT EEG recording system does not support exporting multichannel EEG signals into single ASCII file. Therefore, the continuous multichannel EEG recording is segmented into one file per channel, and each file is approximately 1 h long. Thus, the twenty-one patient FSP

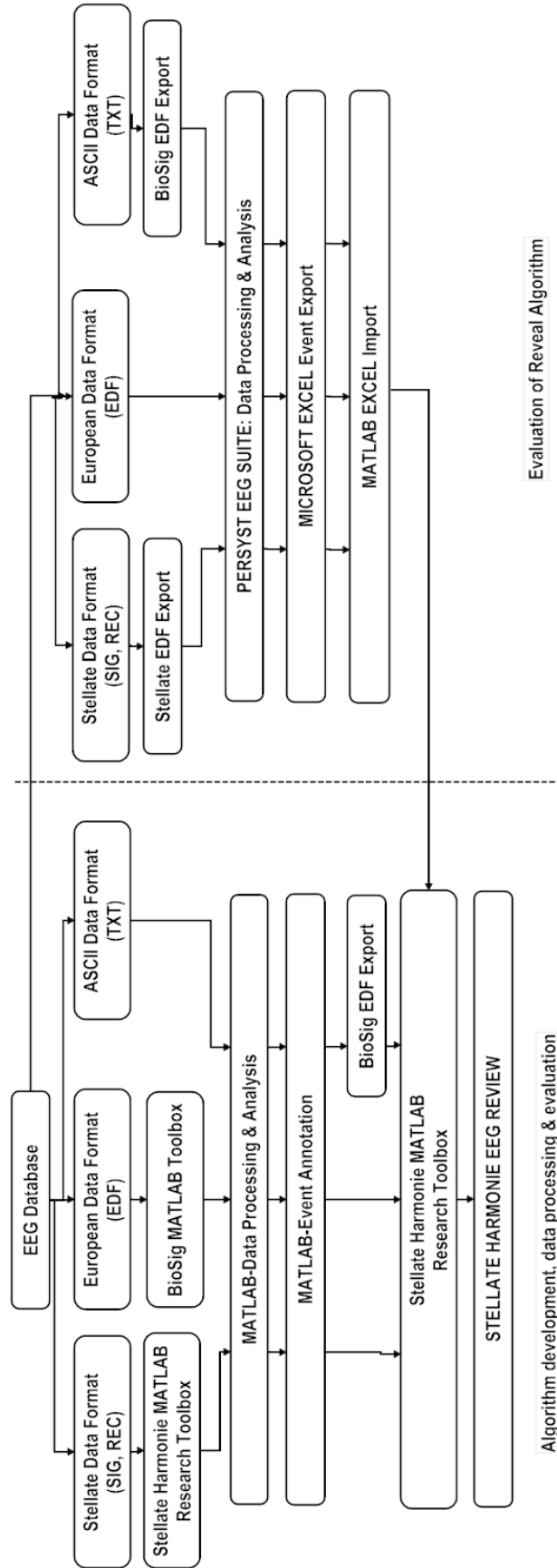


Figure 3.1: Protocol for analysis of the EEG signals.

database contained 4299 ASCII files. ASCII files for each patient were loaded into MATLAB, where the data is converted to bipolar montage. This is done by subtracting the signals of consecutive intracerebral contacts. The resulting single channel bipolar signals are then merged to generate the four-channel record per patient.

Harmonie 6.2e review software (Stellate Systems Inc., Montreal, Canada) is a clinical EEG review software that allows an easy and rapid review of multichannel EEG recordings. Since the MNI and WSU database were originally recorded in the Harmonie software, no additional data conversion is required for this data. However, the ASCII signal files in the FSP database are not compatible with Harmonie. To review FSP data in Harmonie, the data must first be converted to a format that is supported by the Harmonie software. The European Data Format (EDF/EDF+) is a standard data format for exchange and storage of medical time series data such as EEG. This data format is supported by Harmonie. *BioSig* [158] is a toolbox for MATLAB that allows converting ASCII to EDF format. Therefore, the four channel bipolar EEG data in the FSP database were converted to EDF using freely available *BioSig* toolbox [158]. Subsequently, the converted EDF files were imported into Harmonie 6.2e software.

All algorithm developments are done in the MATLAB environment, while data is reviewed in the Harmonie software. This allows an easy evaluation of the algorithm performance and validation of detected events by the EEG experts.

Performance of the newly developed seizure detection systems in this thesis are compared against popular methods from the literature (Gotman (1990) [51], Qu and Gotman (1997) [21], Grewal-Gotman (2005) [32], and *Reveal* Algorithm (2004) [52]). Harmonie software includes Gotman (1990), Qu and Gotman (1997), and Grewal-Gotman (2005) seizure detection methods. The *Reveal* algorithm is included in the Persyst EEG Suite ver. 20090819 (<http://www.eeg-persyst.com>).

In this work, we have used the freely available time-limited Persyst EEG Suite

version that supports the EDF format. The algorithm detections are stored by the software in its own proprietary format, but provides a provision to export results to Microsoft Excel (Microsoft Inc, USA). Performance analysis is done by exporting Reveal detections to Microsoft Excel and then imported into the Harmonie files using the Stellate MATLAB interface toolbox (refer to Fig. 3.1). By doing so, events detected by Reveal algorithm can be easily reviewed and compared with those revealed by the other methods on a common platform.

3.2.5 Data Selection

Seizure Detection

An initial assessment of the data of the complete MNI database revealed that in some patients seizures are present only in a single channel (focal seizures). Therefore, a single channel analysis is considered for the MNI database. Visual inspection of the first seizure section facilitated the selection of the single channel for analysis. For patients with seizures occurring simultaneously on multiple channels, we selected the channel in which the seizure is the most prominent. The selected channel is used to evaluate all data for the given patient.

For the purpose of training and testing, the MNI database was split into two sets. The training dataset for the NPS system includes randomly-selected seven patient data. This subset contains 58 seizures in approximately 145 h of single channel EEG. The remaining seven patient data were used as the test dataset and had 42 seizures in approximately 158 h of single channel EEG. The training dataset for the PS system on the other hand includes the first occurring seizure in the first seizure section of each patient along with 30 seconds of background EEG preceding the seizure onset.

The FSP database is used as a completely blind test data. This database is not considered during the development phase of the methods, and is used for an unbiased performance evaluation of NPS systems.

Spike Sorting

The WSU data are scored for interictal spikes by two different spike detection strategies in the referential montage. The spike detection module in the Stellate Harmonie software v 6.2e (Stellate Inc.) with default settings is utilized to identify interictal spikes [159]. The same data is visually scored by a trained EEGer for interictal spikes. The visually scored data included noise-free polyspikes that were often missed by the automatic spike detector. On the contrary, automatically detected spikes included false positives such as spike-like movement artifacts and mu rhythms. We will hereafter refer to 'AutoSpike' as the spikes detected by the Stellate spike detection module and 'ManuSpike' as the spikes identified by the EEG expert.

The training data consists of randomly selected EEG of five patients while the test data included all the nine patients of the WSU database. The spike sorting algorithm is optimized using the AutoSpike events of the training data. Validation involves the comparison of sorting outcomes using the two spike events (AutoSpike and ManuSpike) of all the nine patients.

3.3 Performance Evaluation Methodology

3.3.1 Seizure Detection

There is quite a bit of inconsistency in the literature in terms of the format of the results reported. For this reason, it is worth defining the measures that we will use to evaluate the proposed methods. In this dissertation, a single channel EEG analysis is considered, since most of the seizure detection methods in the literature detect seizures independently on each channel, and later combine the individual detections from neighboring channels to make a final multi-channel detection. Another reason for single channel analysis is that focal seizures often occur only in one or sometimes

in two neighboring channels. In each EEG recording, we have selected the channel in which seizure is unambiguous and there is no likelihood of disagreement among EEGers by visual inspection of only the first seizure section.

The time instant where the seizure starts first in any given channel is considered as the beginning of the seizure event (seizure onset) and the end of the seizure event is defined as the time instant at which the seizure activity is no longer present in any channel. A manually marked seizure event is a duration event marked across all channels. In this work, since the detections are made on a single channel basis, the channel selected for analysis may not be the channel representing the seizure onset.

The performance is evaluated by examining any overlap of the automatic detection with the manually scored event, as shown in Fig. 3.2. The example shown in Fig. 3.2 contains a multichannel EEG scored for seizure onset (SzO) and end (SzE) based on multichannel information by the EEG expert. The shaded area ('yellow' color) encapsulates seizure section marked by the EEGer. To demonstrate single channel performance evaluation, we select LH1-LH3 as the channel of interest on which automatic detections are enumerated from 1-8. Automatic seizure detection can occur prior to the seizure onset or after the seizure ends depending upon the temporal characteristics of the seizure. Furthermore, multiple seizure events can be detected for a given seizure depending on the classification rule. As a general rule, automatic detection events detected within 30 s of one another are grouped into a single event [19, 30, 32, 54, 81]. As a result of this grouping, it is possible that some algorithm detections occur prior to the manually scored onset. This can be addressed by extending the manually marked seizure sections, allowing a fair assessment of the detected events. In this work, the seizure section is extended on either side by 15 s, ($T_1 = T_2 = 15$ s) for the purpose of performance evaluation. In the example shown in Fig. 3.2, automatic detected events 3, 4, 5, 6 are considered good detection while 1, 2, 7, 8 are considered false events for this seizure.

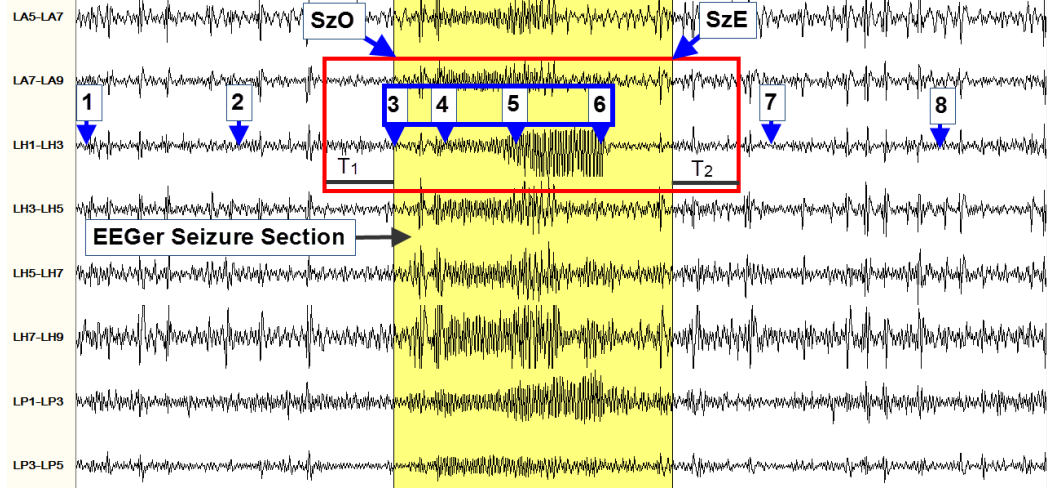


Figure 3.2: Section-based technique of performance evaluation. Numbered events represent the algorithm detections, EEGer section is a multi-channel duration event and the 'red' rectangular box represents the detection section on channel of interest (LH1-LH3).

The performance measures, sensitivity, specificity, false detection rate, average detection latency and receiver operating characteristic curve are used to evaluate the performance of the new seizure detection systems presented in this thesis and to compare it with those of the existing methods. These are defined as follows [21, 32, 51, 52, 54, 101, 160, 161]:

- Sensitivity: Ratio of the number of true seizures detected by the algorithm (TP) to the total number of seizures marked by the EEGer (TE) and is given by $ST = TP/TE$.
- Specificity: Ratio of the number of true seizures detected by the algorithm (TP) to the total number of events detected by the algorithm detected (TD) and is given by $SP = TP/TD = TP/(TP + FP)$, where FP is false positive, i.e., events detected by the algorithm, but not scored by the expert, which is also referred to as false detection (FD).
- False Negative (FN) : Events identified as seizures by the EEGer, but were missed by the algorithm.

- False Detection Rate (FDR): Number of false detections/hour.
- A receiver operating characteristic (ROC) curve is a graphical representation of sensitivity against specificity or FDR, as the detection parameter of interest is varied. The area under the ROC curve (ROC area, calculated using trapezoidal numerical integration) is an effective way of comparing the performance of different features or classifiers. A random discrimination will give an area of 0.5 under the curve, while perfect discrimination between classes will give an area of 1 under the ROC curve. The ROC area is equivalent to the Mann Whitney version of the Wilcoxon rank-sum statistic [162].

It is important to mention at this point that aforementioned definition of the term sensitivity and specificity are often misinterpreted with the accuracy and positive predictive value that are commonly used in the diagnostic testing, where the presence or absence of an event is clear (disease/no disease). True negative (TN) outcome isn't well defined for continuous data. For example, in one-hour section of EEG with one-minute of seizure and 59 minutes of non-seizure, it is not obvious what constitutes a negative event. The definition of the term sensitivity and specificity mentioned above are consistent with the usage in a large number of publications in the seizure detection literature [21, 32, 51, 52, 54, 94, 101, 160, 161].

3.3.2 Spike Sorting

One of the main challenges in the spike sorting is the lack of *a priori* knowledge of the total number of classes or clusters in the data. To address this challenge, we propose a new indirect approach to validate our sorting method and is described in Chapter 7.

Chapter 4

New Non-Patient-Specific Seizure Detection Systems

4.1 Introduction

We propose in this chapter three new non-patient-specific (NPS) seizure detection systems, that track the temporal progression of seizures by simple mathematical descriptors [33, 34, 36, 120, 136]. We select three popular NPS seizure detection systems for a comparative evaluation of the performance. The three selected NPS systems are the Gotman system [51], the Reveal algorithm [52], and the Grewal-Gotman system [32], which will hereafter be referred to as the comparison NPS systems.

The first proposed NPS system employs a simple detection strategy to track the continual increase in the feature value (relative frequency-weighted energy) as a seizure progresses, and hence is termed the *relative frequency-weighted energy (RFWE) system* [36]. The second proposed NPS system quantifies the EEG waveform morphology and tracks the continual increase of abnormally sharp activity to make a detection, and is called as *morphology system* [34, 120]. The third proposed system, termed

the *evolution seizure detection (eSD) system* [33, 136], incorporates the intelligent seizure detection strategy of the EEG experts to make a detection, and quantifies four different EEG features to track the temporal progression of seizures.

First, we introduce the time evolution of seizure that is utilized in the development of the new NPS systems. We then describe each of the new NPS systems and present results of the optimized method on the MNI training data. The results are compared against three existing systems mentioned previously. Each of the new NPS systems aims to address some of the challenges of its predecessor to improve the overall detection results.

4.2 Time-evolution of Seizure

Traditionally, NPS seizure detection techniques treat seizure detection as a binary classification problem, i.e., seizure or non-seizure. A variety of features are considered to quantify and identify the discrimination boundary that separates the two classes. However, features that can perfectly separate seizure and non-seizure classes have not yet been found. Alternatively, we hypothesize that it is possible to make accurate seizure detection by tracking the time evolution of the EEG characteristics.

Epileptic seizure is a dynamic short-time abnormal activity in the brain that starts sporadically, propagates, and after sometime terminates by returning to the normal brain state. This seizure evolution can be mapped as a function of time. A graphical illustration of seizure time evolution is shown in Fig. 4.1. The envelope represents the changes in the amplitude characteristics of the EEG. The example depicts how we encode the time evolution of a seizure using the amplitude feature. Seizure onset is at the point '**A**' and the end of the seizure is at '**D**'. Complete seizure has been segmented into three sections. The section **AB** represents the monotonic increase (growth) in the feature value. The **BC** section represents the stable amplitude segment, and section

CD represents the monotonic decrease (decay). The rate of increase or decrease, and the duration of each of the three sections vary from seizure to seizure, making the seizure detection very challenging. Nonetheless, this observation of continual growth or decay in the EEG characteristics can be employed to design computationally light, robust data-driven NPS systems. We believe that by quantifying the **AB** section of the seizure time evolution, it is possible to detect seizure as close as possible to the onset, which is one of the prerequisites for clinical application of the new system.

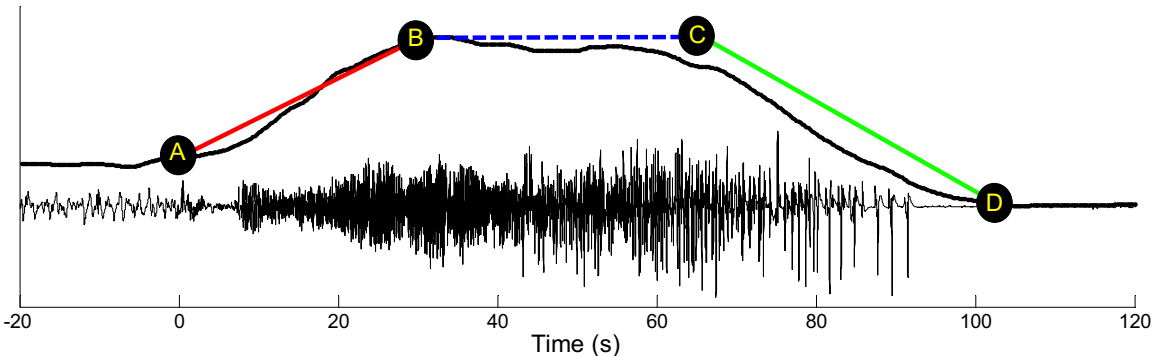


Figure 4.1: Encoding the time evolution of seizure by tracking the EEG characteristics. The example parametrizes temporal changes in EEG amplitude. Seizure onset is at the point 'A'. Seizure is segmented into three sections representing monotonic increase (AB), stable (BC) and monotonic decrease (CD) in the amplitude.

In the following, we present three proposed NPS seizure detection systems, namely, the RFWE system [36], morphology system [34, 120] and eSD system [33, 136].

4.3 Relative Frequency-Weighted Energy System

In this proposed system, the temporal changes in the amplitude and the frequency are quantified using a single EEG feature, namely, the relative frequency-weighted energy (RFWE) to make detections [36]. More specifically, we devise a new seizure detection scheme that uses the RFWE feature to track the continually increasing phase of the seizure onset (**AB** described in Fig. 4.1). The three main steps involved in this system include: (1) pre-processing and artifact rejection, (2) feature extraction,

and (3) classification. The flow chart of the RFWE system is shown in Fig. 4.2, and the following subsections describe the various blocks of the RFWE system in detail.

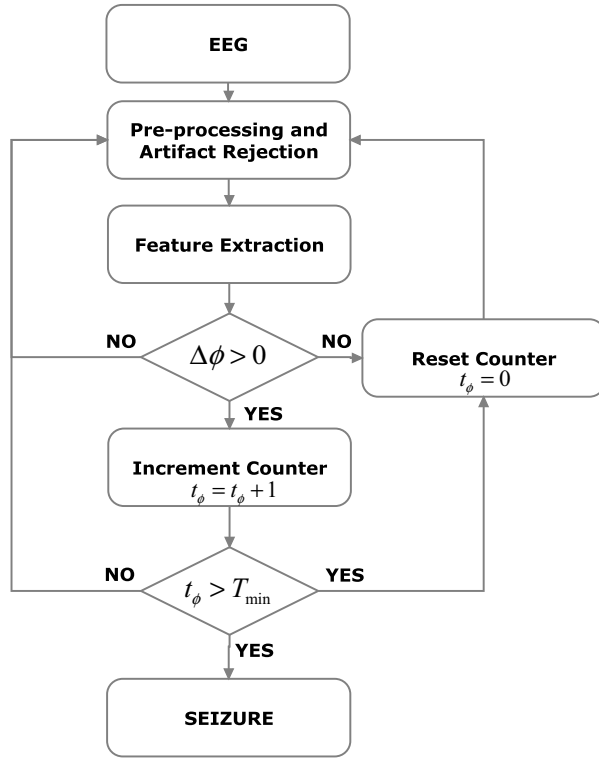


Figure 4.2: Flow chart of the RFWE seizure detection system.

4.3.1 Pre-processing and Artifact Rejection

Intracranial EEG is relatively free from artifacts in comparison to the scalp EEG, but spans a wider frequency spectrum, has a highly variable seizure morphology and a variety of sharp wave complexes, ranging from needle-like fast activity to much slower discharges that can be contaminated by high-amplitude artifacts (HAs), iso-electric artifacts (IEAs), power line noise, and fast electromyography (EMG) activity [5]. The pre-processing and artifact rejection block conditions the signal and incorporates techniques to reject these commonly occurring artifacts.

EMG artifact in the intracranial EEG is observed with substantial energy in the spectral content beyond 30 Hz [163], while the seizure activity in the intracranial

EEG is observed to be within 0.5-70 Hz band and primarily reported to be in 3-30 Hz band [32, 35, 51]. To reduce high frequency interferences and noise, the raw EEG is band-pass (3-30 Hz) filtered using a 5th order digital Butterworth IIR filter [102]. The data is processed in both forward and reverse directions to minimize the non-linear phase distortion caused by the IIR filters [32, 114].

Generally, poor electrode connection is the root cause for EEG contamination by power line noise. A notch filter with null frequency centered at the power supply frequency, i.e., 50/60 Hz is employed to filter the power line noise [164, 165].

Iso-electric artifacts (IEAs) cause false detection in NPS methods that employ techniques to compute features relative to a background EEG [32, 114]. A flat or iso-electric EEG (disconnection artifact) occurs when a patient gets disconnected for one or the other reasons from the recording device while recording continues. An increase in the feature value relative to the flat background is observed upon the patient reconnection. Since we compute the RFWE feature relative to the background EEG, it becomes necessary to handle IEA in this block. A disconnection is identified by computing the variance of the EEG amplitude in small segments. It is expected that during the flat-line, the variance in the EEG amplitude will be zero. On the occurrence of such an event in the data, the detection is suppressed for the next 90 seconds.

High-amplitude artifacts (HAs) are the second most common type of artifact observed in the intracranial EEG that often originate as an abrupt change in the EEG amplitude due to patient or electrode movement [32, 114]. Typically, intracranial EEG is observed to be within $\pm 2500 \mu V$. Therefore, an epoch contaminated by high-amplitude artifact can be easily identified and excluded from the analysis. Any test window in which the amplitude exceeds $\pm 2500 \mu V$ is ignored from further analysis. The example in Fig. 4.3 depicts a 5-hour single channel EEG data contaminated by IEA and HA.

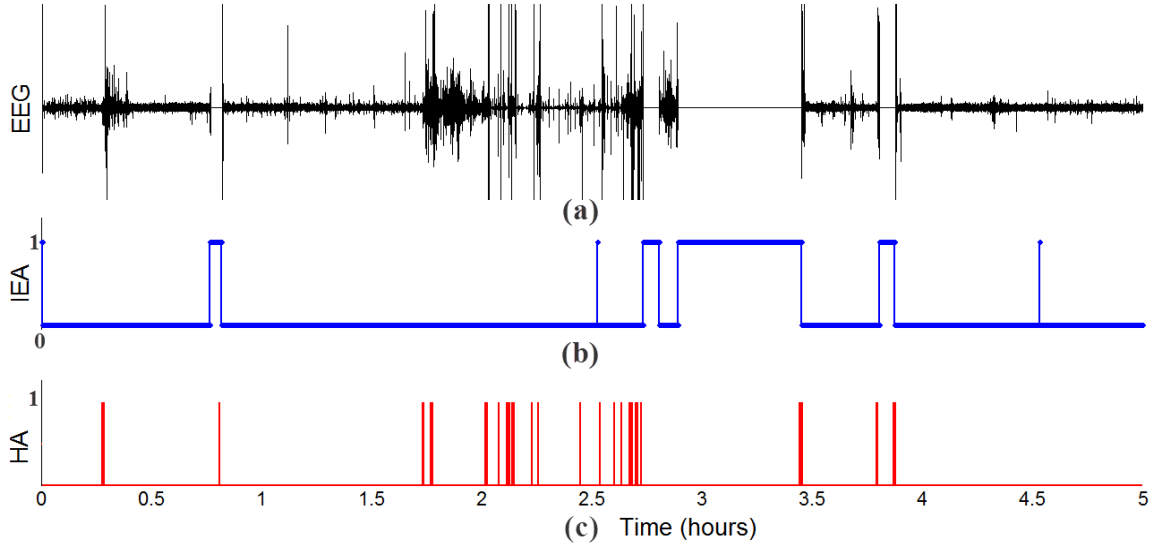


Figure 4.3: (A): Single channel EEG contaminated by the two common artifacts present in the intracranial EEG. (B) represents the time instances of IEAs, and (C) represents the time instances of HAs in (A).

4.3.2 Feature Extraction

Feature Extraction Techniques

In the seizure detection arena, feature extraction is performed using a sliding data frame (window/epoch) approach. There are two popular approaches in the literature: (a) single sliding window, and (b) two sliding windows. In the first approach, the features are computed from the EEG in the test window (x_{test}) which moves through the data in small steps. The size of the test window and the step size are determined by the detection algorithm requirements. In general, the duration of the test window is preferred to be as short as possible to address the rapidly changing EEG, yet it must be large enough to compute the features accurately. Figure 4.4A illustrates the single sliding window feature extraction technique. The second feature extraction technique incorporates two sliding windows and is shown in Figure 4.4B. This feature extraction technique enhances the separability between seizure and non-seizure by computing the features relative to a reference window. Here, the reference window is also known

as the background window (x_{bkg}) that ideally represents the non-seizure EEG. The background window can be fixed or slide synchronously with the test window. The latter is more commonly used to ensure that the most current background EEG state is used for the reference [51, 54]. The gap or separation between the test and background windows reduces the chances of the background window to include seizure EEG. The duration of the background window and gap is generally large compared to the test window.

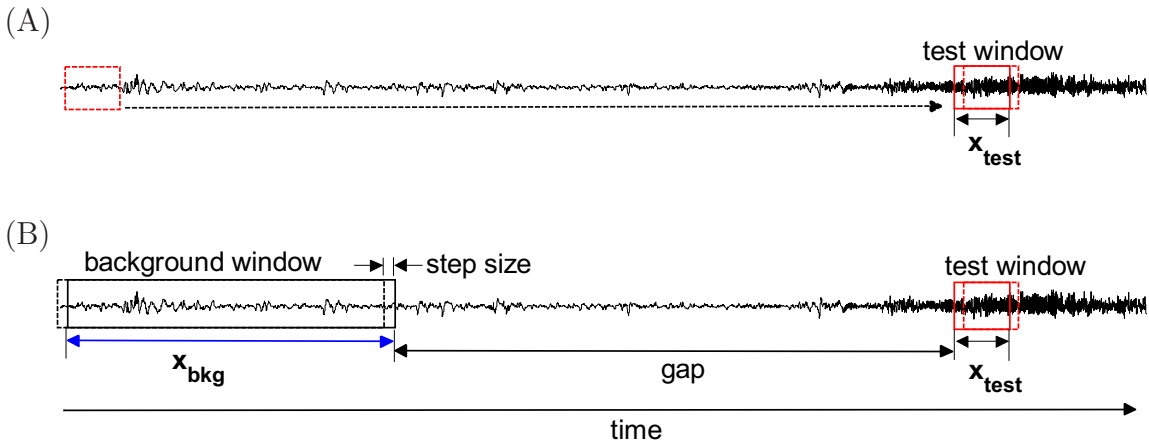


Figure 4.4: Feature extraction techniques: (A) single sliding window, and (B) two sliding window feature extraction.

We experimented with different test window lengths (0.5-30 seconds) and selected 2 seconds to be suitable for the RFWWE system. Detection delay and subtle changes in the ongoing epileptic seizure are captured with a sliding test window that moves in small steps. Empirically determined overlap of 75% is considered suitable for this method. The test window is separated from the background window by a 60 s gap, where the background window duration is chosen to be 30 s. The size of the gap and the background window is taken from the previous studies of Gotman *et al.* [21, 32, 51, 54, 101, 156, 166].

Relative Frequency-Weighted Energy

In general, seizure EEG patterns are distinguished from the background EEG by a change in the amplitude in one or more dominant rhythms for a short duration. However, some seizures show a fast transition in frequency with minimal or no change in the amplitude. It is possible to quantify such seizures using frequency-weighted-energy (FWE). Frequency-weighted-energy is sensitive to variations in both amplitude and frequency resulting in higher energy during the seizure than non-seizure activity [37, 39, 169]. Teager proposed a simple non-linear energy operator (NLEO) to quantify the energy proportional to change in the amplitude or frequency. This operator can be presented in its discrete form as [168]

$$\psi [x(n)] = x^2(n) - x(n-1)x(n-2), \quad (4.1)$$

where $x(n-k)$, $k = 0, 1, 2$ are delayed samples of the EEG signal. One of the key properties of this operator for a pure sinusoid can be summarized by the rule

$$\Psi = \psi[A \cos(\omega_i n + \phi)] = A^2 \sin^2(\omega_i), \quad (4.2)$$

where A is the amplitude and ω_i is the frequency. For ω_i much less than the sampling frequency, $\Psi \approx A^2 \omega_i^2$. In cases where the frequencies of interest are much lower than the sampling frequency, as with EEGs, the output of NLEO can be considered a measure of the spectral content of the signal [39, 167, 169-172]. A more generalized form of the Teager operator had been given earlier by Plotkin and Swamy [170, 171, 172],

$$\psi_g[x(n)] = x(n-l)x(n-p) - x(n-q)x(n-s), \quad l+p = q+s \quad (4.3)$$

where ψ_g denotes generalized NLEO. Agarwal *et al.* [167] showed that for $l \neq p$ and $q \neq s$, ψ_g is more robust to noise. That is, if the input signal x contains additive

white noise, then the output in Eq. (4.3) will not contain a component reflecting the input noise [39, 167, 169]. This is due to the removal of the square term in Eq. (4.3). For this reason, we choose $l = 1$, $p = 2$, $q = 0$ and $s = 3$. The expected value of the output of the generalized NLEO (ψ_g) is referred to as the frequency-weighted-energy (FWE) [39, 167].

Some seizures do not reflect any amplitude evolution, but show a rapid transition from one frequency to another. FWE is useful in the identification of such seizures, since it has been shown to be highly sensitive to amplitude and frequency changes in the EEG [39, 167]. For this method, the feature is extracted using two sliding windows. The ratio of the FWE in the two windows (test and background) is referred to as the relative frequency-weighted energy, $Q'(n)$,

$$Q'(n) = \frac{\frac{1}{N} \sum_1^N \psi_g[x_{test}(n)]}{\frac{1}{M} \sum_1^M \psi_g[x_{bkg}(n)]}. \quad (4.4)$$

An example of the time-evolution of a seizure in the RFWFE is shown in Fig. 4.5.

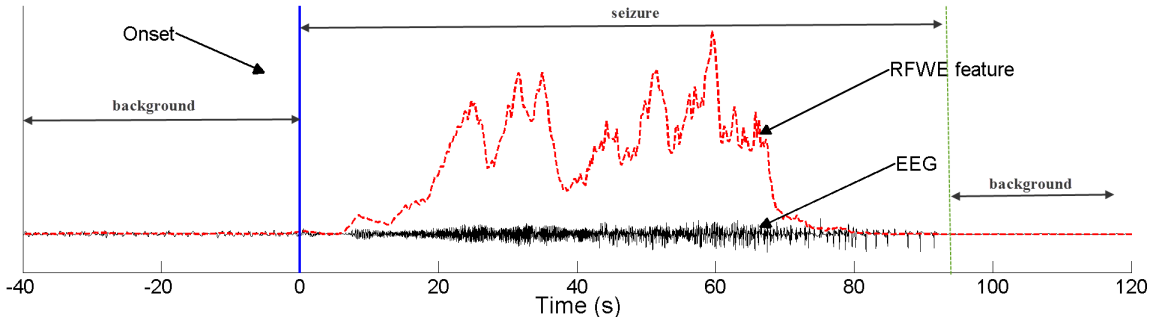


Figure 4.5: The example represents 160 s of EEG activity that includes normal (background) and seizure activity. The RFWFE describes the changes seen in the EEG as it progresses from inter-ictal (background) to ictal (seizure) state, and back to inter-ictal state.

4.3.3 Classification

The RFWFE feature shows a continual increase from the baseline at the onset of seizure, as seen from Fig. 4.5. It was realized that this can be used to track the RFWFE

trajectory for a reliable seizure detection. However, sharp transients and artifacts cause abrupt fluctuations in the time-evolution trends of the RFWE ($Q'[n]$), and must be addressed prior to classification. The spurious fluctuations in $Q'[n]$ can be suppressed by a moving average (MA) filter to generate a smooth time-evolution trend. Therefore, we incorporate a recursive moving average filter to attenuate the effects of spurious fluctuations in $Q'[n]$, given by

$$Q[n] = Q[n - 1] + \frac{Q'[n] - Q'[n - M]}{M}, \quad (4.5)$$

where $Q[]$ is the M -point average output signal and $Q'[]$ represents the unfiltered RFWE input signal.

We experimented with different lengths of the MA filter to determine the filter length that best suits the RFWE system. Figure 4.7 illustrates the effect of the MA filter length on the RFWE feature. It can be seen that with increasing filter length, M , the spurious fluctuations in the $Q'[n]$ are suppressed, resulting in a smooth trend. The amount of spurious noise reduced by the MA filter is equal to the square root of the filter length. That is, a 120 points MA filter reduces the noise by a factor of 10.95 while a 360 point MA filter reduces the noise by a factor of 18.95 [173]. It is also noted that a higher-order MA filter tends to blur the seizure onset and end. In the example of Fig. 4.7, it can be seen that for $M = 360$ the envelop shifts the seizure onset and terminates the seizure far beyond the actual seizure onset and end. Interestingly, the output accurately maps the seizure onset and end for $M = 120$ points. After studying the training data, a 120 points MA filter, which corresponds to 30 seconds of the EEG, was considered suitable.

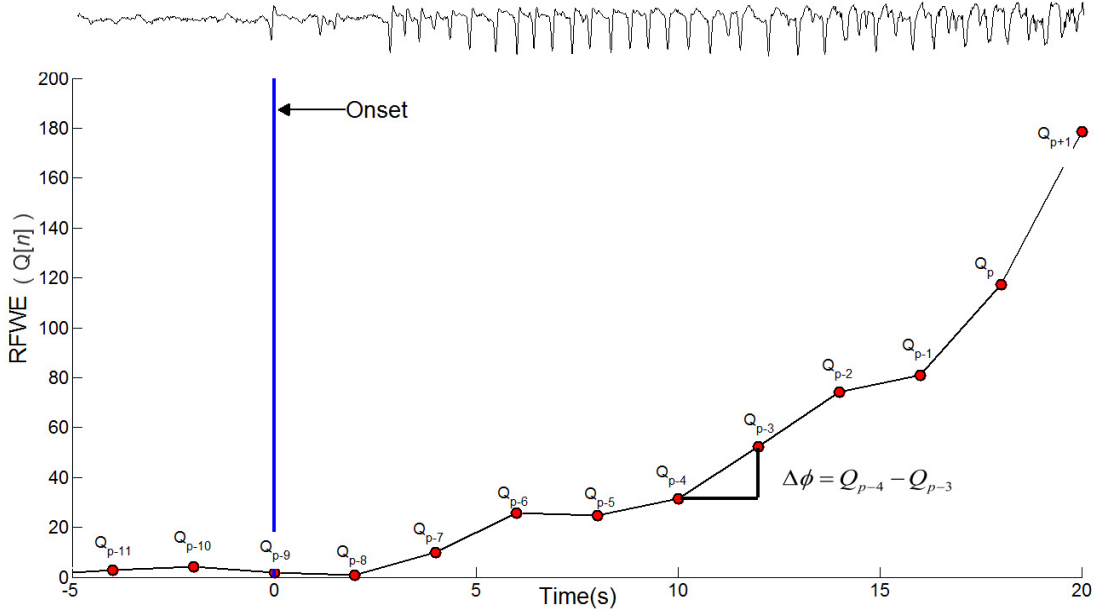


Figure 4.6: Tracking the continual increase of the RFE trajectory at the seizure onset.

In the RFE system, we aim to quantify the time evolution of the seizure to make a detection that does not require *a priori* knowledge of the seizure type. In other words, the method aims to track the continual increase in the feature value, which does not require a default detection threshold with respect to the feature. However, the definition of minimum duration of seizure can be used to control the trade-off between sensitivity and specificity. This is achieved by examining the gradient of $Q[n]$ for continual increase as illustrated in Fig. 4.6. The gradient, $\Delta\phi[n]$, is computed by taking the difference of two successive $Q[n]$ values.

$$\Delta\phi[n] = Q[n] - Q[n - 1], \quad (4.6)$$

Continual increase in the amplitude, frequency or both can be tracked using $\Delta\phi[n]$ by looking for a continual positive gradient. Furthermore, in order to classify the continual increase in the RFE trend to be due to seizure, it must satisfy a minimum duration. This is achieved by extracting the sign of $\Delta\phi[n]$ given by

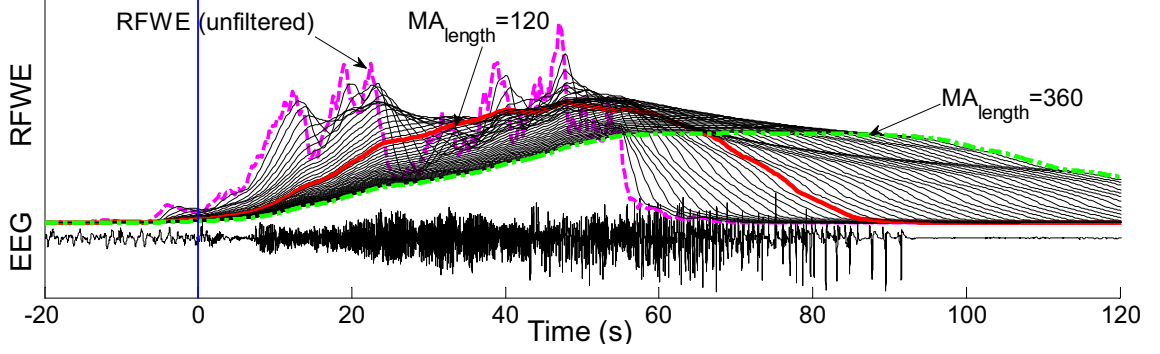


Figure 4.7: Effect of filter length on the feature trajectory.

$$\text{sgn}(\Delta\phi) = \begin{cases} 1, & \Delta\phi > 0 \\ 0, & \Delta\phi = 0, \\ -1, & \Delta\phi < 0 \end{cases} \quad (4.7)$$

and counting the number of times the sign is continually positive ($= 1$). The counter (t_ϕ) is used to find consecutive positive gradients and is incremented by unity, if $\text{sgn}(\Delta\phi)$ equals one (or positive gradient), otherwise it is reset to zero (see Fig. 4.2). When the counter exceeds a minimum duration ($T_{min} = 120$), a seizure is identified, and the counter is reset. In this manner, the RFWE system detects a seizure reflecting the continual increase in the RFWE for the minimum duration. Note that we do not define the discrimination boundary(ies) or the detection threshold(s) needed for the classification, which is typical in most of the existing NPS systems. Instead, the detection parameter in the RFWE system is the continual increase in the RFWE feature for a certain minimum duration. Typically, the EEGer considers various properties of the EEG that sustain for certain minimum duration to identify seizures. However, in the literature, there exists an ambiguity as to what should be the minimum duration to define a seizure, and is often left up to the experts. Our definition of seizure is any paroxysmal EEG activity sustaining for at least six seconds.

4.3.4 Performance Evaluation

The performance of the RFWE system is evaluated on the MNI training dataset and is compared against the three previously mentioned comparison NPS systems (Gotman, Reveal, and Grewal-Gotman systems). Note that the RFWE system is developed using the MNI training dataset, but not the three comparison systems. Therefore, the detection settings of the comparison systems need to be optimized on this dataset. We utilize receiver operating characteristic (ROC) analysis to determine the default detection settings for the comparison systems.

Majority of the seizure detection systems in the literature are dependent on the detection threshold derived using the training data. The detection threshold means that the specified feature(s) must satisfy certain minimum preset value(s) in order to classify the current epoch as a seizure. For example, as default detection threshold, the average amplitude in the test window must be at least three times the average amplitude in the background window in the Gotman system. It is not necessarily true that all seizures will satisfy this condition, resulting in missed seizures. The NPS systems considered for comparison also include a minimum duration threshold to further enhance the detection specificity. Therefore, the detection settings of the comparison systems must be optimized on the same dataset that were utilized in the development of the proposed RFWE system for an unbiased performance evaluation. The optimal detection thresholds for the comparison systems are determined from the ROC analysis using the training dataset. The performance of each of the NPS systems is evaluated at several thresholds in a given range. The threshold value that results in the best compromise between the sensitivity and false detection rate is selected. ROC analysis for the Grewal-Gotman and Reveal algorithm are shown in Fig. 4.8.

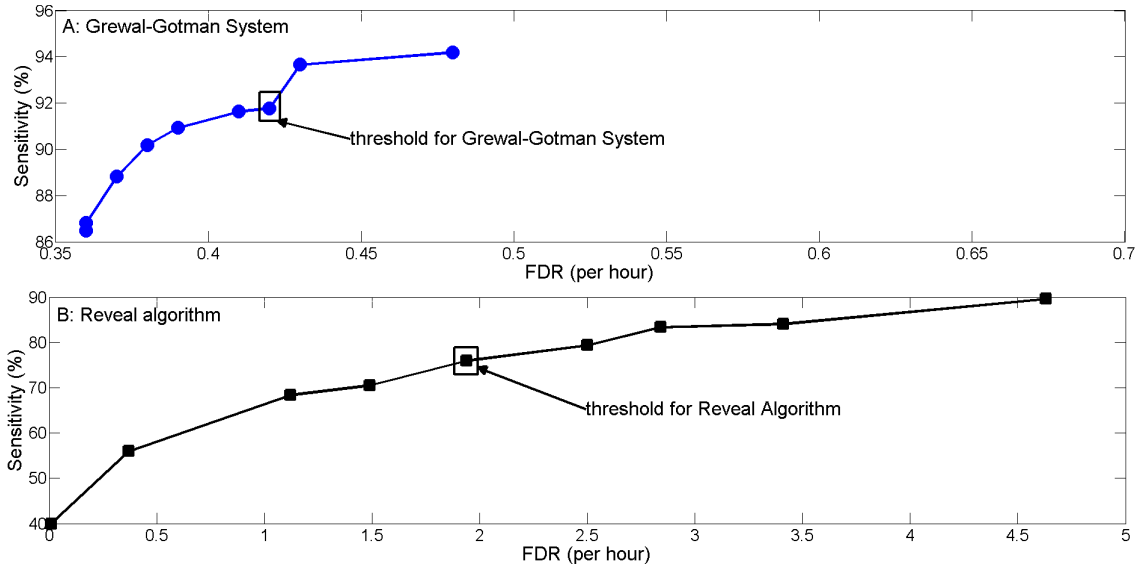


Figure 4.8: ROC analysis for Grewal-Gotman system and Reveal algorithm. The detection threshold of the Grewal-Gotman system and Reveal algorithm is varied from 1 to 10. The selected thresholds for Grewal-Gotman system (detection threshold = 3) and Reveal algorithm (perception value = 5) are selected.

Note that the seizure varies from the patient-to-patient. Therefore, it is very difficult to set a single threshold value at which the detector gives the best result for all patients. One of our aims is to overcome this limitation, which we achieve by tracking the time evolution of the seizure as it progresses.

Prior to any performance evaluation, all automatic detections that are within 30 s of each other are clustered as a single seizure event. An event detected by the proposed algorithm is considered a good detection, if there is any overlap with a manually scored event; otherwise, it is considered a false detection. The performance is assessed with the three most commonly used performance measures in the seizure detection literature: sensitivity, specificity and false detection rate as described in Chapter 3 [32, 160].

4.3.5 Results

The detection results on the MNI training data of the RFWE system for each patient are shown in Table 4.1, while the corresponding results for the three comparison systems are shown in Table 4.2. The RFWE system results in a sensitivity of 95.4%, specificity of 69.2%, and FDR of 0.2/h. The Gotman, Reveal, and Grewal-Gotman systems report a sensitivity of 64.6%, 41.9% and 85.5%, and a specificity of 65.7%, 22.2% and 51.5%, respectively. The RFWE system shows an overall improvement of 30.8%, 53.5% and 9.9% in terms of sensitivity, and 3.5%, 47% and 17.7% in terms of specificity over the Gotman, Reveal and Grewal-Gotman systems, respectively.

Table 4.1: Detection results for the proposed RFWE system on the MNI training dataset

PID	Channel	No. of Files	Hours	TE	TP	FP	FN	SN (%)	SP (%)	FDR (/h)
1	LH1-LH3	5	20	11	9	0	2	75	100	0
2	RC1-RC3	5	20	13	13	8	0	100	61.9	0.4
3	LH1-LH3	5	21	4	4	0	0	100	100	0
4	LA3-LA5	5	20	6	6	6	0	100	50.0	0.3
5	LP1-LP2	5	20	14	13	6	1	92.9	68.4	0.3
6	LS4-LS5	6	24	7	7	6	0	100	53.8	0.3
7	LFC3-LCF5	5	20	3	3	3	0	100	50.0	0.2
TOTAL		36	145	58	55	29	3	95.4	69.2	0.2

PID = patient ID, TE = total expert, TP = true positive, FP = false positive, FN = false negative, SN = sensitivity, SP = specificity, FDR = false detection rate.

4.3.6 Discussion

The main goal of the proposed RFWE system was to quantify the temporal evolution of seizure by a computationally simple approach. This is achieved by quantifying the amplitude and frequency changes in the EEG by a single feature, i.e., the relative frequency-weighted energy (RFWE). Since the RFWE feature is highly sensitive to subtle changes in the EEG amplitude and frequency, sharp transients which occur more frequently in the background EEG can disrupt temporal evolution in the RFWE.

Table 4.2: Detection results for the three comparison systems on the MNI training dataset

PID	RFWE-based Classifier			Gotman System (1990)			Reveal Algorithm (2004)			Grewal-Gotman (2005)		
	SN (%)	SP (%)	FDR per hour	SN (%)	SP (%)	FDR per hour	SN (%)	SP (%)	FDR per hour	SN (%)	SP (%)	FDR per hour
1	75	100	0	100	92	0.0	18.2	100	0	72.7	80	0.1
2	100	61.9	0.4	62	47.1	0.5	23.1	3.1	4.75	61.5	57.1	0.3
3	100	100	0	50	100	0.0	50	7.4	1.19	100	57.1	0.1
4	100	50	0	83.3	63	0.2	33.3	8.7	1.05	100	37.5	0.5
5	92.9	68.4	0.3	28.6	33.3	0.4	78.6	25	1.65	64.3	37.5	0.8
6	100	53.8	0.3	29	50.0	0.1	57.1	3.8	4.21	100	41.2	0.4
7	100	50	0.2	100	75	0.1	33.3	7.7	0.6	100	50	0.2
TOTAL	95.4	69.2	0.2	64.6	65.7	0.2	41.9	22.2	1.9	85.5	51.5	0.3

PID= patient ID, SN = sensitivity, SP = specificity, and FDR = False detection rate

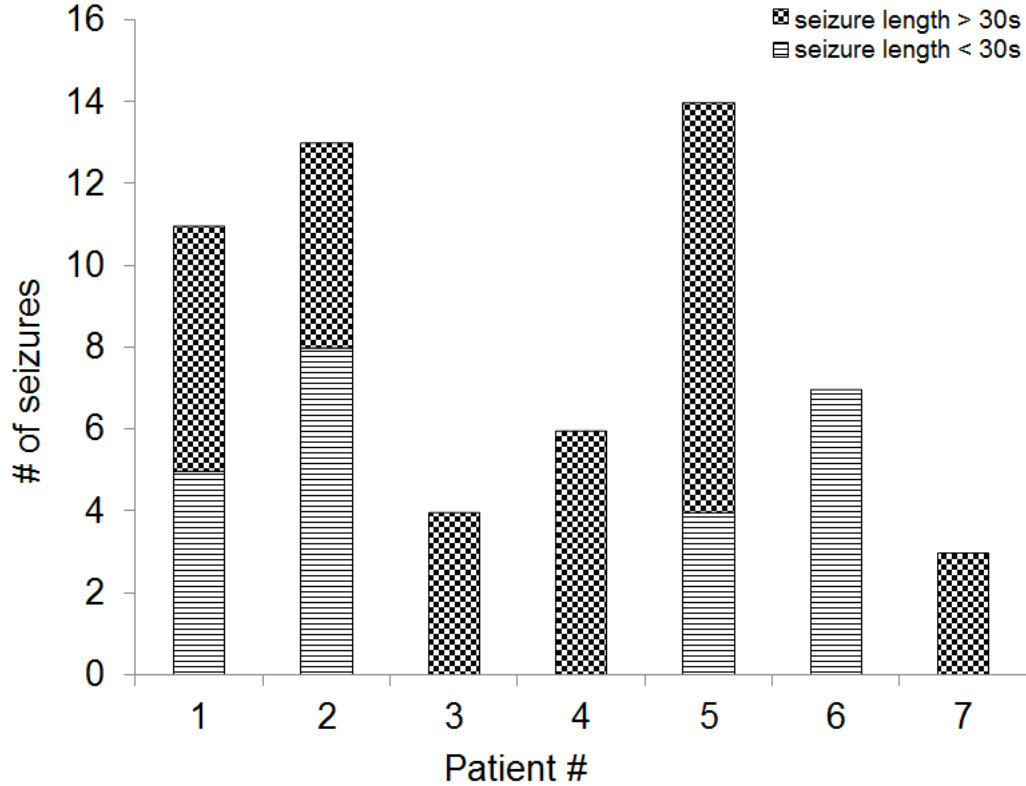


Figure 4.9: Seizure classification-based on duration.

Therefore, any spurious fluctuation in the RFWE feature is suppressed by a moving average filter. Then, the gradient of the filtered RFWE is examined for a continual increase to make a detection. An advantage of the RFWE system is that it does not require *a priori* knowledge of seizures to set the detection threshold. Training-data results demonstrate a significantly improved detection sensitivity over the NPS systems in [51], and [52] with a nearly similar detection specificity.

To better assess the limitations of the new NPS, we categorized the seizures based on their duration and according to their characteristics upon visual review of the training data. Seizure activity sustaining for more than 30 s were defined as long seizures, otherwise they were considered short seizures. The distribution of short and long seizures based on this classification is shown in Fig. 4.9. Patients 1, 2 and 5 had both long- and short- length seizures, while Patients 3, 4, and 7 had only long-length seizures and Patient 6 had only short-length seizures.

Sensitivity

The proposed RFWE system detected at least one seizure in all the patients, with an overall sensitivity of 95.4% for the MNI training dataset. However, any seizure that occurs within the first 98 s of the start of the EEG recording will not be detected by this system. This is because of the feature extraction technique employed in this method, and the definition of paroxysmal activity utilized to make a detection. Similarly, seizures occurring immediately following disconnection (IEA) artifact will not be detected by the RFWE system.

In terms of sensitivity, the proposed RFWE system performs relatively better over the three comparison NPS systems, as shown in Fig. 4.10. Grewal-Gotman system has a sensitivity similar to that of the RFWE system. A significant improvement in sensitivity is observed over the Gotman system and the Reveal algorithm.

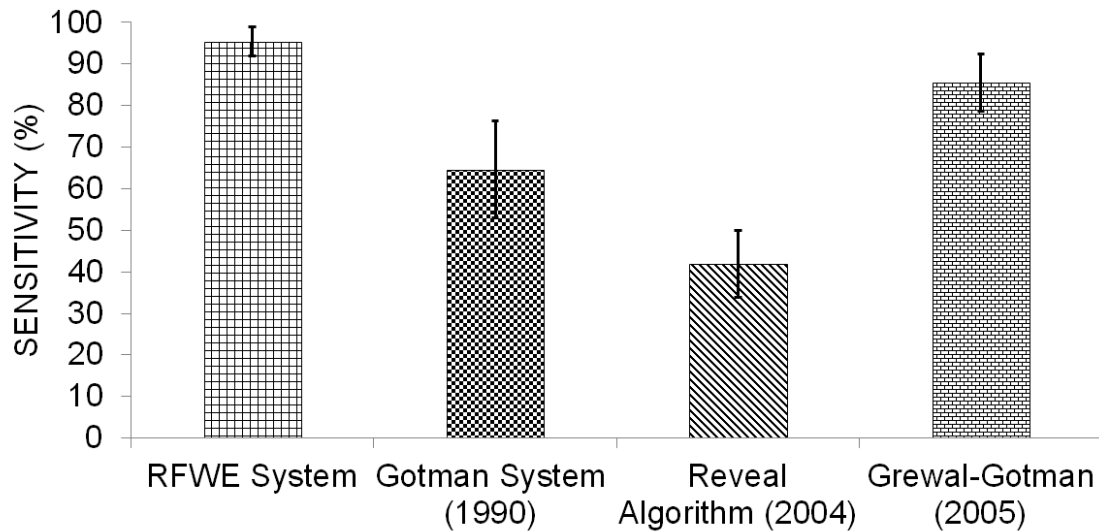


Figure 4.10: Comparison of sensitivity against comparison systems. The error bars represent standard error.

The RFWE system missed two seizures in Patient 1 and one seizure in Patient 5. An example of missed seizure in Patient 1 is shown in Fig. 4.11. The missed seizure is a short seizure that was also missed by the Gotman system, Reveal algorithm and the

Grewal-Gotman system. Majority of the NPS systems in the literature report difficulty in detecting short seizure including the three NPS systems considered for performance comparison. This may be a possible reason as to why all the three comparison NPS systems missed this seizure. It was observed in the review of this patient EEG that several minutes (> 30 min) of the background EEG before the seizure onset consisted frequent discharges of sharp transients. This could be a possible reason for missing this seizure by the RFWE system as it relies on relative characteristics.

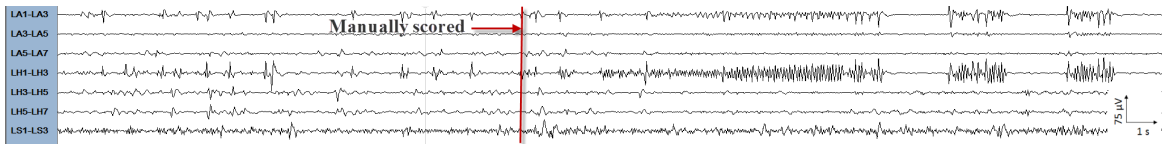


Figure 4.11: Missed 30 s long seizure in Channel LH1-LH3 in Patient 1. The seizure was missed by the RFWE system as well as all three comparison systems.

The missed seizure in Patient 5 is shown in Fig. 4.12. The missed seizure evolves with low amplitude and mixed frequency characteristics. This seizure was detected by the Reveal algorithm and Grewal-Gotman system. The likely cause for its detection by these two NPS systems could be due to prominent seizure activity in the neighboring channel. The Grewal-Gotman and Reveal algorithm rely on multiple channels to make a detection, but not the proposed RFWE and the Gotman systems.

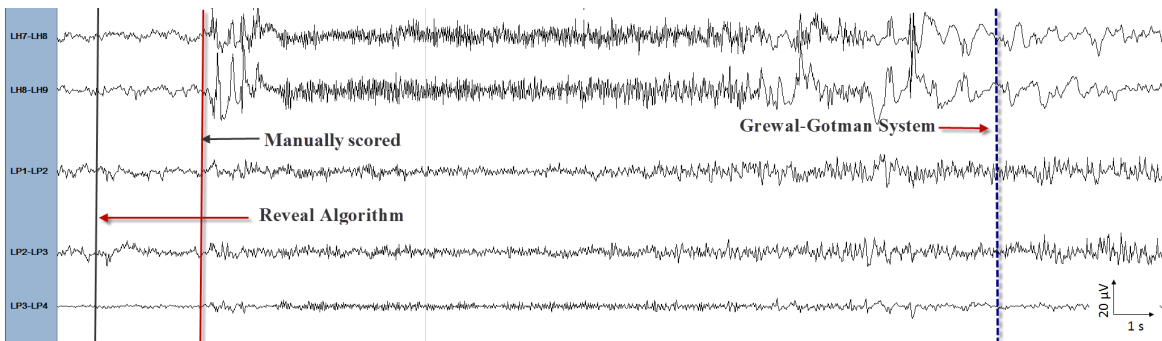


Figure 4.12: An example of low amplitude, mixed frequency seizure in Patient 5 that was missed by the RFWE and Gotman systems, but detected by the Reveal algorithm and Grewal-Gotman system.

An example of good detection in Patient 2 is shown in Fig. 4.13. The example

represents short focal seizure detected by the RFWE system and Grewal-Gotman system, but missed by the Gotman system and the Reveal algorithm.

The examples of missed and good detections show that the proposed RFWE system fails to detect short-length seizure if the background is contaminated by the presence of sharp transients. It is observed that in some patients, the frequency of occurrence of sharp transients increases several folds prior to the seizure. Onset of frequent discharges compared to sporadically occurring sharp transients in the background EEG can lead to detection of events several minutes to several seconds before the actual seizure. In other words, frequent discharge of sharp-transients over-shadows the evolution of short seizures, thereby missing the detection of such events.

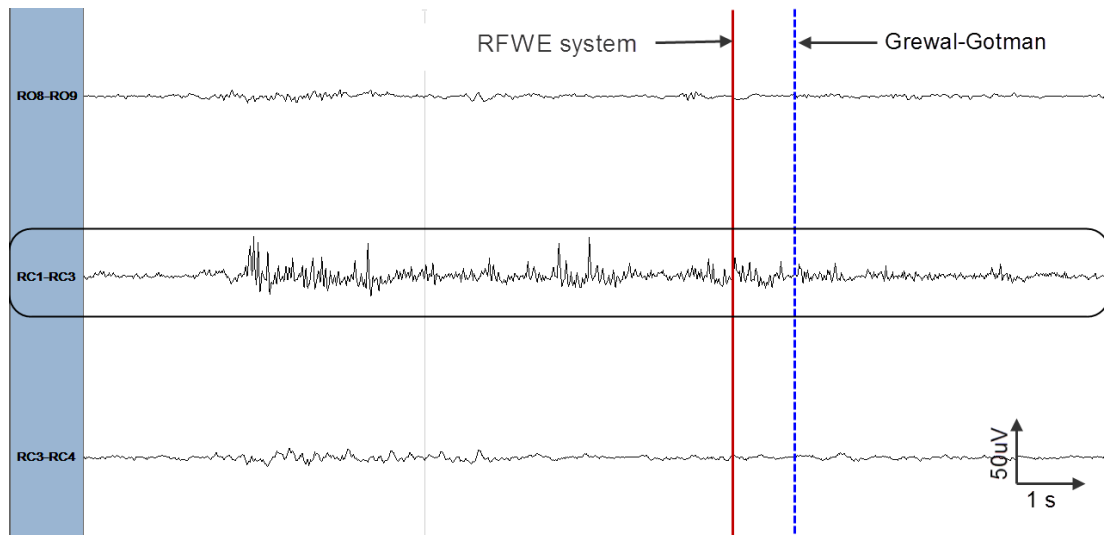


Figure 4.13: Good detection in Patient 2 (channel: RC1-RC3) of the MNI training dataset. The multichannel EEG (15 s) containing a seizure that was detected by RFWE system and Grewal-Gotman system but missed by Gotman system and Reveal algorithm. The detection time instance is shown by vertical line.

Specificity

Specificity indicates the quality of the detections made by the seizure detection method. Majority of the false detections are due to sporadically occurring sharp transients with a relatively higher amplitude or due to contamination by high-amplitude artifacts. An

example of false detection in Patient 5 is shown in Fig. 4.14. This event was detected by all NPS systems.

In Patient 2, some of the false detections were due to the presence of low amplitude fast activity. An example of such a false event is shown in Fig. 4.15. Detection of such an event is possible probably due to the fact that the RFWE feature is highly sensitive to changes in the amplitude and the frequency. On careful examination of these false events by the RFWE system, it was realized that some of these events were very similar to the seizures detected by the experts. It may indeed be possible that the experts missed such events in their manual scoring. Validating these false events may further improve the detection specificity.

In terms of specificity, with the exception of the Reveal algorithm, the other two comparison NPS systems had a specificity nearly similar to that of the proposed RFWE system, as shown in Fig. 4.16.

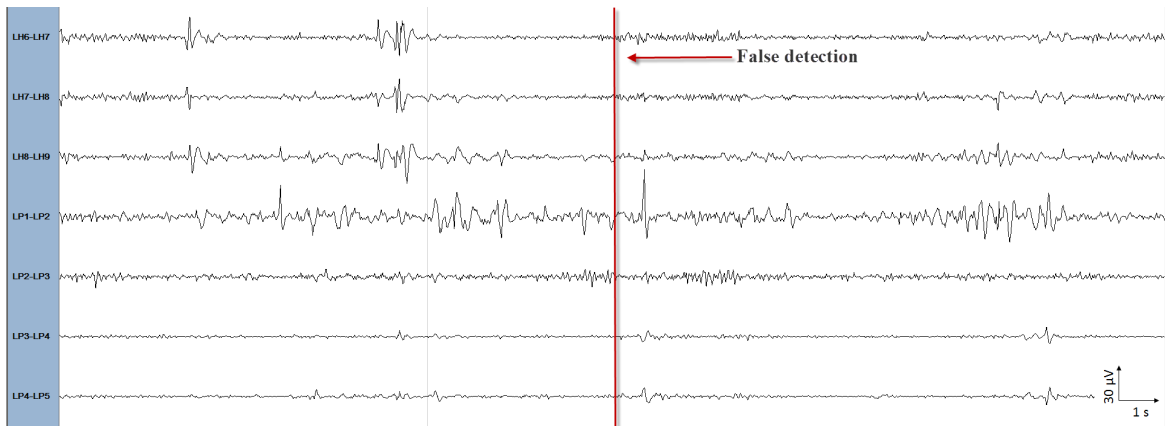


Figure 4.14: Multichannel EEG (30 s) with an example of false detection in Patient 5 (channel: LP1-LP2) of the MNI training dataset that was detected by the RFWE system and the three comparison systems. The detection time instance is shown by the vertical line.

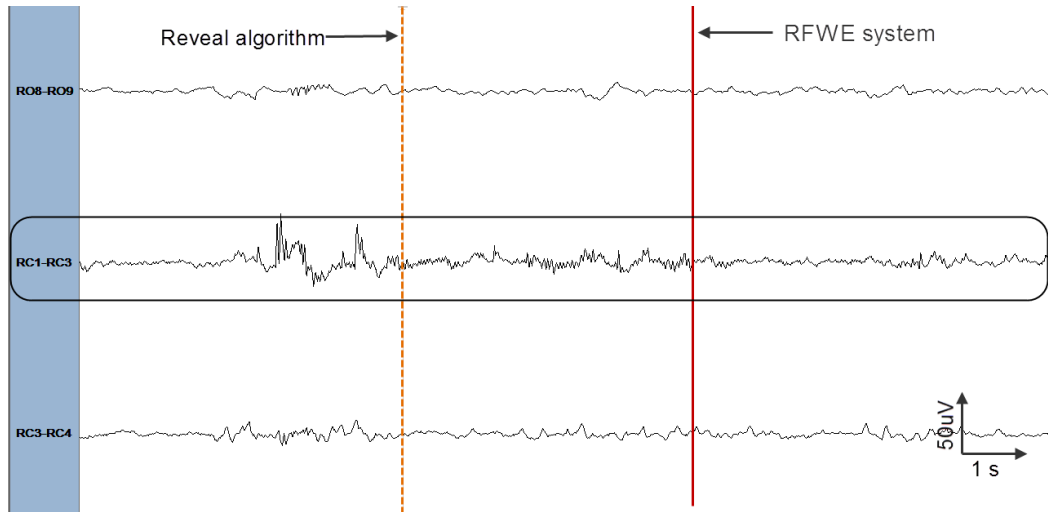


Figure 4.15: An example of false detection in Patient 2 (channel: RC1-RC3) of the MNI training dataset. The multichannel EEG (15 s) containing a seizure-like event that was detected by RFWE system and Reveal algorithm, but missed by Gotman and Grewal-Gotman systems. The detection time instance is shown by the vertical line.

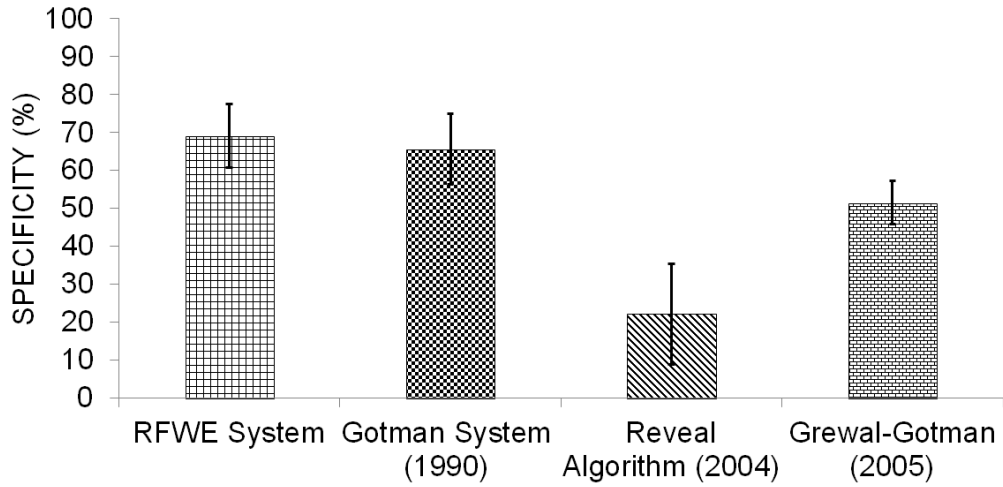


Figure 4.16: Comparison of specificity against comparison systems. The error bars represent standard error.

4.4 Morphology System

A large number of seizures contain rhythmic discharges with increasing amplitude and sustained dominant rhythm. Such epileptiform activities are easily detected by many seizure detection methods. However, these methods often fail to detect

short duration seizures or those with non-rhythmic mixed frequency characteristics [32, 51, 100, 114, 88]. As noted in the previous section, a large number of false events are detected in the presence of sharp transients and high-amplitude artifacts by the proposed RFW system as well as the three NPS systems selected for comparison. This needs to be addressed in order to improve the overall detection performance for widespread applicability of the NPS methods in the EMU.

In general, one common property of all epileptic seizures is the increase in the number of sharp-wave complexes (SWCs) as the seizure progresses. Sharp wave complexes include sharp transients, sharp waves and polymorphic epileptogenic waveforms that are distinct from the background EEG [51, 174, 175]. Figure 4.17 illustrates the evolution of epileptic seizure in the context of sharp-wave complexes (SWCs) as the seizure progresses. By quantifying this unique morphological property of the EEG, it may be possible to make more accurate seizure detections with improved system performance. In our initial investigation of various EEG properties, we discovered that sharpness of the half-waves (SHWs) can grossly characterize the EEG morphology. It was noted that the number of SHWs profoundly increase as the seizure progresses. This characteristic morphological property of the seizure is utilized to design a new NPS system that we refer to as the *morphology system* [34, 120]. We note that this is the first reported use of the sharpness feature to track temporal evolution of seizure for detection.

The Morphology system is composed of the following six blocks.

1. Pre-processing and artifact rejection
2. Half-wave (HW) decomposition
3. Estimation of sharpness of the half-waves
4. Identification of sharp epileptiform activity
5. Median filtering

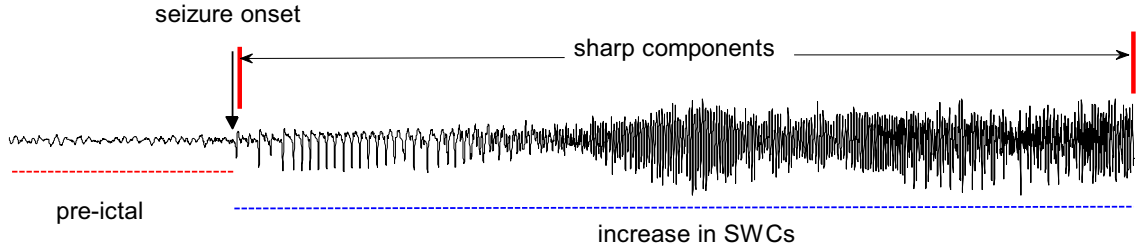


Figure 4.17: Illustration of gradually increasing number of sharp components (sharp wave complexes and spike-like activities) as the seizure evolves. The number of sharp components prior to seizure onset is non-existent compared to post-onset.

6. Detection criteria

All epileptic seizures whether rhythmic, non-rhythmic or mixed-frequency, exhibit increased sharp-wave like activity as they evolve. To quantify this increased sharp-wave activity, the raw EEG is decomposed into half-waves (HW). Prior to HW decomposition, the pre-processing block screens each epoch for high amplitude artifact contamination. The sharpness of each half-wave is estimated by the slope of the best-fit least-square estimated straight line. Median filtering is used to reduce the effect of very sharp outlier HWs, and a seizure is detected on the continual presence of SHWs. To track the persistence of SHWs, the data is processed in 0.5 s non-overlapping epochs. The continual detection of the SHWs represents an ongoing epileptic activity. The flow chart of the proposed method is shown in Fig. 4.18. The details of each of the six blocks of the *morphology system* are described below.

4.4.1 Pre-processing and Artifact Rejection

The pre-processing block screens each epoch for contamination by HA artifacts as in the case of the proposed RFWE system. Epochs contaminated by HA artifacts are excluded from the analysis. The preprocessed data is utilized to compute the morphological feature as described below.

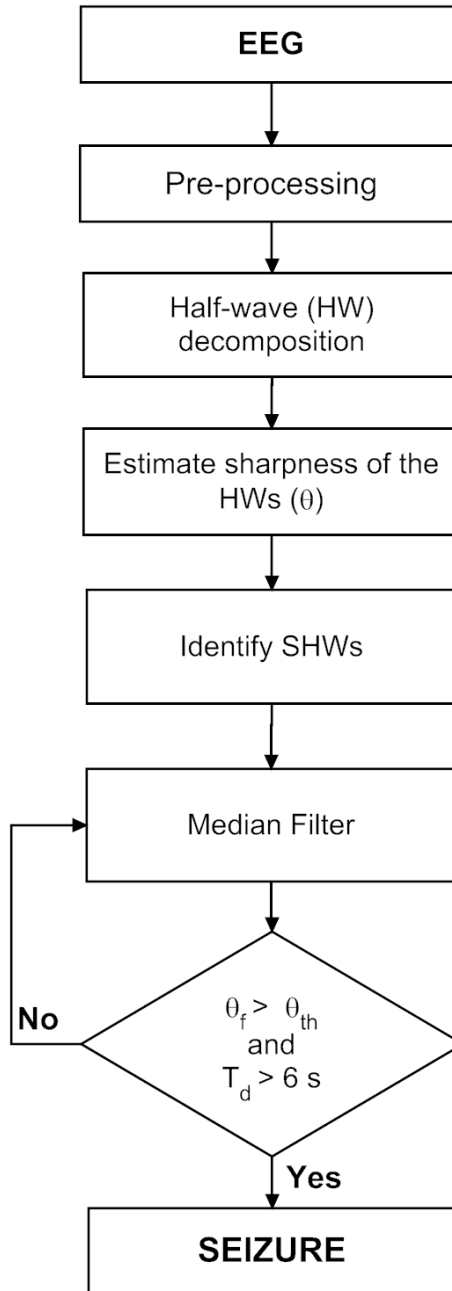


Figure 4.18: Flow chart of the morphology system.

4.4.2 Feature Extraction

Seizures occurring at the start of data recording are missed due to the unavailability of the background EEG in the two sliding-window feature extraction scheme as observed in the proposed RFWE system. Therefore, in this proposed system, the feature is computed using a single window technique, i.e., no background EEG is utilized. A small test epoch (0.5 s) is employed to capture subtle changes in the EEG to detect seizure as close as possible to the onset.

Half-wave Decomposition

Majority of the false detections in the RFWE system and the three comparison NPS systems were due to the discharge of sharp transients. These systems failed to make a clear distinction between the seizure and sharp transients. As described earlier in this section, one of the key properties of seizure is the persistent increase in the sharp wave complexes (SWC) as the seizure evolves. By devising a method to quantify this property, it is possible to improve the detection specificity. To do so, the EEG is first decomposed into a series of half-waves, where a half-wave (HW) is defined as the segment of EEG waveform located between two adjacent extrema (i.e., a minimum and a maximum, or vice versa), as shown in Fig. 4.19. The extremas are detected by the change in the sign of slope, which we measure as the difference between two adjacent samples [22, 176]. To reduce the effect of small fluctuations due to noise and artifacts, HWs less than 15 ms (3 samples) in duration are ignored.

Sharpness of a Half-wave

Each half-wave is characterized by its sharpness feature, *sharpness* being defined as the slope (m) of the best-fit straight line of each half-wave. Since the slope is a function of both amplitude and duration (frequency) of the HW, the sharpness feature is highly sensitive to both of these. Some approaches in the literature have utilized the HW

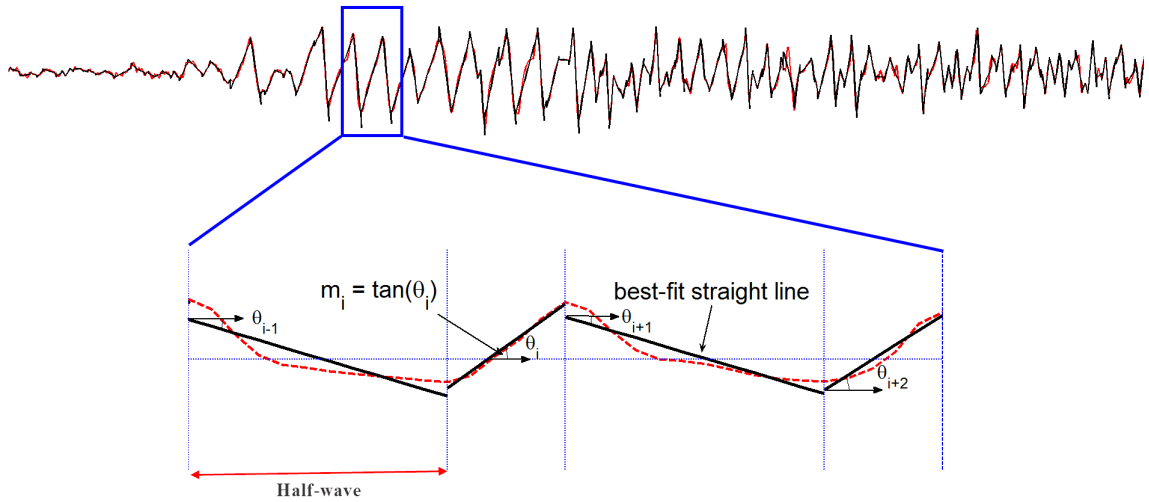


Figure 4.19: A section of EEG is zoomed in to illustrate half-wave decomposition and estimation of sharpness of the half-wave. The slope of the best-fit line between the local extrema (thick-black line) is the sharpness feature.

peak-to-peak amplitude and their duration as features for detection of epileptiform EEG [22, 97, 110, 176]. In the same spirit, we quantify the amplitude and frequency changes in the EEG by a single feature, the sharpness of the half-wave (SHW), defined as the absolute value of m . It may be noted that this has not been previously reported for the detection of epileptic seizures. The evolution of EEG sharpness as a function of time is illustrated by the example in Fig. 4.20. Clearly, the SHW is profoundly greater and increases during the seizure compared to that during the non-seizure activity. We utilize this observation in the proposed morphology system to differentiate between normal and epileptic activity.

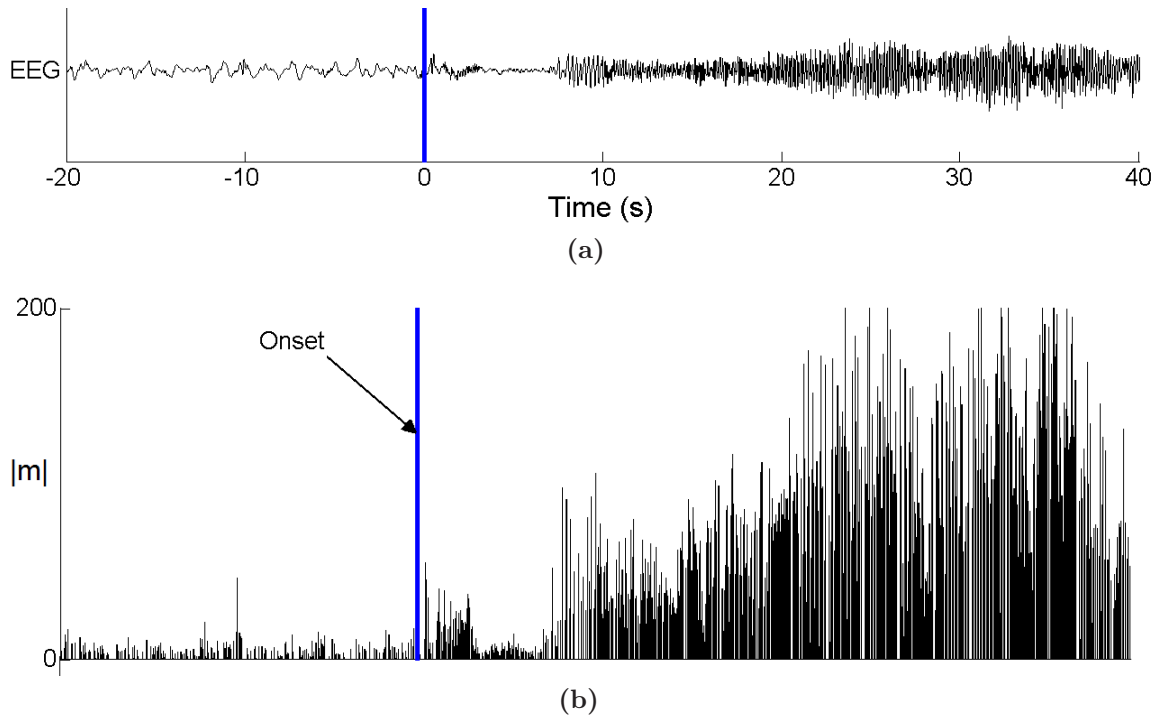


Figure 4.20: Evolution of SHW as the seizure progresses. (A) Seizure with background. (B) SHW corresponding to the EEG in (A).

4.4.3 Classification

Identification of Sharp Epileptiform Activities

As noted in the example shown in Fig. 4.20, it is possible to discriminate between the seizure and the normal EEG by applying a threshold that highlights abnormally sharp activities linked with the seizure. This can be achieved by applying a scaled-heaviside step function (activation function) [177] that limits the SHWs to a minimum sharpness, and is given by

$$g(n) = \begin{cases} m & \text{for } m \geq m_{th} \\ 0 & \text{otherwise} \end{cases}, \quad (4.8)$$

where m_{th} is the threshold to identify candidate HWs that may correspond to the seizures. Receiver operator characteristic (ROC) analysis on the training data is

utilized to determine the default value of m_{th} that provides a suitable separation between seizure and non-seizure EEG. Using the MNI training data, the sensitivity and the FDR are computed for each m_{th} in the range of 5 – 50. We use the knee of the ROC curve to select m_{th} and is shown in Fig. 4.21.

Median Filter

The output of the activation filter is shown in Fig. 4.22C, which indicates that not all sporadically occurring SWCs in the EEG (see Fig. 4.22C prior to seizure onset) are removed. Such occasionally occurring SWCs may lead to an increase in the detection of false events. Therefore, such sporadic SWCs must be removed prior to classification. The impact of spurious SWCs can be suppressed or smoothed by a moving average or a median filter. A median filter is preferred to eliminate the effect of a few SWCs over the moving average filter, since it is insensitive to outliers and the extreme values [100, 129, 178, 179].

The median filter is defined as follows: To compute the output of a median filter, an odd number of sample values are ranked (sorted numerically) and the middle value is used as the filter output. For a filter of window length ($L = 2k + 1$), the filtering procedure for the input SHW sequence is given by

$$G(n) = \text{med}[g(n - k), \dots, g(n), \dots, g(n + k)] \quad (4.9)$$

where $g(n)$, and $G(n)$ are the input values and the output of the window centered at the n th value, respectively. In Eq. (4.9), 'med' denotes the median value. Equation (4.9) represents a non-recursive median filter [178, 180]. Computational cost can be reduced by employing a recursive median filter that replaces the center point $g(n)$ of the window by the median value of all the points inside it, and uses these values to calculate the median in the subsequent window positions. The output of recursive median filter is given by

$$G(n) = \text{med}[G(n - k), \dots, G(n), g(n), \dots, g(n + k)], \quad (4.10)$$

which replaces at every step, the leftmost k -points in the moving window with the previously k output points [181, 180]. The filter length (L) is empirically determined considering the low-frequency seizure activity. We hypothesize that each 0.5-second epoch will have at least one abnormally sharp activity, therefore, a total of 12 in the six seconds, we round this number to 15 for robustness due to potential influence by noise.

An added advantage of this layer is that it preserves continual increase of the SHWs as the seizure evolves. Figure 4.22 illustrates the process of quantifying SWCs using half-waves. In this example, a 10 s section of epileptic seizure is shown in Fig. 4.22A, and best-fit straight lines for each HW are shown in Fig.4.22B. The sharpness measure (m) of the HWs that satisfy the requirement for SHWs are shown by the bar plot in Fig. 4.22C. $G(n)$ clearly reveals absence of SHWs prior to seizure onset while during the post onset there is sudden increase in the number of SHWs (Fig. 4.22D).

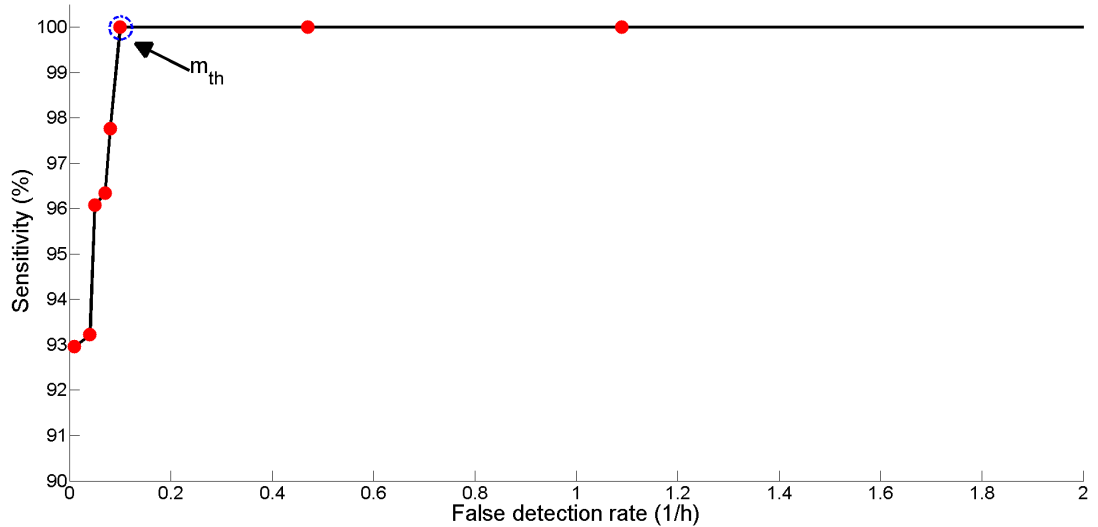


Figure 4.21: Threshold estimation using the receiver operating characteristics (ROC) analysis. The threshold m_{th} is varied from 5 to 50 and for each m_{th} , the average sensitivity and false detection rate is computed to generate the ROC curve. The default threshold ($m_{th} = 25$) which we use for morphology system is shown encircled.

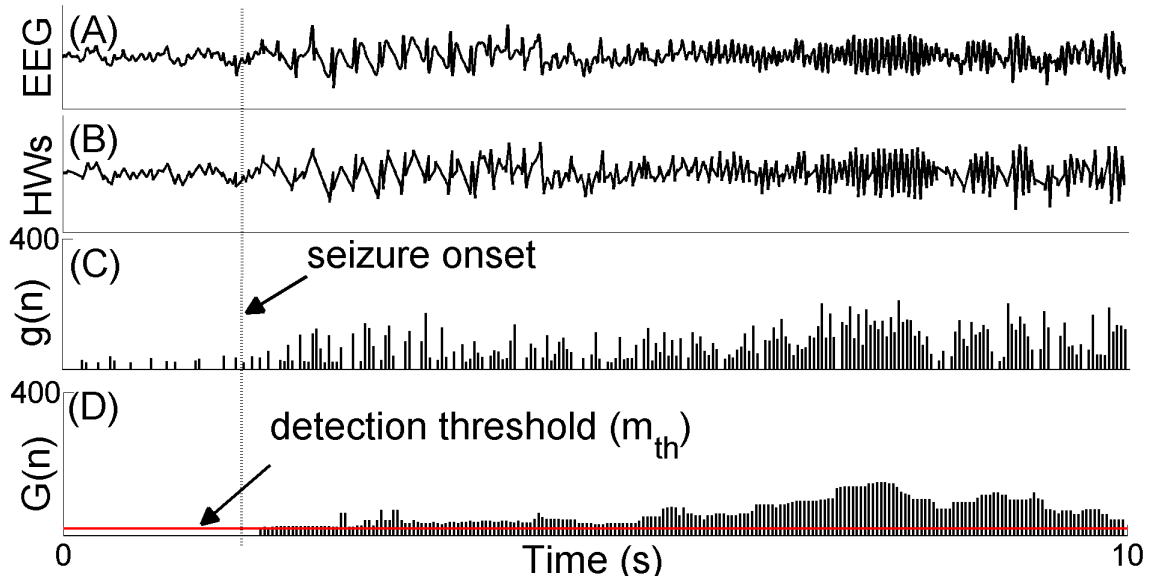


Figure 4.22: Epileptic seizure recognized by the morphology system. (A) Detected seizure event. (B) Raw EEG in A is decomposed into half-waves as modeled by the best-fit straight line. (C) represents bar graph of the absolute slope ($|m|$) for each half-wave after processing by the activation function, and (D) is median filtered $g(n)$. The horizontal line represents the detection threshold.

Detection Criteria

An electrographic seizure is detected on a sustained discharge of SWCs for at least 6 s, i.e., $G(n)$ exceeding m_{th} as illustrated in Fig. 4.22D. The number of SWCs in an epoch depends on the morphology and rhythm of the sharp wave complex. A 0.5 second epoch may contain a single or burst of SWCs. In order to make a seizure detection, at least 12 consecutive 0.5 second epochs must contain at least one SWC greater than m_{th} in the time series $G(n)$. Such a stringent detection criterion may not be fulfilled in cases where there are short pauses in the seizures. Therefore, we relax the detection criterion to a minimum 10 epochs within 12 consecutive epochs (6 s).

4.4.4 Performance Evaluation

Like the RFWE system of the previous section, the proposed morphology system is also assessed in the single channel configuration, and is compared against the RFWE

system and the three NPS systems considered earlier. The performance is evaluated with the same rules as was done for the RFWE system. All detections within 30 s are grouped prior to performance evaluation.

4.4.5 Results

The automatic detection results of the proposed morphology system for each patient are shown in Table 4.3. The morphology system resulted in 100% sensitivity, specificity of 84.5% and a FDR of 0.2/h. The results of the RFWE and the three comparison NPS systems on the training dataset are given in Table 4.4. It is seen from this table that the proposed morphology system shows an improvement of 4.6%, 35.4%, 58.1% and 14.5% in terms of sensitivity and an improvement of 15.3%, 18.8%, 62.3%, and 33% in terms of specificity over the RFWE system, Gotman system, Reveal algorithm and Grewal-Gotman system, respectively.

Table 4.3: Single channel evaluation of the MNI training dataset

PID	Channel	No. of Files	Hours	TE	TP	FP	FN	SN (%)	SP (%)	SP* (%)	FDR (/h)	FDR* (/h)
1	LH1-LH3	5	20	11	11	2	0	100	84.6	84.6	0.1	0.1
2	RC1-RC3	5	20	13	13	22	0	100	37.1	81.3	1.1	0.2
3	LH1-LH3	5	21	4	4	0	0	100	100	100	0	0
4	LA3-LA5	5	20	6	6	0	0	100	100	100	0	0
5	LP1-LP2	5	20	14	14	6	0	100	70	70	0.3	0.3
6	LS4-LS5	6	24	7	7	0	0	100	100	100	0	0
7	LFC3-LCF5	5	20	3	3	0	0	100	100	100	0	0
TOTAL		36	145	58	58	30	0	100	84.5	90.8	0.21	0.08

PID = Patient ID, TE = total expert, TP = true positive, FP = false positive, FN = false negative, SN = sensitivity, SP = specificity, SP* = specificity after re-classification of FDs in Patient 2, FDR = false detection rate, and FDR*= FDR after re-classification.

4.4.6 Discussion

Majority of the existing NPS systems in the literature fail to detect seizures that are of short duration (sub-clinical electrographic seizures without significant change in the EEG amplitude) or seizures that do not show a sustained rhythmic component. False

Table 4.4: Comparison results of the MNI training dataset

PID	Morphology System		RFWE System		Gotman System (1990)		Reveal Algorithm (2004)		Grewal-Gotman (2005)	
	SN (%)	SP (%)	SN (%)	SP (%)	SN (%)	SP (%)	SN (%)	SP (%)	SN (%)	SP (%)
1	100	84.6	75	100	100	91.7	18.2	100	72.7	80
2	100	81.3	100	61.9	61.5	47.1	23.1	3.1	61.5	57.1
3	100	100	100	100	50	100	50	7.4	100	57.1
4	100	100	100	50	83.3	62.5	33.3	8.7	100	37.5
5	100	70	92.9	68.4	28.6	33.3	78.6	25	64.3	37.5
6	100	100	100	53.8	28.6	50	57.1	3.8	100	41.2
7	100	100	100	50	100	75	33.3	7.7	100	50
TOTAL	100	90.8	95.4	69.2	64.6	65.7	41.9	22.2	85.5	51.5

PID= patient ID, SN = sensitivity, SP = specificity.

detection in the presence of artifacts and sharp transients significantly increases, and often some true events are missed. Such a limitation was also noted in the RFWE system considered in the previous section. The overall goal was to overcome these challenges in the seizure detection by designing a computationally simple system that detects a wide-variety of seizure patterns with high sensitivity and high specificity (low false detection rate).

Sensitivity

The proposed morphology system detected all seizures in the MNI training dataset. Approximately, 5% improvement in terms of sensitivity over the RFWE system is obtained. Comparison of the sensitivity with the three NPS systems is shown in Fig. 4.23. The proposed morphology system performs better in terms of sensitivity over the other NPS systems considered.

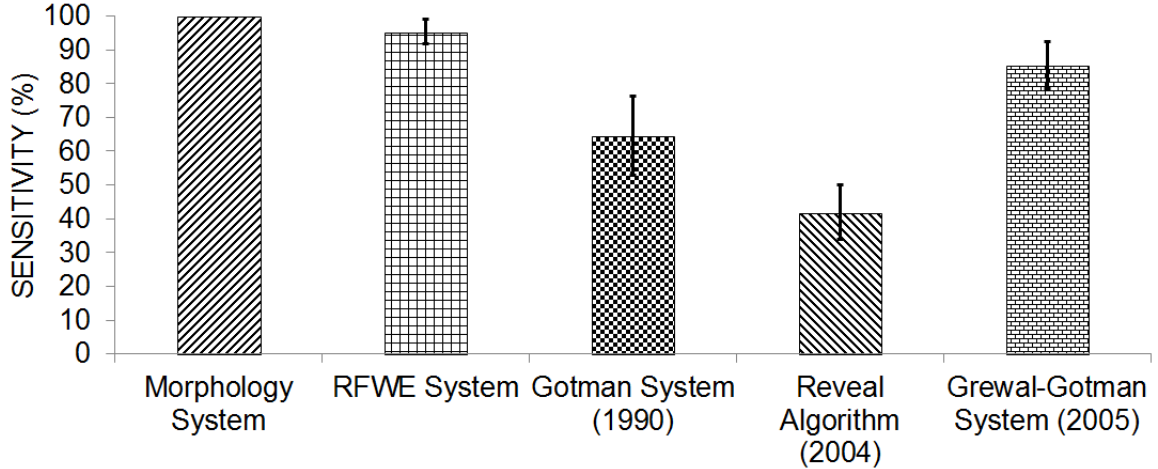


Figure 4.23: Comparison of sensitivity of the proposed morphology system against other systems. Error bars represent the standard error.

An example of good detection by the proposed morphology system that was missed by the other NPS systems is shown in Fig. 4.24. The missed seizure manifests in the EEG with low amplitude and mixed frequency. As noted in the previous section, such mixed frequency seizures are difficult to detect by the three NPS systems considered

for performance comparison. The seizures missed by the RFWE system were detected by the proposed morphology system, demonstrating the robustness of this system in the presence of artifacts and sharp transients.

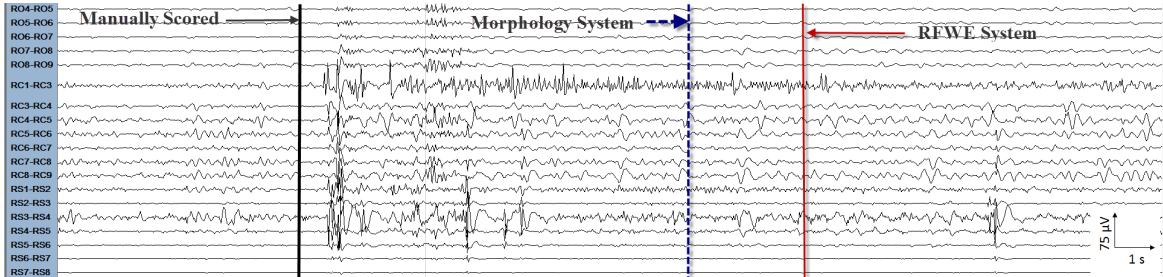


Figure 4.24: An example of good detection in Patient 2 of the MNI training dataset. Multichannel EEG (20 s) containing a seizure that was detected by both the new NPS systems but missed by all three comparison systems. The channel of interest is RC1-RC3 and detection time instance is shown by vertical line.

An example of good detection for all the comparison systems is shown in Fig. 4.25. The detection time instances for the various systems are shown by vertical lines.

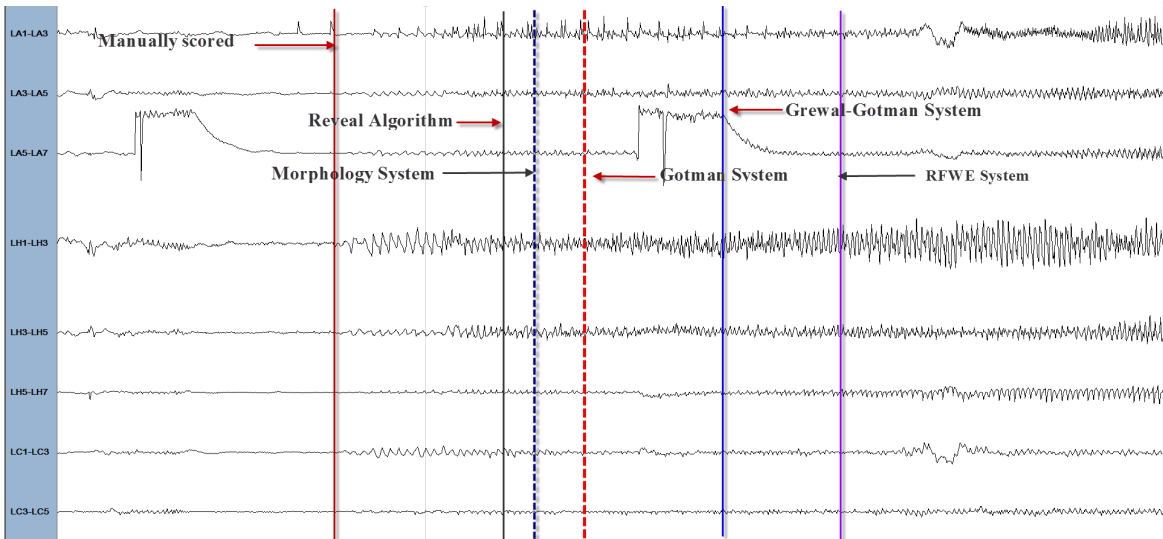


Figure 4.25: An example of good detection in Patient 3 of the MNI training dataset. Multichannel EEG (30 s) containing a seizure that was detected by all NPS systems. The channel of interest is LH1-LH3 and detection time instance is shown by the vertical line.

Specificity

Visual inspection of the events detected by the proposed morphology system revealed that majority of the false detections in Patients 1, 2, and 5 were mainly due to short duration high amplitude bursts or mixed frequency activity. Patient 2 had a significantly higher FDR. Example of events detected by the morphology system in Patient 2 (channel: RC1-RC3) are shown in Fig.4.26. Figure 4.26A is an event marked by the expert that was detected by the morphology system, while Fig.4.26B and C are events detected by the morphology System, but not by the expert. In this example, the false events detected have characteristics resembling the manually scored event in Fig.4.26A. We manually re-classified all false events detected by the proposed morphology system that matched the EEGer marked events for this patient, and considered all false events $> 6s$ to be events missed by the expert. Nearly, 80% of the false events fell into this category, which demonstrates that the morphology system may highlight electrographic seizures that are missed by the experts. The remaining 20% of the false events also had characteristics similar to the manually marked event, but did not fit our seizure definition in terms of the minimum seizure length. An example of such a false event is shown in Fig. 4.26C. We re-evaluated the performance for this patient by validating false events ($\geq 6 s$) similar to events detected by the expert as true events. By doing so, the overall specificity (SP^*) improved by 6% (Table 4.3).

Overall, the proposed morphology system shows an improvement in the detection specificity over the three NPS systems including the proposed RFWF system as shown in Fig. 4.27.

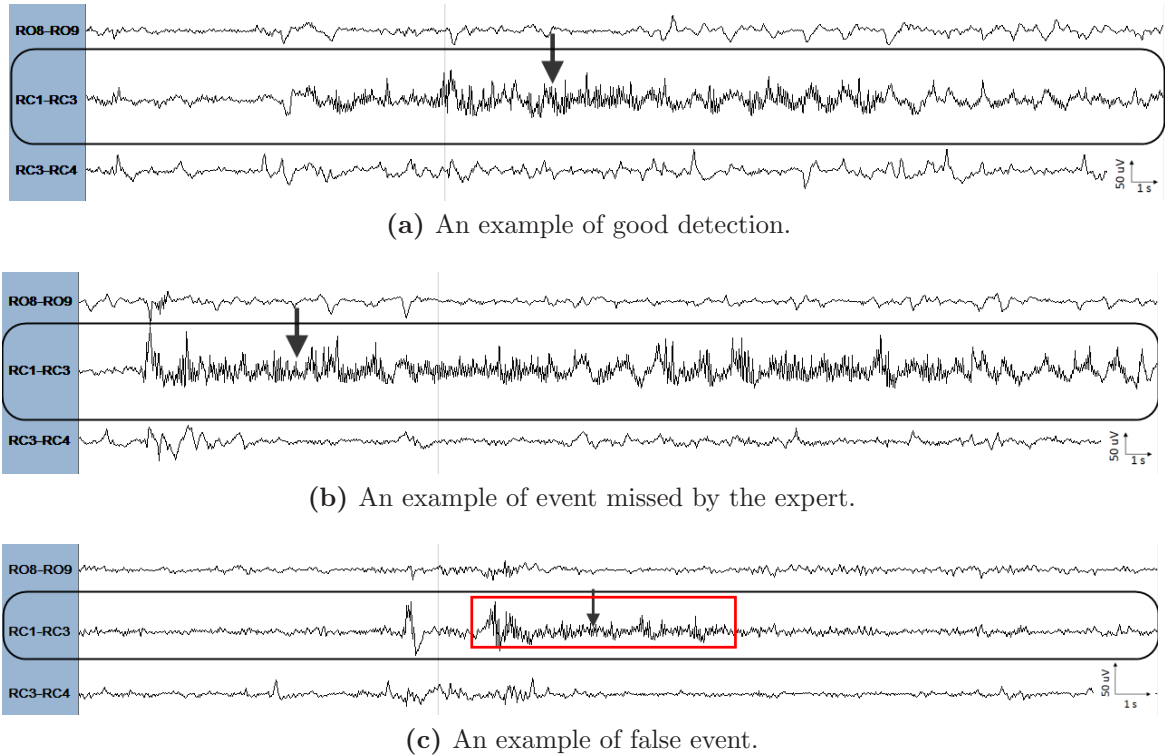


Figure 4.26: Detections by the morphology system in Patient 2 (channel: RC1-RC3). All examples are 30 s in duration and the detection time intervals are shown by downward pointing arrows. The 'red' rectangle in (C) denotes six seconds of electrographic event that we considered as false event.

4.5 Evolution Seizure Detection System

The proposed morphology system addressed some of the limitations in the RFWE system, but its performance is dependent on the pre-determined threshold. It is also noted that the presence of high-amplitude activity and fast electromyographic (EMG) activity can degrade the detection specificity of the morphology system. In this system, the EEG is not filtered to reject high-frequency interferences (> 30 Hz) as was done in the RFWE system to preserve the EEG waveform morphology. However, a new NPS seizure detection system can be designed taking into account the respective advantages of the two previously proposed NPS systems, the RFWE and the morphology systems, to improve the overall detection performance, *i.e.*, to reduce false detections without affecting the detection sensitivity. We propose a new NPS system that quantifies the

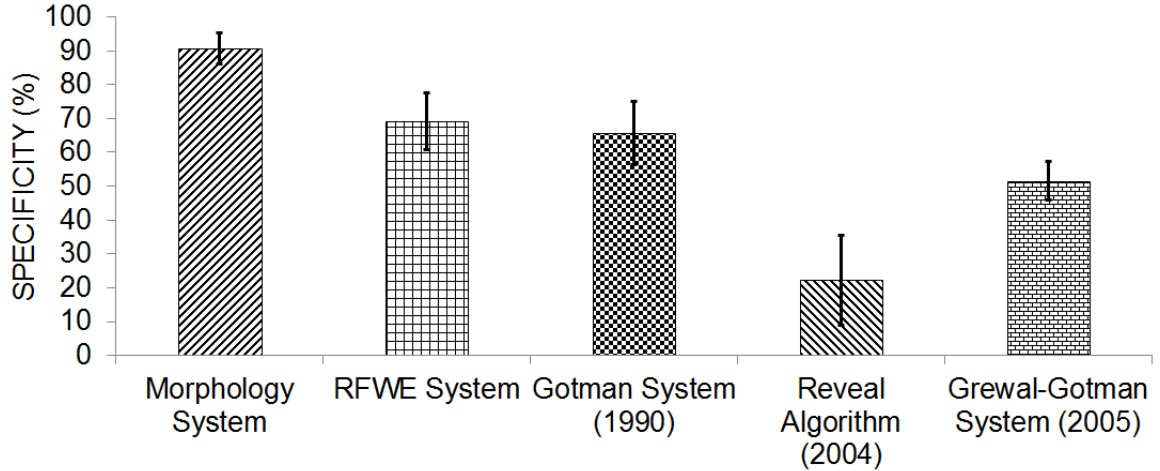


Figure 4.27: Comparison of specificity of the morphology system with the other systems on the MNI training dataset. Error bars represent standard error.

evolving changes in the EEG characteristics as the seizure progresses, and will be called the evolution seizure detection (eSD) system [33, 136].

The seizure identification in the proposed eSD system is done in two steps. The concept utilized in the eSD system is to first identify candidate seizure (CSZ) events based on the evolving changes in the amplitude, frequency and the rhythmicity, and then verify the CSZ event sharpness characteristics to make the final detection. The proposed eSD system scheme gains its strength from (a) a novel computationally simple scheme, which continuously examines the evolving characteristics of the EEG features to set unique detection threshold to identify the candidate seizure event, and (b) then use a computationally simple approach to validate and classify the candidate seizure event. The proposed eSD system is composed of the following four blocks.

1. Pre-processing and artifact rejection
2. Feature extraction
3. Identification of candidate seizure event
4. Validation of candidate seizure event

The flowchart of the eSD system is shown in Fig. 4.28, and each of the four blocks is described below.

4.5.1 Pre-processing and Artifact Rejection

The pre-processing and artifact rejection techniques employed in the RFWE system (described in Section 4.3.1) are also utilized in the proposed eSD system.

4.5.2 Feature Extraction

The two popular approaches of feature extraction in the literature are (a) single sliding window and (b) two sliding windows as discussed in Section 4.3. In the proposed eSD system, we employ both of these techniques, since some of the features are computed relative to a dynamically changing background, while some others do not require the reference window for their computation. For computing features relative to a background, the length of the test epoch must be sufficiently large to compute reliable estimates of the features, and must have a small step-size to capture subtle changes in the EEG. Subtle changes in an ongoing epileptic seizure are captured with a sliding test epoch (\mathbf{x}_{test}) of 2 s that moves in steps of 0.25 s. The test epoch (\mathbf{x}_{test}) is separated from the background window (\mathbf{x}_{bkg}) by a 60 s gap. The length of the background window duration is 30 s. The test window that slides in small steps allows smooth tracking of the seizure evolution as well as reduces the risk of missing seizures.

Features computed using the single sliding window must be time synchronized with the two sliding windows feature extraction technique, and at the same time must provide reliable estimates of the EEG parameters. Therefore, the length of the test epoch (= 2 s) is kept the same for both the feature extraction techniques.

In the proposed eSD system, four non-redundant features are utilized to quantify changes in the seizure EEG compared to the two single feature methods of Sections 4.3 and 4.4. The four features are relative amplitude (RA) that captures changes

in the EEG amplitude, RFWE that quantifies the spectral content of the seizure, coefficient of variation of the amplitude (CVA) that quantifies the EEG rhythmicity, and sharp-wave complex density (SWCD). The features RA and RFWE are calculated relative to a dynamically changing background, while the features CVA and SWCD are computed from the single sliding window.

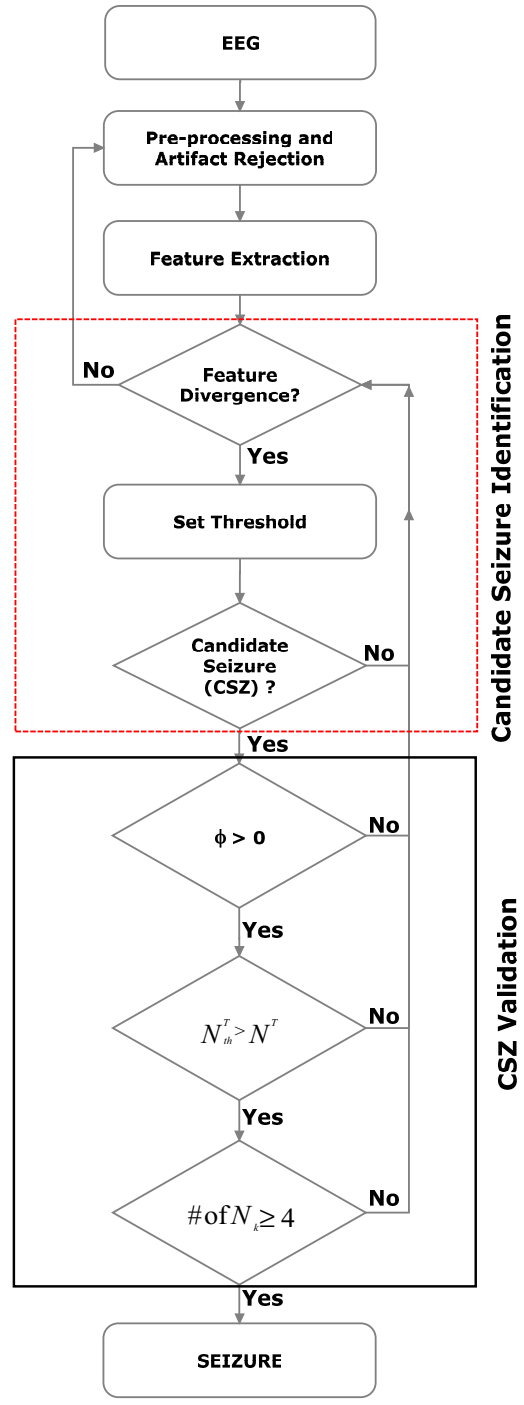


Figure 4.28: Flowchart of the eSD system.

Sharp-Wave Complex Density

One of the key properties of seizure evolution is the continual increase in the number of sharp components, as previously discussed in Section 4.3 [34]. Patterns due to artifacts can be isolated by examining this characteristic property of seizure evolution. We compute the SWC density feature to establish the increase in the number of sharp components as the seizure evolves. This is achieved by decomposing the EEG into half-waves and quantifying the sharpness of the half-waves by the slope of the best-fit line, as was done in the morphology system in Section 4.4. As was done in that system, the sharpness of the half-waves is restricted to highlight the potential epileptiform sharp activity. The SWC density (SWCD) is then defined as the number of SHWs in the test epoch. Computational load can be significantly reduced by computing the density of SWCs in a non-overlapping test window instead of a sliding window that moves in small steps. Therefore, the density of SWCs is computed from a two-second non-overlapping test window. This feature is computed along with the other three features, but used only to validate a candidate seizure event (CSZ). The validation of CSZ involves establishing evolving changes in terms of sharp-components to differentiate between seizure and artifact.

Coefficient of Variation of the Amplitude

The coefficient of variation of the amplitude (CVA) quantifies in a simple way the increased regularity in the amplitude during a seizure. It is defined as the ratio of variance of the absolute amplitude to the square of the mean absolute amplitude.

$$\text{CVA} = \frac{\sigma_{|x_{test}|}^2}{\mu_{|x_{test}|}^2}, \quad (4.11)$$

where $\sigma_{|x_{test}|}^2$ is the variance and $\mu_{|x_{test}|}$ is the mean of the absolute of the x_{test} . The CVA is computed from the 2 s test epoch that slides in small steps. Signals exhibiting

strong rhythmic characteristics are likely to have regularity both in the frequency and the amplitude as typically observed in the seizures [32]. An example of CVA feature before and after a seizure onset is shown in Fig. 4.29. The CVA decreases with the increased rhythmic EEG activity and vice versa. It is seen in Fig.4.29 that CVA decreases and remains below some arbitrary baseline value during the seizure.

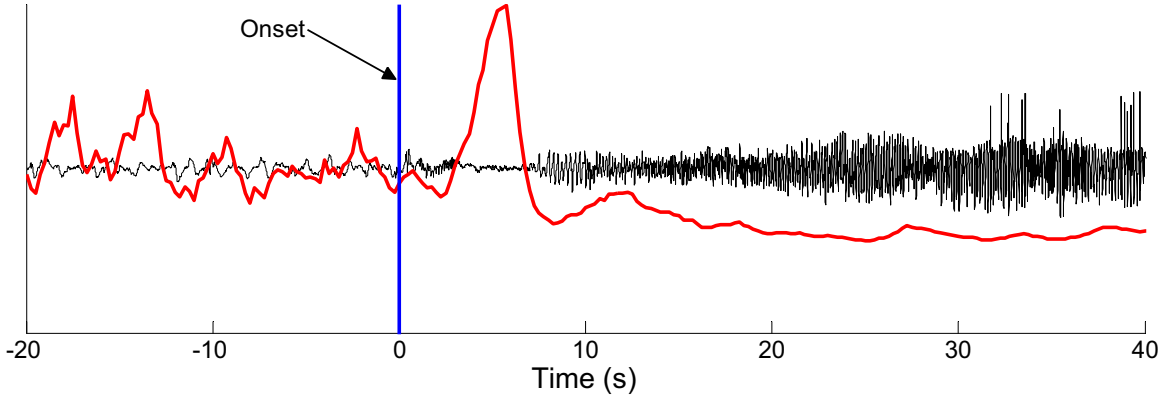


Figure 4.29: Time evolution of coefficient of variation of amplitude superimposed on the EEG.

Relative Amplitude

The widely accepted definition of epileptic seizure states that during an epileptic seizure, a new type of EEG rhythm appears, hesitantly, and then more distinctly, and soon it boldly dominates the EEG tracing. It tends to become slower with increasing amplitude and the more distinct spiky phases of the rhythmical waves appear [5]. Our observation is consistent with this definition with respect to the increase in the amplitude relative to the background during a seizure evolution, and is therefore, considered as one of the hallmark features suitable for the identification of seizures. The relative amplitude (RA) is computed using the two sliding window technique. It is defined as the ratio of the mean absolute amplitude in the test window (\mathbf{x}_{test}) and the background window (\mathbf{x}_{bkg}) and is given by

$$RA = \frac{E(|x_{test}|)}{E(|x_{bkg}|)}, \quad (4.12)$$

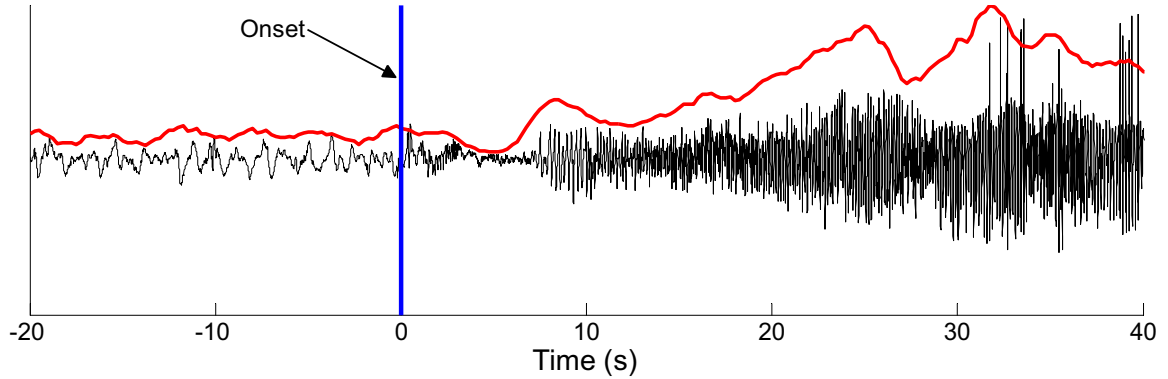


Figure 4.30: Time evolution of relative amplitude superimposed on the EEG.

where \mathbf{E} is the expectation operator.

This feature allows the quantification of the amplitude changes observed during seizure evolution as shown in Fig. 4.30. The example illustrates changes in the EEG amplitude before and after the seizure onset.

Relative Frequency-Weighted-Energy

The RFWE feature is described in Section 4.3 towards the development of the RFWE system. This feature is incorporated in the proposed eSD system to quantify the spectral changes in the EEG.

4.5.3 Identification of Candidate Seizure Event

Our initial assessment of the features revealed that RA and RFWE tend to increase at the seizure onset while CVA decreases. The features RA/RFWE and CVA change in opposite directions at the seizure onset; this guided us in developing a technique that can adapt the detection threshold for each ongoing seizure activity. We define this characteristic property at the seizure onset as the divergence in the features. Figure 4.31 illustrates the concept of divergence observed in the features at the seizure onset. It can be seen that at the seizure onset, a continual increase in the RA and RFWE is observed, while a continual decrease in the CVA is observed. In randomly

selected non-seizure epochs from the training dataset, we observed no such divergence or sustained increase or decrease in the feature values during non-seizure activity.

A candidate seizure event can be identified by looking for sections in the EEG with a continual increase/decrease in the above features for a minimum duration. At such instances, the detection threshold for each feature can be set. We define this process of identifying and setting the detection threshold as the learning phase of the proposed eSD system as illustrated in Fig. 4.31. In the learning mode, the instantaneous feature values of the RA, RFWE and CVA are continuously examined. The system continuously monitors for instances, where RA and RFWE increase, while CVA decreases. This is achieved by comparing the current feature value with the previous one, to detect the onset of the divergence (κ). That is, we evaluate the following:

$$\kappa = ((F_A \vee F_B) > 0) \wedge (F_C < 0), \quad (4.13)$$

where,

$$F_A = RA_p - RA_{p-1}. \quad (4.14)$$

$$F_B = RFWE_p - RFWE_{p-1}. \quad (4.15)$$

$$F_C = CVA_p - CVA_{p-1}. \quad (4.16)$$

and p represents the test epoch number. The operators utilized in the determination of κ are mathematical (logical) operators, i.e., ‘OR’ (\vee) and ‘AND’ (\wedge). At the onset of the divergence, the detection thresholds (δ_{RA}^p , δ_{RFWE}^p , and δ_{CVA}^p) are set as the current epoch (p th epoch) feature values.

In the detection mode, the feature values in the subsequent epochs must satisfy the detection thresholds for at least 6 s to identify a CSZ. Due to the presence of artifacts or non-stationary nature of the seizure evolution, it is possible that there may be some spurious fluctuations or pauses during the detection phase, where the detection criteria may not be satisfied for a continuous 6 s period. In such conditions, the detection criteria must be satisfied for at least a minimum of 6 s within eight seconds.

The eSD system switches between the learning and detection modes to identify a CSZ. At any given time point, only one of the two modes is active. That is, the learning mode is active when the system examines the EEG features for divergence, and, on the occurrence of divergence in the features, the system switches to the detection mode. The system returns to the learning mode after the CSZ is validated or when the conditions to identify a CSZ are not fulfilled.

4.5.4 Validation of Candidate Seizure Event

The proposed eSD system validates a CSZ by establishing a continual increase in the sharp components via the SWC density. One simple approach to quantify the progressive or continual increase in the SWCs is by examining the slope of a regression line fitted to the SWC density of the CSZ. Figure 4.32 illustrates this concept. On detection of a CSZ, the most recent five SWCDs are examined, which corresponds to 10 s of the EEG. The 10 s CSZ pattern shown in Fig. 4.32A is decomposed into half-waves and modeled by fitting a straight line (Fig. 4.32B), as described in the morphology system described in Section 4.3. The absolute value of the slope (m) of the best-fit line for each half-wave is shown in Fig. 4.32C. SWCs are identified by comparing the sharpness feature (m) to a minimum (m_{th}). We compute the density of SWCs as the number (N_k) of SHW in the 2 s epochs shown in Fig. 4.32D. A regression line is fit to the N_k of the five two-second epochs of the CSZ. The slope

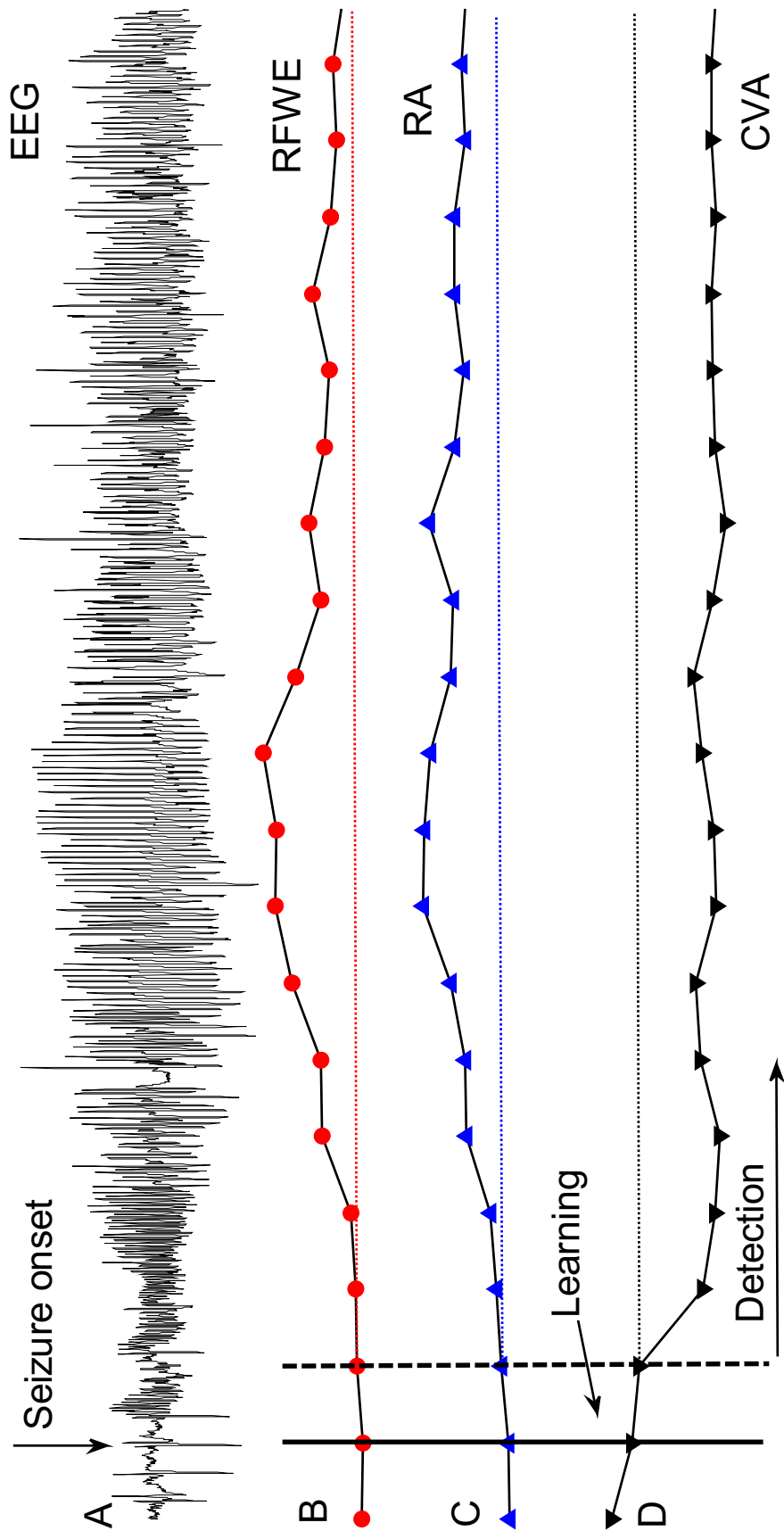


Figure 4.31: Illustration of dynamically setting a local detection threshold. (A) A 30-second EEG obtained from one patient with a short seizure (~ 40 s), and the three features: (B) relative frequency-weighted-energy (C) relative amplitude and (D) coefficient of variation of amplitude (CV). The dots represent the feature at every m -point. The ‘thick’ and ‘dashed’ vertical line encloses the learning phase.

(μ) of the resulting regression line is used to determine the continual increase in the sharp components. A positive slope ($\mu > 0$) establishes a continual increase in the density of sharp components.

Normal EEG rhythms with occasionally occurring sharp transients can at times meet the condition of $\mu > 0$, and are detected as the CSZ. Such false events plagued both the RFWF and the morphology systems. One way to reject such events is by enforcing a minimum number of SWCs in the CSZ. The total number of SWCs in the CSZ ($N^T = \sum_{k=1}^5 N_k$) is examined against a default threshold (N_{th}^T), where N_k represents SWCD in the k th two-second epoch.

It is a well-known fact that the best-fit line is sensitive to extreme values which may pass the first validation criterion ($\mu > 0$) of the CSZ, that is establishing a continual increase in the N_k . Furthermore, a single instance of high-frequency burst in the CSZ can satisfy the second validation criterion, namely, $N^T > N_{th}^T$, which can lead to a false classification of the CSZ. Such CSZ patterns can be rejected by examining the characteristic property of seizure as a continual increase in the sharp components at the seizure onset. That is, in addition to the above two conditions, the CSZ must have $N_k > 0$ in at least 4 of 5 two-second epochs. A seizure is detected when all the three conditions are met, otherwise the CSZ is rejected as due to artifacts.

4.5.5 Performance Evaluation

The performance of the proposed eSD system is also assessed in single channel configuration, and is compared against the two proposed NPS systems, and the three comparison NPS systems. The performance is evaluated with the same rules as was done for the two NPS systems proposed earlier in this chapter. Any detections within 30 s were grouped prior to performance evaluation.

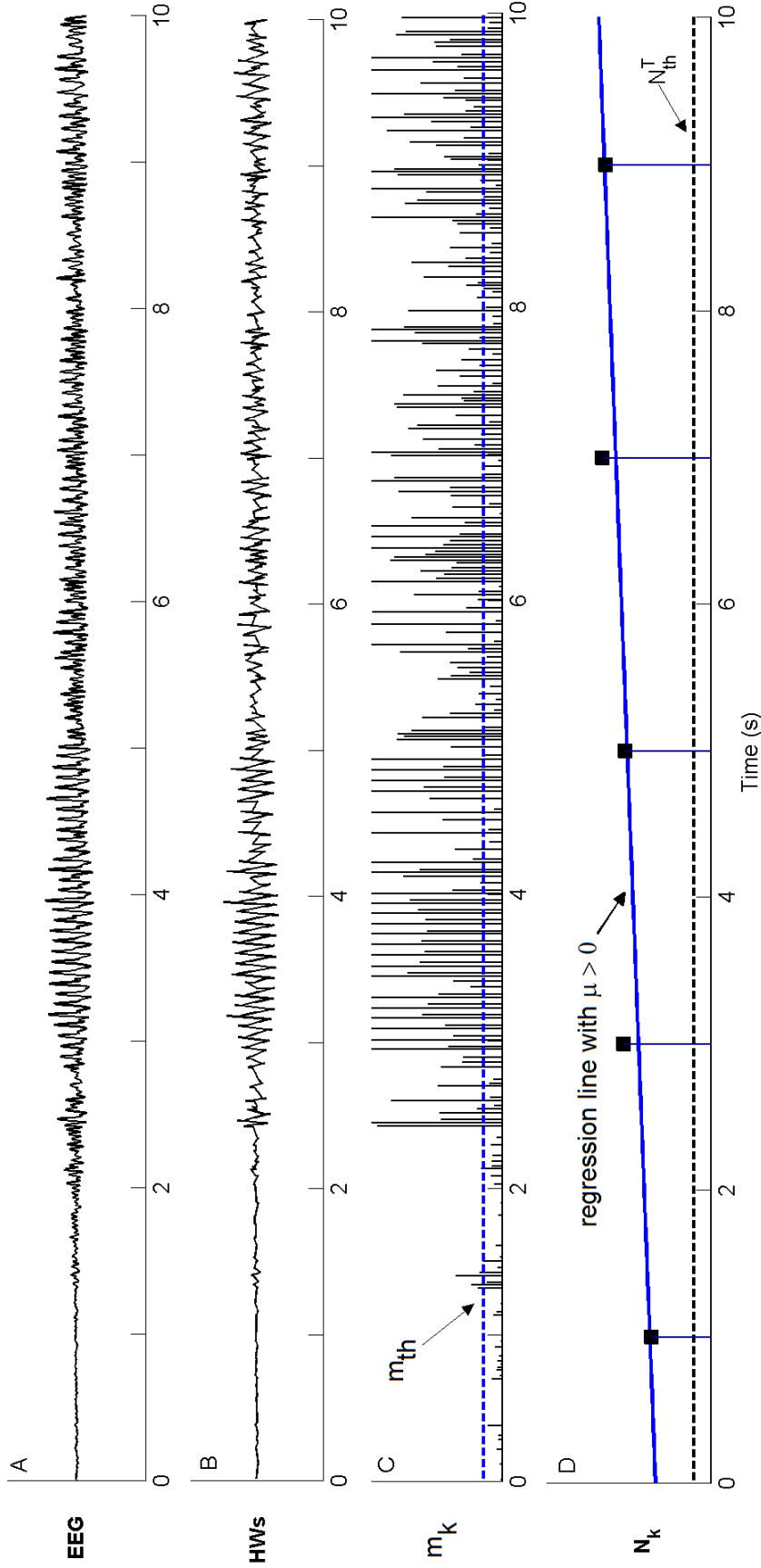


Figure 4.32: Illustration of the quantification of evolution of SWC density. (A) is 10-second candidate seizure (CSZ) pattern, (B) transformation of the CSZ pattern into elementary waveform obtained by fitting straight line on the half-waves, (C) the slope of the half-wave (m) shown as bar graph and slope threshold m_{th} by horizontal ‘dashed’ horizontal line. (D) The total number of SHW ($m > m_{th}$) N_k , in 2-second bins is shown by vertical lines. The minimum number of sharp component (N_{th}^T) in a candidate seizure event is represented by horizontal ‘dashed’ line. The continual increase of the sharp components is estimated by the slope of the regression line μ fitted on the five SHW density data point.

4.5.6 Results

As with the two previous new NPS systems proposed, the eSD system is also optimized using the single-channel MNI training dataset. The threshold to identify SHWs is adapted from the morphology system described in the previous section.

The detection results for the proposed eSD system for each patient are shown in Table 4.5. The eSD system resulted in an average sensitivity of 91.8%, specificity of 82.1% and a FDR of 0.1/h. Table 4.6 compares the results with the two new NPS systems proposed in this chapter, and the three NPS systems considered for the performance evaluation. It is seen that in terms of sensitivity, the proposed eSD system is inferior to both the morphology system and the RFWE system. However, the proposed eSD system shows significantly improved detection specificity over the two new NPS systems, and improved sensitivity as well as specificity over all three NPS systems considered for comparison.

Table 4.5: Single channel analysis of eSD system on the MNI training dataset.

PID	Channel	No. of Files	Hours	TE	TP	FP	FN	SN (%)	SP (%)	FDR (/h)
1	LH1-LH3	5	20	11	11	8	0	100	57.9	0.4
2	RC1-RC3	5	20	13	13	1	0	100	92.9	0.1
3	LH1-LH3	5	21	4	4	0	0	100	100	0.0
4	LA3-LA5	5	20	6	6	0	0	100	100	0.0
5	LP1-LP2	5	20	14	8	1	6	57.1	88.9	0.1
6	LS4-LS5	6	24	7	6	4	1	85.7	60	0.2
7	LFC3-LCF5	5	20	3	3	1	0	100	75	0.1
TOTAL		36	145	58	51	15	7	91.8	82.1	0.1

PID = patient ID, TE = total expert, TP = true positive, FP = false positive, FN = false negative, SN = sensitivity, SP = specificity, and FDR = false detection rate.

4.5.7 Discussion

The main goal of the eSD system was to overcome the limitations of the RFWE and morphology systems proposed in Section 4.3 and 4.4, that is, to improve the detection specificity. The results obtained on the MNI training data suggests that the proposed

Table 4.6: Single channel evaluation of eSD system on the MNI training dataset in comparison with the two new systems and comparison systems.

PID	eSD System		Morphology System		RFWE System		Gotman System (1990)		Reveal Algorithm (2004)		Grewal-Gotman (2005)	
	SN (%)	SP (%)	SN (%)	SP (%)	SN (%)	SP (%)	SN (%)	SP (%)	SN (%)	SP (%)	SN (%)	SP (%)
1	100	57.9	100	84.6	75	100	100	91.7	18.2	100	72.7	80
2	100	92.9	100	81.3	100	61.9	61.5	47.1	23.1	3.1	61.5	57.1
3	100	100	100	100	100	100	50	100	50	7.4	100	57.1
4	100	100	100	100	100	50	83.3	62.5	33.3	8.7	100	37.5
5	57.1	88.9	100	70	92.9	68.4	28.6	33.3	78.6	25	64.3	37.5
6	85.7	60	100	100	100	53.8	28.6	50	57.1	3.8	100	41.2
7	100	75	100	100	100	50	100	75	33.3	7.7	100	50
TOTAL	91.8	82.1	100	84.5	95.4	69.2	64.6	65.7	41.9	22.2	85.5	51.5

PID = patient ID, TE = total expert, TP = true positive, FP = false positive, FN = false negative, SN = sensitivity, SP = specificity, and FDR = false detection rate.

eSD system clearly improves the detection specificity, but at the cost of sensitivity.

Sensitivity

The proposed eSD system detected at least one seizure in every patient with an overall sensitivity of 91.8%. Comparison of sensitivity with other NPS systems is shown in Fig. 4.33. The proposed eSD and RFWE systems, and Grewal-Gotman system, all had a similar sensitivity. The best sensitivity is reported for the morphology system while the worst performance is obtained from the Reveal algorithm.

The proposed eSD system detected all seizures in the training data with the exception of Patients 5 and 6. The events missed in Patient 1 (channel: LH1-LH3) by the RFWE system were detected by the eSD system. The eSD system missed six out of 14 seizures in Patient 5 (channel: LP1-LP2). Typically, the missed seizures in this patients had minimal change in the amplitude from the background and had mixed frequency characteristics. An example of missed detection in Patient 5 (channel: LP1-LP2) by the eSD system is shown in Fig. 4.34. The missed seizure is a very low amplitude mixed-frequency seizure lasting for more than 30 s.

In Patient 6, the eSD system missed one seizure event that was also missed by all the three comparison NPS systems. The missed seizure in Patient 6 (channel: LS4-LS5) is shown in Fig. 4.35 . The example illustrates a very low amplitude mixed frequency seizure lasting for more than 30 s that was detected by the proposed RFWE and morphology systems. Such low amplitude seizures are often considered difficult to detect even by the experts. The expert scoring of such a seizure is highly subjective and eventually require consensus from a group of experts before classifying it as a seizure.

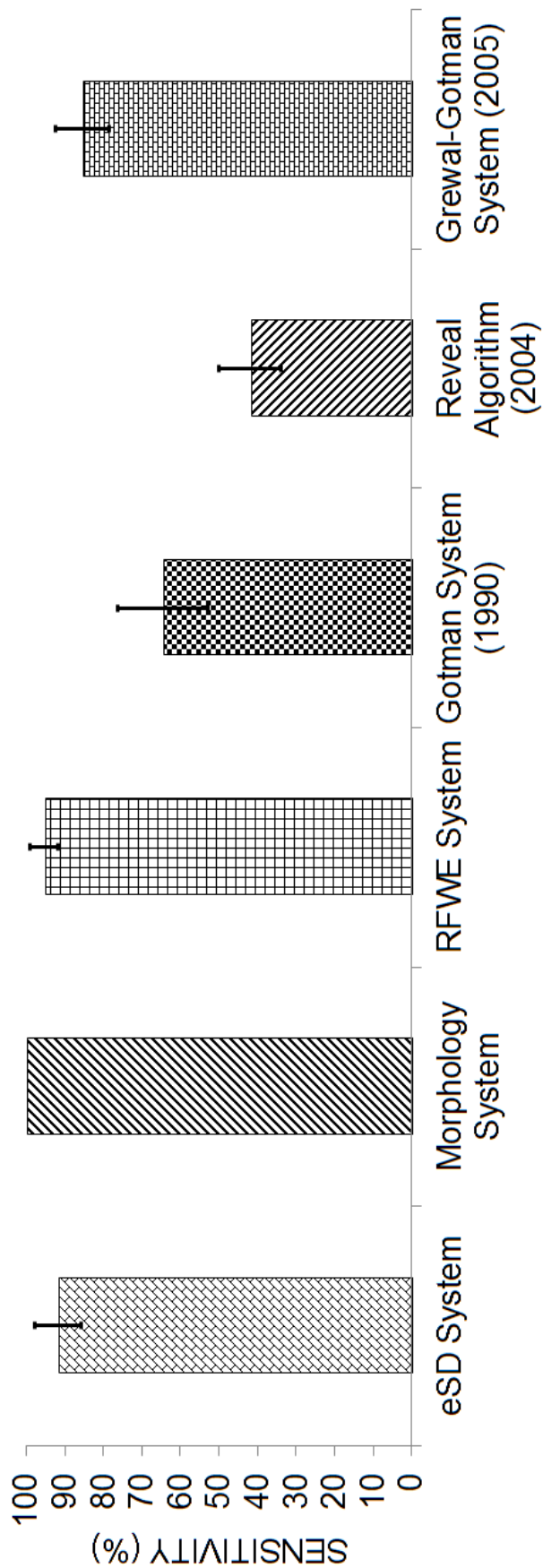


Figure 4.33: Comparison of sensitivity of the eSD system with morphology system, RFWE system and comparison systems on the MINI training data. Error bars represent standard error.

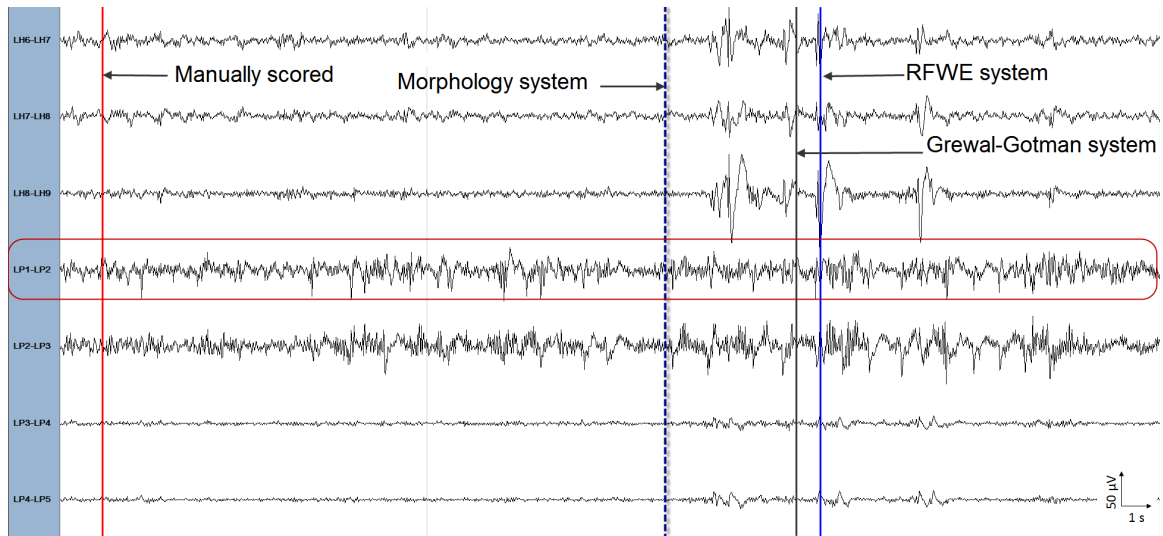


Figure 4.34: Seizure embedded in the 60 s EEG section in Patient 5 (channel: LP1-LP2) missed by the eSD system, Gotman System and Reveal algorithm. The vertical downward arrow represents the detection time instances.

Specificity

Comparing the specificity of the proposed RFWE and morphology systems with that of the three NPS systems, both the morphology and eSD systems report similar specificity, but significantly improved specificity over the other NPS systems. The eSD system reports improved specificity over the RFWE system by 12.9%, the Gotman system by 16.4%, the Reveal algorithm by 59.9% and the Grewal-Gotman system by 30.6%. Comparison of specificity with all the NPS systems is shown in Fig. 4.36.

An example of false detection in Patient 1 is shown in Fig. 4.37. The example represents a false detection due to a burst of sharp transients. The event was detected by the proposed morphology system, and the Grewal-Gotman system. The detected event resembles some true events. However, this event cannot be considered a true seizure, because it does not evolve in a manner similar to that of the EEGer-scored seizures in this patient. EEGers may find such events interesting and often require consensus from a group of experts before classifying it as a seizure.

The two new NPS systems of Section 4.3 and 4.4 detected several false events in

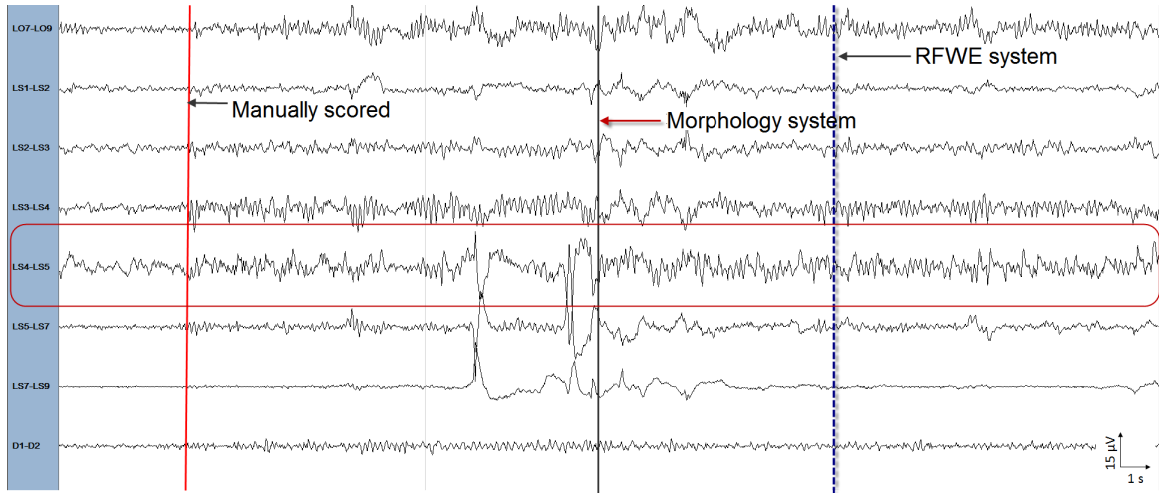


Figure 4.35: Seizure embedded in the 30 s EEG section in Patient 6 (channel: LS4-LS5) missed by the eSD system, and also by all three comparison systems. The vertical downward arrow represents the detection time instances.

Patient 2 resulting in a poor specificity. On the contrary, the proposed eSD system did not detect such low amplitude mixed-frequency events in this patient, thereby improving the detection specificity. It is important to note that several false events detected by the morphology system in this patient were actually true events that experts missed. False detections in other patients were also due to sharp transients. It is observed that eSD system in general has difficulty in detecting low-amplitude mixed frequency seizures.

4.6 Summary

In this chapter, we have presented three new simple NPS systems to detect seizures by tracking the temporal evolution of seizures. Among the three new NPS systems, the RFWE and the morphology systems are based on a single-feature, while the eSD system utilizes multiple features to detect seizures.

The first NPS system proposed in this chapter is the RFWE system that tracks the temporal evolution of a seizure by the relative frequency-weighted energy feature. The RFWE feature is highly sensitive to the amplitude and the frequency changes

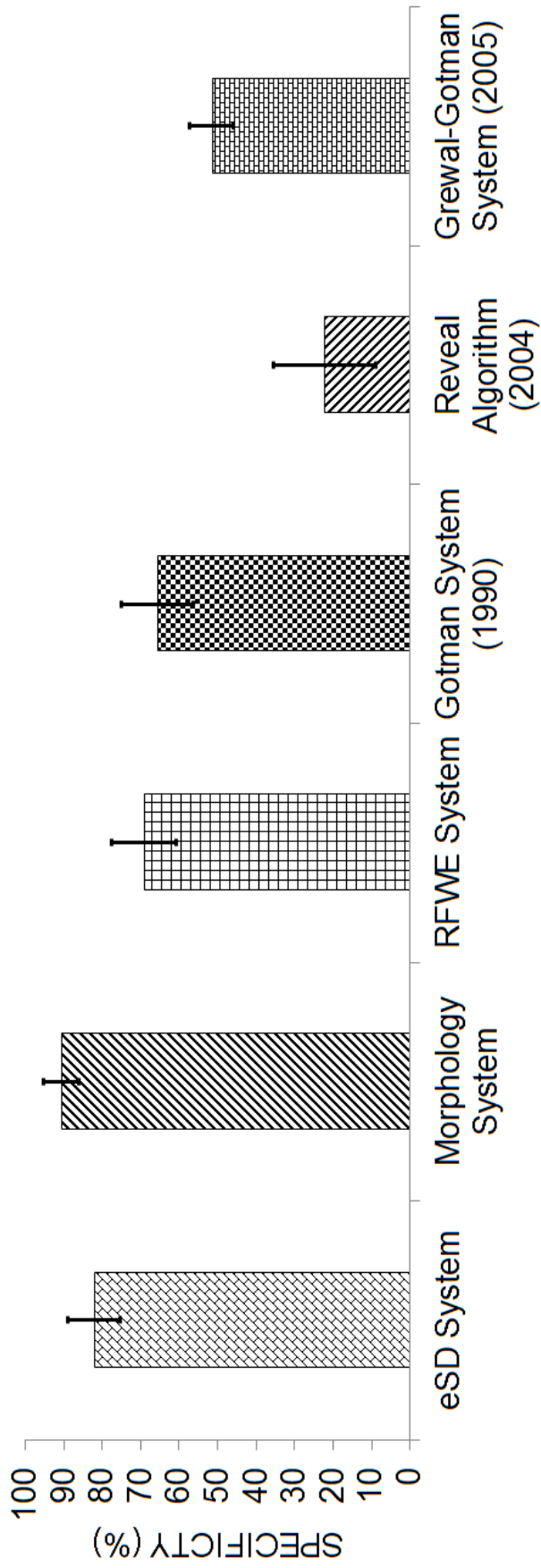


Figure 4.36: Comparison of specificity of the eSD system with morphology system, RFWF system and comparison systems on the MNI training data. Error bars represent standard error.

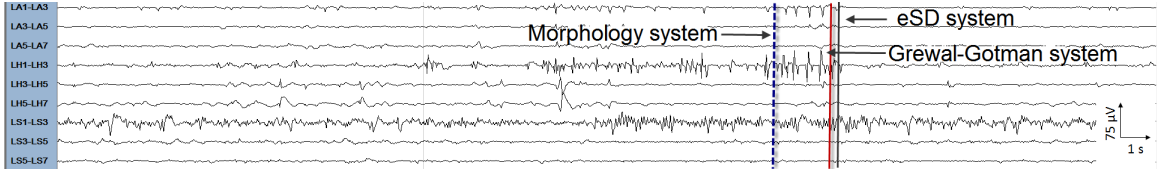


Figure 4.37: An example of false detection in Patient 1 (channel: LH-Lh3) of the MNI training dataset. The multichannel EEG (30 s) containing a false event detected by the morphology, eSD and Grewal-Gotman system. The detection time instance is shown by the vertical line.

in the EEG. Most of the existing NPS systems in the literature rely upon some pre-defined/patient-tunable detection threshold to classify the EEG as seizure or non-seizure. The RFWE system does not require a detection threshold to classify the EEG as it maps the continual increase in the RFWE feature as seizure progresses to make a detection. The results on the training data has shown a significant improvement in the detection sensitivity, but not in the specificity over the three comparison NPS systems. The false detections in the RFWE system were mainly due to the discharge of sharp transients and high-amplitude artifacts. It is noted that the background EEG contaminated by these two artifacts preceding the seizure resulted in missing some short duration seizures.

The second NPS system proposed in this chapter is the morphology system, which incorporates a new morphological feature to quantify the temporal evolution of seizure. The morphological feature, the *sharpness of the EEG waveform*, is one of the most important electrographic features utilized by the experts for accurate and reliable identification of seizures. The waveform morphology is characterized by a measure of sharpness as defined by the slope of the half-waves. Further filtering of the sharp waves along with the duration of the train of sharp waves is used to identify seizures. The morphology system detected a wide range of seizure patterns that included rhythmic and non-rhythmic seizures of varying length, including those missed by the experts. False detection in this system were mainly due to sharp transients, and high-amplitude artifacts. Contamination of the EEG by electromyographic artifacts can lead to an

increase in the number of false detections. Nonetheless, the proposed morphology system offers improved performance over all the three comparison NPS systems, and establishes a definitive role in the review of long-term EEG recordings.

The third NPS system proposed in this chapter is the eSD system, which incorporates the intelligent approach of EEG experts in the identification of seizures by quantifying and validating the temporal evolution of seizure characteristics. The eSD system first identifies a candidate seizure event by examining the temporal evolution of EEG in the relative amplitude, the RFWE, and the coefficient of variation of amplitude features. The morphological properties of the candidate seizure event is then assessed to make a detection with an attempt to improve the drawbacks of the RFWE and morphology systems. The eSD system significantly improved detection specificity over the RFWE and morphology systems as well as the three comparison NPS systems. However, on the training data, it is noted that majority of the low-amplitude mixed frequency seizures are difficult to be detected by the eSD system. Overall, the eSD system offers a performance comparable to that of the morphology system and can aid in a rapid review of long-term EEG recordings.

Chapter 5

Performance Evaluation and Rapid EEG Review Tool

5.1 Introduction

Three new NPS seizure detection systems were proposed and optimized using the MNI training dataset in Chapter 4. In this Chapter, we evaluate the performance of these new systems on a previously unseen MNI test dataset. Among the three proposed NPS systems, the one with the best performance is selected for final performance assessment on a completely blind test data (FSP database). We conclude this chapter by demonstrating a novel tool to aid in a rapid review of voluminous multichannel EEG recordings for application in EMU [119, 182].

5.2 MNI Database Results

In Chapter 4, we proposed three new NPS systems and presented results on the seven patients (Patients 1-7) belonging to the training dataset of the MNI database. We compared the performance of the new NPS system against three popular NPS systems from the literature. Training data results of the new systems revealed an

improvement in the overall performance over all the three popular NPS systems from the literature. However, this performance evaluation is biased, since we optimized the proposed NPS systems using the same data that was used for the performance evaluation. Therefore, to make meaningful comparisons, we evaluate all the three proposed systems on a previously unseen test data. We utilize the remaining seven patients (Patients 8-14) of the MNI database to evaluate the performance of the proposed RFWE, morphology, and eSD systems. The performance of these new NPS systems are compared against that of the popular NPS systems: Gotman system, Reveal algorithm and Grewal-Gotman system. The default setting for each of the NPS systems considered for the performance evaluation is determined using the ROC analysis, as described in the previous chapter. The performance is evaluated using the same technique as was done for the training data. A summary of the results obtained on the test dataset are shown in Table 5.1. For comparative assessment, we also include results obtained on the training dataset.

Table 5.1: MNI database results.

Method	Training Data		Test Data	
	Sensitivity (%)	Specificity (%)	Sensitivity (%)	Specificity (%)
RFWE System	95.4	69.2	98.7	41.1
Morphology System	100	84.5	86.7	71.3
eSD System	91.8	82.1	88.0	81.4
Gotman System	64.6	65.7	47.9	46.3
Reveal Algorithm	41.9	22.2	46.2	30.7
Grewal-Gotman System	85.5	51.5	90.2	40.5

Figure 5.1 shows single channel performance of the various NPS systems on the MNI test dataset. It is seen that for all the three new NPS systems proposed in Chapter 4 and the Grewal-Gotman system have similar sensitivity.

The proposed RFWE system reported the highest sensitivity on this unseen test data (98.7%) followed by the Grewal-Gotman system (90.2%), the proposed eSD system (88%), the proposed morphology system (86.7%), the Gotman system (47.9%) and the Reveal algorithm (46.2%).

In terms of specificity, both the morphology and the eSD systems result in a significantly improved specificity over the RFWE and the three NPS systems used for comparison. The eSD system reported 40.3%, 10.1%, 35.1%, 50.7% and 40.9% improvement in the specificity over the RFWE, morphology, Gotman, Reveal and Grewal-Gotman systems, respectively. Similarly, the morphology system reported 30.2%, 25%, 40.6%, and 30.8% improvement in the specificity over the RFWE, Gotman, Reveal and Grewal-Gotman systems, respectively. The eSD system had specificity similar to that of the morphology system.

Performance comparison between the training and test MNI dataset for the various NPS systems are indicated by 'up' and 'down' pointing arrows in Fig. 5.1. The 'up' arrow represents improved results on the test data while 'down' arrow represents improved results on the training data. No change or similar results on both the training and test data is represented by 'dash'.

5.3 Discussion

Sensitivity

On the MNI test dataset, the RFWE system reported highest sensitivity while missing one short length seizure in Patient 8. One possible reason for missing this seizure is due to the complex background activity that is precursor to the missed seizure. In Patient 9, the morphology and eSD systems missed one seizure. This patient mainly had seizures of very low amplitude that were difficult to detect. An example of the missed seizure in this patient is shown in Fig. 5.2.

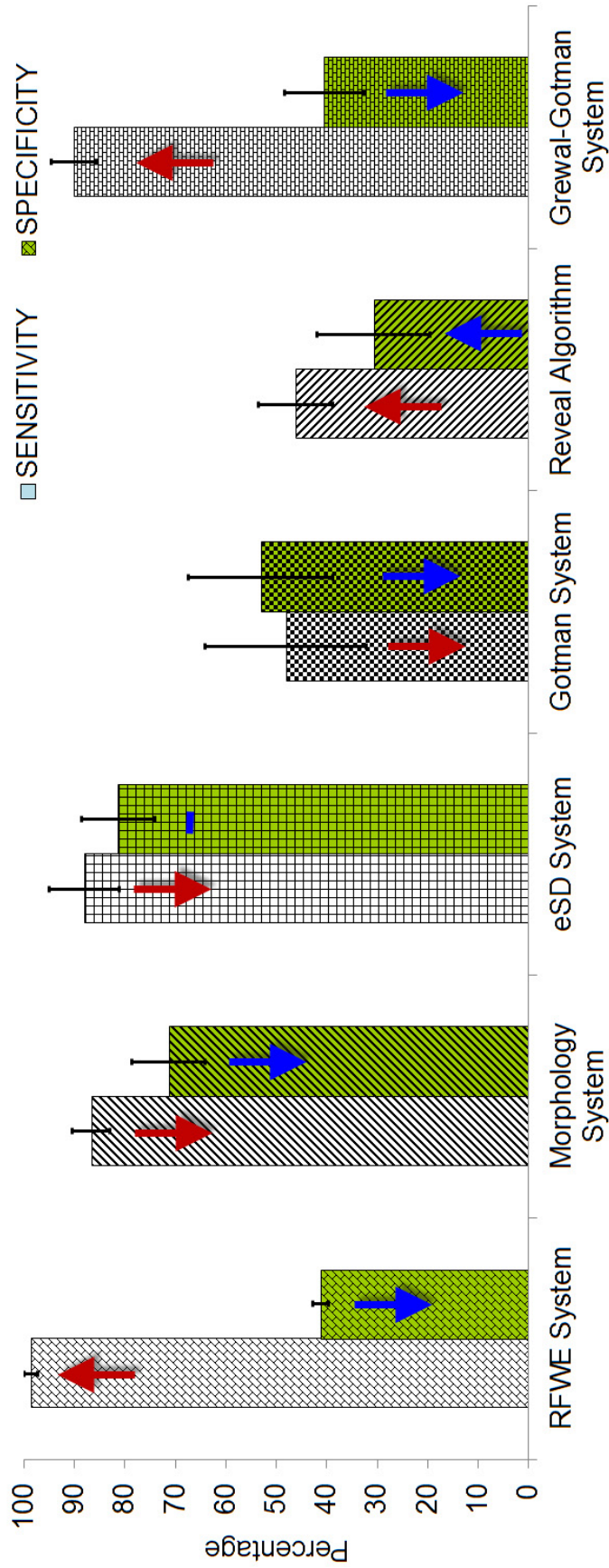


Figure 5.1: Comparison of the sensitivity and specificity on the MNI test dataset. Error bars represents the standard error. Specificity bar plots are in 'GREEN' background color for each system. The 'up' arrow represents improved results on the test data while 'down' arrow represents improved results on the training data. No change or similar results on both the training and test data is represented by 'dash'.

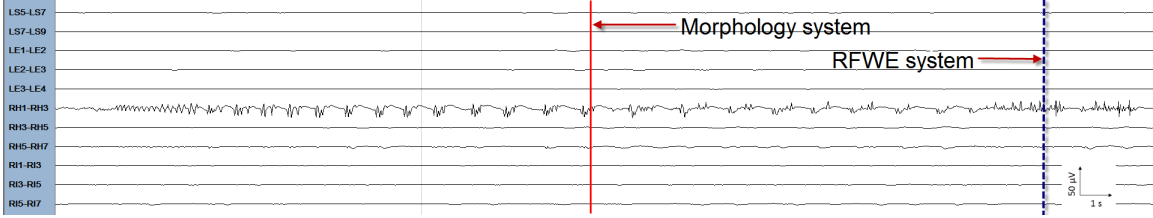


Figure 5.2: An example of low amplitude seizure in Patient 9 of the MNI test dataset. The example contains 30 s of multichannel EEG (channel: RH1-RH3) containing a seizure that was detected by the morphology and RFE systems, but missed by the eSD, Gotman, Reveal, and Grewal-Gotman systems. The detection time instance are shown by the vertical line.

An example of missed seizure by the Gotman system and Reveal algorithm in Patient 10 is shown in Fig. 5.3. The probable cause of missing this seizure by the Gotman and Reveal systems is the frequent sharp transients that constituted most of the background EEG prior to the seizure onset. It is also observed that both of these comparison systems had difficulty detecting low-amplitude seizures resulting in a poor sensitivity.

In Patient 9, the morphology and eSD systems missed one seizure, while the Grewal-Gotman system missed three seizures. In Patient 12, the morphology and Grewal-Gotman systems missed one seizure, while the eSD system missed four seizures. Similarly, in Patient 14, the morphology system missed five seizures, the Grewal-Gotman system missed four seizures, while the eSD system missed only one seizure. An example of missed seizure in Patient 14 by all the methods except for the RFE and Gotman systems, is shown Fig. 5.4. This example depicts a very short, low amplitude mixed frequency seizure. It is realized that the morphology, eSD and Grewal-Gotman systems, all had difficulty detecting low-amplitude as well as short seizures. Note that the MNI test data had nearly 87% of seizures with an average length of 72.6 seconds, and the remaining 13% seizures had an average length of 15.4 seconds.

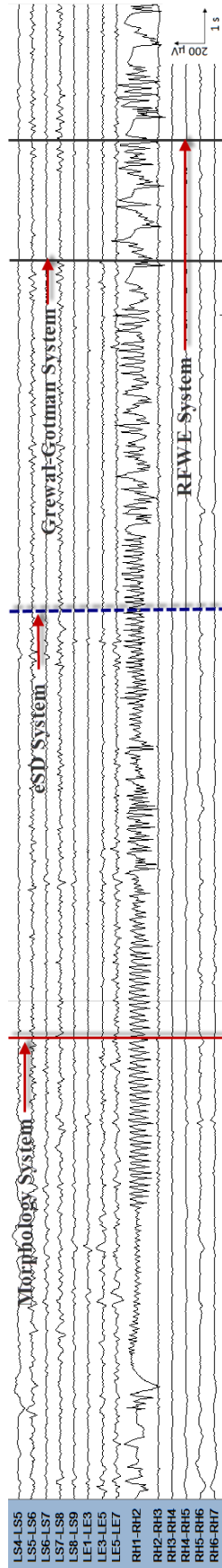


Figure 5.3: An example of seizure in Patient 10 of the MNI database. The example contains 30 s of multichannel EEG (channel: RH1-RH2) containing a seizure that was detected by all systems except the Gotman system and Reveal algorithm. The detection time instances are shown by the vertical lines.

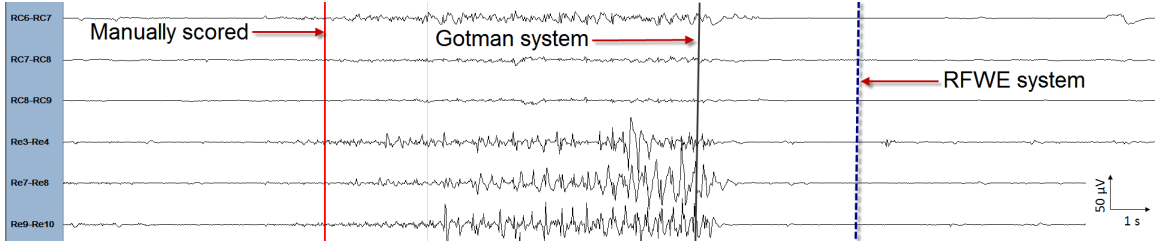


Figure 5.4: An example of short length seizure in Patient 14 of the MNI database. The example contains 30 s of multichannel EEG (channel: RE3-RE4) containing a seizure that was detected by Gotman system and Reveal algorithm, and missed by all other systems. The detection time instances are shown by the vertical lines.

Specificity

On the test data, among the three new NPS systems, the RFWE system reported 28% drop in the specificity on the test data compared to the MNI training data. The likely cause for the drop in the specificity is due to a fairly large number of sharp transients in some of the patients in the MNI test data. The performance of the morphology system also deteriorates in the presence of sharp transients, and is one possible reason as to why the system reports 13% drop in the specificity. An example of the false event detected by the RFWE and morphology systems is shown in Fig. 5.5. Among all the three new systems, only the eSD system is minimally affected by the presence of sharp transients with a 1% drop in the specificity compared to that for the training data. The false detections are mainly due discharge of high-frequency activity or sharp transients. It is noted that computing features relative to a running background EEG improves the detection specificity by suppressing the effect of such a complex background EEG. Although the false detection shown in Fig. 5.5 does not match the seizure characteristics in this patient, it seems to have traits of a seizure. The EEGer may find such events interesting, and may consider retaining them for further analysis. Morphology system also highlighted several seizures missed by the expert on the training data. False detections made by the morphology system on the MNI test dataset are revisited in Section 5.4 with further detailed analysis.

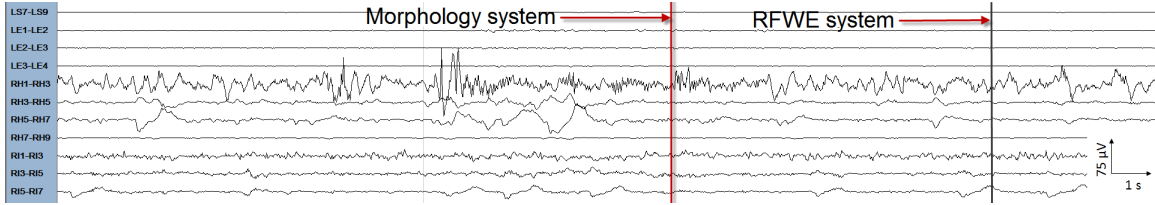


Figure 5.5: An example of false detection in Patient 9 of the MNI test data. The example contains 30 s of multichannel EEG (channel: RH1-RH3) detected by RFWE system and morphology system, but not by other NPS systems. The detection time instances are shown by the vertical lines.

5.4 FSP Database Results

The performance assessment on the MNI test data can still be viewed as biased for several reasons. Since the proposed methods were developed in sequence, after the assessment of first method, that test data is no longer blind to subsequent methods even though the test data was not used in the development of the other methods. Our channel selection criterion and single channel vs. multichannel performance evaluation are among several possible reasons. Depth recordings are made using the grid, strip or depth electrodes. The strip and grid electrodes are disk electrodes of 4 mm in diameters that are placed on brain surface (cortex). On the other hand, depth electrodes penetrate the brain and have multiple electrodes along their length with smaller surface area compared to the grid and strip electrodes. They may be closer to the generators of the epileptic discharges and hence, the EEG may be of higher amplitude. Thus, electrode configuration can cause variations in the overall system performance [47, 183]. In addition, the digital EEG acquisition systems within the same center and across different EMUs, have different front-end settings such as amplifier gains, filter settings and sampling rates. These settings can also lead to variation in the performance. Therefore, we evaluate the performance of one of the new NPS systems proposed in Chapter 4, and compare it with one of the popular comparison NPS systems, on a totally new EEG dataset recorded using a different

hardware (different front-end settings) consisting of varied type of intracranial EEG recordings (depth, strip, and grid electrodes).

For this purpose, we select the new NPS system that reports the best overall performance on the MNI database. It is seen from Table 5.1 that the NPS systems with the best overall sensitivity and specificity are the morphology system, the eSD system and the Grewal-Gotman system. Both the morphology and eSD systems report a similar sensitivity, but the latter reports 10% improvement in the specificity on the MNI test dataset. It is important to mention here that re-assessment of false detections made by the morphology system revealed several events that were in fact true events, i.e., events not scored by the expert. In addition, the morphology system is computationally light compared to the eSD system. Considering all these factors, we selected the morphology system from the new NPS systems, and the Grewal-Gotman system from the literature, for performance evaluation on the blind test dataset.

The performances of the morphology and Grewal-Gotman systems are assessed in multichannel configuration on the FSP database (see detailed description of the database in Chapter 3). The performances are evaluated with the same rules as was done for the MNI database.

On the multichannel FSP database, the morphology system resulted in an average sensitivity of 81% and specificity of 58.9%, respectively, whereas the Grewal-Gotman system reported an average sensitivity of 65.6% and specificity of 57.7%, as shown in the Table 5.2. For this database, the morphology system shows an overall improvement in the sensitivity by 15.4% over the Grewal-Gotman system with a similar specificity. It is interesting to note that the Grewal-Gotman system did not make any detection (missed all seizures) in Patients 1, 8 and 19. Excluding these patients from the performance evaluation, the morphology system reports an additional 9.4% and 11.6% improvement in the sensitivity and specificity, respectively, over the Grewal-Gotman system.

Table 5.2: Multichannel evaluation of the FSP database

PID	Hours	TE	Morphology System			Grewal-Gotman System		
			SN (%)	SP (%)	FDR (/h)	SN (%)	SP (%)	FDR (/h)
1	31	4	75	20	0.39	0	100	0
2	29.6	3	100	37.5	0.17	100	37.5	0.17
3	32.2	5	100	31.3	0.34	100	71.4	0.06
4	34	5	100	100	0	80	80	0
5	33.9	5	20	50	0.03	60	25	0.27
6	30.4	3	100	100	0	66.7	50	0.07
7	30.6	3	66.7	33.3	0.13	66.7	25	0.20
8	27.7	2	50	33.3	0.07	0	100	0
9	33.9	5	100	11.6	0.17	80	11.4	0.91
10	35.2	5	60	33.3	0.17	40	20	0.23
11	32	4	75	100	0	75	100	0
12	57.6	4	75	100	0	75	100	0
13	28	2	100	100	0	100	66.7	0.04
14	30.9	4	100	22.2	0.45	100	30.8	0.29
15	34	4	75	75	0.03	75	42.9	0.12
16	35.7	5	100	27.8	0.36	80	28.6	0.28
17	38.9	5	100	83.3	0.03	100	100	0
18	37.9	5	80	7	1.42	20	2.3	1.11
19	37.3	4	25	100	0	0	100	0
20	38.5	5	100	71.4	0.05	80	80	0.03
21	35.9	5	100	100	0	80	40	0.17
TOTAL	725.2	87	81	58.9	0.18	65.6	57.7	0.19
			86	60	0.19	76.6	50.6	0.22

Total excluding Patients 1, 8 and 19

PID = Patient ID, TE = Total number of seizure events identified by the experts, SN = Sensitivity, and SP = Specificity. The overall performance result for all 21 patients is in the first row of the TOTAL while results obtained by excluding highlighted patients is shown in the bottom row of the 'TOTAL'.

Both the NPS systems report a poor specificity compared to the MNI test dataset. A possible cause for an increase in the false detection rate (specificity) could be due to the fact that the EEGer scored the FSP database only in the sections of clinical seizures. That is, the EEGer did not score seizures in sections in which there were no clinical seizures. False detections may in fact be real seizures, which warrant studying the characteristics of false detections by the experts. Typical classifications of seizures that an EEGer may consider during a normal EEG review are: seizure-like (SL), interesting events (IE) or false detection (FD). Seizure-like events are those that match characteristics of seizures. Interesting events include detections such as sharp transients, including events difficult to classify as seizure-like, however display some

properties of the seizures. False detections are clearly non-seizure like activity. Two neurophysiologists (EEGer A & B) independently re-assessed all the false detections, and classified them in the above three categories for the proposed morphology system and the Grewal-Gotman system. We define the three category classification of the FDs by the experts as Assessment I. The performance is re-assessed using Assessment I approach and the results are shown in Table 5.3. Re-assessment of the FDs for the two methods showed improvement in the specificity for all data.

It is not uncommon to note variability in the EEG scoring by the experts. We too note a variation in the EEGer scoring. Therefore, we estimated the Cohen’s κ score, a popular measure employed to measure inter-rate variability. We used κ statistics to adjust the observed inter-observer agreement (p_o) for the proportion of random agreement (p_e): $\kappa = (p_o - p_e)/(1 - p_e)$. If both the EEGers are in complete agreement, then $\kappa = 1$. If there is no agreement other than what would be expected by chance, then $\kappa \leq 0$ [116, 184]. A moderate agreement between the two EEGers is achieved ($\kappa = 0.43$) on re-assigning these false detections into the three categories (SL, IE, and FD).

Some EEGers consider classifying the EEG into two categories: seizure-like and false detection [52, 185]. This motivated us to evaluate the performance using the two category classification, which we define as Assessment II. In this assessment of false detections, we combine the seizure-like and interesting as seizure-like events. The specificity for the Assessment II validation approach is also shown in Table 5.3. Re-assessment using Assessment II showed an improvement in the detection specificity for the two systems. This classification mode resulted in a substantial agreement ($\kappa = 0.81$) between the EEGers, establishing expert’s agreement on a clear demarcation between the two categories: SL and FD. Re-assessment of the false detection is discussed in the next section.

Table 5.3: Re-assessment of false detections in the FSP Database

PID	Hours	TE	Morphology System					Grewal-Gotman System					
			SP	EEGer A		EEGer B		SP	EEGer A		EEGer B		
				SP*	SP**	SP*	SP**		SP*	SP**	SP*	SP**	
(%)	(%)	(%)	(%)	(%)	(%)	(%)	(%)	(%)	(%)	(%)	(%)		
1	31	4	20	56.4	64.1	28.2	61.5	100	100	100	100	100	
2	29.6	3	37.5	50	100	50	75	37.5	44.4	100	44.4	77.8	
3	32.2	5	31.3	33.3	50	27.8	27.8	71.4	85.7	85.7	71.4	85.7	
4	34	5	100	100	100	100	100	80	80	80	80	80	
5	33.9	5	50	100	100	100	100	25	17.6	17.6	17.6	17.6	
6	30.4	3	100	100	100	100	100	50	50	75	50	50	
7	30.6	3	33.3	33.3	50	33.3	33.3	25	38	50	25	25	
8	27.7	2	33.3	33.3	100	33.3	33.3	100	100	100	100	100	
9	33.9	5	11.6	60.6	98.5	45.5	80.3	11.4	54.9	98	47.1	80.4	
10	35.2	5	33.3	21.4	21.4	21.4	28.6	20	20	20	20	20	
11	32	4	100	100	100	100	100	100	100	100	100	100	
12	57.6	4	100	100	100	100	100	100	100	100	100	100	
13	28	2	100	100	100	100	100	66.7	66.7	66.7	66.7	66.7	
14	30.9	4	22.2	78.6	88.1	47.6	59.5	30.8	56.3	56.3	50.0	56.3	
15	34	4	75	75	75	75	75	42.9	42.9	57.1	42.9	42.9	
16	35.7	5	27.8	68.2	68.2	68.2	68.2	28.6	94.7	94.7	94.7	94.7	
17	38.9	5	83.3	100	100	83.3	83.3	100	100	100	100	100	
18	37.9	5	6.9	58.6	85.2	7.6	74.3	2.3	58	83.8	9.1	86.4	
19	37.3	4	100	100	100	100	100	100	100	100	100	100	
20	38.5	5	71.4	100	100	100	100	80	100	100	100	100	
21	35.9	5	100	100	100	100	100	40	40	40	40	40	
TOTAL	725.2	87	58.9	74.7	85.7	67.7	76.2	57.7	69	77.4	64.7	72.5	
			60.2	76.6	85.4	70.0	78.1	50.6	63.8	73.6	58.8	68.0	

Total excluding Patients 1, 8, and 19

TE = Total number of seizure events identified by the experts, SP = Specificity, SP* = Specificity by Assessment I approach, and SP** = Specificity by Assessment II approach. The overall performance result for all 21 patients is in the first row of the TOTAL while results obtained by excluding highlighted patients is shown in the bottom row of the 'TOTAL'.

5.5 Discussion

In the literature, it is reported that majority of the existing systems for seizure detection fail to detect seizures that are of short duration or seizures that do not show a sustained rhythmic component, and are of low-amplitude. We too observed that the selected NPS systems from the literature, as well as the proposed NPS systems report difficulty in detecting such seizures in the MNI database. Our overall goal was to overcome these challenges in seizure detection by designing a system that detects a wide-variety of seizure patterns with high sensitivity and high specificity (low false

detection rate).

The performance evaluation results are shown in Figure 5.6, which compares the sensitivity and specificity of the proposed morphology system against the Grewal-Gotman system on the two databases. The results depict that the proposed morphology system reports improved sensitivity and specificity on the FSP database, and improved specificity with nearly similar sensitivity on the MNI database over the Grewal-Gotman system.

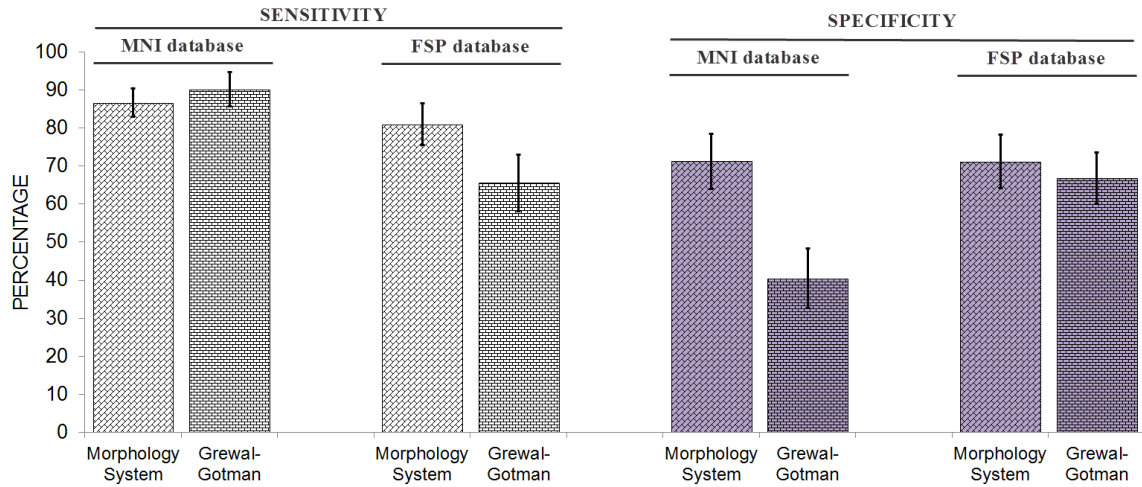


Figure 5.6: Comparison of sensitivity and specificity of the morphology system with Grewal-Gotman system on the MNI and FSP database. Error bars represent standard errors. Specificity results for FSP database are after re-classification of false detections by the EEGer A and B using 'Assessment I' technique.

Sensitivity

The proposed morphology system detected at least one seizure in all the patients, with an overall sensitivity of 86.7 % for the MNI test database and 81% for the FSP test database using the default threshold (obtained using the MNI training dataset). On the contrary, Grewal-Gotman system failed to detect any seizure in Patients 1, 8, and 19 of the FSP database. The detected seizures consisted of a wide variety of patterns in the frequency range of 0.5 to 70 Hz that included focal seizures (seizure occurring only on a single channel), rhythmic as well as seizures of mixed characteristics (non-

rhythmic, discharge of spikes and sharp-wave complexes). However, seizures having subtle changes in the EEG amplitude were often missed.

Comparing the sensitivity with the Grewal-Gotman system, our system performed much better ($\sim 15\%$ improvement) on the FSP database and with nearly similar results on the MNI database (Fig. 5.6A). The Grewal-Gotman system, however, had difficulties in detecting seizures that were present on a single channel, seizures that were of short duration, and seizures with slow evolution or non-rhythmic characteristics. An example of good detection is shown in Fig. 5.7 and an example of seizure missed by both the systems in the FSP database is shown in Fig. 5.8. The EEGer identified this electrographic seizure because of the associated clinical component. The missed seizure is about 27 seconds in duration with subtle changes in the EEG amplitude and ending with low-frequency complexes (< 1 Hz). Detection of this seizure is questionable without the clinical components, as it does not follow the typical definition for electrographic seizures. In general, both the methods failed to detect seizures having a subtle change in the EEG amplitude.

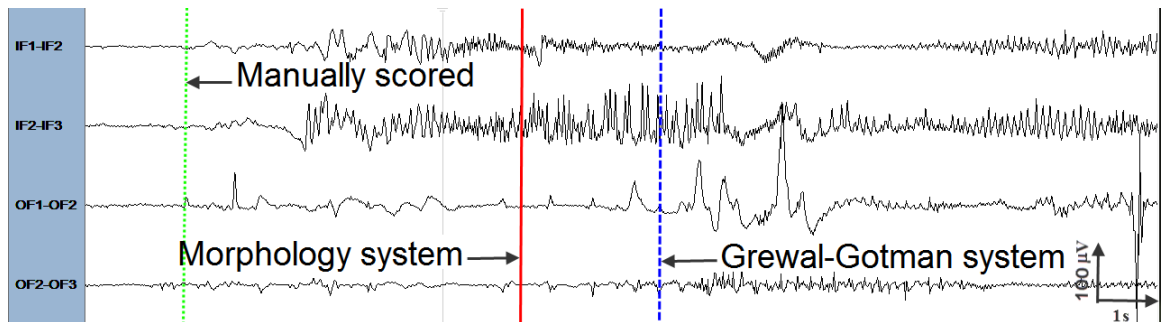


Figure 5.7: An example of good detection in Patient 7 of FSP database. Multichannel EEG (20 s) containing a seizure that was detected by both systems. The detection time instance is shown by vertical line.

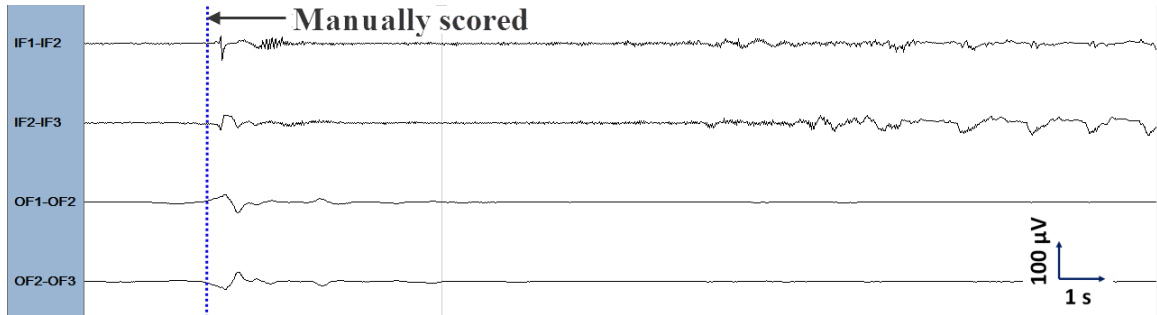


Figure 5.8: An example of missed event in Patient 5 of FSP database. Multichannel EEG (20 s) containing a seizure that was missed by both systems. The detection time instance by EEGer is shown by the dotted vertical line.

Specificity

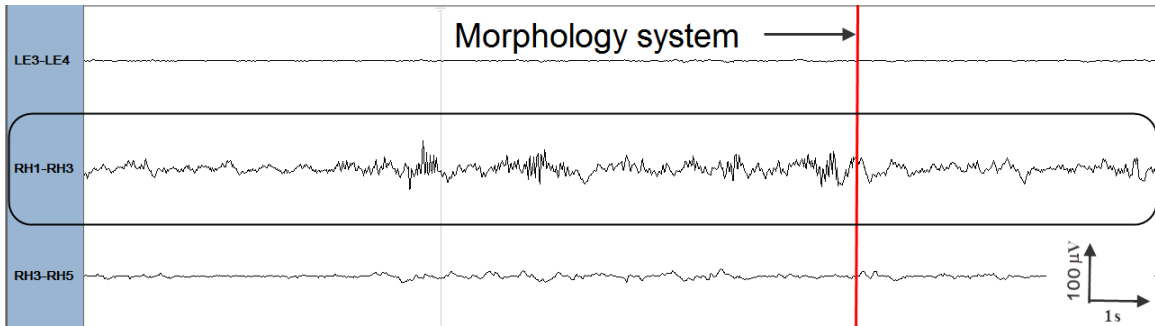
As previously mentioned, specificity indicates the quality of detections made by the seizure detection method. On the MNI database, using the default threshold, the morphology system had an average specificity of 91.2 % on the training data [34] and 71.3% on the test data. A specificity of 58.9% is obtained on the FSP test database. The specificity on the FSP test database is poor compared to that on the MNI database, thus indicating a higher false detection rate. It is possible that some of these false detections may in fact be sub-clinical seizures that were not identified by the EEGer in the original review of this data. Re-evaluating these false detections may provide more insight into the detection specificity.

The average number of false detections in the MNI database as well as in the FSP database were quite uniform in majority of the patients. In the MNI database, two patients (Patient 9 and 11) had a significantly large number of false detections. In both cases, majority of the false detections occurred prior to the seizures. The false detections included a discharge of sharp-wave complexes (~ 5 s), low amplitude fast activity, or were due to bursts of sharp transients in addition to high amplitude artifacts (see Fig. 5.9). A large proportion of the false detections occurred several seconds to several minutes before the seizure onset. A recent study by Marsh *et al.*

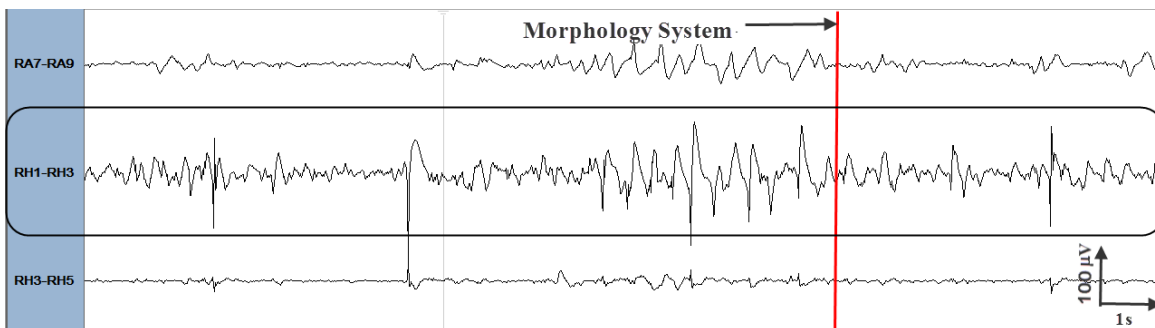
[45] has demonstrated the role of interictal epileptic discharge (IED) for improved localization of seizure focus in children with intractable epilepsy. The authors report that electrodes with highest frequency of IEDs over long periods of intracranial EEG correlate with the electrodes involved in the seizure onset in about two-thirds of patients [45]. Furthermore, IEDs are used clinically in a variety of ways to help identify the regions of surgical resection [186]. Several other studies, using long-term depth EEG, report that in addition to resection of the seizure onset zone, resection of regions generating 'significant' interictal spikes and sharp waves improves seizure freedom postoperatively [187, 188]. It may be possible that in some patients increased false detections by our system, due to increased sharp activity, are precursors to seizures or markers for seizure onset zones. Therefore, such events can be potentially used as a clinical tool to identify regions of interest that warrant further review.

Similarly, a large proportion of false detections in the FSP database were due to discharges of sharp-wave complexes and fast rhythmic activities. Two patients (Patient 9 and 18) had a significantly higher number of false detections. An example of false detection for Patient 9 is shown in Fig. 5.10 and for Patient 18 in Fig. 5.11. The examples in Fig. 5.10 and 5.11 in fact resemble sub-clinical electrographic seizures that were not marked by the EEGer. As noted above, this is because the FSP database is annotated by experts based on the knowledge of clinical seizures. That is, the data was reviewed for the presence of electrographic discharges only at the instances of clinical seizures. It is possible that some of the false detections (EEG sections without clinical events) are indeed electrographic seizures. To further evaluate these false detections, two neurophysiologists (EEGer A and B) re-classified these events into three categories (Assessment I), seizure-like (SL) activity, interesting events (IE) and false detections (FD). Seizure-like activity included detections that matched characteristics of seizures (as in, Fig. 5.10 and 5.11). Interesting events included detections such as discharge of sharp transients that may be considered interesting events to the EEGer. False

detection included those that were clearly non-seizure. Performance was re-assessed using this approach (Assessment I) and results of the re-classification are shown in Table 5.3. The inter-reviewer variability was evaluated by calculating Cohen's κ between the EEGers.



(a) Example of false detection in Patient 9 (channel: RH1-RH3) which represents low amplitude fast activity.



(b) An example of false detection in Patient 11 (channel: RH1-RH3) which represents a burst of high amplitude sharp wave complexes.

Figure 5.9: A 20 s example for false detections in the Patient 9 and 11 belonging to the test dataset from the MNI database. The channel of interest is enclosed in the rounded rectangle box with detection made by the proposed system shown by solid vertical line.

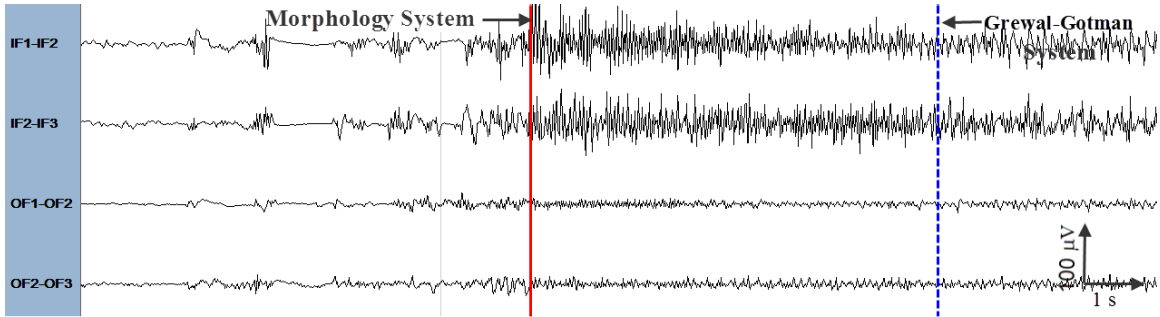


Figure 5.10: An example of false event detected in Patient 9 of FSP database. Multichannel EEG (20 s) with detection by our system (represented by solid vertical line) and Grewal-Gotman system (represented by dashed vertical line). The detection time instance is shown by vertical line.

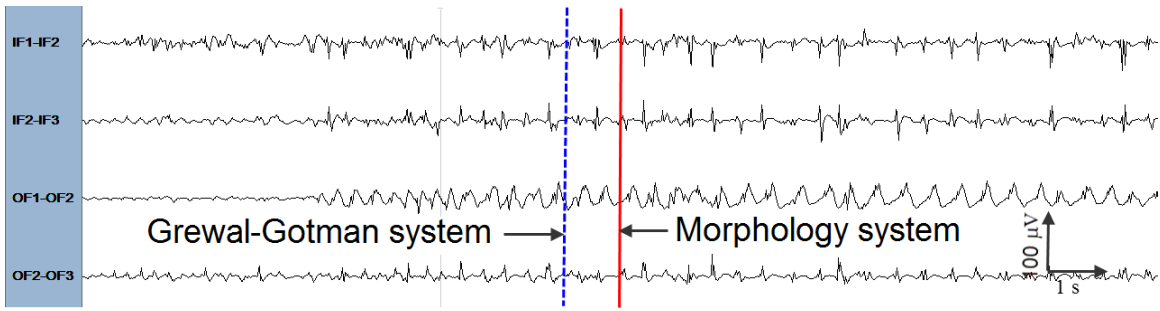


Figure 5.11: An example of false event detected in Patient 18 of FSP database. A 20 s of multichannel EEG with detection by our system (represented by solid vertical line) and Grewal-Gotman system (represented by dashed vertical line). The detection time instance is shown by vertical line.

An unweighted κ coefficient of 0.430 is obtained representing a moderate agreement between the EEGers. This might be explained by differences in the interpretation of certain seizure-like and interesting events by the two EEGers. Seizure-like events identified by one EEGer were considered interesting events by the other EEGer and vice versa. It may be difficult to interpret certain epileptiform discharges leading to differences in the opinion among the EEGers. Limited number of channels (four channels) could be one possible explanation for this disagreement among the EEGers. A limited number of channels do not provide any anatomical orientation information. Availability of all channels, anatomical orientation and baseline EEG for review will significantly improve the inter-rater agreement. Nevertheless, previous studies

have shown that EEGers (based on their experience) report perfect to near perfect agreement when the EEG is categorized into seizure and false detections [116, 184, 189]. In our data, near perfect agreement ($\kappa = 0.81$) between the EEGers is achieved when all events that were scored seizure-like by one EEGer and interesting by the other are treated as true positives, i.e., the two categories (seizure-like + interesting = seizure-like) are combined. Therefore, we computed specificity for two category reclassification (Assessment II). As expected, an overall improvement in the specificity is observed (see Table 5.3 and Fig. 5.12), which suggests that several FDs are in fact seizures that were not originally scored in the FSP database.

It can be seen that the specificity is poor in some patients in both the MNI and FSP databases. That is, there are a large number of false detections in these patients due to short paroxysmal activities. For clinical application of the method, a tunable threshold must be considered, which can be used to address the trade-off between the detection sensitivity and specificity. In our NPS systems, we have aimed to remove the dependence on the preset detection thresholds. However, the use of a minimum duration as part of the definition of seizures can be considered as a threshold that can be tunable. The EEGer can increase the duration threshold on observing a large number of short false events to reduce these false detections.

It is important to mention here that MNI database are all depth recordings while FSP database is a mix of depth, strip and grid recordings. Seizure manifestations in the depth EEG are likely to be similar for both the databases, while strip and grid electrodes are likely to have a different manifestation. This is because seizure manifestation is different for different brain regions. Depth electrodes can be placed into deeper brain regions such as hippocampus, hypothalamus, and deep frontal lobes, where there is inadequate coverage provided by subdural strip and grid electrodes. Furthermore, the two database were acquired using two different hardware (Stellate Harmonie and Neurofile NT systems) and at two different sampling rates. The

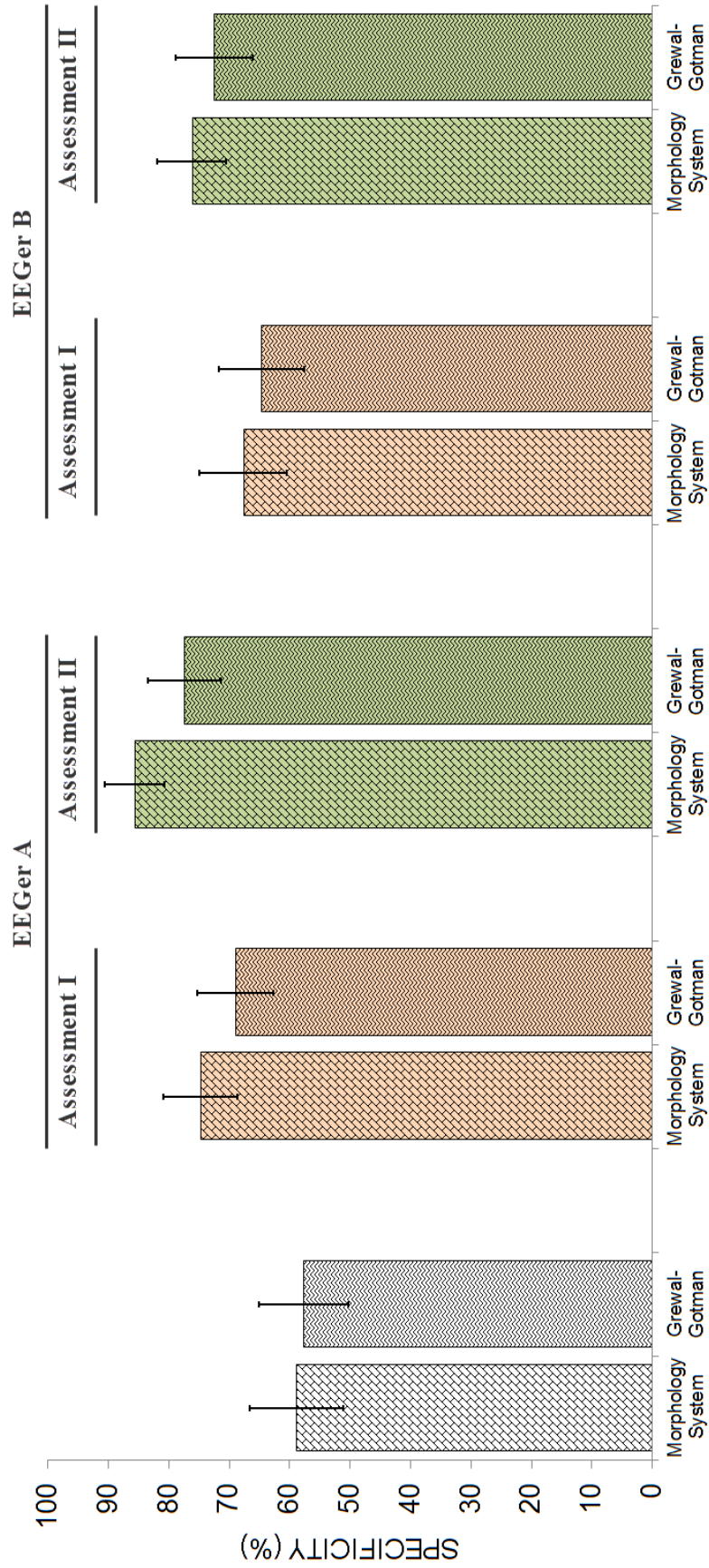


Figure 5.12: Re-assessment of false detections in the FSP database.

performance of the morphology system, however, did not change significantly for the two databases.

We also assessed the computational cost of the proposed morphology system on the FSP database. Running our system on MATLAB 2008b (MathWorks Inc.) on a laptop with Intel dual core 1.8 GHz processor, 3 GB RAM, having the 32-bit Microsoft Windows 7 operating system, our system processed 24-h four channel EEG in approximately 30 minutes. Computational performance of the system can be significantly enhanced by developing a standalone version in C++. In addition, running on systems with faster processors with multiple cores can further reduce the computation time. The performance and computational speed suggests that the proposed morphology system can be clinically useful in the review of long-term EEG recordings.

As with other systems, the morphology system generally failed to detect seizure events that occurred with minimal changes in the EEG amplitude. In addition, a large number of false events may be detected by our system in the presence of discharge of sharp wave complexes, spikes, high-amplitude artifacts, and fast EMG artifacts. We anticipate that by including additional artifact removal techniques to handle some of the mentioned artifacts, it would be possible to further improve the specificity, and is considered as part of future work.

5.6 Rapid Review of Prolonged EEG Recordings

5.6.1 Background

In the EMU, the main role of automatic seizure detection method is to aid in a rapid review of the voluminous EEG data. The seizure detection method helps to identify seizures along with false events in the prolonged recordings. The detected events are visually examined by the experts to filter the false events and accurately localize the

epileptogenic sites, which is a tiresome task. Mapping channel-by-channel timeline of seizures and the epileptiform activities can provide visualization of seizure onset and spread (both temporally and spatially), and can be a powerful tool for planning of surgical resection. This type of 2D visualization is generally unavailable for the review of intracranial EEG. Therefore, it becomes very important to develop adjunctive tools that allow quick identification of seizures, provide a view of seizure activity over prolonged durations, seizure recurrence frequency, and the sites involved in the seizure generation for therapeutic interventions and management [5, 38-41].

Rapid identification of epileptogenic sites and evaluation of spatio-temporal dynamics is possible by digital trending tools [38-40]. Tools such as amplitude integrated EEG (aEEG), envelope trend (ET), compressed spectral array (CSA), color density spectral array (CDSA), and compressed EEG pattern analysis (CEPA) allow graphical display of the EEG trends [38-40]. The process typically involves splitting EEG data into small epochs, and extracting features for graphical display. For example, CSA displays time, frequency, and power in a three-dimensional graphical view. However, CSA display has a practical limitation of a few channels [38, 40, 42, 190]. CDSA is a modified CSA that allows the display to accommodate a few more channels. Typically, intracranial EEG recording consist of 32 to 256 channels. The large number of channels increases the computational complexity. EEGer experience in the interpretation of such graphical display is yet another limiting factor [38-40]. These factors limit the utility of the compressed EEG display in the EMU. Computationally simple and easy-to-interpret compressed EEG display, specially designed to review multichannel intracranial EEG for paroxysmal or seizure activity is much needed.

5.6.2 Method

Note that the seizure onset zone is the single most definitive localizing feature of the epileptogenic region. For this reason, it is important to identify all channels (electrodes)

in the seizure onset and their recurrence frequency for anatomical localization [38-40]. As previously mentioned in Chapter 4, an electrographic seizure is a discharge of sharp wave complexes evolving in frequency and amplitude, including repetitive spikes. Furthermore, discharge of sharp waves (sharp transients, spikes, and epileptiform discharges) occur more frequently than seizure, and can be linked to the brain regions involved in the epileptogenesis [5]. It is realized that the sharpness of the EEG waveform can be a robust marker to highlight epileptogenic areas (both temporally and spatially). The sharpness measure to parametrize the EEG waveform morphology proposed in Chapter 4 is utilized to generate the new compressed display.

Easy, reliable and intuitive interpretation is important to maintain patient safety in the EMU, where experienced EEGer may not be available round-the-clock. Color-intensity plots are intuitive, easy-to-interpret and require minimal training. Therefore, we quantify the level of sharp activity in the EEG, and graphically display it as a color-intensity plot. To do so, we split the EEG into short segments (epochs) and extract a feature for the graphical display. For compressed display, the EEG is processed in 10 s non-overlapping epochs. The feature for graphical display is the level of sharp activity in an epoch referred to as relative sharpness index (RSI), and is given by

$$RSI = \frac{\# \text{ of } m > m_{th}}{\text{Total } \# \text{ of } m}, \quad (5.1)$$

where m is a measure of the sharpness of the half-waves in the epoch (see Chapter 4, Section 4.4). The resulting RSI is displayed as a color-intensity plot that allows the compression of several hours of multichannel EEG on a single page display. We randomly selected two patients from the MNI database to illustrate the RSI display to aid in a rapid review of prolonged intracranial EEG recordings.

5.6.3 Results and Discussion

The performance evaluation of the compressed displays is done by examining the display size, interpretation, and computational complexity. To do a comparative assessment of these complexities, we selected CDSA and aEEG displays. Compressed EEG displays using all three techniques (RSI, CDSA and aEEG) were generated for the two patient EEG recordings from the MNI database. Seizure, epileptiform activity, and areas of potential seizure development were visually identified and correlated with the EEG. This evaluation allowed us to decide on the best method among the three techniques.

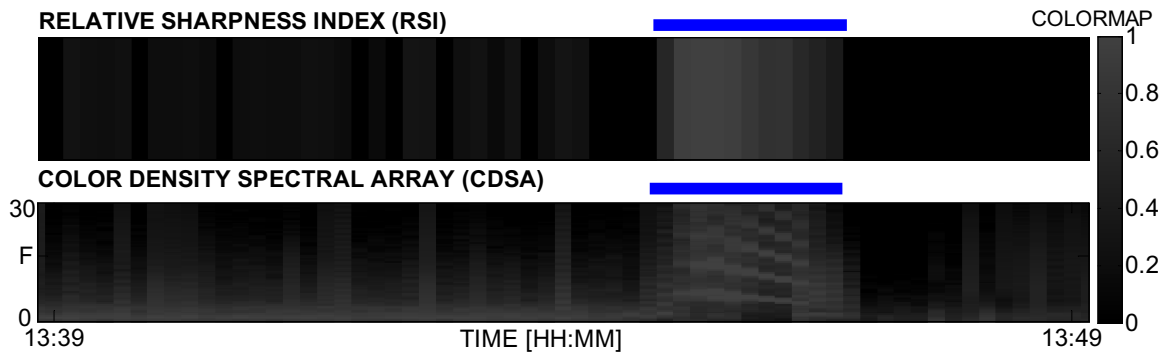


Figure 5.13: Identification of seizure in the compressed EEG display. The example represents 10 min single channel RSI and CDSA displays. Seizure detected by the EEGer is annotated with 'horizontal bar' on both the displays.

First, it is important to describe how compressed displays are interpreted for seizures. Note that compressed display represents EEG activity in a transformed domain as a function of time. The features utilized are the level of sharpness in the RSI display, power at the different frequencies in the CDSA, and the amplitude activity in the aEEG. These features are represented as color-intensity (RSI and CDSA) or trend (aEEG) graphs. An electrographic seizure evolves in both the amplitude and frequency; therefore, the intensity or the magnitude of the feature will be lower during non-seizure and maximum during a seizure. A seizure can be identified by looking for high-intensity segments in the compressed display. An example to illustrate the

interpretation of RSI and CDSA display is shown in Fig. 5.13. The example represents 10 min single channel EEG that contains a seizure (horizontal bar above the graph). Each vertical block in the RSI display represents RSI in a 10 s epoch. The RSI reaches maximum ($= 1$) during the early part of the seizure and slowly decreases as seizure evolves and eventually terminates. In our experimentation, we found that the RSI is minimal (< 0.2) during normal background activity, between 0.2 and 0.5 in the presence of paroxysmal discharges and above 0.5 during the seizure. We believe seizures can be identified by looking for instances with higher color intensity (RSI > 0.5) in the display. Similarly, high power at several frequencies is observed in the CDSA display during the seizure, resulting in a plateau formation (see Fig. 5.13). Thus, seizures can be identified in the CDSA display by looking for the sections with plateaus.

All displays were scored for seizures using the above mentioned approach. The EEG corresponding to the scored events were visually examined to confirm the detection accuracy. Figure 5.14 depicts an example of 30 channel 4 h compressed display using the three techniques for Patient 1. The EEGer marked seizure events are annotated on top of each display by downward pointing 'blue' arrow. All seizures of this patient were longer than 60 s with an average amplitude above $200 \mu V$. It was easy to identify seizure for all three methods. An example of the seizure obtained around the time instant '1' is shown in Fig. 5.15A. Referring to Fig. 5.14, seizures do not occur on all the channels according to RSI and CDSA display. However, seizure occurs on most channels according to the aEEG display (Fig. 5.14). EEG review confirmed that seizures actually occur only on specific channels, and RSI mapping of seizure channels were more accurate and precise than the CDSA mapping.

Similarly, identification of seizure was easier using RSI display in Patient 2 (see Fig. 5.16). It was found that seizures in this patient were of short duration (30-60 s) with average amplitude below $200 \mu V$. Identification of all the six EEGer-marked seizures

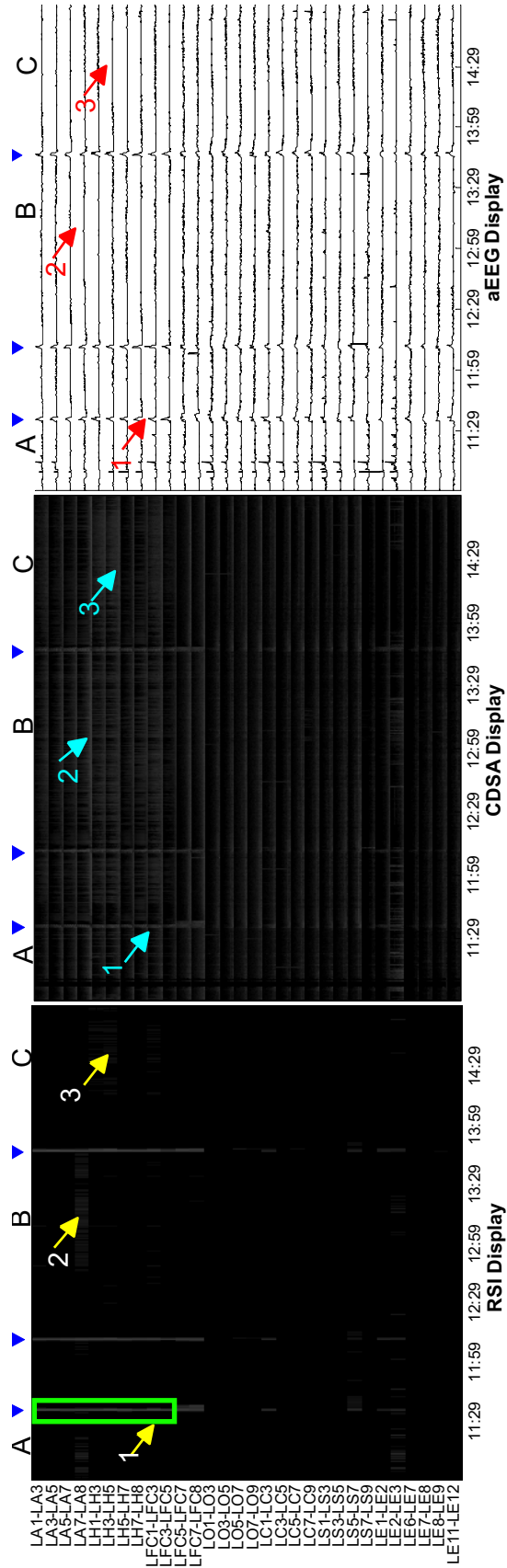


Figure 5.14: Example of multichannel compressed EEG display. The display represents 30 channel 4 h EEG section of Patient 1 for the three schemes (RSI, CDSA and aEEG). The section contains three seizure identified by the EEGer and is annotated by 'downward pointing (blue)' arrows on top of each display. Three events are selected from the RSI display (A, B, and C) with corresponding EEG shown in Fig. 5.15. Location of the selected event is shown by enumerated arrows on the RSI display.

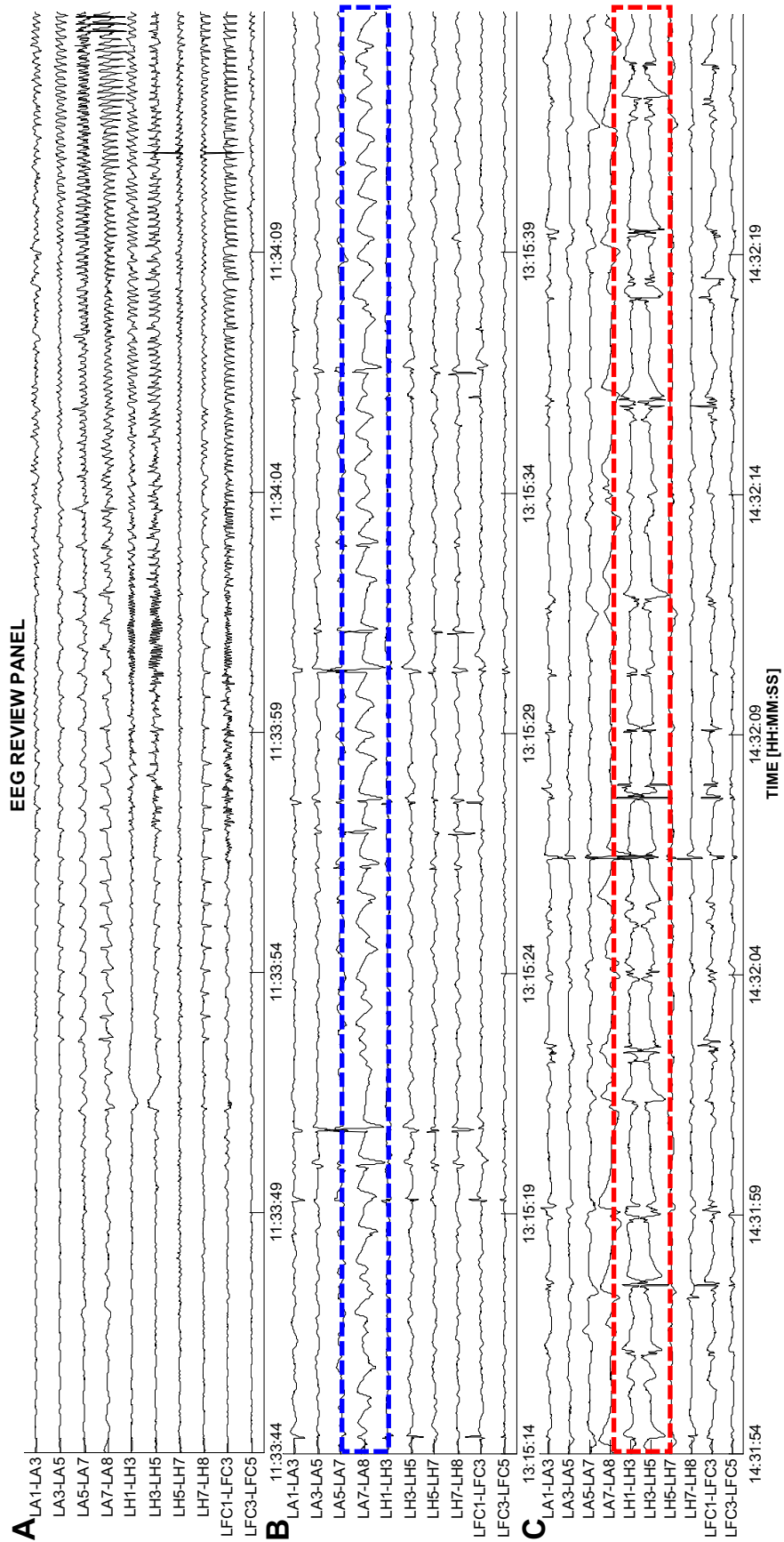


Figure 5.15: EEG corresponding to the events selected from the RSI display in Fig. 5.14. (A) represents a seizure around the time point '1', (B) represents the pre-ictal rhythmic discharge of sharp waves around the time point '2', and (C) represents discharges of sharp wave complexes around the time point '3' in Fig. 5.13, respectively. Each segment represents 30 s of 10 channel EEG.

using CDSA and aEEG was difficult. This is probably due to the fact that seizures in this patient were focal and low amplitude (channel: RH1-RH2 and RC1-RC2). This is consistent with the observations in [5, 191]. As with the CDSA and aEEG, detection of seizures with no or minimal change in the EEG amplitude ($< 20 \mu\text{V}$) is also challenging for the RSI display. However, RSI is still able to clearly and accurately highlight the epileptogenic sites, i.e., channels with profoundly increased sharp activity (confirmed by the EEG review) than the comparison displays. Increased sharp activities are often associated with regions involved in the seizure generation [190]. Therefore, this information may be clinically vital in the identification of neuronal areas involved in the seizure generation. In Patient 1, we observed such activity to be present, predominantly and consistently in all seizure EEG sections on the channels LA7-LA8, LFC1-LFC3 and LE2-LE3 (see Fig. 5.14) that disappears at the seizure onset. The corresponding raw EEG of such an activity is shown in Fig. 5.15B (obtained around the time instant shown by arrow '2' in Fig. 5.14). In this patient, RSI display also reveals increased sharp activity on other sites as well (channel: LH1-LH3, LH3-LH5 and LH7-LH8). Figure 5.15C depicts an example of such activity (around the time instant shown by arrow '3' in Fig. 5.14). Similarly, in Patient 2, such sharp activity predominantly occurs only on two specific channels (RH1-RH2 and RC1-RC2) as seen in Fig. 5.16 (RSI display). CDSA display also confirmed presence of such activity but not the aEEG display (not shown).

A compressed display is advantageous in the EMUs when timely intervention becomes important on seizure detection to prevent secondary brain damages [5, 38, 39, 192]. The main limiting factor of the compressed display is the display-size complexity [38, 193]. In CDSA and aEEG, the spatio-temporal resolution of the display decreases with an increase in the number of channels and the duration of monitoring, making the interpretation very difficult. On the contrary, an increase in the number of channels minimally affects the RSI display. This effect can be seen on the multichannel

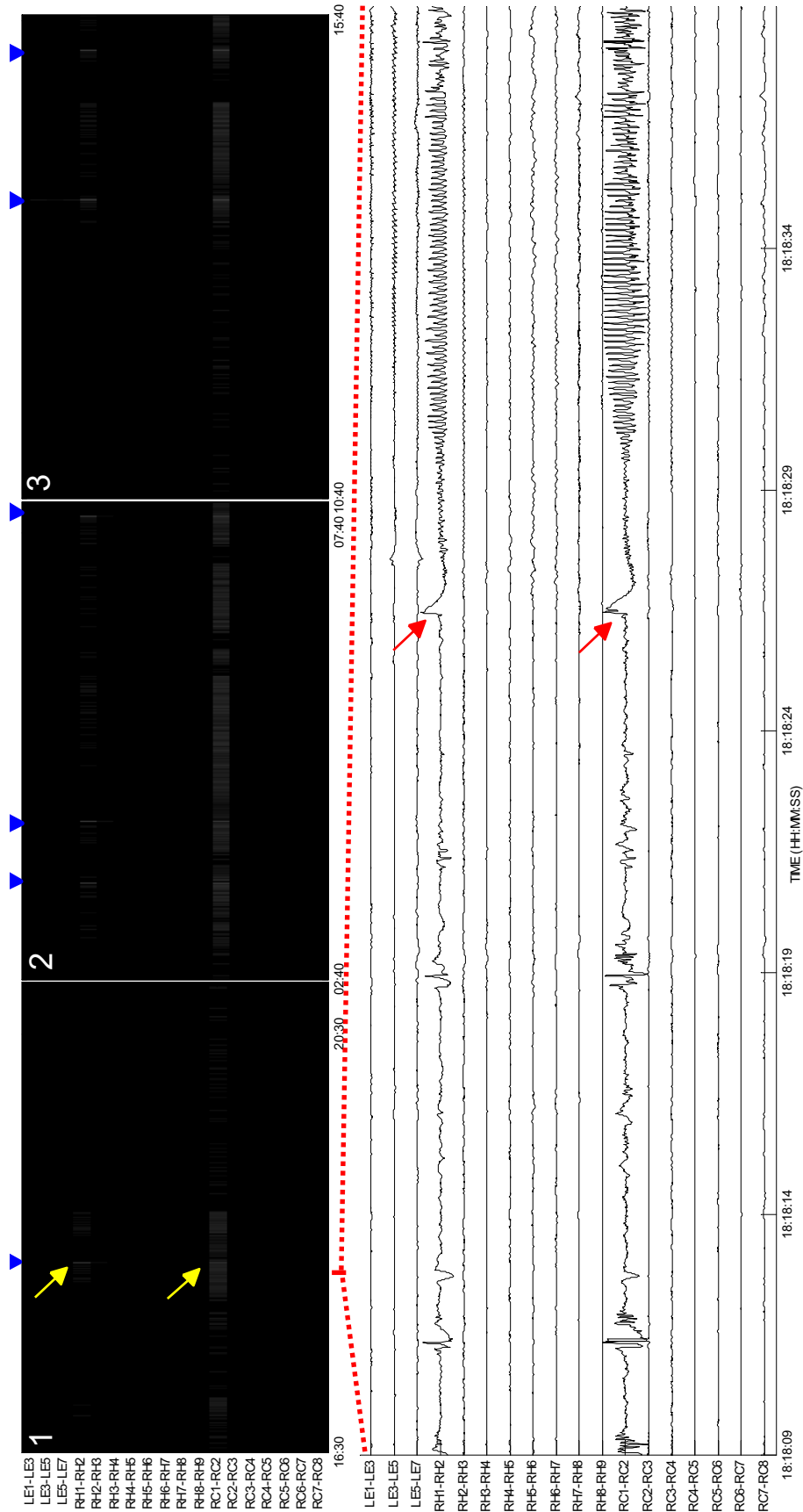


Figure 5.16: Example of 18 channel RSI display for Patient 2. The RSI display represents 16 h of data in three segments (1, 2, and 3), and contains a total of six seizures. Downward pointing 'blue' arrows denote EEGer identified seizures. EEG review panel displays 30 s of an event selected from RSI display for segment #1.

compressed display in Fig. 5.14. An added advantage of the RSI display is that it is easy-to-interpret, and hence can be used by experienced as well as inexperienced staff to monitor and flag ongoing or ensuing abnormalities.

5.7 Summary

In this chapter, we have evaluated the performance of three new NPS systems proposed in Chapter 4 and compared against the three popular NPS systems from the literature on the MNI test dataset. We have selected one of the new NPS systems and one of the comparison NPS systems to make a head-to-head comparison on a completely blind test data.

Among the new NPS systems, the morphology and eSD systems both outperformed the comparison NPS systems in terms of sensitivity as well as specificity on the seven patients single-channel MNI test dataset. Furthermore, the morphology system and the Grewal-Gotman system were selected for further performance assessment on a completely blind test data (FSP database). The FSP database consists of 21 patient intracranial EEG recordings that were recorded using a different EEG system with a different sampling rate and included varied types of electrodes (depth, grid and strip electrode). The morphology system does not require any *a priori* knowledge of patient-specific seizures. It is based on quantifying the morphology of the EEG waveform. The method does not require a background EEG in computing the 'sharpness' feature, which improves the overall computational cost, and the results do indeed show an improvement in the sensitivity and specificity on the FSP database. The performance suggests that the morphology system can be clinically useful in the review of long-term depth EEG recordings.

The chapter also described a clinical tool for the EMU, aimed to rapidly review prolonged recordings, and to identify epileptogenic sites by a novel multichannel

compressed (RSI) display. The new RSI display is compared for computational, interpretation and display complexities against two popular digital trending tools from the literature. The RSI display has been shown to be easy-to-interpret compared to the compressed EEG displays for multichannel prolonged intracranial EEG recordings.

Chapter 6

A New Model-Based Patient-Specific Seizure Detection System

6.1 Introduction

Patient-specific (PS) seizure detection systems are those that allow the recognition of recurring seizure patterns tailored for individual patients. It is based on the observations that one or two, and sometimes even more types of seizures, tend to occur repeatedly within a patient. To build such a system, experts utilize the knowledge of previously identified seizure and non-seizure EEG to train a classifier for the given patient. The trained classifier for the given patient is used to detect similar seizures in all subsequent EEG recordings/monitoring. Even though PS systems report significantly improved detection performance over the NPS systems, they are at present, impractical due to (a) supervised selection of the seizure pattern that serves as the template pattern, (b) supervised selection of the non-seizure EEG (or a set of non-seizure EEG patterns), and (c) supervised training of the classifier. It is believed

that removing the latter two dependencies would lead to a more practical solution in the design of PS systems.

In Chapter 1, we introduced the framework of a fully automatic PS system that aims to address the existing challenges in the seizure detection by combining the NPS and PS systems. New computationally light NPS systems were developed in Chapter 4 and 5 for this framework. In this chapter, we develop a new PS seizure detection system that eliminates the need for supervised selection of non-seizure data and for the supervised training of the classifier. Such a PS system is able to detect recurring seizure patterns of non-equal duration. The new PS system builds a seizure model for a previously identified seizure that can be used with the statistically optimal null filter (SONF) for subsequent detection of similar seizures [37, 134, 135, 194]. The performance of the new PS system is evaluated on the 304 h of single channel EEG obtained from 14 patients of MNI database and is compared with the clinically used PS system proposed by Qu and Gotman [21].

6.2 Problem Formulation

We assume seizure to be a narrow-band signal in comparison to the disproportionately large background EEG and define the problem as the detection of rhythmic narrowband seizure activity, $s(n)$, from the observed EEG consisting of signal and noise, $x(n) = s(n) + n(n)$. It is important to note that the rhythmic narrowband seizure activity evolves as the seizure progresses over time. In other words, a seizure is composed of short piecewise stationary rhythmic discharges that change from one rhythm to another as the seizure progresses. Figure 6.1 illustrates the temporal progression of a seizure in short piecewise stationary rhythms. The problem can be re-defined as the detection of these narrowband piecewise stationary rhythms, i.e., the template seizure, $s(n)$, consisting of a set of components, $s_1(n), s_2(n), \dots, s_N(n)$, with a specific order of

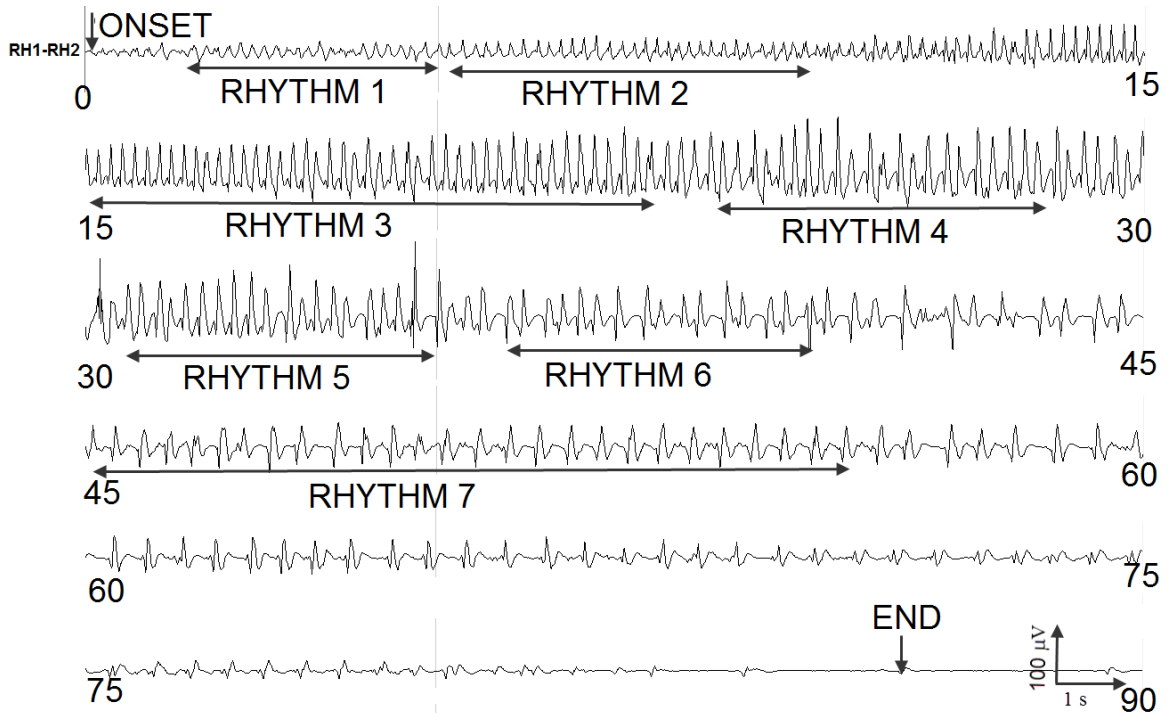


Figure 6.1: The example illustrates temporal evolution of a seizure which is observed as piecewise stationary rhythms. This example encapsulates a 90 s single channel EEG (channel: RH1-RH2) of a patient, which is considered as the template pattern in this patient. The piecewise stationary rhythms (template epochs) in the template pattern are enumerated and is obtained by the proposed STFT-based adaptive segmentation algorithm.

temporal occurrence.

The proposed PS seizure detection system must be capable of

1. detecting the seizure components (piecewise rhythms) of non-equal duration, and
2. quantifying the time-order sequences of the occurrence of these components for the final seizure detection.

We aim to address these challenges by a new PS system that is computationally light, generates a seizure model and maps the time-ordered occurrence of the seizure components in order to make an accurate detection. To address the existing challenges listed above, the new PS system must utilize techniques that estimate seizure components from the observed EEG ensuring maximal separation between the two categories:

seizure and non-seizure. We select statistically optimal null filters (SONF) for the proposed model-based PS system. The use of SONF is a novel approach for the problem of enhancement/suppression of narrowband signals of short-record length based on combining maximum signal-to-noise ratio (SNR) and least-square optimization criteria [170, 172]. Its intrinsic property is the ability to track signals rapidly leading to a more practical processing of short-duration signals and has been shown to be equivalent to the well-known Kalman filter, but with a much simpler implementation [195-199]. SONF is a linear time-varying filter, and can be implemented as a number of parallel filters. Thus, SONF becomes an obvious choice for processing time-varying, narrowband seizure components that may lead to a practical PS system. However, SONF requires *a priori* knowledge of the signal components or the basis functions constituting the signals to be estimated.

In the proposed PS system, the first step involves partitioning the seizure signal $s(n)$ into a set of piecewise stationary seizure components, $s(n), s_2(n), \dots, s_N(n)$. Here, an *a priori* known seizure is considered as the template seizure pattern T_{PAT} , the piecewise stationary segments as seizure components or epochs, and the unknown seizures for a given patient as the candidate seizure pattern (C_{PAT}). The second step involves extracting ' k ' non-redundant rhythmic components of T_{PAT} that constitute the set of '*template epochs*'. The third step involves identifying the composing basis functions for each template epoch that are required to implement the SONF. The seizure model is a set of basis functions for each of the k -template epochs. Finally, the PS classifier is trained using T_{PAT} and the derived seizure model. The trained PS system is employed to detect narrowband template epochs in all subsequent data. The tracking of the time-ordered occurrence of k -template epochs is possible by a parallel implementation of the SONFs, where each of the SONFs corresponds to a different template epoch of T_{PAT} . That is, at any given time only one SONF will track a template epoch. By tracking the time-ordered estimation of the components by the

SONF, it is possible to identify the subsequent seizures with similar characteristics. An added advantage of this detection strategy is the ability to minimize the detection of non-epileptic rhythms that have similar rhythmic characteristics as T_{PAT} , but not the time-ordered component occurrence. This is due to the fact that the dominant rhythm of an epileptic seizure evolves in short bursts as shown in Fig. 6.1, while normal EEG rhythms do not typically evolve. The non-epileptic rhythms include the non-ictal rhythmic discharges such as the alpha rhythms, mu rhythms, lambda waves, sleep spindles, and sub-clinical rhythmic discharges (SREDA) [5, 134].

6.3 Model-Based Seizure Detection

The block diagram of the proposed PS system is shown in Fig. 6.2, and consists of the blocks: (a) pre-processing and artifact rejection, (b) seizure model, (c) SONF, (d) detection criterion (energy ratio), and (e) evolution-based classification. SONF is used to estimate the seizure waveform (rhythmic components) from the observed EEG. If the observed EEG contains the same type of seizure as described by the *a priori* known model, the output of the SONF will represent an estimate of the seizure $\hat{s}(n)$. In this case, the energy ratio γ between the seizure estimate $\hat{s}(n)$ and the observed EEG $x(n)$ should be large; conversely, if the EEG contains no seizure ($x(n) = n(n)$), then the SONF output should be near zero with little energy. The energy ratio in this case will be small. Thus, the energy ratio γ of the seizure estimate $\hat{s}(n)$ and the observed EEG $x(n)$ can be used as a metric to decide whether the input EEG contains a seizure or not [132]. In terms of k -parallel SONFs, one for each of the k -template epochs, the energy ratio γ_k of the estimate of the k th template epoch, $\hat{s}_k(n)$, and the observed EEG $x(n)$ is used as a metric to decide whether the input EEG contains the k th template epoch or not. The time-ordered sequence in which the template epochs occur in the T_{PAT} and C_{PAT} are matched to determine whether the T_{PAT} and C_{PAT}

are similar or not.

As previously mentioned, the first step in building the seizure model involves segmenting the template seizure pattern (T_{PAT}) into stationary epochs (piece-wise stationary rhythms as seen in Fig. 6.1). The first 60 s of *a priori* known seizure or the complete seizure, if it lasts less than 60 s, is considered as the T_{PAT} . Short-time Fourier transform (STFT)-based segmentation algorithm is developed to partition the T_{PAT} into quasi-stationary segments or epochs [37, 167, 169]. Redundant epochs (epochs with similar characteristics) reduce the robustness of the classifier while increasing the computational load. Therefore, we incorporate an unsupervised clustering scheme to identify and reject similar epochs as well as epochs that may be due to noise. This results in disjoint, noise-free, non-redundant epochs that are utilized for building the seizure model, and are referred to as 'template epochs'. Seizure model is a set of orthogonal basis functions (required in the SONF) that represent the dominant rhythm of each template epoch, e.g., each rhythmic epoch of the seizure in Fig. 6.1. The data is processed in short segments (test epochs) that slide in small steps (step-size = 0.25 s). A small step-size allows tracking subtle changes in the EEG. The epoch length ranges from 2 to 6 s, determined by the segmentation algorithm [37]. The following sections describe each block of Fig. 6.2 in detail.

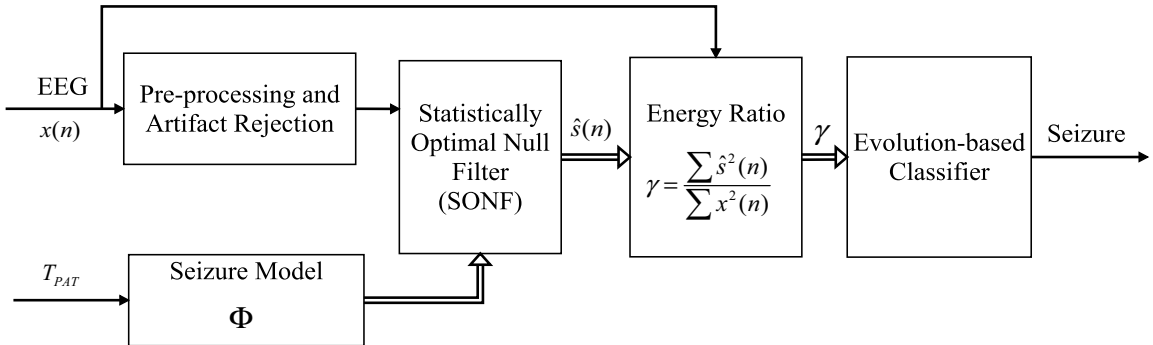


Figure 6.2: Model-based PS seizure detection scheme. $x(n)$ = observed EEG, T_{PAT} = template seizure pattern, Φ = seizure model (basis functions) derived from template seizure pattern, $\hat{s}(n)$ = estimated seizure waveform, γ = detection metric

6.4 Pre-processing and Artifact Rejection

As discussed previously in Chapter 4, intracranial EEG is relatively free from artifacts as compared to the scalp EEG, but spans a wider frequency spectrum, has a highly variable seizure morphology and a variety of sharp wave complexes, ranging from needle-like fast activity to much slower discharges [5]. Generally, most of the seizure activity is reported to be dominant in 3-30 Hz band [31, 102]. Therefore, we employ a 5th order Butterworth low-pass digital filter (cut-off frequency $f_c = 30 Hz$) to remove unwanted high frequency interferences as was done in Chapter 4 for NPS systems. High-amplitude and iso-electric artifacts are also addressed in a manner similar to what was done in the NPS systems.

Since the SONF has properties similar to the recursive least-square (RLS) estimation technique, it is expected that it may not work well for data that contains randomly occurring data points with extreme values. That is, the tracking capability of the SONF may be impaired or reduced in the presence of sporadically occurring high-amplitude transients. Such high-amplitude transients need to be suppressed before estimating the desired signal by the SONF. We employ the idea of *instantaneous matched filter* (IMF) proposed by Agarwal *et al.* [195-199] as a key building block in the SONF to identify and suppress instantaneous time-points of high-amplitude transients within each processing epoch. If a matched filter (MF) is used to detect the signal at any given time, then at the output we obtain a signal that provides the maximum output signal-to-noise ratio (SNR_o), for the considered time interval - 0 to n . Because the time interval or frame of observation is continually increasing, at each considered time instant, the MF provides a new output signal and a new SNR_o , and hence it is termed the *instantaneous matched filter* [197, 199]. Figure 6.3 depicts the IMF.

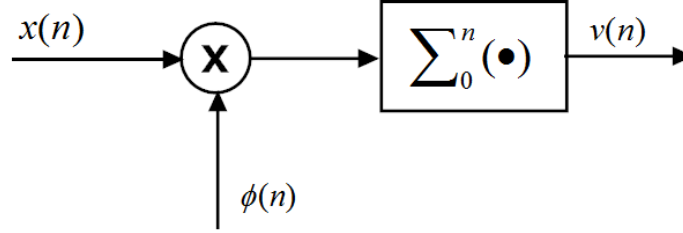


Figure 6.3: Instantaneous matched filter

The IMF provides at each instant of time the maximum SNR_o at the output, $v(n)$, and the effect of sporadically occurring high-amplitude transients on $v(n)$ is seen as sudden jumps or shifts. An example illustrating an input signal $x(n)$ contaminated with such artifacts (encircled areas) and estimated output $\hat{s}(n)$ without any artifact rejection from the SONF is shown in Fig. 6.4A. The corresponding IMF output is shown in Fig. 6.4B, which reflects (encircled areas) sudden jump due to the presence of transients. Examining $v(n)$ can assist in identifying the time-instances in the input signal, where these artifacts occur. As IMF provides maximum SNR_o at the output, it is expected that a continual increase (linear) in the IMF output is observed. We first remove such trends in the $v(n)$ by taking the first order difference of the $v(n)$ time series.

$$w(n) = v(n) - v(n - 1), \quad (6.1)$$

where $v(n)$ is the output of the IMF and $w(n)$ is the first-difference series. The new time series $w(n)$ is examined to identify the considerably dissimilar points with respect to the remaining data. Chebyshev's inequality is employed to determine a lower bound of the percentage of data that is within b number of standard deviations from the mean [134, 200]. In the case of data with normal distribution, it is known that about 95% of the data will fall within two standard deviations from the mean.

When data distribution is unknown, Chebyshev's inequality, given by

$$P(|W - \mu| \leq b\sigma) \geq (1 - \frac{1}{b^2}) \quad (6.2)$$

can be used, where W represents a random variable of the detrended $w(n)$ of unknown distribution with the expected mean, μ , and variance σ^2 . The number of standard deviations from the mean is represented by b that gives a lower bound for the percentage of data that is within a certain number of standard deviations from the mean. Equation (6.2) can be re-arranged to focus on the amount of data away from the mean, and is given by

$$P(|W - \mu| \geq b\sigma) \leq (\frac{1}{b^2}). \quad (6.3)$$

Assuming that a relatively small percentage of outliers (high-amplitude transients) exists in the input $x(n)$, then outliers are the sample points outside the boundary, $b\sigma$, due to the high amplitude transients [134, 200]. The amplitude of the corresponding sample points in the input signal are attenuated by empirically determined factor of 75 % [134, 135]. The resulting non-linearly modified signal is used as the input to the SONF. Figure 6.4 represents the non-linearly modified input signal $x(n)$ along with its estimate $\hat{s}(n)$ by the SONF. The corresponding IMF output is shown in Fig. 6.4D which clearly reflects the suppression of the transients present in $x(n)$.

6.5 Seizure Model

The fully automated process of modeling T_{PAT} involves

- Segmentation of T_{PAT} into piecewise stationary segments.
- Identification and rejection of redundant epochs resulting from the segmentation of T_{PAT} .
- Modeling of each remaining template epoch.

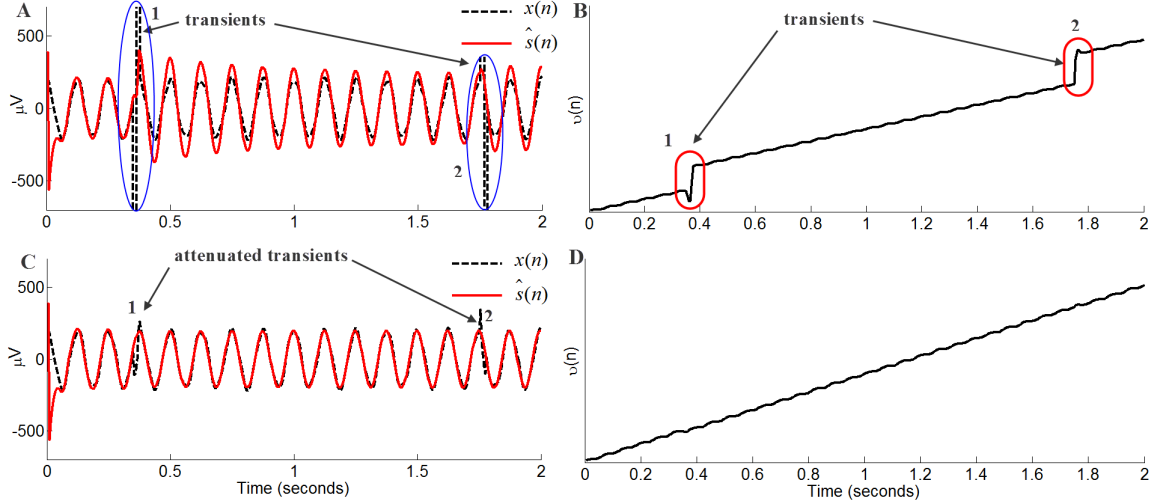


Figure 6.4: An illustration of impact of high-amplitude transients on the tracking ability of the SONF. (A) depicts the input signal $x(n)$ containing two sharp transients labeled as 1 and 2 (enclosed by the ellipse) along with its estimate $\hat{s}(n)$ using SONF, and (B) represents the corresponding IMF output ($v_i(n)$). (C) represents the sharp transients attenuated input signal $x(n)$ along with the its estimate $\hat{s}(n)$ using SONF, and (D) represents the corresponding IMF output ($v_i(n)$).

6.5.1 STFT-based Segmentation

The first step in modeling the template pattern (T_{PAT}) involves partitioning T_{PAT} into disjoint stationary epochs corresponding to the piece-wise stationary rhythms. In the original work of Shi *et al.* [132], the template seizure pattern was visually segmented into 6 s non-overlapping epochs. Since a fixed length of the epochs may not be ideal for all types of seizures, we determine the length of the epochs using adaptive segmentation. The segmentation process is automated by introducing a short-time Fourier Transform (STFT)-based segmentation technique to identify the stationary sections [36, 135]. The Fourier transform of the template pattern is computed for sliding data frames of 2 s with a step size (τ) of 0.25 s. The dominant rhythm frequency F_m in each data frame is defined as the frequency with maximum power in the discrete Fourier transform (DFT), $X(f)$, and m denotes the frequency index with the maximum power. The resulting set is a new discrete time series of the dominant frequency with a sampling interval of τ as shown in Fig. 6.5B. The changes in the

dominant rhythm of T_{PAT} are observed as a change in $F_m(\tau)$. The points of change in the dominant frequencies are identified as segmentation boundaries given by

$$g_\tau = |F_m(\tau) - F_m(\tau - 1)| < \Delta, \quad (6.4)$$

where $\Delta = 0.25$ is the tolerance threshold defined as the maximal allowable change in two consecutive F_m samples [36, 135].

Segmented epochs shorter than 2 s are rejected. By doing so, we retain only the epochs with sustained dominant rhythm. The length of the final basis functions is set as the average duration of all identified epochs. The length of the sliding test window required in the SONF is set to the length of the basis functions.

In the example of Fig. 6.5, T_{PAT} is segmented into a set of seven stationary epochs ($p = 7$), $E = \{E_1, E_2, \dots, E_7\}$. Some epochs in this set represent the same dominant rhythms, that is, epochs E_1 and E_2 , E_3 and E_4 , and E_5 , E_6 and E_7 shown in Fig. 6.5B have the same dominant rhythm. Computational cost in the PS system can be reduced by rejecting redundant epochs prior to constructing the basis functions. Additionally, in some complex template seizures, it is possible that some of the epochs resulting from the segmentation algorithm are due to background noise. Such epochs must also be eliminated prior to the construction of the seizure model.

6.5.2 Rejection of Artifacts and Redundant Epochs in T_{PAT}

A simple approach to keep only one of the several epochs with the same dominant rhythm is possible by examining the dominant frequency. Alternatively, cross-validation techniques can be explored to identify and reject redundant epochs. We use the latter method to identify and reject redundant epochs. The idea is to use the p th template epoch to derive a model for use in the SONF to process the remaining $(p - 1)$ template epochs. The classifier of the p th template epoch is trained using the p th epoch and

model derived for the SONF and tested on the remaining $(p - 1)$ epochs. All of the epochs detected by the p th model are observed to be similar. The epoch with the highest energy ratio is retained as one of the template epochs to model the seizure. The process is repeated until all the epochs are unique. An epoch due to noise consists of a mixture of frequencies without any sustained rhythm; the model derived using such epochs will fail to detect the epoch itself. These epochs are therefore rejected from further considerations [134, 135].

The resulting k epochs are disjoint, noise-free and non-redundant, and are utilized to build the final seizure model. As seen in the example of Fig. 6.5, segmentation of T_{PAT} resulted in seven stationary epochs ($E = \{E_1, E_2, \dots, E_7\}$) of which only three epochs are unique ($k = 3$). These three disjoint template epochs are utilized to build the final seizure model that uses 3-SONF branches, one SONF for each template epoch.

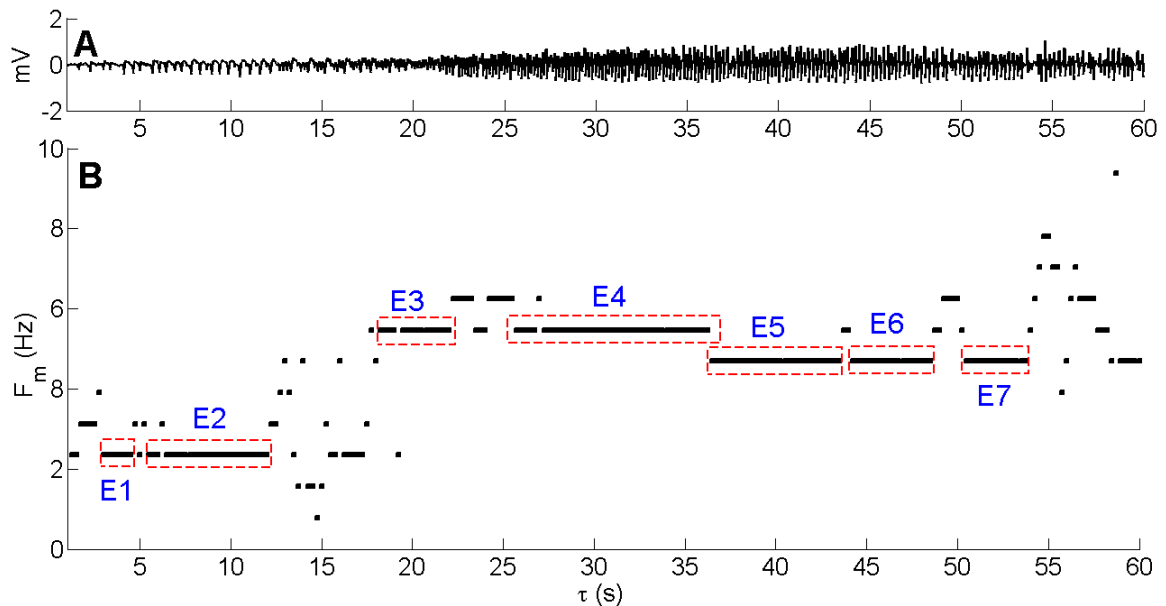


Figure 6.5: STFT-based segmentation of T_{PAT} . The 60 s long template seizure pattern (T_{PAT}) is shown in (A) along with evolution of dominant (peak) frequency F_m obtained from Fourier transform in (B). The dashed-boxes represent the stationary epochs identified by the adaptive segmentation algorithm in the T_{PAT} , and are labeled E_1, E_2, \dots, E_7 .

6.5.3 Modeling of T_{PAT} Epochs

In using the SONF, an orthogonal linear expansion of the signal to be estimated is required. The basis functions in this expansion constitute the model for the signal. We, therefore, consider representing an EEG rhythm (template epoch) in terms of a linear combination of sinusoids, which is the one of the more popular approaches employed in signal analysis. One approach of constructing basis functions to model the template epochs in the wavelet domain is proposed in [132]. In this method, each template epoch is decomposed into wavelet scales in 3-25 Hz band. At the sampling rate of 200 Hz, scales 3, 4, 5 corresponds to the 3-25 Hz band. The scale contributing maximum energy is selected and peak frequency in the spectrum of the selected scale signal is used to construct the sinusoid. Since the phase information is unknown, the Hilbert transform is also required. This approach of constructing the basis functions is limited by the sampling rate at which the EEG is digitized. We propose three additional techniques of modeling the template epochs [36, 134, 135].

- *Sinusoidal Basis Function (SBF)* [36, 134, 135]: The first and second dominant frequencies corresponding to the two largest peaks in the power spectrum of the template epochs are selected and modeled by sinusoids. Hilbert transforms (quadrature component) of the sinusoids of the selected frequencies are also considered since the phase of the input is unknown.
- *Harmonic Basis Function (HBF)* [135]: It is observed that power spectral density of some template epochs consists of dominant peaks as well as their harmonic components. As with the SBF method, the first and second dominant frequencies corresponding to the largest peaks in the spectrum are selected to formulate the basis functions. Additionally, the harmonics of the two dominant rhythms are also identified. Sinusoids corresponding to the frequencies of the two dominant rhythms and their relevant harmonic components (and their Hilbert transform)

are used as the basis functions to model each template epoch.

- *Ratio-spectrum Basis Function (RBF)* [128, 135]: In this approach, the ratios of the power spectral densities of the template epochs and the background EEG are taken to highlight the dominant seizure frequencies. The dominant frequencies resulting from the ratio-spectrum are selected and modeled using the SBF approach. The reference EEG is the 30 s of background EEG preceding the template seizure pattern.

Of the three, the model that best represents T_{PAT} is selected to identify similar seizures in the remaining data. Selection of the best model representing T_{PAT} is described in the classifier training section. The main building block of the model-based PS seizure detection is the SONF, which is described in the next section.

6.6 Statistically Optimal Null Filter

The use of statistically optimal null filter (SONF) was proposed by Agarwal *et al.* [195-199] for the enhancement/suppression of narrowband signals, and is based on combining the maximum output signal-to-noise ratio (SNR_o) and the least-square (LS) optimization criteria. SONFs are obtained by scaling the output (optimal in the maximum output SNR ratio sense) of the instantaneous matched filter (IMF). Its intrinsic property is the ability to track signals rapidly leading to a more practical processing of short-duration signals. It has been shown that SONF is equivalent to the well-known Kalman filter, but with a much simpler implementation [195-199].

In the SONF-based estimation of a signal with unknown shape, we assume that the desired signal $s(n)$ can be represented as a linear combination of *a priori* known set of orthogonal basis function, $\{\phi_i(n), i = 1, 2, \dots, N\}$, i.e.,

$$s(n) = \sum_{i=1}^N a_i \phi_i(n) \quad (6.5)$$

where a_i are the unknown scaling variables.

In a model-based PS system, T_{PAT} represents the signal $s(n)$ of interest that is to be estimated, and consists of k -narrowband components, $s(n) = \{s_1(n), s_2(n), \dots, s_k(n)\}$, in a specific-time ordered sequence. We consider implementing k -parallel SONF branches, one for each template epoch as shown in Fig. 6.6. The k th epoch can be represented as $s_k(n) = \sum_{i=1}^N a_{ik}\phi_{ik}(n)$. The signal $s_k(n)$ in the presence of additive white Gaussian noise (AWGN) can be estimated by the SONF with \mathbf{N} parallel branches – one corresponding to each term in the expansion of $s_k(n)$, as shown in Fig. 6.6B.

Since only one seizure component $s_k(n)$ can occur at any given time, then at the l th time instance, the input mixture $x_k(n)$ to the SONF can be written as

$$x_k(n) = s_k(n) + n(n), \quad (6.6)$$

$$= \sum_{i=1}^N a_{ik}\phi_{ik}(n) + n(n). \quad (6.7)$$

The output of the i th IMF in Fig. 6.6 is,

$$v_{ik}(n) = \sum_m^N x_k(m)\Phi_{ik}(m), \quad (6.8)$$

$$= \sum_m^{n-1} x_k(m)\phi_{ik}(m) + x_k(n)\phi_{ik}(n), \quad (6.9)$$

$$= v_k(n-1) + x_k(n)\phi_{ik}(n), \quad (6.10)$$

scaled by $\lambda_k(n)$'s (obtained through LS optimization) to produce the estimate of the desired seizure signal (Fig. 6.6B),

$$\hat{y}_k(n) = \sum_{i=1}^N \lambda_{ik}(n)v_{ik}(n), \quad (6.11)$$

and

$$s_k \hat{\nu}(n) = \sum_{i=1}^N y_{ik} \hat{\nu}(n) \quad (6.12)$$

The above can be summarized in general vector notation (without any subscript) as,

$$\lambda(n) = [\lambda_1(n) \lambda_2(n) \lambda_3(n) \dots \lambda_N(n)]^T$$

$$\nu(n) = [\nu_1(n) \nu_2(n) \nu_3(n) \dots \nu_N(n)]^T$$

$$\Phi(n) = [\phi_1(n) \phi_2(n) \phi_3(n) \dots \phi_N(n)]^T$$

where $\lambda(n)$, $\nu(n)$ and $\phi(n)$ are the post-IMF scaling functions, output of the IMF and the set of known basis functions, respectively. The complete recursive algorithm for implementing the SONF for the k th branch of Fig. 6.6 can be written as

$$\nu_k(n) = \nu_k(n-1) + x(n)\Phi_k(n)$$

$$P_k(n) = P_k(n-1) - \frac{P_k(n-1)\Phi_k(n)\Phi_k^T(n)P_k(n-1)}{1 + \Phi_k^T(n)P_k(n-1)\Phi_k(n)}$$

$$\lambda_k(n) = P_k(n)\Phi_k(n)$$

$$\hat{s}_k(n) = \nu_k^T(n)\lambda_k(n)$$

The gain matrix $P(n)$ is initially chosen to be positive-definite. As a general rule, one may choose $P(0) = SNR \bullet I$, where I is the identity matrix of order N and $\nu(0) = x(0)\Phi(0)$. A detailed description of the statistically optimal null filter can be found in [195-199].

6.6.1 Classifier Training

The SONF estimates the desired signal using the model. The output of the SONF is nearly zero except when the input EEG matches the model. That is, the output of the SONF for the k th template epoch is nearly zero except at the time instance where the k th template epoch is present in T_{PAT} . The energy ratio, γ_k , of the k th estimated component and the input signal can be used to discriminate parts of the seizure that are similar to the k th template epoch, and is given by (Fig. 6.7)

$$\gamma_k = \frac{\sum \widehat{s}_k^2(n)}{\sum x^2(n)}. \quad (6.13)$$

The detection threshold for the k th model, δ_k^{th} , is set as 1/3 of the maximum γ_k where the input is the template pattern itself. The strategy for selection of δ_k^{th} is based on the observation on simulated EEG and MNI training dataset. Different values of the thresholds were explored that included maximum γ_k , 1/3rd of the maximum γ_k , 1/2 of the maximum γ_k , and average γ_k at the instance of template epoch. The remaining data for a given patient is evaluated using the SONF at the set thresholds. The threshold that reported best sensitivity and specificity was selected, which was found to be 1/3rd of the maximum γ_k .

6.6.2 Model Selection

In Section 6.5.3, we proposed three techniques for constructing the basis functions for the template epoch. The resulting set of basis functions for the template epoch is known as a model. Model selection involves selecting the model that best represents the template epoch, i.e., the model which results in maximum separation between non-seizure and seizure EEG in the SONF framework. The energy ratio is computed using a model during background EEG (γ^{bkg}) and at the time instances where the model matches the template epoch (γ^{sez}). The Euclidean distances between γ^{bkg}

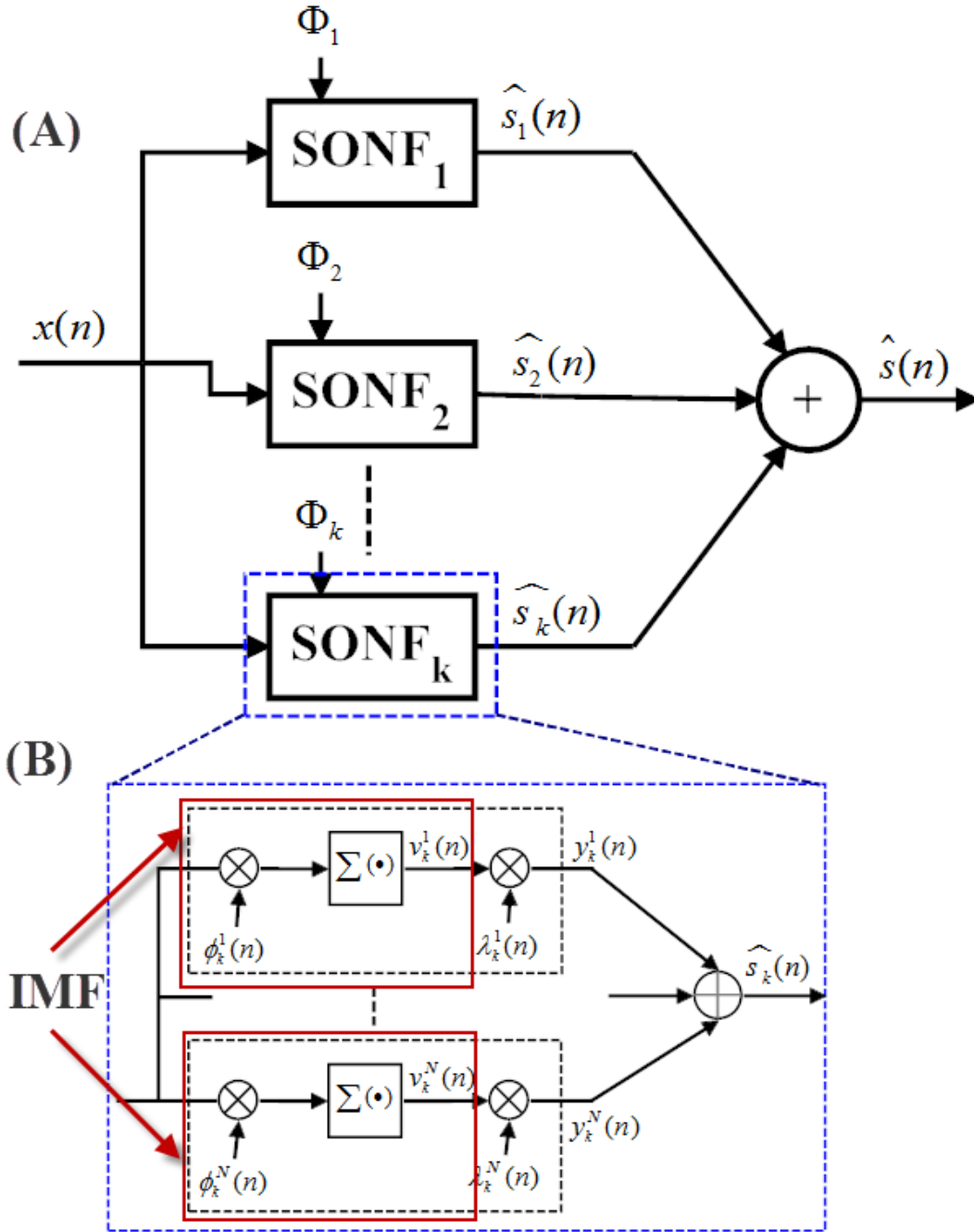


Figure 6.6: Estimation of signal using statistically optimal null filter (SONF). (A) represents block diagram of k -branches of SONF utilized to track the temporal evolution of seizures. Model (basis function) for the template epoch, represented by Φ_k is employed in the SONF to estimate seizure waveform ($\hat{s}(n) = \sum_{i=1}^k \hat{s}_i(n)$) in the input signal $x(n)$. (B) represents the estimation counterpart of the k th discrete SONF.

and γ^{sez} are evaluated using all three models for the template epoch. The Euclidean distance d_{lk} for l th modeling technique for k th template is given by

$$d_{lk} = \sqrt{\left(\frac{1}{N_k} \sum_{n=1}^{N_k} \gamma_{lk}^{sez}(n)\right) - \left(\frac{1}{N_{bkg}} \sum_{n=1}^{N_{bkg}} \gamma_{lk}^{bkg}(n)\right)}, \quad (6.14)$$

where N_k is the length of template epoch, N_{bkg} is 30 s of the background EEG, γ_{lk}^{sez} and γ_{lk}^{bkg} are the energy ratios of the k th template epoch and background EEG obtained using l th modeling technique. Among three models for each template epoch, the one that results in maximal separation between seizure and non-seizure segments as quantified by the metric d_{lk} is selected for the template epoch under consideration.

6.6.3 Evolution-based Classification

One of the primary goals of the PS system is to identify seizure events C_{PAT} that are similar to T_{PAT} . Existing PS systems identify patterns similar to the template patterns, but do not use the sequence of time-ordered occurrence of piecewise rhythmic discharges. In our approach, we track this time-ordered sequence of the occurrence of template epochs that constitute T_{PAT} . By doing so, it is possible to improve the detection specificity. Such a tracking of temporal evolution of the seizure results in a reduction of false detections caused by non-epileptic rhythms that may have matching dominant rhythms with the template epochs of T_{PAT} , but not the time-ordered evolution.

For a given T_{PAT} , the modeling step results in k -disjoint, non-redundant, noise-free template epochs. The sequence of their occurrence is remembered and matched with the time-order sequence of the candidate seizure pattern. This matching of time-sequence within a given time-frame is what we define as the *evolution-based classification*. A seizure similar to the template is detected when the time sequence of the epochs matches T_{PAT} epochs with in a 60 s time-frame.

Figure 6.7 illustrates this novel evolution-based classification approach employed in the proposed model-based PS system. The modeling process resulted in two disjoint non-redundant epochs for the given T_{PAT} . The two template epochs of T_{PAT} are labeled E_1 and E_2 and shown in Fig. 6.7A. Enumerated subscripts denote the time-order in which they occur in T_{PAT} . The power spectral density plot confirms the non-overlapping dominant rhythm of the template epochs (Fig. 6.7B). The model-based PS system for this T_{PAT} consists of two parallel branches of SONF, one for each template epoch. The detection thresholds are set using the model and the training data, as described in the classifier training section (Section 6.6.1). The trained PS system is utilized to detect candidate seizure patterns similar to T_{PAT} . An example of detected C_{PAT} similar to T_{PAT} is shown in Fig. 6.7C. Raw EEG is shown to map the detection by the evolution-based classifier. The energy ratios (γ_1, γ_2) are shown in Fig. 6.7D. The time-sequence of the detected epochs in C_{PAT} is matched to the template epochs of T_{PAT} to make final detection. In this example, the sequential detection of template epoch 1 followed by template epoch 2 matches the sequence of the template epochs in T_{PAT} . The final detection decision is represented by vertical 'dashed' line in Fig. 6.7. In this example, there are two instances where the time-ordered template epochs match. Therefore, there are two detections as indicated by the two dashed vertical lines.

6.7 Performance Evaluation

The performance of the proposed model-based seizure detection system is assessed on the MNI database. The MNI database consists of intracranial EEG recordings from 14 patients that was originally scored based on all channels for another study [32]. We selected the most prominent seizure channel from the multichannel EEG of individual patients for evaluating the performance of the proposed system, as was done for the

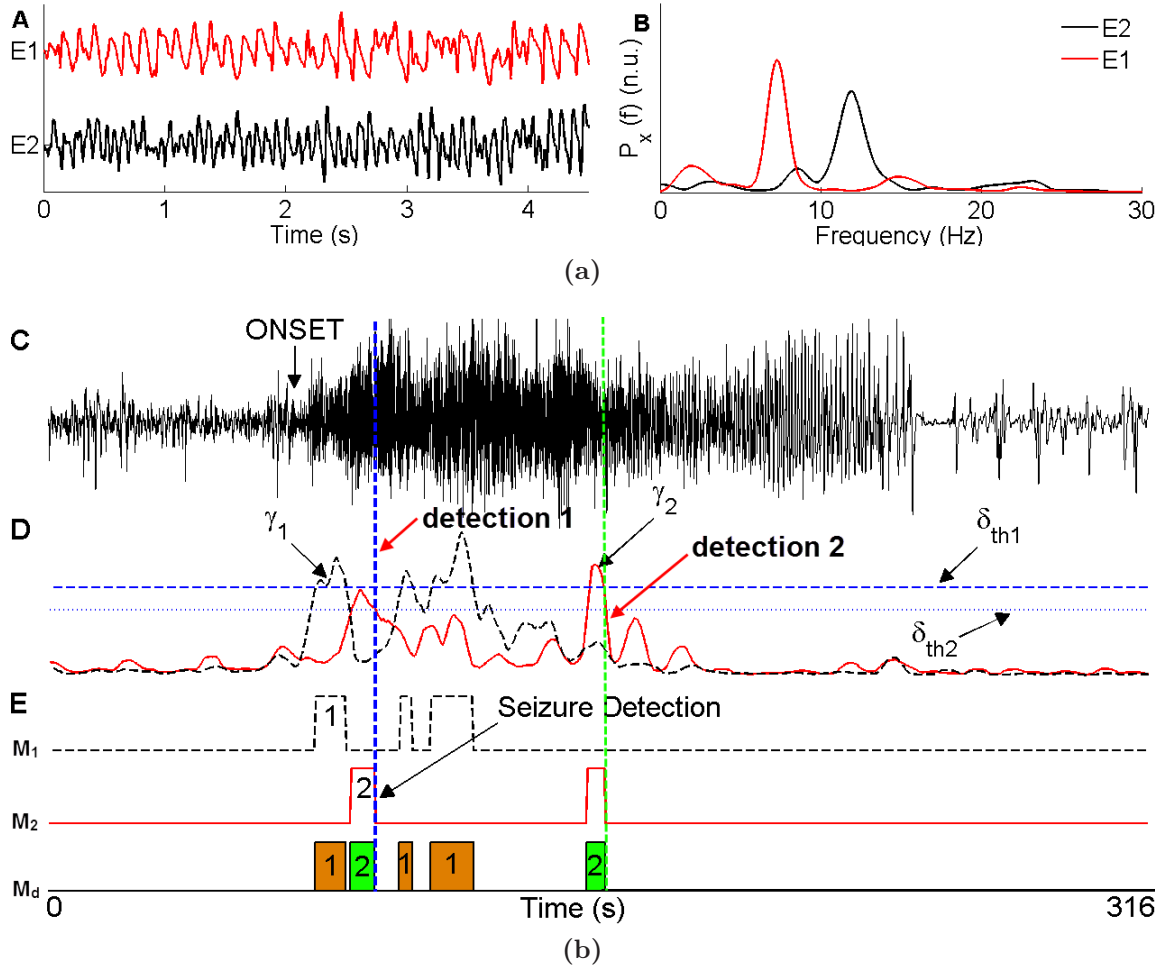


Figure 6.7: Evolution-based classification. (A) represents two disjoint ($k = 2$) template epochs of T_{PAT} along with their power spectral density plot. A candidate seizure pattern C_{PAT} similar to T_{PAT} detected using the seizure model is shown in (B). (C) represents the C_{PAT} and (D) the energy ratios γ_k for the k -SONF branches (one model for each template epochs), and (E) depicts detection by the individual SONF branches. The 'number' represents time-order in which the template epochs constitute the $T_{PAT} = \{E_1, E_2\}$ that are examined by the evolution-based classifier to make a detection. The vertical 'dashed' line denotes the final detection of an event similar to T_{PAT} .

NPS systems in Chapter 4. For each patient, the first occurring seizure is used as the *template* seizure pattern (T_{PAT}) for the training of the proposed PS system. The training data includes 30 s of EEG preceding the seizure template. The trained PS system is used to detect all other seizures that are similar to the template seizure for the given patient. Same template seizure pattern is used to train the Qu-Gotman system which, in addition, requires a minimum of 30 minutes of non-seizure EEG. We selected 30 min section of non-seizure EEG preceding the template pattern. The background EEG in some patients included one or two patient-disconnection artifacts. The background EEG is visually inspected for such artifacts. When the background EEG contains these artifacts, additional seizure-free EEG data is added to compensate the disconnection artifacts. In all 14 patients, we did not find any manually scored seizures within the 30 min seizure-free section preceding T_{PAT} for the Qu-Gotman system. For both the methods, the training data consisted of the first seizure in each patient (14 template seizures) and the test data included the remaining 4 sections of data for each patient consisting of a total of 68 seizures in the 304 hours of single channel EEG for the 14 patients. We used hold-out validation technique in evaluating the performance of the proposed and Qu-Gotman systems. The test data for each patient included all EEG sections except the training sections. That is, the test and training data are mutually exclusive or do not overlap.

A good detection in the proposed system is an event that is detected within 60 s of the manually scored seizure onset. Prior to performance evaluation, detections within 30 s of one another were grouped as a single detection. We evaluate the Qu-Gotman system [21] using the same dataset and the same criterion. The performance is assessed by the three popular measures in the seizure detection literature: sensitivity, specificity, and false detection rate (FDR), described in Chapter 3.

6.8 Results

Results of the proposed PS system and the Qu-Gotman system for the individual patients on the test data are shown in Table 6.1. The model-based PS system resulted in an overall 100% specificity (FDR = 0/h) and 92.2% sensitivity. Qu-Gotman system resulted in an overall specificity of 66.6%, sensitivity of 93.7% and a FDR of 0.2/h. The new PS system reflects a significant improvement (approximately by 33%) in the specificity when compared to the Qu-Gotman system, but at the cost of a 2% drop in the sensitivity.

6.9 Discussion

The main goal of the patient-specific seizure detection system in the EMU is to identify reproducible phenomena that characterize epileptic seizures. The advantage of a PS system is that it improves the detection sensitivity and reduces the false detection rate. The proposed model-based PS system significantly improves the detection specificity resulting in no false detection, while the Qu-Gotman system resulted in a FDR of 0.2/h on the same dataset. Clearly, our method outperforms the popular Qu-Gotman system.

Although the existing patient-specific seizure detectors show improved sensitivity and FDR over the generic methods, they are not practical. The main limiting factors are (a) selection of the template seizure pattern, (b) selection of the background EEG, and (c) supervised training of the classifier. We have overcome these challenges by using a novel model-based scheme with SONFs as the building blocks, which can rapidly track narrowband signals buried in noise [195, 197]. Adaptive modeling and unsupervised classifier training are some of the key attributes of this new system. Unlike the multiresolution-based detectors, our PS system is not limited by the sampling rate. Additionally, seizures with minimal change in the EEG amplitude are

Table 6.1: Detections of the Proposed and Qu-Gotman Systems

Patient	Channel	Hours	TPE	Proposed System						Qu-Gotman System					
				TP	FP	FN	SN (%)	SP (%)	FDR (/h)	TP	FP	FN	SN (%)	SP (%)	FDR (/h)
1	LH1-LH3	20	9	9	0	0	100	100	0	9	2	0	100	81.8	0.1
2	LFC1-LFC3	17.3	4	4	0	0	100	100	0	4	0	0	100	100	0
3	RC1-RC3	20	9	4	0	5	44.4	100	0	8	11	1	88.9	42.1	0.55
4	LH1-LH3	21	3	2	0	1	66.7	100	0	3	9	0	100	25	0.4
5	LA3-LA5	20	5	5	0	0	100	100	0	5	1	0	100	83.3	0.05
6	LP1-LP2	20	7	7	0	0	100	100	0	7	5	0	100	58.3	0.25
7	RH1-RH3	32	9	9	0	0	100	100	0	2	0	7	22.2	100	0
8	RH1-RH2	26	5	5	0	0	100	100	0	5	0	0	100	100	0
9	RH1-RH3	20	2	2	0	0	100	100	0	2	4	0	100	33.3	0.2
10	LH1-LH3	20	5	4	0	1	80	100	0	5	7	0	100	41.7	0.35
11	LE1-LE2	17	1	1	0	0	100	100	0	1	1	0	100	50	0.1
12	LS4-LS5	24	5	5	0	0	100	100	0	5	25	0	100	16.7	1.0
13	LFC3-LCF5	20	2	2	0	0	100	100	0	2	0	0	100	100	0
14	RE3-RE4	26.5	2	2	0	0	100	100	0	2	0	0	100	100	0
TOTAL		303.8	68	61	0	7	92.2	100	0	60	65	8	93.7	66.6	0.2

TPE = Total numbers of seizure events identified by the expert, TP = Number of true positives, FP = Number of false positives, FN=Number of false negatives, SN = Sensitivity, SP = Specificity, FDR = False detection rate.

reported to be generally very difficult to detect by experts as well automatic seizure detectors. The proposed PS system is capable of detecting low-amplitude seizures, since it estimates the seizure signals while suppressing the non-seizure EEG, thereby enhancing the discrimination boundary between the two categories. We have studied the ability of the proposed system to detect low amplitude seizures using simulated data¹ in [134].

The new PS system resulted in no false detections while missing five out of nine seizures in Patient 3, one out of three seizures in Patient 4 and one out of five seizures in Patient 10. An example of the missed seizure and the corresponding template pattern for Patient 3 (channel: RC1-RC3) is shown in Fig. 6.8. The initial few seconds of the template pattern contain the mixed frequency characteristics (4 to 34 s) that later evolve into rhythmic activity. The missed seizure is similar to the mixed seizure part of the template seizure in the initial seconds (6 to 20 s), but did not continue to evolve into the rhythmic part. On careful examination of the four derived template epochs for this patient data, it is observed that the first template epoch corresponded to the mixed frequency part, while the other three template epochs came from the rhythmic part of the template pattern (T_{PAT}). The proposed system is designed to detect seizures when the candidate seizures match the time-ordered occurrence of the template epochs in the T_{PAT} . All of the missed seizures in this patient did not meet this criterion. Clearly, the missed seizure do not match the template seizure.

¹Simulated EEG under varying SNR conditions and durations were used in the development of the model-based PS system. These are not presented in this thesis.

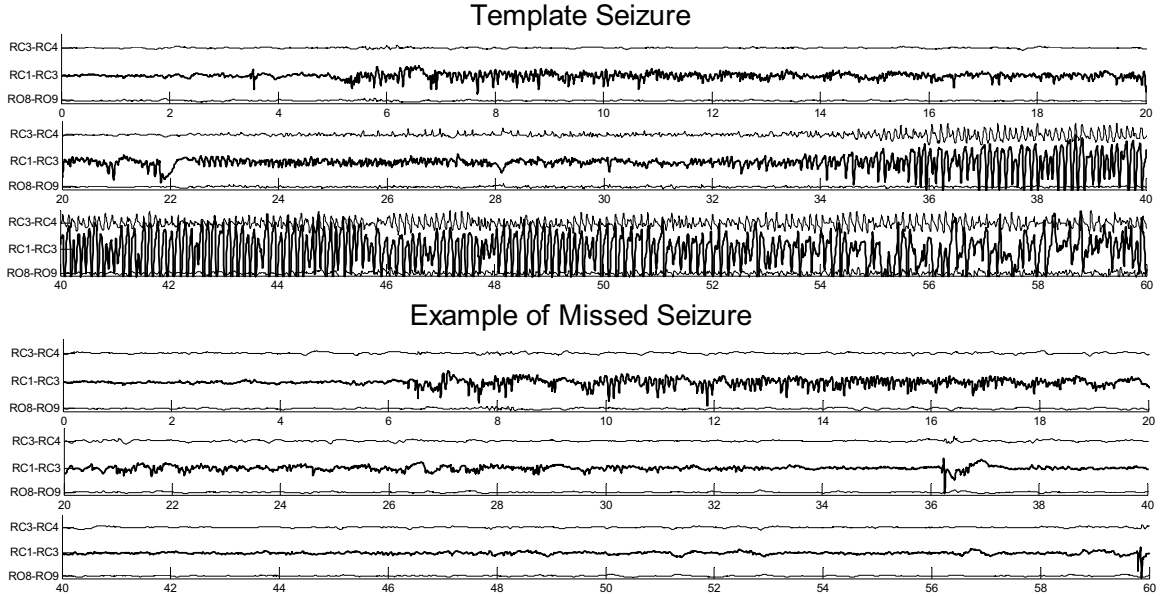


Figure 6.8: Examples of T_{PAT} and a missed seizure by the proposed model-based seizure detection system. Plot represents 60 s of the template seizure and a missed seizure in Patient 3 (channel: RC1-RC3) shown in 20 s segments.

Since the first 20 s of all seizures in Patient 3 were very similar, we tested the idea of using only the first 20 s of the template pattern to build the seizure model. However, this was not successful as a minimum of two disjoint template epochs could not be found. Our method is designed to detect seizures evolving with sustained dominant rhythms. Therefore, it is not surprising that seizures that do not evolve with sustained dominant rhythms were not detected. In contrast, the Qu-Gotman system detected majority of the seizures for this patient, but at the cost of eleven false detections.

Figure 6.9 depicts the template seizure pattern and a missed seizure in Patient 4. The missed seizure partially matches the template seizure pattern and is also contaminated by high-amplitude artifacts. Since it did not evolve similar to T_{PAT} , this seizure was eventually not detected by the proposed PS system. The Qu-Gotman system detected all the seizures in Patient 4 at the cost of several false detections resulting in 100% sensitivity, but at a much lower specificity (25%).

The Qu-Gotman system detected all the seizures in Patient 10 with no false detections. On the other hand, it missed seven out of nine seizures in Patient 7, while

our system detected all of them with no FDs. The likely cause for the Qu-Gotman system to miss some of them is the very low EEG amplitude. Additionally, the seizures missed by the Qu-Gotman system did not evolve in a way similar to the multichannel template seizure within first 20 s. Seizures can go undetected in the Qu-Gotman system due to spatial constraints, which require the seizure onsets to occur in the same channel as those of the template seizure [21]. An example of a training seizure and a missed seizure in the Qu-Gotman system is shown in Fig. 6.10. Clearly, in this example, the test seizure in channels other than RH1-RH3 were of low amplitude and did not evolve in the same manner as the template seizure. No such spatial constraints exists in our PS system.

Majority of the false detections made by the Qu-Gotman system were brief rhythmic bursts ($< 4-6$ s). These short rhythmic discharges did not evolve like the template seizure pattern, and hence were not detected by our system, resulting in a significantly improved detection specificity².

As with other systems, our system too has limitations. It cannot detect mixed frequency seizures. The system requires a minimum of two template epochs in order to make a detection.

Isolating precisely reproducible phenomena in EEG signals remains a difficult task and is vitally important to answer several fundamental questions and can highlight possible pathways of the propagation of epileptic discharges. The proposed evolution-based classification in the PS system allows the identification of recurring seizure patterns that can accurately map the propagation of epileptic discharges by incorporating multichannel information; this warrants further research and is considered as part of future work.

²It must be noted that Qu-Gotman system is designed as a seizure warning system which requires the method to have a short detection delay. Our system, while improving the detection specificity, cannot be used as a seizure warning system because of the constraints imposed in the evolution-based classification which increases the detection delay.

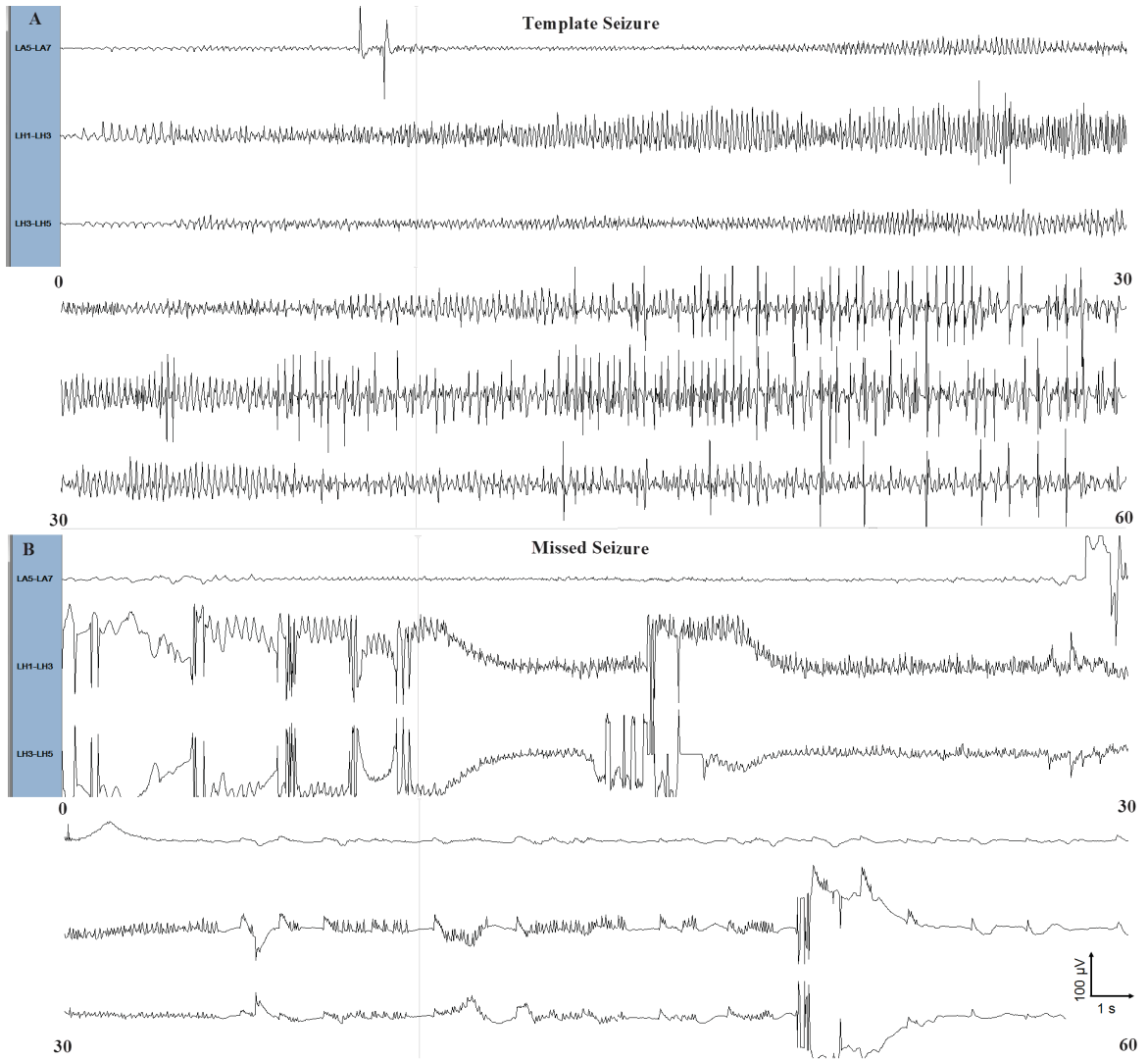


Figure 6.9: Examples of T_{PAT} and a missed seizure by the proposed PS system. Plot represents 60 s of the template seizure and a missed seizure in Patient 4 (channel: LH1-LH3) broken in segments of 30 s. The missed seizure did not evolve similar to T_{PAT} , therefore, did not satisfy the detection criterion.

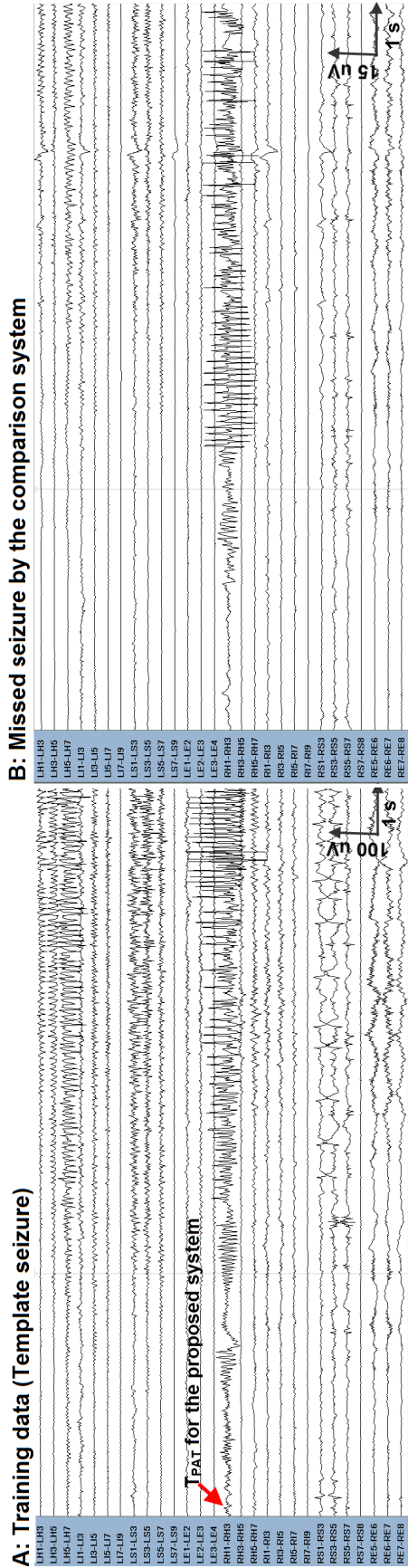


Figure 6.10: Examples of a template seizure and a missed seizure by the comparison system in Patient 7. Data represents 20 s of the training data and 20 s of a missed seizure.

6.10 Summary

We have presented a novel fully-automated patient-specific seizure detection method that is based on the idea that epileptic seizures of one or more type tend to recur within each patient. Piece-wise sustained rhythms of each types of seizure were modeled from the *a priori* known template seizure pattern. Resulting model formulates the required kernel for the SONF to detect similar seizures in subsequent EEG recordings. The process of building a dedicated seizure detection method for each type of seizure (template seizure) has been fully automated. We have assessed the performance of the detection on simulated EEG as well as on 14 patient recordings. The results have shown a sensitivity greater than 92% without any false detections on the 14 patient recordings. Comparison with one of the seminal patient-specific seizure detection methods on the same data has shown a greatly improved performance.

Chapter 7

Unsupervised Spike Sorting

7.1 Introduction

In epilepsy, little is known as to how normal brain regions become and remain epileptic. Regardless of the original brain insult, the neocortical epileptic foci show remarkably similar electrophysiological patterns of localized abnormal electrical discharges. These discharges become rhythmic and spread to widespread brain regions to produce clinical seizures. A lot more frequently than seizures, the focal brain regions generate localized 'interictal' discharges that can be used to identify regions of seizure onset [49, 50, 201]. Interictal discharges commonly known as interictal spikes (ISs) are expressed by high-amplitude ($> 50\mu V$), fast transients often followed by a slow wave for several hundreds of milliseconds. The hallmark property of interictal spikes are the increased tendency to recur periodically and often cluster in brief paroxysms [49, 202]. Because normal neuronal activity is a critical force that shapes nervous system development and plasticity, it appears that ongoing ictal and interictal epileptic activities influence the functional and structural changes that lead to hyper-excitability and hyper-connectivity. Consistent with this idea, gene encodings, neurotransmitter receptors, ion channels, transcription and neurotrophic factors have been found to be differentially expressed in

various animal models of epilepsy and in the human epileptic brain tissues [49, 50, 201]. Therefore, it is possible to elucidate activity-dependent molecular pathways linked with epilepsy. This can be achieved by comparing “electrically-active neocortex” to “control neocortex” within the same patient to search for common gene expression changes across many patients [49, 50, 201]. Furthermore, even though as to how exactly interictal spikes develop, propagate and contribute to the generation of seizures is not well understood, several studies report a better surgical outcome when regions of frequent interictal spikes are also removed [45, 203]. Qualitative and quantitative analysis of interictal spikes thus become vitally important for epilepsy management. However, no such tool exists for use with intracranial EEG recordings.

In this chapter, we propose a new unsupervised spike sorting method to facilitate rapid qualitative and quantitative analysis of interictal spikes for intracranial EEG [204, 205]. The performance of the proposed sorting method is compared against a popular unsupervised spike sorting technique (WAVE_CLUS¹) [151] that is designed for extracellular potentials.

Keeping in mind the heavy workload of the clinical staff in the EMUs, we unify the proposed spike sorting algorithm with a simple, easy-to-use graphical user interface (GUI). Hereafter, we will refer to complete spike classification software package as the automatic spike classification (ASC) package.

7.2 Challenges in Spike Sorting

Spike sorting is the first step in the qualitative and quantitative analysis of neural spikes. The process involves detecting spikes and clustering or mapping each spike to its source. It is generally considered a high dimensional clustering problem that still remains incompletely-solved due to issues of signal-to-noise ratio (SNR), non-stationarity, and

¹Wave_Clus spike sorting system is designed for sorting action potentials and not for the interictal spikes.

non-Gaussianity. Artifacts resembling spikes lead to erroneous classification [147, 153, 154, 206-210]. The two major challenges to be faced in the analysis of interictal spikes, are the wide variety of spike morphologies and the lack of *a priori* knowledge of spike information for each patient. Manual correction of the sorting errors and the sorting results thus become mandatory; this is time-intensive and subjective [211].

A large number of electrodes introduces computational complexity that can vary from patient to patient. Furthermore, EEG is digitized at different sampling rates (200 to 5000 Hz) across various laboratories. Sorting methods based on multi-resolution analysis, such as the wavelet transform, are dependent on the sampling rate, which ultimately limits their widespread application [155, 209]. Majority of the spike sorting algorithms in the literature parametrize spikes into a high dimensional feature space to overcome the data sparsity and low SNR. However, representation of spikes in terms of features loses the morphology of the spikes, which can be important in the invasive studies [155, 209].

Validation of the spike sorting results is another challenge, since spike classes are not known *a priori*. Typically, the sorting results are evaluated using one or more cluster validity metrics on simulated data for varying SNR and with a limited number of spike classes. The popular performance evaluation measures are intra- and inter- cluster distance, Folkes and Mallows index, Huberts Γ statistics, cophenetic correlation coefficient, Dunn index, Davies-Bouldin index, and Xie-Beni index [212]. These measures give an indication of the cluster quality, which requires experts to visually screen the spikes and validate the automatic sorting results.

In this chapter, we propose a new spike sorting method, designed for prolonged depth EEG recordings, that address some of the above practical issues. This chapter also proposes an easy-to-interpret cluster validation method.

7.3 Automatic Spike Classification

In the literature, it has been reported that template matching sorting methods outperform other sorting techniques. These methods, however, require complete knowledge of the data, and often employ principal component analysis (PCA) and wavelet transformations to generate the templates [209, 213]. Taking into account the superior performance of the template matching sorting techniques, we propose a sorting algorithm that uses template matching at its core, but does not require *a priori* knowledge of all the data to generate the templates. That is, the templates are created on-the-fly as the data becomes available. Thus, one of the primary goals in the proposed method is to generate the best representation of the template, as the clustering outcomes are heavily dependent on the templates. Since spike wave complexes are crucial in epilepsy research, we propose a full waveform-based sorting algorithm. Challenges in waveform-based sorting techniques mainly arise due to noise, data dimensionality and sparsity. In multichannel recordings, adjacent channels sometimes contain the same type of spike activity. In these cases, correlations between channels can be exploited to generate templates for which we consider a morphological correlator and the PCA. Waveform-based sorting methods suffer from transient and unavoidable gradual changes in the spike waveform (waveform nonstationarities), resulting in the creation of a large number of overlapping clusters. To eliminate this type of sorting errors, we employ an offline method (hierarchical clustering and validation) that uses *a priori* knowledge of the templates and the spike waveforms to improve the quality of the sorting results. The proposed sorting algorithm is shown in the block diagram enclosed by thick 'blue' rectangular box in Fig. 7.1 and is composed of five blocks: (a) spike alignment, (b) morphological correlator, (c) principal component analysis, (d) template matching, and (e) hierarchical clustering and validation.

It is important to define the various terms used in the proposed method before

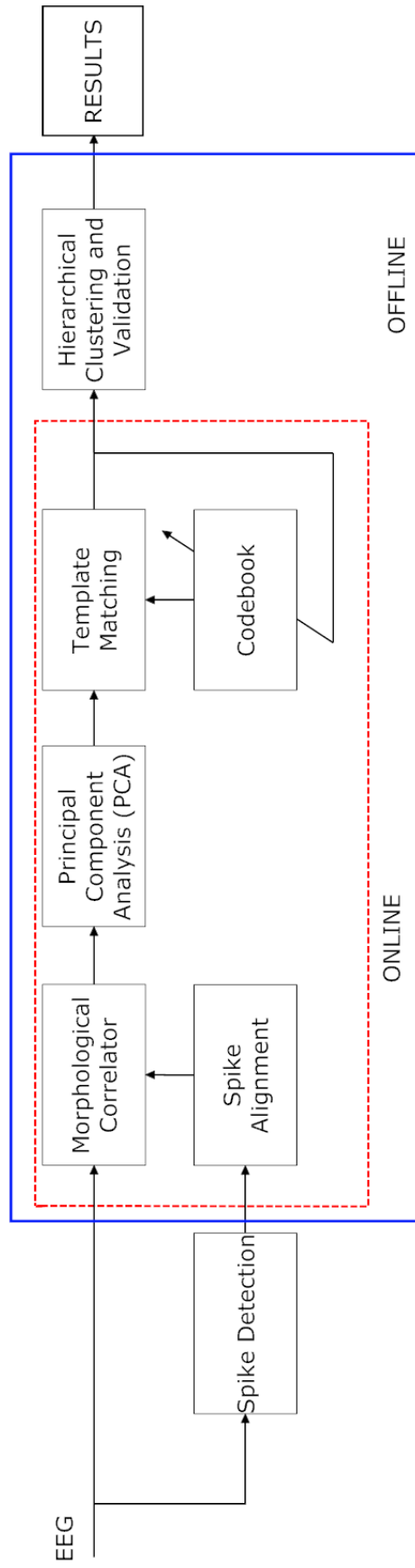


Figure 7.1: Block diagram of the proposed unsupervised sorting algorithm (enclosed in blue box).

describing each of the building blocks. We define a single channel detected spike as the reference spike irrespective of whether the spike was detected automatically or manually. Multichannel EEG centered around the vertex of the reference spike is defined as the multichannel spike event. Let $\mathbf{X} = [x_1, x_2, \dots, x_N]$ represent the multichannel spike event, where N is the number of channels and the column x_i represents the i th channel spike data of length n . A variety of clinical studies examine not only the spike, but also the waveform following the spike which we define as the spike-wave-complex (SWC). Therefore, 150 ms of the EEG following the spike event is added to create the SWC. Let $\mathbf{Y} = [y_1, y_2, \dots, y_N]$ represent the N -channel SWCs, where each column is a vector of length m . In our analysis, $m = 250$ ms (± 50 ms of spike data around the spike vertex and 150 ms of data following the spike event) was empirically found to be optimal in this development. Since the proposed method generates templates on-the-fly by exploiting the spatial correlation between adjacent channels, aligning spikes to a common reference point (which is the vertex of reference spike) becomes inevitable and is the first step in the proposed method. Both \mathbf{X} and \mathbf{Y} represent aligned multichannel spike data. Figure 7.2 illustrates the multichannel EEG extracted around the reference spike, aligned multichannel spike and the resulting SWC event. A template is defined as the optimal or best single-channel representation for a group (class) of similar SWC events and a codebook is defined as a collection of SWC templates for a patient.

7.3.1 Spike Data (Spike Detection)

The state-dependent spike detection algorithm of [159] available in the Stellate Harmonie v6.2e software (Stellate Inc, Montreal, Canada) is employed to identify spikes, which we refer to as the *AutoSpike* events. Same patient data is also scored for spike events by an experienced EEGer. Manually identified spikes will be referred to as the *ManuSpike* events. Even though previously detected spikes are utilized for spike

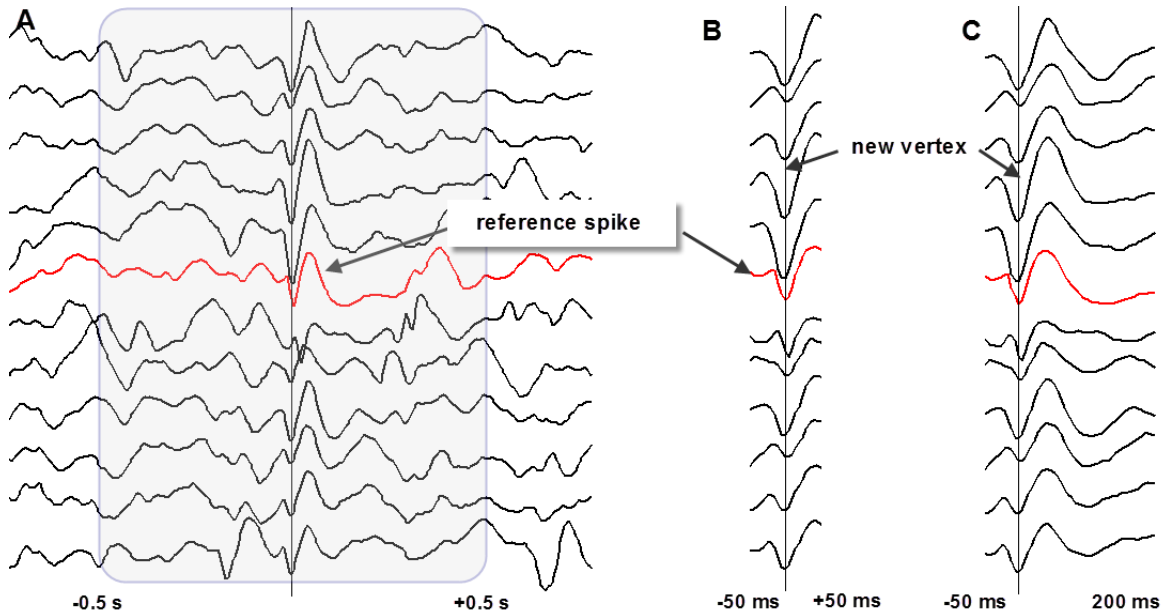


Figure 7.2: Multichannel spike and spike-waveform complex event. (A) represents multichannel EEG event extracted around the vertex of the reference (detected) spike. Vertical line represents the vertex of the detected spike. (B) represents 100 ms of multichannel spike data (\mathbf{X}), and (C) represents example of multichannel spike-waveform complex (\mathbf{Y}), both aligned to the reference spike vertex.

clustering, the classification is done in an online manner. The detected spikes are processed sequentially; one at a time as they would be in an online application.

7.3.2 Spike Alignment

One of the most difficult and complex parts of sorting process is the unsupervised clustering where no *a priori* knowledge of the templates or clusters is available. In the case of template-matching, it is a well established fact that the shape, phase, and length of the templates have a significant effect on the algorithm's performance. Therefore, it is important to generate a noise-free estimate of the template. In a multichannel EEG, noise-free template can be generated on-the-fly by exploiting the spatial correlation between adjacent channels. However, it is observed that interictal spikes do not occur perfectly aligned across multiple channels. This generally happens due to sequential activation of unidirectional dynamical neural networks. Therefore,

it becomes important to first align the multichannel spike event to the vertex of the reference spike to minimize the effect of time-shift.

The considered spike event labeled at the vertex serves as the reference spike. The vertex is used as the reference point along which spikes in all the other channels will be aligned. To do so, we extract 50 ms of the multichannel data around the vertex of the reference spike. The local maxima or minima within ± 25 ms of the reference spike vertex is considered as the correct vertex in each of the other channels. Local maxima or minima in each channel is shifted so that it occurs at the same time instance as the reference spike vertex. This rule is applied to all channels whether there exists a spike or not.

7.3.3 Morphological Correlator

As previously mentioned, we want to exploit the spatial correlation between adjacent channels in the creation of a noise-free template using PCA. In multichannel EEG data, not all channels contain the same type of interictal spike as the reference spike, and not all channels contain spike events. It becomes very difficult to automatically select the principal component that best represents the reference spike. Therefore, channels without interictal spikes and/or channels with dissimilar spikes from the reference must be ignored in the analysis. This step is aimed at increasing the data sparsity, enhancing the SNR, and reducing the computational load in the PCA. Channels with waveforms similar to that of the reference spike channel are extracted from the multichannel spike event, $\mathbf{X} \in \mathbf{R}^{N \times n}$ by using the correlation measure. Since the wave-complex following the spike is highly variable, including it would significantly affect the identification of similar spikes. Therefore, we consider only the multichannel spike event and not the multichannel SWC event in the morphological correlator.

The correlation coefficient ρ_{ij} between the reference spike channel, x_i , and all the other channels, x_j is computed by

$$\rho_{ij} = \frac{n \sum x_i x_j - (\sum x_i)(\sum x_j)}{\sqrt{n(\sum x_i^2) - (\sum x_i)^2} \sqrt{n(\sum x_j^2) - (\sum x_j)^2}}, \quad (7.1)$$

where n is the length of the spikes. The correlation coefficient ρ_{ij} between the i th reference spike and j th channel is compared to a threshold, ρ_{MC} . If ρ_{ij} exceeds ρ_{MC} , then channels with spikes similar to the reference spike are identified. In this manner, only those channels similar to the reference spike channel are retained for further analysis, as shown in Fig. 7.3. This step reduces the data dimension and is similar to subtractive clustering technique in [213]. In subtractive clustering, similar spikes around the defined cluster center point (reference spike) are searched and extracted, and the process iterates until all of the data belongs to unique classes.

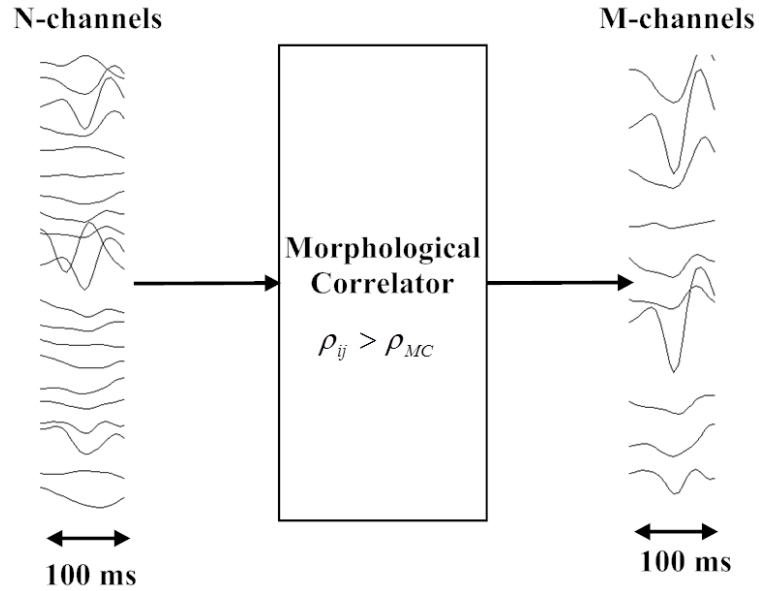


Figure 7.3: Identification of channels with spikes similar to the reference spike using morphological correlator.

7.3.4 Principal Component Analysis

The output of the morphological correlator along with the wave-complexes following the spike represents the multichannel SWC event, \mathbf{Y} . We apply PCA to the resulting multichannel SWC event to generate a noise-free estimate of the template spike. PCA

is a linear mathematical transform that seeks a projection of the correlated data to a new uncorrelated coordinate system called principal components. These coordinates are an ordered set of orthogonal basis vectors that capture the directions of the largest variation in the data. It has been shown that incorrectly aligned spike waveforms affect the projection bases in the PCA and thus, the clustering outcome [214, 215]. It is for this reason that we align the spike vertex across channels.

For the implementation of PCA, the mean-centered signals, \mathbf{Y}_c are whitened using the following equation:

$$\mathbf{Z} = \mathbf{V} \cdot \mathbf{Y}_c, \quad (7.2)$$

where $\mathbf{V} = \mathbf{\Lambda}^{-1/2}\mathbf{U}^T$ is the whitening matrix, $\mathbf{\Lambda} = \text{diag}[\lambda_1, \dots, \lambda_k]$ and \mathbf{U} are the eigenvalue and eigenvector matrices, respectively, of the covariance matrix of \mathbf{Y}_c . Mean centering is necessary for performing PCA to ensure that the first principal component describes the direction of maximum variance. In Eq. (7.2), each column z_i corresponds to the projection of y on the i^{th} principal component \mathbf{u}_i , and the variance of the component \mathbf{z}_i is λ_i such that $\lambda_1 > \lambda_2 > \dots > \lambda_k$.

In high SNR conditions, the first principal component (highest variance) corresponds to the signal (reference SWC) while low variance components correspond to noise. In low SNR conditions, the selection of principal components corresponding to the SWC event becomes more complex. In the framework of unsupervised spike sorting, we want to automatically select the component that best represents the SWC. By employing the morphological correlator as a preprocessing step, we eliminate channels that do not contain information related to the reference spike. This results in a high SNR condition, where the best representation of the reference SWC is the first principal component. Therefore, the first principal component is considered as the candidate SWC, \mathbf{w}_i , as shown in Fig. 7.4.

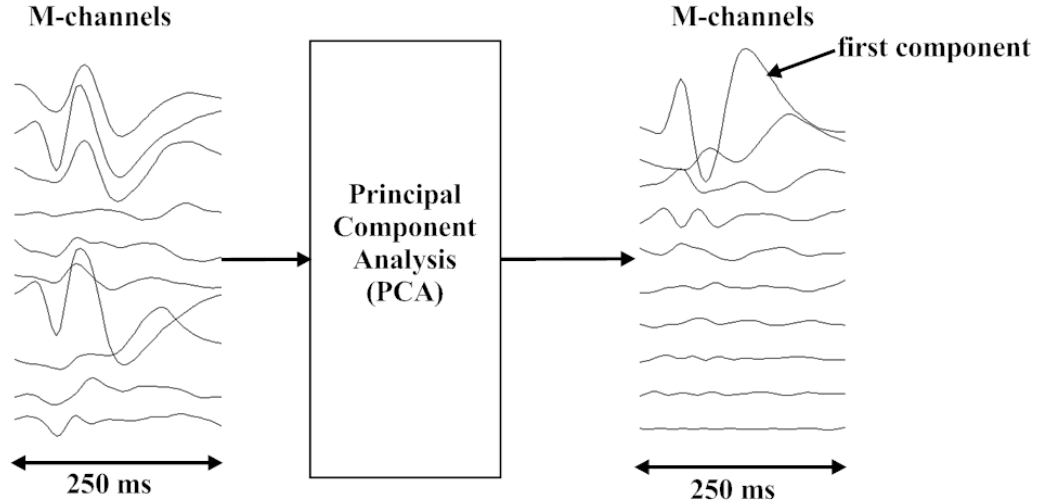


Figure 7.4: Principal component analysis of the multi-channel SWC.

7.3.5 Codebook-based Template-Matching

The codebook (\mathbf{T}) stores the SWC templates ($\mathbf{T} = \{\mathbf{t}_1, \mathbf{t}_2, \dots, \mathbf{t}_r\}$), class membership details such as SWC time and channel of occurrence, and various properties of individual SWCs. The i th candidate SWC, \mathbf{w}_i , is matched with SWC templates in \mathbf{T} . The correlation coefficient metric given by Eq. (7.1) is utilized to identify the best match for \mathbf{w}_i .

The correlation coefficient of \mathbf{w}_i and j th template, $\rho_{w_i t_j}$ (where $j = 1, 2, \dots, r$), is compared to a preset threshold, ρ_{TM} . When $\rho_{w_i t_j}$ exceeds the threshold ($\rho_{TM} > 0.9$), a match is found, and \mathbf{w}_i is assigned to the j th class. Sometimes, it is possible that there may be more than one template matching the candidate SWC. In such situations, \mathbf{w}_i is assigned to the class with the highest correlation coefficient. The j th SWC template is updated by averaging with \mathbf{w}_i , *i.e.*, $\mathbf{t}_j = 0.5 * (\mathbf{t}_j + \mathbf{w}_i)$. If no match is found for \mathbf{w}_i in the codebook \mathbf{T} , then a new class is created and the codebook is updated with the new SWC template, *i.e.*, $\mathbf{T} = \{\mathbf{t}_1, \mathbf{t}_2, \dots, \mathbf{t}_j, \mathbf{t}_{j+1}\}$, where $\mathbf{t}_{j+1} = \mathbf{w}_i$. The process is continued until all SWCs have been classified.

7.3.6 Hierarchical Clustering and Post-classification

Since the SWC templates evolve over time, they are highly susceptible to noise and EEG non-stationarity, resulting in the creation of redundant classes. Furthermore, since interictal spike-wave-complexes tend to recur periodically, a large number of these events will be concentrated in clusters with large number of members. Therefore, sorting results can be further improved by identifying and rejecting overlapping and insignificant clusters.

Kaneko *et al.* [153] utilized the bottom-up approach (agglomerative) hierarchical clustering to identify and merge similar classes. We too employ agglomerative clustering using single linkage rule, where the similarity parameter is the Mahalanobis distance to identify and merge similar classes. In this approach, the process iterates until all objects are aggregated into a single class using the distance measure. The distance, $d_{i,j}$, between i th and j th class is evaluated using the Mahalanobis distance given by

$$d_{i,j} = \sqrt{(\boldsymbol{\mu}_i - \boldsymbol{\mu}_j)^T \boldsymbol{\Sigma}^{-1} (\boldsymbol{\mu}_i - \boldsymbol{\mu}_j)} \quad (7.3)$$

where $\boldsymbol{\mu}$ and $\boldsymbol{\Sigma}$ are the SWC classes and the covariance matrix, respectively. The threshold to merge clusters based on the Mahalanobis distance between cluster centers is set to 0.1 and is adapted from [216]. This results in well-separated clusters.

In our application, we are only interested in clusters with a significantly large number of members. Since rarely occurring SWC events and events due to noise and artifacts are expected to have a relatively low number of members in the clusters. By applying a threshold relative to the highest-ranking cluster (cluster with the highest number of members), we can reject clusters that contain rarely occurring events and events due to noise and artifacts, thus improving the codebook quality. Therefore, we examined the number of spikes lost with this relative threshold on the five patients training data. Figure 7.5 illustrates the effect of the relative threshold on the number

of spikes lost. It is observed that at 10% threshold relative to the highest-ranking cluster retains the maximum number spike events. Therefore, we selected a threshold of 10% relative to the most significant cluster to reject the insignificant clusters.

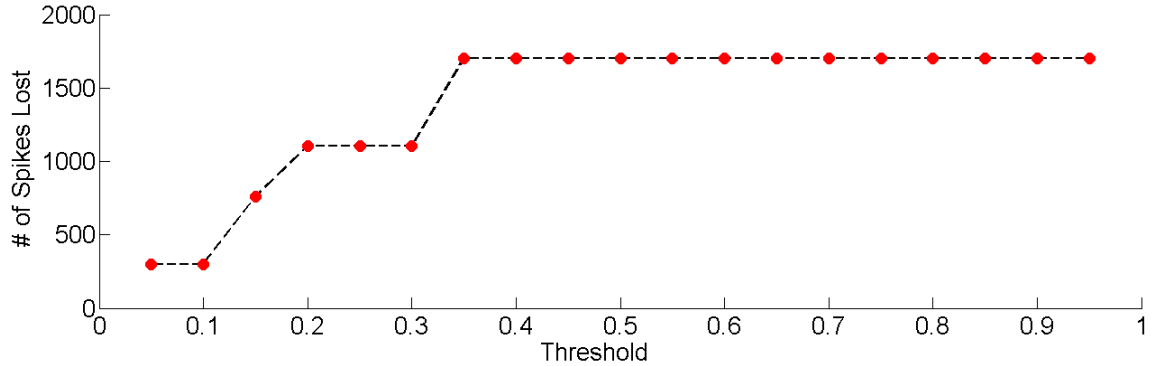


Figure 7.5: Events lost in the insignificant clusters on thresholding relative to the most significant cluster.

7.3.7 Graphical User Interface and Result Display

For clinical use of the proposed sorting algorithm, we have designed a simple graphical user interface (GUI). The GUI is designed keeping in mind the heavy workload of the clinical staff in the EMU. It has preset settings to automate the sorting process while including a variety of tunable parameters to help manually set the parameters of choice and export results in a variety of formats. The display of the results contains the SWC templates in the codebook. Each class template and its members are superimposed along with the total number of members in each class. Summarized result also includes projection of codebooks onto their two principal components, 3-dimensional representation indicating the cluster quality, inter- and intra- cluster distance, and dendrogram chart. Morphological descriptors of codebook are exported to the pre-defined Microsoft excel compatible format.

7.4 Performance Evaluation

A popular unsupervised spike sorting technique 'WAVE_CLUS' [151] for extracellular recordings is considered for comparison. The inputs to the WAVE_CLUS are AutoSpike and ManuSpike events. The sorting results are visually assessed for the number of overlapping clusters in the codebook.

One of the main challenges in the spike sorting is the lack of *a priori* knowledge of the total number of classes or clusters in the data. Researchers, therefore, often validate their spike sorting methods using simulated data with a fixed number of spike classes [155, 207]. On real data, algorithm performance may vary and requires mandatory visual inspection of the sorting results. Evaluating the clustering results by traditional approaches is time-consuming and highly subjective.

We propose a new indirect approach to validate our sorting method, which establishes a definite role for automatic spike detection and sorting methods for clinical application. In this approach, we compare the sorting results of spike events detected by two different approaches - automatic spike detector (AutoSpike) and the gold standard manual spike scoring by the EEGer (ManuSpike). Codebooks generated using the two sets of spike data for the same patient are expected to have the same number and type of classes. Therefore, the spike sorting method can be indirectly validated by visually comparing the codebooks for the two sets of spikes. We refer to these two codebooks as the AutoSpike- and Manuspike-codebooks for each patient. To facilitate easy visual assessment of the sorting result, we employ visual cluster analysis techniques.

Visualization mitigates the challenges in traditional approaches of cluster validation. It maps the high-dimensional data to a 2D or 3D space and aids users having an intuitive and easily understood graph/image to reveal the grouping relationship between the data [217, 218]. Several techniques have been proposed for visual cluster analysis such as icon-based, pixel-oriented, and geometric techniques, and multidimensional

scaling maps such as hierarchical blob, self-organizing maps, and PCA [217, 218]. However, visual assessment of quality of clustering result still heavily relies on the user’s visual perception and understanding on cluster distribution. We include two different easy-to-interpret cluster visualizations: (a) geometric technique, and (b) dendrogram.

7.4.1 Geometric Technique

The basic idea of geometric technique is to visualize transformations and projections of the data to produce useful and insightful visualizations. We propose a new easy-to-interpret visual cluster analysis technique, which is a combination of visualization and cluster analysis. We represent the cluster quality metrics in 3D space as spheres. The center of the sphere is the centroid of the cluster and radius of the sphere is the variation within the cluster (intra-cluster distance). The centroid of a cluster is the average of all SWC points for the given cluster. Since waveform variations in a cluster can lead to shift in the actual cluster center, we compute the cluster centroid using the first principal component from PCA instead of directly deriving it from the cluster. The i th cluster is represented as sphere S_i at center P_i of radius $r_i = \sigma_i^2$, where $P_i = \{c_i, c_i, c_i\}$ and c_i is the centroid of the first principal component of the i th cluster in the codebook. The inter-cluster distance is the Mahalanobis distance between the i th and j th cluster. The resulting 3D visualization allows an easy identification of overlapping clusters, where disjoint spheres symbolize non-overlapping clusters. The example in Fig. 7.6 shows the 3D representation of the inter- and intra-cluster distances obtained using the AutoSpike events of a patient before applying the hierarchical clustering. At this stage, the codebook contains six clusters of which two are well separated and compact (A and B), while two pairs of clusters overlap (C, D) and (E, F). It is noted that in the pair (E, F), one of the overlapping clusters (F) appears to be much less compact than the other (E), i.e., larger intra-cluster distance.

The EEGer can rapidly identify in his or her visual assessment that the two pairs of clusters overlap and can further scrutinize the SWC templates of the overlapping clusters.

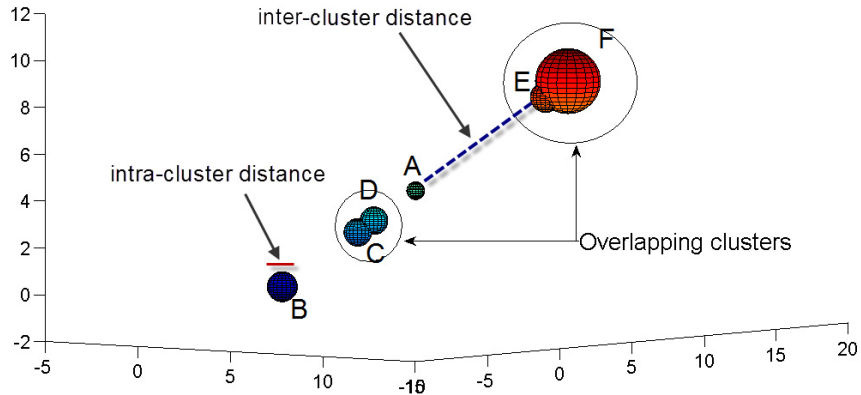


Figure 7.6: Visual analysis of the cluster quality

7.4.2 Dendrogram Analysis

We want to compare the two codebooks for each patient resulting from the two sets of spikes (AutoSpike and ManuSpike) using the proposed sorting method in order to validate the sorting results. This can be achieved by dendrogram, which can highlight similarity and dissimilarity between codebooks via a simple tree-like diagram. A dendrogram is generated using hierarchical clustering method (bottom-up, complete linkage rule with Euclidean distance metric). Identical SWC templates in Auto-codebook and Manu-codebook for each patient will be at the same node in the dendrogram that can be visually confirmed. We compute the accuracy (%), which is defined as the percentage of correct matching between the two codebooks, that is, the number of templates in the AutoSpike codebook that correctly matches the templates in the ManuSpike codebook and vice versa. When no match for a cluster in one codebook is found in the other codebook, they are assigned as unmapped clusters. Additionally, for each method, the total number of significant and insignificant clusters

are also calculated.

7.5 Results

The results of quantitative analysis of the two codebooks for each patient in the WSU database for the proposed method are shown in Table 7.1. On the average, the proposed sorting method loses 19.7% of AutoSpike and 21.6% of ManuSpike events in the respective codebooks for all the nine patients. The average number of spikes in the insignificant classes were 6 for AutoSpike and 4 for ManuSpike events (not shown). Visual inspection of the codebooks via the 3D geometric technique revealed the clusters to be disjoint. The comparison of significant clusters in the two codebooks for each patient via the dendrogram resulted in 79.3% accurate matching.

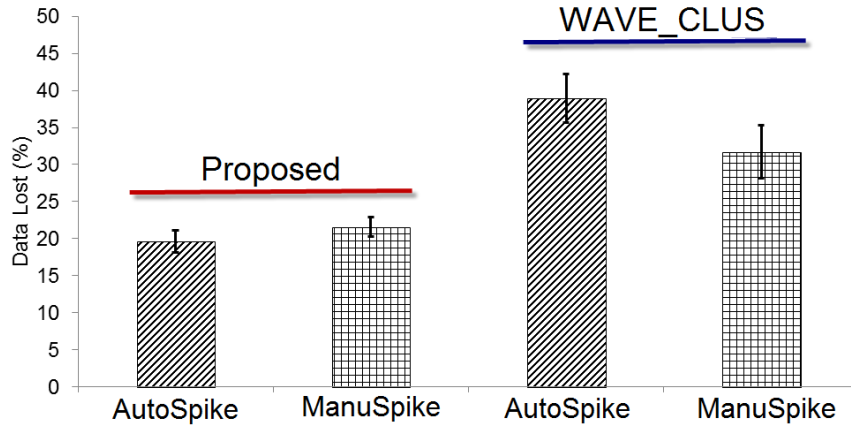


Figure 7.7: Percentage of events lost by the proposed ASC and WAVE_CLUS methods. Error bar represents standard error.

Similarly, the results of quantitative analysis of the two codebooks for the WAVE_CLUS method are shown in Table 7.2 for all the nine patients. On the average, the WAVE_CLUS sorting algorithm loses 38.9% of AutoSpike and 31.7% of ManuSpike events in the respective codebooks. In several patients, WAVE_CLUS clustering results were observed to be imprecise. In such situations and without a knowledge of the true class labels, it was difficult to match the two codebooks. Therefore, matching

Table 7.1: Quantitative analysis of the proposed sorting results.

PID	# of significant clusters		# of SWCs per significant cluster		# of unmapped clusters		Accuracy (%)	% of data lost	
	AutoSpike	ManuSpike	AutoSpike	ManuSpike	AutoSpike	ManuSpike		AutoSpike	ManuSpike
1	5	4	629	2	1		80	48.9	0
2	7	7	337	41			100	26.2	20.8
3	3	4	11	68		1	75	0	16.3
4	4	6	1463	81		2	66.7	21.3	36
5	3	2	3129	4000	1		66.7	10.5	15.8
6	3	2	692	147	1		66.7	15.6	22.2
7	5	6	215	206		1	83.3	13.5	17.8
8	4	3	247	9	1		75	23.9	25
9	2	2	4547	419			100	17	40.8
Average	4	4	1252	553			79.3	19.7	21.6

accuracy is not reported for the WAVE_CLUS algorithm.

7.6 Discussion

The purpose of this study was to develop an unsupervised sorting technique to aid in the rapid quantitative analysis of interictal spikes and establish definite role of spike detection and sorting techniques for clinical application in the EMU.

Template matching-based sorting methods are the most preferred technique in the literature because of their superior performance. These methods, however, require a knowledge of the complete data to derive the templates. Therefore, template-matching sorting methods are generally not well suited for online analysis. We have proposed a novel online spike sorting technique that employs template-matching at its core and dynamically derives the templates as the data becomes available.

Majority of the spike sorting methods in the literature extract various features of spikes such as spike height, width, peak-to-peak amplitude, half-wave duration, slopes, and wavelet coefficients. These features are utilized to measure similarity between spikes to perform sorting. Classifying spikes directly using waveforms in high dimensional space is considered very challenging because data points are sparse and noisy, resulting in imprecise clusters [147, 211, 219]. Waveform morphology is vitally important in invasive EEG studies. Therefore, representation of the spike wave complex into features is not generally suitable. To address this clinical need, we have proposed a multistage complete waveform-based sorting technique.

We have incorporated PCA to generate the noise-free estimate of the templates. However, PCA requires a set of synchronized spikes to perform PCA. We have used the reference spike (defined earlier) to align data on other channels prior to processing the multichannel SWC by PCA to generate the best estimate for the SWC candidate. When multichannel SWC events are not available for PCA, the SWC event is considered

Table 7.2: Quantitative analysis of the WAVE_CLUS sorting results.

PID	# of significant clusters		# of SWCs per significant cluster		# of unmapped clusters		% of data lost	
	AutoSpike	ManuSpike	AutoSpike	ManuSpike	AutoSpike	ManuSpike	AutoSpike	ManuSpike
1	4	2	974	613	1	2	36.8	100
2	3	2	258	172		2	75.7	5.7
3	3	2	11	157		2	0	3.4
4	5	2	916	291	1	2	38.3	23
5	6	5	866	701	3		50.5	63.1
6	2	2	1072	165	2	2	12.8	12.7
7	3	2	234	541	3	2	43.3	28
8	2	1	601	21	2		7.3	41.7
9	3	2	496	652	1	2	86.4	7.6
Average	3	2	603	368			38.9	31.7

as the SWC candidate.

In the literature, there exist a few template-matching sorting techniques that dynamically derive templates, but such methods have been shown to result in overlapping clusters [206, 220-222]. Visual assessment of sorting results, therefore, becomes very difficult. The challenges arise due to (1) overlapping clusters, and (2) unknown number of clusters. The latter is application dependent and does not have a general solution. However, the issue of overlapping clusters that arises due to noise and artifacts can be resolved. It has been shown in [153] that tracking spike-amplitude changes improves the quality of the spike templates and reduces the number of overlapping clusters. We have also followed a similar approach to minimize the influence of noise and artifacts. The templates are continually updated over time whenever a matching event is found. This is advantageous as it improves the SNR of the SWC template and results in a reduction of number of overlapping clusters.

Kaneko et al. [153] showed that tracking spike clusters by repeatedly applying bottom-up hierarchical clustering to spike data recorded during temporally overlapping frames helps in improving the quality of the sorting results. However, repeatedly applying hierarchical clustering is computationally expensive. Instead of repeatedly performing hierarchical clustering on each subsequent frame, the same can be applied on the codebook once the online analysis has been completed. Our method identifies and merges overlapping clusters in the codebook using hierarchical clustering once the online analysis has been completed. This improves the quality of the sorting results.

The codebook contains clusters that are due to interictal spikes as well as rarely occurring events and artifacts. The EEGer is mainly interested in the significant clusters. This is because significant clusters are likely to contain the highly stereotypical recurring interictal spikes. Therefore, clusters with lower membership can be deleted from the codebook. We reject clusters with number of SWC members below some percentage of the most significant cluster membership. This improves the quality of

the sorting results; and also reduces the visual inspection workload of the EEGer. However, it may result in eliminating some small clusters and rarely occurring SWCs that may be important.

Another challenge lies in the visual assessment and validation of the sorting results. We have proposed a new indirect technique to validate the quality of the clusters. In this approach, the EEGer visually examines the 3D cluster quality for overlapping clusters. To validate the sorting accuracy of the proposed method, we have compared the AutoSpike and ManuSpike codebooks for each patient using dendrogram. The two codebooks matched with 79.3% accuracy, i.e., 79.3% of the templates of AutoSpike codebook matched correctly with the ManuSpike codebook. The codebooks obtained using the two sets of spikes for Patient 5 are shown in Fig. 7.8, which represents SWC members along with its template (in 'red' bold) for each class. The 3D plots to assess the cluster quality are shown in Fig. 7.9. The size of the sphere represents the variation within the cluster (compactness), while disjoint spheres symbolize non-overlapping clusters. Visual inspection of these plots reveals that the resulting clusters from the proposed sorting method to be disjoint (non-overlapping). Comparison of the two codebooks using the proposed indirect approach is shown in Fig. 7.10 in terms of the dendrogram. It is seen that two-of-three clusters of AutoSpike (A) codebook perfectly matches the two clusters of ManuSpike (B) codebook. For the additional cluster in the AutoSpike codebook, no match was found in the ManuSpike codebook. Similarly, Patients 1, 6, and 8 also had additional SWC classes for which no match was found in the ManuSpike codebook. In these patients, it is possible that EEGer missed these frequently occurring spike events, which were detected by the automatic method. The EEGer can decide whether to retain or reject such additional SWC classes by examining the codebooks. Patients 3, 4 and 7 had additional classes in the codebook derived using ManuSpike events. It is possible that either the automatic spike detection method missed spikes belonging to these classes or were filtered by the validation

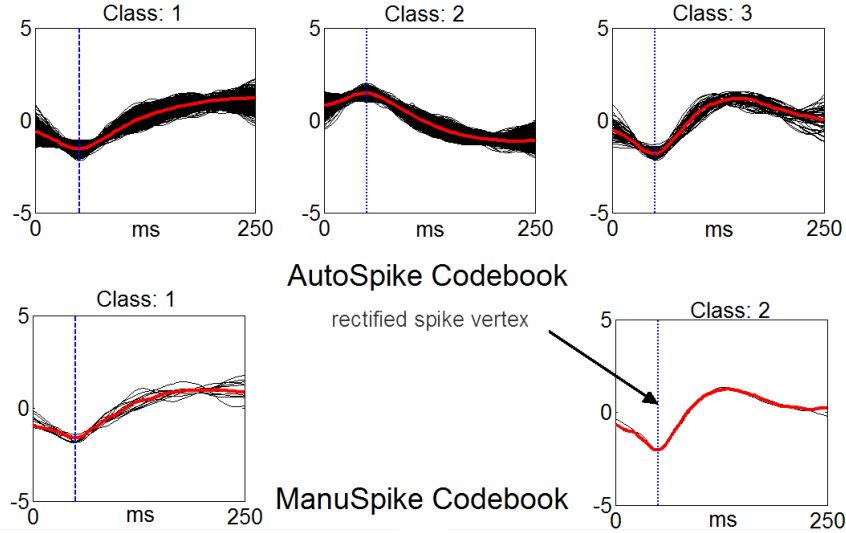


Figure 7.8: Codebook generated using AutoSpike and ManuSpike events for Patient 5 using the proposed spike sorting algorithm.

block (due to lower cluster membership). The cut-off threshold in the validation block is a function of the class with the highest membership. Therefore, some of the SWC classes with lower membership may have been rejected. It is important to mention that the EEGer may not have access to both the AutoSpike and ManuSpike codebooks. The two codebooks were employed to validate the sorting results in the absence of true class labels. Validation of the sorting results with this indirect approach reported good matching between the two codebooks. This establishes a definite role for spike detection and the proposed sorting method for clinical use. The EEGer can rapidly examine the codebook, thereby significantly reducing the cost of identifying and classifying events by the experts.

We have also compared our sorting method with a popular spike sorting technique WAVE_CLUS [151]. The AutoSpike and ManuSpike events were input to the WAVE_CLUS sorting algorithm to generate the two codebooks. Sorting was performed at the default settings of the algorithm and summary of the sorting results are shown in Table 7.2. The sorting results for Patients 4 and 9 obtained using the AutoSpike events by the proposed and WAVE_CLUS techniques, respectively, are shown in Fig.

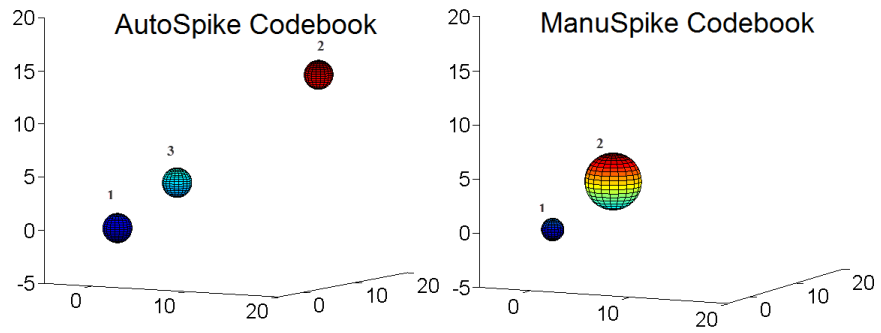


Figure 7.9: Illustration of cluster validation in terms of inter- and intra- cluster distance for the two codebooks of Patient 5.

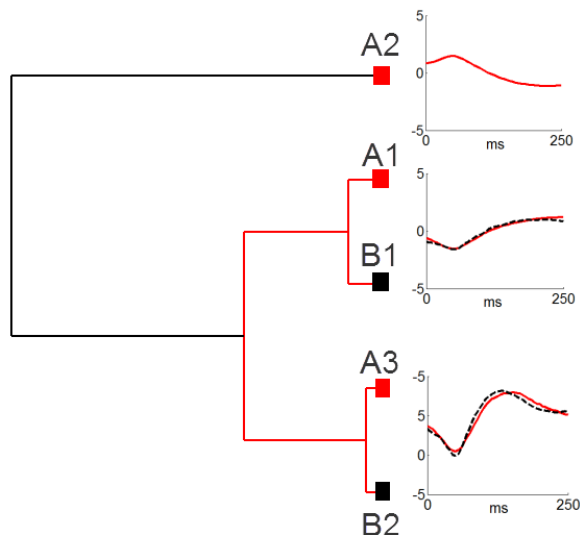


Figure 7.10: Visual comparison of the AutoSpike and ManuSpike codebooks using dendrogram for Patient 5.

7.11 and 7.12. Visual inspection of the sorting results confirms that WAVE_CLUS clusters have large intra-cluster distance, which could be due to the wave-complex following the spike. This is because WAVE_CLUS algorithm is designed for spikes and not for spike-wave-complexes. The wave-complexes following spikes are highly variable and act as noise source causing imprecise clustering results from the WAVE_CLUS algorithm. It is important to mention here that clustering is a data-driven process, which means that there is no absolutely superior clustering method. Each method is designed for certain type of data and without the knowledge of true spike classes, comparison of sorting results is extremely difficult.

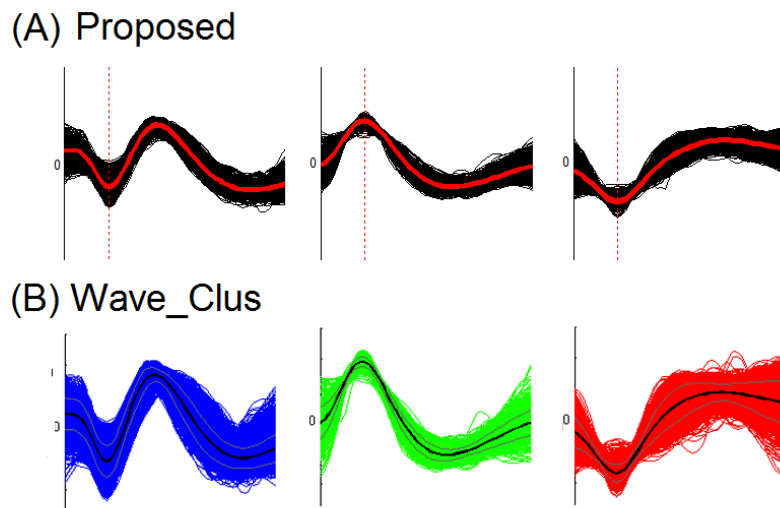


Figure 7.11: Sorting results for Patient 4 using the AutoSpike SWC events. (A) contains three most significant clusters obtained with the proposed sorting algorithm. (B) contains results obtained from the WAVE_CLUS sorting algorithm.

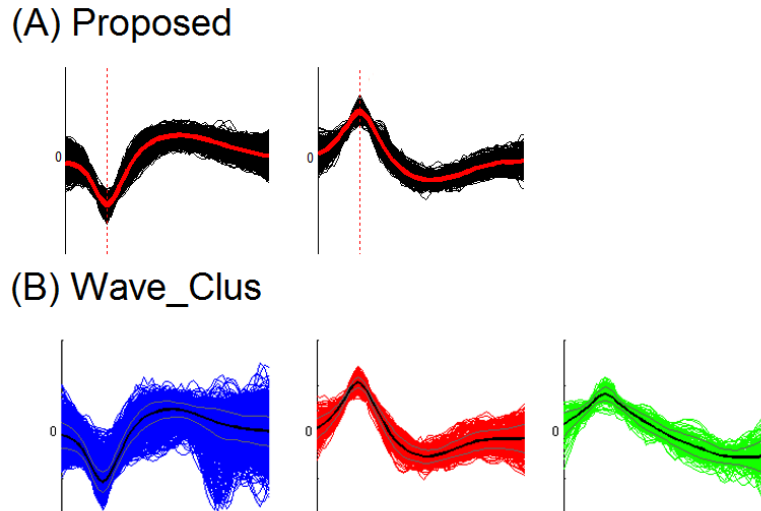


Figure 7.12: Sorting results for Patient 9 using the AutoSpike SWC events. (A) represents three most significant clusters obtained with the ASC algorithm, and (B) depicts results obtained using the WAVE_CLUS sorting algorithm.

As previously mentioned, sorting is a multi-step process, which requires selection of a number of parameters that can increase the learning time of the software. A simple GUI with preset parameters reduces the learning time of the software. Keeping in mind the heavy workload and challenges in the clinical setting, we have developed a simple GUI. The algorithm requires minimal input from the user. The learning time, therefore, is significantly reduced by allowing the algorithm to process data in the sequential pagination framework. Pagination is a process of formatting information into ordered pages that streamlines the information flow and reduces the complexity in its application. The screen-shot of the ASC software GUI is shown in Fig. 7.13. The first step in the ASC software requires the user to provide basic information regarding the data such as file path, montage and spike events of interest. It allows the comparison of events within the same file. The next step allows the user to set parameters of choice or to use default settings that are easy to remember. This step also allows the selection of features and data formats for exporting the results. The user can then execute the sorting process by clicking the 'RUN' button. However, it is activated only if all the information necessary for sorting are correctly entered.

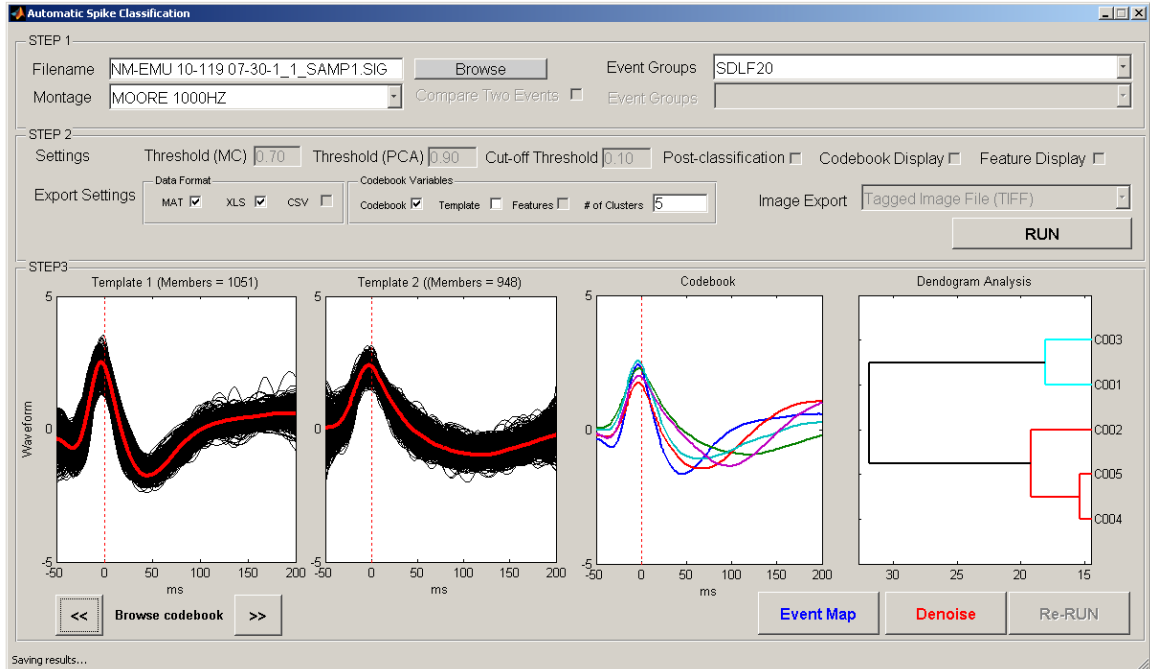


Figure 7.13: Graphic user interface of the ASC software.

The third step displays sorting results and allows a quick review of the codebook². The software also includes basic artifact rejection methods to improve the SNR. The current version of the ASC is designed to work with Stellate Harmonie (ver. 6.2e) EEG system and allows exporting results in various formats such as MATLAB native format, Excel, CSV, JPEG, EMF and TIFF.

7.7 Summary

This chapter has presented a new automatic spike classification (ASC) software package for analyzing neural signals. It is designed to assist researchers in performing easy quantitative analysis of neural data by combining a number of advanced neural signal processing algorithms in a unified GUI. The ASC can easily process massive amounts of neural data and generate clusters of neural signal without loss in the waveform

²Note that even though the sorting results are shown in the GUI as single channel traces, the EEGer can examine the sorting results in multichannel configuration using the EEG review 'Harmonie' software since the spike classification results are exported to the EEG file on an event-by-event basis.

morphology. The ASC is designed to improve the quality of analysis. A new indirect approach to validate sorting results has also been proposed in this chapter. Visual assessment of the sorting results revealed disjoint and compact clusters. The method has been compared against a popular spike sorting algorithm, WAVE_CLUS. Results have shown greatly improved performance compared to that of the WAVE_CLUS algorithm.

Chapter 8

Conclusion

This chapter presents the overall conclusions of this research, including the summary of achievements and contributions towards the classification of neural signals followed by directions for future research.

8.1 Concluding Remarks

In epilepsy, EEG is the primary and the only continuous monitoring tool available to the clinicians. However, its interpretation is notoriously difficult. The success of an epilepsy treatment, such as resective surgery, relies heavily on accurate identification and localization of the abnormal brain regions involved in epilepsy for which patients undergo continuous EEG monitoring. The two main biomarkers of epilepsy in the EEG are (a) the seizures and (b) interictal spikes. They are identified by visually inspecting the prolonged EEG recordings. However, visual screening in the voluminous EEG is highly subjective, labor-intensive, tiresome and expensive. Therefore, automatic techniques to quantify spikes and seizures are much needed in the EMUs. In this thesis, we have developed automatic techniques to detect and classify these two biomarkers of epilepsy to facilitate easy and rapid analysis of the prolonged EEG recordings.

Epilepsy therapies are individualized for numerous reasons; therefore, automatic

detection and classification techniques must also be patient-specific. In the seizure detection arena, patient-specific seizure detection techniques are needed not only in the presurgical evaluation of prolonged EEG recordings, but also in the emerging neuro-responsive therapies. However, to date, there does not exist any fully automatic patient-specific seizure detection system.

One of the possible design frameworks for a fully-automatic patient-specific (PS) seizure detection system may involve combining the PS and the more generalized non-patient-specific (NPS) seizure detection techniques. In this framework, a NPS technique (which does not require any *a priori* seizure information) can be employed to bootstrap the PS technique with the necessary seizure-related information. This information then can be utilized for on-the-fly (unsupervised) training of the PS scheme and subsequently, the PS system can detect recurring patterns similar to the template. However, the inherent tradeoff between the detection accuracy and the algorithm complexity in the NPS and PS techniques limit the possibility of such a fully automatic PS system. Thus, one of the primary goals of this research was to develop robust computationally-simple NPS and PS seizure detection methods that may serve as building blocks of a fully automatic PS seizure detection system.

The design process of a new seizure detection system involves the determination of discriminating boundaries between seizure and non-seizure EEG by parametric representation of seizure EEG. Majority of the NPS and PS systems in the literature are based on this design approach. However, these systems report difficulty in detecting short-duration seizures, slow evolving seizures, seizures with minimal change in the amplitude and frequency, and seizures occurring on a single channel. Alternatively, in the seizure detection literature, it has been observed that reliable detection can be made by quantifying the seizure evolution. However, quantifying time-evolution of seizure in a low-complexity domain has been considered very challenging. Thus, one of the objectives of this research was to develop new computationally simple NPS and

PS seizure detection systems that quantify seizure evolution.

In Chapter 4, three new NPS systems, namely the RFWE, morphology and the eSD systems were proposed that quantify the time-evolution of seizures. The main focus in the design of NPS systems was to ensure that the proposed systems can detect a wide variety of seizure patterns and seizures occurring on a single channel, and at the same time is computationally light. This led to the investigation of a variety of EEG features in order to design the new NPS systems. The performance of the new systems have been evaluated against three popular NPS systems, namely, the Gotman system, Reveal algorithm, and the Grewal-Gotman system.

The evaluation in single channel configuration of the RFWE, morphology and the eSD systems on the MNI test data yielded an average sensitivity of 98.7%, 86.7% and 88%, and detection specificity of 41.1%, 71.3% and 81.4%, respectively. The new NPS systems reported improvement in both the sensitivity and the specificity over the compared systems. Among the three new NPS systems, the morphology system detected a wide range of seizure patterns that included rhythmic and non-rhythmic seizures of varying length, including those missed by the experts. This system was robust to noise and artifacts, and computationally light compared to the RFWE and eSD systems. Therefore, this system was selected for performance evaluation in multichannel configuration using previously unseen FSP database. Among the comparison systems, Grewal-Gotman system outperformed the other two comparison systems on the MNI test data. Therefore, this system was selected for multichannel evaluation on the FSP database. Multichannel evaluation of the morphology system against the Grewal-Gotman system yielded significantly improved detection performance. The comparison systems generally failed to detect seizures occurring on a single channel, seizures with minimal change in the amplitude and frequency, and short-duration seizures. The new NPS systems detected seizures that are often difficult to detect by the comparison system, and also revealed several electrographic seizures missed by

the experts. The performance results suggest that new NPS system can aid in the rapid review of prolonged EEG recordings in the EMUs.

The focus of this research was not limited only to the design of NPS system, but also to explore and develop new tools that can provide visualization of seizure onset and spread, and allow easy mapping of channel-by-channel timeline of seizure. In Chapter 5, a new adjunctive tool (RFI display) that allows easy and quick identification of paroxysmal activities in the intracranial EEG has been proposed. RFI display has been compared against two other methods in the literature. It was demonstrated that the RFI display is easy-to-interpret and minimally affected by the display size complexity.

The second objective of this research was to address the main limitations in the automation of patient-specific seizure detection. The limiting factors are due to (1) the supervised selection of the seizure EEG, (2) the supervised selection of non-seizure EEG, and (3) the supervised training of the classifier. In Chapter 6, we have addressed these challenges with a new model-based PS system. The model-based PS system requires only the knowledge of the seizure pattern to derive the seizure model consisting of a set of basis functions necessary to utilize the statistically optimal null filters (SONF) for the detection of seizures. The process of modeling involves several steps that have been automated. The seizure classification is based on tracking the temporal evolution of the seizure rhythm to enhance the detection specificity. The new model-based PS system has been compared against a popular patient-specific system (Qu-Gotman system) from the literature on the MNI database. The evaluation of the new PS system yielded an average sensitivity of 92% with no false detection and resulting in significantly improved performance over the compared system. This translates into a very promising reliable system with enormous clinical potential.

The development of a fully-automatic patient-specific system based on the new NPS and PS systems presented in this thesis, will open the doors to the investigation

of numerous unanswered questions in epilepsy and find a variety of clinical applications. Nonetheless, the new NPS and PS systems can work independently and can be clinically used to review prolonged intracranial EEG recordings.

The third objective in this research was to develop an unsupervised spike classification system to aid in the rapid quantitative and qualitative analysis of interictal spikes. Such a tool for the intracranial EEG is unavailable for clinical use. In this thesis, we have developed a new unsupervised spike sorting algorithm based on the spike waveform template matching, which does not require *a priori* knowledge of the spike templates. A graphical user interface (GUI) has also been developed to assist easy integration of the automatic spike sorting system in clinical setting. In Chapter 7, the new spike sorting system has been described and compared against one of the popular spike sorting systems (WAVE_CLUS) for extracellular recordings on the nine patients' EEG of the WSU database. Due to the unavailability of all spike classes, it becomes extremely difficult to validate the sorting results. We have introduced a simple easy-to-interpret visual analysis technique to validate the sorting results. Visual inspection of the sorting results has confirmed that the proposed system had non-overlapping clusters with improved sorting accuracy over the WAVE_CLUS system.

8.2 Contributions

The main contributions of this research are (1) introduction of a new feature to quantify seizures, (2) design of three new NPS seizure detection systems that quantify temporal evolution of seizures, (3) a new adjunctive 2D visualization tool for rapid review of long-term intracranial EEG recordings, (4) semi-automatic PS seizure detection system that includes a new adaptive EEG segmentation algorithm, a new technique for artifact rejection, unsupervised modeling of the template seizure, and unsupervised

training of the PS classifier, and (5) a new unsupervised spike classification system for intracranial EEG recordings. The following provides further details on each of these contributions:

1. The main limitation in NPS detection schemes is the lack of simple robust markers for seizures. This has resulted in seizure detection schemes that often employ a large number of features and a complex detection strategy to address the highly varying seizure EEG morphologies. One of the hallmark properties of seizure evolution is the increase in the number of sharp waveform complexes as the seizure evolves. We have introduced a novel approach to quantify EEG sharpness that allows reliable detection of seizures. This has not been done previously.
2. Tracking temporal progression (evolution) of seizure to detect seizure in low complexity detection schemes is considered extremely challenging. We have developed three computationally simple NPS detection schemes by tracking the temporal progression of the seizures. The performances of the newly developed detection systems have been shown to be superior to the current state-of-the-art NPS systems.
3. We have introduced a new adjunctive compressed EEG display to aid in the rapid review of voluminous intracranial EEG recording. It is based on a new relative sharpness index measure which quantifies the frequency of abnormally sharp activity in the EEG and provides a birds-eye-view of potential epileptiform activity. Such a display is currently unavailable for the intracranial EEG recordings.
4. A novel PS system, that requires only the knowledge of the template seizure patterns, has been developed. The key building blocks of this new system are (1) a new adaptive segmentation method, (2) new adaptive modeling approach,

(3) novel evolution-based classifier and (4) a new technique for artifact rejection. Underlying each of the building blocks is the SONF. While current state-of-the-art requires one or more template seizure patterns, a large amount of carefully selected background EEG and supervised training of the classifier, our proposed PS system requires only the selection of a single template pattern to build a patient-specific seizure classifier. The new PS system is computationally light compared to the existing PS detection systems. The performance of the new PS system has been shown to be superior in terms of the detection specificity over the current state-of-the-art PS system.

5. A spike sorting system for quantitative analysis of interictal spike in the EMU is unavailable. We have developed a new unsupervised spike sorting system based on waveform template matching and principal component analysis (PCA) for quantitative analysis of the interictal spikes. The new system does not require *a priori* knowledge of the complete data or the spike templates. The spike templates are dynamically derived and a patient-specific template codebook generated. It has been shown that the new system is capable of handling a large number of electrodes. The performance of the new sorting system results in disjoint clusters, in contrast to the current state-of-the-art spike sorting system. A GUI is also designed keeping in mind the heavy workload of the clinical staff in the EMU.

8.3 Future Perspectives

8.3.1 Non-Patient-Specific System

- High-frequency activity up to 1000 Hz in the EEG has been shown to be linked to epilepsy. These patterns have come to be known as high-frequency oscillations

(HFOs). HFOs are low-amplitude transient events that are thought to play a role in the physiological and pathological neural process [223-227]. We have demonstrated that the new *sharpness of EEG waveform* feature is highly sensitive to changes in the amplitude and frequency. We believe that this feature can be utilized to make computationally light and robust HFO detector.

- The ideal spike detector does not exist as the specificity and sensitivity remain difficult to assess when there exists a large variability in the visual classification by the experts [228]. Nonetheless, the waveform sharpness is one of the most important characteristics of an interictal spike, which can be explored with respect to the new feature proposed in this thesis to develop a reliable spike detector.
- It has been noted that the detection specificity of the new NPS system proposed in this thesis may deteriorate in the presence of sharp transients, high-frequency electromyographic activity and high-amplitude artifacts. New artifact rejection strategies need to be explored to handle such artifacts. Since scalp EEG is prone to additional artifacts, extending the new NPS systems to scalp EEG would require additional considerations.
- The RSI display allows rapid identification of epileptogenic sites. However, the new compressed EEG display does not provide any quantitative information of the epileptiform activity. Information such as seizure recurrence, onset zone, and spreads, are manually identified by the expert. Manual identification of these crucial informations is extremely tiresome and subjective. These informations can be made available by combining the RSI display, NPS and the PS systems developed in this thesis, which could improve the care and management of epilepsy patients, and therefore, must be investigated.

8.3.2 Patient-Specific System

- The patient-specific seizure detection system developed in this thesis is based on a single channel EEG. In practical applications, EEG is analyzed in multichannel configuration. An extension of the model-based PS system to the multi-channel scenario can be developed by (a) modeling the template seizure epochs across multiple channels, (b) removing the redundant epochs, (c) finding spatio-temporal sequence, and (d) then looking for similar sequence in the remaining data. A match across multichannel in spatio-temporal sequences would likely increase the detection specificity.
- One of the limitations in the proposed PS system is that it fails to detect non-rhythmic mixed frequency seizures along with short duration seizures. New techniques to model mixed-frequency and short rhythmic seizures need to be explored.
- As described earlier in this chapter, automatic PS systems are needed in view of their unmatched detection accuracy for a variety of diagnostic and therapeutic applications. We have developed individual building blocks of such a fully-automatic PS system. The obvious next step would be to implement and validate the fully-automatic PS system, where the NPS system bootstraps the PS system to supply the template seizure.
- The extension of the proposed PS system for the scalp EEG would require inclusion of additional artifact management. This is due to fact that the scalp EEG is generally affected by artifacts to a greater degree than the intracranial EEG. Since the proposed PS system examines the sequential occurrences of specific rhythmic discharges, rhythmic artifacts may not be a problem as they will not satisfy the stringent criterion of the sequential occurrences. However, motion, electro-oculogram (EOG), electrocardiogram (EKG) and electromyogram (EMG)

artifacts must be removed to ensure that components representing EEG activity are preserved [229]. Therefore, extending the new PS system to scalp EEG would require additional considerations to handle these artifacts.

8.3.3 Spike Sorting System

The proposed spike sorting system provides the basic tool necessary for the analysis of interictal spikes. The method can be improved on several fronts, and some of the possible avenues are listed below.

- Alignment of the spikes to its maximum amplitude plays a pivotal role in the success of the proposed method. However, local maximum of the spike may get corrupted by the noise causing misalignment. Smoothing techniques such as cubic spline interpolation can be explored to minimize the effect of noise. Aligning spikes to the point of its maximum slope or frequency-weighted energy can also be explored; these should further improve the classification results.
- Aligning spikes in the multichannel EEG distorts the spike propagation pathways, which are vitally important in some clinical studies such as epilepsy. Instead of aligning multichannel EEG with the reference spike, the multichannel spike event can be used directly as a template. This will result in multichannel templates instead of a single-channel template and will preserve the spike propagation pathways. However, this will lead to templates with poor SNR that can result in an increased number of misclassification and overlapping clusters. Effect of noise in the multichannel template can be minimized by exploring techniques such as independent component analysis (ICA). The benefits of ICA are many, including the ability to automatically detect artifacts and overlapping spikes and to handle waveform non-stationarities [230]. However, it must be noted that the ICA, an iterative algorithm, is computationally expensive.

An obvious extension of the proposed sorting method would be in the statistical characterization of the spatio-temporal distribution of interictal spikes in a large dataset and identifying the subsets of brain structures frequently and conjointly involved in the generation of interictal spikes [228].

References

- [1] World Health Organization, *ATLAS : Epilepsy care in the world*. World Health Organization, 2005.
- [2] R. S. Fisher, G. Harding, G. Erba, G. L. Barkley, and A. Wilkins, “Photic- and pattern-induced seizures: a review for the epilepsy foundation of america working group,” *Epilepsia*, vol. 46, no. 9, pp. 1426–41, 2005.
- [3] F. Mormann, R. G. Andrzejak, T. Kreuz, C. Rieke, P. David, C. E. Elger, and K. Lehnertz, “Automated detection of a pre seizure state based on a decrease in synchronization in intracranial electroencephalogram recordings from epilepsy patients,” *Physical Review E*, vol. 67, no. 2 Pt 1, p. 021912, 2003.
- [4] I. Kotsopoulos, T. Van Merode, F. Kessels, M. De Krom, and J. Knottnerus, “Systematic review and meta-analysis of incidence studies of epilepsy and unprovoked seizures,” *Epilepsia*, vol. 43, no. 11, pp. 1402–1409, 2002.
- [5] E. Niedermeyer and F. L. D. Silva, *Electroencephalography: Basic Principles, Clinical Applications, and Related Fields*. Lippincott Williams & Wilkins, 2004.
- [6] “ILAE classification of epilepsies: its applicability and practical value of different diagnostic categories,” *Epilepsia*, vol. 37, no. 11, pp. 1051–9, 1996.

- [7] D. Schmidt and S. C. Schachter, *Puzzling cases of epilepsy*. Academic Press, 2008.
- [8] C. G. Wasterlain and D. M. Treiman, *Status Epilepticus : mechanisms and management*. MIT Press, 2006.
- [9] G. Adelman and B. H. Smith, *Encyclopedia of Neuroscience*. Elsevier, 1999.
- [10] X. F. Yang and S. M. Rothman, “Focal cooling rapidly terminates experimental neocortical seizures,” *Annals of Neurology*, vol. 49, no. 6, pp. 721–6, 2001.
- [11] X. F. Yang, D. W. Duffy, R. E. Morley, and S. M. Rothman, “Neocortical seizure termination by focal cooling: temperature dependence and automated seizure detection,” *Epilepsia*, vol. 43, no. 3, pp. 240–5, 2002.
- [12] B. Litt and J. Echauz, “Prediction of epileptic seizures,” *Lancet Neurology*, vol. 1, no. 1, pp. 22–30, 2002.
- [13] W. S. Anderson, E. H. Kossoff, G. K. Bergey, and G. I. Jallo, “Implantation of a responsive neurostimulator device in patients with refractory epilepsy,” *Neurosurgical Focus*, vol. 25, no. 3, p. E12, 2008.
- [14] T. L. Skarpaas and M. J. Morrell, “Intracranial stimulation therapy for epilepsy,” *Neurotherapeutics*, vol. 6, no. 2, pp. 238–43, 2009.
- [15] S. Wong, G. H. Baltuch, J. L. Jaggi, and S. F. Danish, “Functional localization and visualization of the subthalamic nucleus from microelectrode recordings acquired during DBS surgery with unsupervised machine learning,” *Journal of Neural Engineering*, vol. 6, no. 2, p. 026006, 2009.
- [16] K. B. Baker, B. H. Kopell, D. Malone, C. Horenstein, M. Lowe, M. D. Phillips, and A. R. Rezai, “Deep brain stimulation for obsessive-compulsive disorder: using functional magnetic resonance imaging and electrophysiological techniques:

- technical case report,” *Neurosurgery*, vol. 61, no. 5 Suppl 2, pp. E367–8; discussion E368, 2007.
- [17] S. M. Rothman, “The therapeutic potential of focal cooling for neocortical epilepsy,” *Neurotherapeutics*, vol. 6, no. 2, pp. 251–7, 2009.
- [18] S. Raghunathan, S. K. Gupta, M. P. Ward, R. M. Worth, K. Roy, and P. P. Irazoqui, “The design and hardware implementation of a low-power real-time seizure detection algorithm,” *Journal of Neural Engineering*, vol. 6, no. 5, p. 56005, 2009.
- [19] H. Qu and J. Gotman, “Improvement in seizure detection performance by automatic adaptation to the EEG of each patient,” *Electroencephalography and Clinical Neurophysiology*, vol. 86, no. 2, pp. 79–87, 1993.
- [20] H. Qu, *Self-adapting algorithms for seizure detection during EEG monitoring*. PhD thesis, Department of Biomedical Engineering, McGill University, 1994.
- [21] H. Qu and J. Gotman, “A patient-specific algorithm for the detection of seizure onset in long-term EEG monitoring: possible use as a warning device,” *IEEE Transactions on Biomedical Engineering*, vol. 44, no. 2, pp. 115–22, 1997.
- [22] J. Gotman, “Automatic recognition of interictal spikes,” *Electroencephalography and Clinical Neurophysiology*, vol. 37, pp. 93–114, 1985.
- [23] D. Zumsteg, D. M. Andrade, and R. A. Wennberg, “Source localization of small sharp spikes: low resolution electromagnetic tomography (LORETA) reveals two distinct cortical sources,” *Clinical Neurophysiology*, vol. 117, no. 6, pp. 1380–7, 2006.
- [24] E. Niedermeyer, “The clinical relevance of EEG interpretation,” *Clinical Electroencephalography*, vol. 34, no. 3, pp. 93–8, 2003.

- [25] E. Niedermeyer, “Ultrafast EEG activities and their significance,” *Journal of Clinical EEG and Neuroscience*, vol. 36, no. 4, pp. 257–62, 2005.
- [26] T. Yu, Y. Wang, G. Zhang, L. Cai, W. Du, and Y. Li, “Posterior cortex epilepsy: Diagnostic considerations and surgical outcome,” *Seizure*, 2009.
- [27] M. Zijlmans, J. Jacobs, Y. U. Kahn, R. Zelman, F. Dubeau, and J. Gotman, “Ictal and interictal high frequency oscillations in patients with focal epilepsy,” *Clinical Neurophysiology*, vol. 122, no. 4, pp. 664–71, 2011.
- [28] F. Wendling, J. J. Bellanger, J. M. Badier, and J. L. Coatrieux, “Extraction of spatio-temporal signatures from depth EEG seizure signals based on objective matching in warped vectorial observations,” *IEEE Transactions on Biomedical Engineering*, vol. 43, no. 10, pp. 990–1000, 1996.
- [29] F. Wendling, M. B. Shamsollahi, J. M. Badier, and J. J. Bellanger, “Time-frequency matching of warped depth-EEG seizure observations,” *IEEE Transactions on Biomedical Engineering*, vol. 46, no. 5, pp. 601–5, 1999.
- [30] R. Meier, H. Dittrich, A. Schulze-Bonhage, and A. Aertsen, “Detecting epileptic seizures in long-term human EEG: a new approach to automatic online and real-time detection and classification of polymorphic seizure patterns,” *Journal of Clinical Neurophysiology*, vol. 25, no. 3, pp. 119–31, 2008.
- [31] J. Gotman, “Automatic detection of seizures and spikes,” *Journal of Clinical Neurophysiology*, vol. 16, no. 2, pp. 130–40, 1999.
- [32] S. Grewal and J. Gotman, “An automatic warning system for epileptic seizures recorded on intracerebral EEGs,” *Clinical Neurophysiology*, vol. 116, no. 10, pp. 2460–72, 2005.

- [33] R. Yadav, R. Agarwal, and M. N. S. Swamy, "A novel dual-stage classifier for automatic detection of epileptic seizures," *Proceedings of IEEE Engineering in Medicine and Biology Society Conference*, pp. 911–914, 2008.
- [34] R. Yadav, R. Agarwal, and M. N. S. Swamy, "A novel morphology-based classifier for automatic detection of epileptic seizures," *Proceedings of IEEE Engineering in Medicine and Biology Society Conference*, pp. 5545–5548, 2010.
- [35] A. S. Zandi, M. Javidan, G. A. Dumont, and R. Tafreshi, "Automated real-time epileptic seizure detection in scalp EEG recordings using an algorithm based on wavelet packet transform," *IEEE Transactions on Biomedical Engineering*, vol. 57, no. 7, pp. 1639–51, 2010.
- [36] R. Yadav, R. Agarwal, and M. N. S. Swamy, "Detection of epileptic seizures in stereo-EEG using frequency-weighted energy," *Proceedings of IEEE Midwest Symposium on Circuits and Systems*, pp. 77–80, 2007.
- [37] R. Yadav, R. Agarwal, and M. N. S. Swamy, "STFT-based segmentation in model-based seizure detection," *Proceedings of IEEE Canadian Conference on Electrical and Computer Engineering*, pp. 729–732, 2007.
- [38] C. I. Akman, V. Micic, A. Thompson, and J. J. Riviello, "Seizure detection using digital trend analysis: Factors affecting utility," *Epilepsy Research*, vol. 93, pp. 66–72, Jan 2011.
- [39] R. Agarwal, J. Gotman, D. Flanagan, and B. Rosenblatt, "Automatic EEG analysis during long-term monitoring in the ICU," *Electroencephalography and Clinical Neurophysiology*, vol. 107, pp. 44–58, Jul 1998.
- [40] A. K. Shah, R. Agarwal, J. R. Carhuapoma, and J. A. Loeb, "Compressed EEG pattern analysis for critically ill neurological-neurosurgical patients," *Neurocritical Care*, vol. 5, no. 2, pp. 124–33, 2006.

- [41] C. P. Stewart, H. Otsubo, A. Ochi, R. Sharma, J. S. Hutchison, and C. D. Hahn, “Seizure identification in the ICU using quantitative EEG displays,” *Neurology*, vol. 75, no. 17, pp. 1501–8, 2010.
- [42] V. Gnatkovsky, S. Francione, F. Cardinale, R. Mai, L. Tassi, G. L. Russo, and M. de Curtis, “Identification of reproducible ictal patterns based on quantified frequency analysis of intracranial EEG signals.,” *Epilepsia*, vol. 52, pp. 477–488, Mar 2011.
- [43] R. Wagner, D. M. Feeney, F. P. Gullotta, and I. L. Cote, “Suppression of cortical epileptiform activity by generalized and localized ECoG desynchronization,” *Electroencephalography and Clinical Neurophysiology*, vol. 39, no. 5, pp. 499–506, 1975.
- [44] T. E. Peters, N. C. Bhavaraju, M. G. Frei, and I. Osorio, “Network system for automated seizure detection and contingent delivery of therapy,” *Journal of Clinical Neurophysiology*, vol. 18, no. 6, pp. 545–9, 2001.
- [45] E. D. Marsh, B. Peltzer, r. Brown, M. W., C. Wusthoff, J. Storm, P. B., B. Litt, and B. E. Porter, “Interictal EEG spikes identify the region of electrographic seizure onset in some, but not all, pediatric epilepsy patients,” *Epilepsia*, vol. 51, no. 4, pp. 592–601, 2010.
- [46] R. G. Emerson, C. A. Turner, T. A. Pedley, T. S. Walczak, and M. Forgione, “Propagation patterns of temporal spikes,” *Electroencephalography and Clinical Neurophysiology*, vol. 94, no. 5, pp. 338–48, 1995.
- [47] E. Asano, O. Muzik, A. Shah, C. Juhasz, D. C. Chugani, S. Sood, J. Janisse, E. L. Ergun, J. Ahn-Ewing, C. Shen, J. Gotman, and H. T. Chugani, “Quantitative interictal subdural EEG analyses in children with neocortical epilepsy,” *Epilepsia*, vol. 44, no. 3, pp. 425–34, 2003.

- [48] J. Bourien, F. Bartolomei, J. J. Bellanger, M. Gavaret, P. Chauvel, and F. Wendling, "A method to identify reproducible subsets of co-activated structures during interictal spikes. application to intracerebral EEG in temporal lobe epilepsy," *Clinical Neurophysiology*, vol. 116, no. 2, pp. 443–55, 2005.
- [49] S. N. Rakhade, B. Yao, S. Ahmed, E. Asano, T. L. Beaumont, A. K. Shah, S. Draghici, R. Krauss, H. T. Chugani, S. Sood, and J. A. Loeb, "A common pattern of persistent gene activation in human neocortical epileptic foci," *Annals of Neurology*, vol. 58, no. 5, pp. 736–47, 2005.
- [50] S. N. Rakhade, A. K. Shah, R. Agarwal, B. Yao, E. Asano, and J. A. Loeb, "Activity-dependent gene expression correlates with interictal spiking in human neocortical epilepsy," *Epilepsia*, vol. 48 Suppl 5, pp. 86–95, 2007.
- [51] J. Gotman, "Automatic seizure detection: improvements and evaluation," *Electroencephalography and Clinical Neurophysiology*, vol. 76, no. 4, pp. 317–24, 1990.
- [52] S. B. Wilson, M. L. Scheuer, R. G. Emerson, and A. J. Gabor, "Seizure detection: evaluation of the Reveal algorithm," *Clinical Neurophysiology*, vol. 115, no. 10, pp. 2280–91, 2004.
- [53] J. R. Ives, "Video recording during long-term EEG monitoring of epileptic patients," *Advances in Neurology*, vol. 46, pp. 1–11, 1987.
- [54] J. Gotman, "Automatic recognition of epileptic seizures in the EEG," *Electroencephalography and Clinical Neurophysiology*, vol. 54, no. 5, pp. 530–40, 1982.
- [55] J. Kay, "Continuous EEG monitoring in the intensive care unit," *Canadian Journal Neurological Sciences*, vol. 25, no. 1, pp. S12–5, 1998.

- [56] K. G. Jordan, “Continuous EEG monitoring in the neuroscience intensive care unit and emergency department,” *Journal of Clinical Neurophysiology*, vol. 16, no. 1, pp. 14–39, 1999.
- [57] J. Claassen and S. A. Mayer, “Continuous electroencephalographic monitoring in neurocritical care,” *Current Neurology and Neuroscience Reports*, vol. 2, no. 6, pp. 534–40, 2002.
- [58] M. Casazza, G. Avanzini, P. Ferroli, F. Villani, and G. Broggi, “Vagal nerve stimulation: relationship between outcome and electroclinical seizure pattern,” *Seizure*, vol. 15, no. 3, pp. 198–207, 2006.
- [59] A. M. Chan, F. T. Sun, E. H. Boto, and B. M. Wingeier, “Automated seizure onset detection for accurate onset time determination in intracranial EEG,” *Clinical Neurophysiology*, vol. 119, no. 12, pp. 2687–96, 2008.
- [60] M. D’Alessandro, R. Esteller, G. Vachtsevanos, A. Hinson, J. Echauz, and B. Litt, “Epileptic seizure prediction using hybrid feature selection over multiple intracranial EEG electrode contacts: a report of four patients,” *IEEE Transactions on Biomedical Engineering*, vol. 50, no. 5, pp. 603–15, 2003.
- [61] G. R. Minasyan, J. B. Chatten, M. J. Chatten, and R. N. Harner, “Patient-specific early seizure detection from scalp electroencephalogram,” *Journal of Clinical Neurophysiology*, vol. 27, no. 3, pp. 163–78, 2010.
- [62] A. M. Murro, D. W. King, J. R. Smith, B. B. Gallagher, H. F. Flanigin, and K. Meador, “Computerized seizure detection of complex partial seizures,” *Electroencephalography and Clinical Neurophysiology*, vol. 79, no. 4, pp. 330–3, 1991.

- [63] P. Hilfiker and M. Egli, "Detection and evolution of rhythmic components in ictal EEG using short segment spectra and discriminant analysis," *Electroencephalography and Clinical Neurophysiology*, vol. 82, no. 4, pp. 255–65, 1992.
- [64] S. J. Schiff, A. Aldroubi, M. Unser, and S. Sato, "Fast wavelet transformation of EEG," *Electroencephalography and Clinical Neurophysiology*, vol. 91, no. 6, pp. 442–55, 1994.
- [65] N. Pradhan, P. K. Sadasivan, and G. R. Arunodaya, "Detection of seizure activity in EEG by an artificial neural network: a preliminary study," *Computers and Biomedical Research*, vol. 29, no. 4, pp. 303–13, 1996.
- [66] W. G. Hofmann and M. P. Spreng, "Unsupervised classification of EEG from subdural seizure recordings," *Brain Topography*, vol. 10, no. 2, pp. 121–32, 1997.
- [67] A. Klatchko, G. Raviv, W. R. Webber, and R. P. Lesser, "Enhancing the detection of seizures with a clustering algorithm," *Electroencephalography and Clinical Neurophysiology*, vol. 106, no. 1, pp. 52–63, 1998.
- [68] H. S. Park, Y. H. Lee, N. G. Kim, D. S. Lee, and S. I. Kim, "Detection of epileptiform activities in the EEG using neural network and expert system.," *Studies in Health Technology and Informatics*, vol. 52 Pt 2, pp. 1255–1259, 1998.
- [69] K. Lehnertz, "Non-linear time series analysis of intracranial EEG recordings in patients with epilepsy—an overview.," *International Journal of Psychophysiology*, vol. 34, pp. 45–52, Oct 1999.
- [70] F. Sartoretto and M. Ermani, "Automatic detection of epileptiform activity by single-level wavelet analysis," *Clinical Neurophysiology*, vol. 110, no. 2, pp. 239–249, 1999.

- [71] B. Boarshash and M. Mesbah, "A time-frequency approach for newborn seizure detection," *IEEE Engineering in Medicine and Biology Magazine*, vol. 20, no. 5, pp. 54–64, 2001.
- [72] H. S. Liu, T. Zhang, and F. S. Yang, "A multistage, multimethod approach for automatic detection and classification of epileptiform EEG," *IEEE Transactions on Biomedical Engineering*, vol. 49, no. 12, pp. 1557–1566, 2002.
- [73] P. E. McSharry, T. He, L. A. Smith, and L. Tarassenko, "Linear and non-linear methods for automatic seizure detection in scalp electro-encephalogram recordings," *Medical and Biological Engineering and Computing*, vol. 40, no. 4, pp. 447–61, 2002.
- [74] J. Altenburg, R. J. Vermeulen, R. L. Strijers, W. P. Fetter, and C. J. Stam, "Seizure detection in the neonatal EEG with synchronization likelihood," *Clinical Neurophysiology*, vol. 114, no. 1, pp. 50–5, 2003.
- [75] M. K. Kiyimik, A. Subasi, and H. R. Ozcalik, "Neural networks with periodogram and autoregressive spectral analysis methods in detection of epileptic seizure," *Journal of Medical Systems*, vol. 28, no. 6, pp. 511–22, 2004.
- [76] V. P. Nigam and D. Graupe, "A neural-network-based detection of epilepsy," *Journal of Neurology Research*, vol. 26, pp. 55–60, Jan 2004.
- [77] N. Acir, I. Oztura, M. Kuntalp, B. Baklan, and C. Guzelis, "Automatic detection of epileptiform events in EEG by a three-stage procedure based on artificial neural networks," *IEEE Transactions on Biomedical Engineering*, vol. 52, no. 1, pp. 30–40, 2005.
- [78] A. Alkan, E. Koklukaya, and A. Subasi, "Automatic seizure detection in EEG using logistic regression and artificial neural network," *Journal of Neuroscience Methods*, vol. 148, no. 2, pp. 167–76, 2005.

- [79] A. Subasi, "Epileptic seizure detection using dynamic wavelet network," *Expert Systems with Applications*, vol. 29, no. 2, pp. 343–355, 2005.
- [80] C. M. L. Lommen, P. J. M. Cluitmans, J. J. M. Kierkels, J. W. Pasman, P. Andriessen, L. G. Van Rooij, K. D. Liem, and S. B. Oetomo, "Sensitivity of 98% in automatic seizure detection of neonatal amplitude-integrated EEG," *Pediatric Research*, p. 225, 2005.
- [81] A. Aarabi, F. Wallois, and R. Grebe, "Automated neonatal seizure detection: a multistage classification system through feature selection based on relevance and redundancy analysis," *Clinical Neurophysiology*, vol. 117, no. 2, pp. 328–40, 2006.
- [82] A. B. Gardner, A. M. Krieger, G. Vachtsevanos, and B. Litt, "One-class novelty detection for seizure analysis from intracranial EEG," *Journal of Machine Learning Research*, vol. 7, pp. 1025–1044, 2006.
- [83] H. Adeli, S. Ghosh-Dastidar, and N. Dadmehr, "A wavelet-chaos methodology for analysis of EEGs and EEG subbands to detect seizure and epilepsy," *IEEE Transactions on Biomedical Engineering*, vol. 54, no. 2, pp. 205–11, 2007.
- [84] S. Ghosh-Dastidar, H. Adeli, and N. Dadmehr, "Mixed-band wavelet-chaos-neural network methodology for epilepsy and epileptic seizure detection," *IEEE Transactions on Biomedical Engineering*, vol. 54, no. 9, pp. 1545–51, 2007.
- [85] A. Subasi, "Application of adaptive neuro-fuzzy inference system for epileptic seizure detection using wavelet feature extraction," *Computers in Biology and Medicine*, vol. 37, no. 2, pp. 227–44, 2007.
- [86] A. T. Tzallas, M. G. Tsipouras, and D. I. Fotiadis, "The use of time-frequency distributions for epileptic seizure detection in EEG recordings," *Proceedings*

- of *IEEE Engineering in Medicine and Biology Society Conference*, vol. 2007, pp. 3–6, 2007.
- [87] B. R. Greene, P. de Chazal, G. B. Boylan, S. Connolly, and R. B. Reilly, “Electrocardiogram based neonatal seizure detection,” *IEEE Transactions on Biomedical Engineering*, vol. 54, no. 4, pp. 673–82, 2007.
- [88] M. A. Harrison, M. G. Frei, and I. Osorio, “Detection of seizure rhythmicity by recurrences,” *Chaos*, vol. 18, no. 3, p. 033124, 2008.
- [89] L. Kuhlmann, A. N. Burkitt, M. J. Cook, K. Fuller, D. B. Grayden, L. Seiderer, and I. M. Y. Mareels, “Seizure detection using seizure probability estimation: Comparison of features used to detect seizures,” *Annals of Biomedical Engineering*, vol. 37, no. 10, pp. 2129–2145, 2009.
- [90] B. Abibullaev, M. S. Kim, and H. D. Seo, “Seizure detection in temporal lobe epileptic EEGs using the best basis wavelet functions,” *Journal of Medical Systems*, vol. 34, no. 4, pp. 755–65, 2010.
- [91] L. Guo, D. Rivero, J. Dorado, J. R. Rabunal, and A. Pazos, “Automatic epileptic seizure detection in EEGs based on line length feature and artificial neural networks,” *Journal of Neuroscience Methods*, 2010.
- [92] E. M. Thomas, A. Temko, G. Lightbody, W. P. Marnane, and G. B. Boylan, “Gaussian mixture models for classification of neonatal seizures using EEG,” *Physiological Measurement*, vol. 31, no. 7, pp. 1047–64, 2010.
- [93] G. E. Polychronaki, P. Y. Ktonas, S. Gatzonis, A. Siatouni, P. A. Asvestas, H. Tsekou, D. Sakas, and K. S. Nikita, “Comparison of fractal dimension estimation algorithms for epileptic seizure onset detection,” *Journal of Neural Engineering*, vol. 7, no. 4, p. 046007, 2010.

- [94] A. Temko, E. Thomas, W. Marnane, G. Lightbody, and G. Boylan, "EEG-based neonatal seizure detection with support vector machines," *Clinical Neurophysiology*, vol. 122, no. 3, pp. 464–73, 2011.
- [95] A. W. Chiu, M. Derchansky, M. Cotic, P. L. Carlen, S. O. Turner, and B. L. Bardakjian, "Wavelet-based Gaussian-mixture hidden markov model for the detection of multistage seizure dynamics: a proof-of-concept study," *BioMedical Engineering OnLine*, vol. 10, p. 29, 2011.
- [96] F. Pauri, F. Pierelli, G. E. Chatrian, and W. W. Erdly, "Long-term EEG-video-audio monitoring: computer detection of focal EEG seizure patterns," *Electroencephalography and Clinical Neurophysiology*, vol. 82, no. 1, pp. 1–9, 1992.
- [97] G. W. Harding, "An automated seizure monitoring system for patients with indwelling recording electrodes," *Electroencephalography and Clinical Neurophysiology*, vol. 86, no. 6, pp. 428–37, 1993.
- [98] A. J. Gabor, R. R. Leach, and F. U. Dowla, "Automated seizure detection using a self-organizing neural network," *Electroencephalography and Clinical Neurophysiology*, vol. 99, no. 3, pp. 257–66, 1996.
- [99] A. J. Gabor, "Seizure detection using a self-organizing neural network: validation and comparison with other detection strategies," *Electroencephalography and Clinical Neurophysiology*, vol. 107, no. 1, pp. 27–32, 1998.
- [100] I. Osorio, M. G. Frei, and S. B. Wilkinson, "Real-time automated detection and quantitative analysis of seizures and short-term prediction of clinical onset," *Epilepsia*, vol. 39, no. 6, pp. 615–27, 1998.

- [101] Y. U. Khan and J. Gotman, "Wavelet based automatic seizure detection in intracerebral electroencephalogram," *Clinical Neurophysiology*, vol. 114, no. 5, pp. 898–908, 2003.
- [102] M. E. Saab and J. Gotman, "A system to detect the onset of epileptic seizures in scalp EEG," *Clinical Neurophysiology*, vol. 116, no. 2, pp. 427–42, 2005.
- [103] L. D. Iasemidis, "Epileptic seizure prediction and control," *IEEE Transactions on Biomedical Engineering*, vol. 50, no. 5, pp. 549–58, 2003.
- [104] L. D. Iasemidis, J. C. Sackellares, H. P. Zaveri, and W. J. Williams, "Phase space topography and the Lyapunov exponent of electrocorticograms in partial seizures," *Brain Topography*, vol. 2, no. 3, pp. 187–201, 1990.
- [105] M. C. Casdagli, L. D. Iasemidis, R. S. Savit, R. L. Gilmore, S. N. Roper, and J. C. Sackellares, "Non-linearity in invasive EEG recordings from patients with temporal lobe epilepsy," *Electroencephalography and Clinical Neurophysiology*, vol. 102, no. 2, pp. 98–105, 1997.
- [106] L. D. Iasemidis, D.-S. Shiau, W. Chaovalitwongse, J. C. Sackellares, P. M. Pardalos, J. C. Principe, P. R. Carney, A. Prasad, B. Veeramani, and K. Tsakalis, "Adaptive epileptic seizure prediction system," *IEEE Transactions on Biomedical Engineering*, vol. 50, no. 5, pp. 616–627, 2003.
- [107] L. D. Iasemidis, D. S. Shiau, J. C. Sackellares, P. M. Pardalos, and A. Prasad, "Dynamical resetting of the human brain at epileptic seizures: application of nonlinear dynamics and global optimization techniques," *IEEE Transactions on Biomedical Engineering*, vol. 51, no. 3, pp. 493–506, 2004.
- [108] L. D. Iasemidis, D. S. Shiau, P. M. Pardalos, W. Chaovalitwongse, K. Narayanan, A. Prasad, K. Tsakalis, P. R. Carney, and J. C. Sackellares, "Long-term pro-

- spective on-line real-time seizure prediction,” *Clinical Neurophysiology*, vol. 116, no. 3, pp. 532–44, 2005.
- [109] S. Sabesan, L. B. Good, K. S. Tsakalis, A. Spanias, D. M. Treiman, and L. D. Iasemidis, “Information flow and application to epileptogenic focus localization from intracranial EEG,” *IEEE Transactions on Neural Systems and Rehabilitation Engineering*, vol. 17, pp. 244–53, Jun 2009.
- [110] M. A. Navakatikyan, P. B. Colditz, C. J. Burke, T. E. Inder, J. Richmond, and C. E. Williams, “Seizure detection algorithm for neonates based on wave-sequence analysis,” *Clinical Neurophysiology*, vol. 117, no. 6, pp. 1190–203, 2006.
- [111] J. Gotman, D. Flanagan, B. Rosenblatt, A. Bye, and E. M. Mizrahi, “Evaluation of an automatic seizure detection method for the newborn EEG,” *Electroencephalography and Clinical Neurophysiology*, vol. 103, no. 3, pp. 363–9, 1997.
- [112] A. Liu, J. S. Hahn, G. P. Heldt, and R. W. Coen, “Detection of neonatal seizures through computerized EEG analysis,” *Electroencephalography and Clinical Neurophysiology*, vol. 82, no. 1, pp. 30–7, 1992.
- [113] W. R. S. Webber, R. P. Lesser, R. T. Richardson, and K. Wilson, “An approach to seizure detection using an artificial neural network (ANN),” *Electroencephalography and Clinical Neurophysiology*, vol. 98, no. 4, pp. 250–272, 1996.
- [114] A. Aarabi, R. Fazel-Rezai, and Y. Aghakhani, “Seizure detection in intracranial EEG using a fuzzy inference system,” *Proceedings of IEEE Engineering in Medicine and Biology Society Conference*, vol. 1, pp. 1860–3, 2009.
- [115] V. Srinivasan, C. Eswaran, and N. Sriraam, “Artificial neural network based epileptic detection using time-domain and frequency-domain features,” *Journal of Medical Systems*, vol. 29, no. 6, pp. 647–60, 2005.

- [116] K. M. Kelly, D. S. Shiau, R. T. Kern, J. H. Chien, M. C. Yang, K. A. Yandora, J. P. Valeriano, J. J. Halford, and J. C. Sackellares, "Assessment of a scalp EEG-based automated seizure detection system," *Clinical Neurophysiology*, 2010.
- [117] J. Duun-Henriksen, T. W. Kjaer, R. E. Madsen, L. S. Remvig, C. E. Thomsen, and H. B. D. Sorensen, "Channel selection for automatic seizure detection.," *Clinical Neurophysiology*, Jul 2011.
- [118] K. Majumdar and P. Vardhan, "Automatic seizure detection in ECoG by differential operator and windowed variance.," *IEEE Transactions on Neural Systems and Rehabilitation Engineering*, May 2011.
- [119] R. Yadav, M. N. S. Swamy, and R. Agarwal, "Rapid identification of epileptogenic sites in the intracranial EEG recordings," *Proceedings of IEEE Engineering in Medicine and Biology Society Conference*, pp. 7553–7556, 2011.
- [120] R. Yadav, A. K. Shah, J. A. Loeb, M. N. S. Swamy, and R. Agarwal, "Morphology-based automatic detection of epileptic seizures," *IEEE Transactions on Biomedical Engineering*, vol. 59, p. 11 pages, 2012 (accepted).
- [121] R. A. Wagner and M. J. Fisher, "The string-to-string correction problem," *Journal of the Association for Computing Machinery*, vol. 21, no. 1, pp. 168–173, 1974.
- [122] F. Wendling and F. Bartolomei, "Modeling EEG signals and interpreting measures of relationship during temporal-lobe seizures: an approach to the study of epileptogenic networks," *Epileptic Disorders*, vol. Special Issue, pp. 67–78, 2001.
- [123] F. Wendling, F. Bartolomei, J. J. Bellanger, J. Bourien, and P. Chauvel, "Epileptic fast intracerebral EEG activity: evidence for spatial decorrelation at seizure onset," *Brain*, vol. 126, no. Pt 6, pp. 1449–59, 2003.

- [124] A. Shoeb, H. Edwards, J. Connolly, B. Bourgeois, S. T. Treves, and J. Guttag, "Patient-specific seizure onset detection," *Epilepsy and Behavior*, vol. 5, no. 4, pp. 483–98, 2004.
- [125] N. Verma, A. Shoeb, J. Bohorquez, J. Dawson, J. Guttag, and A. P. m. Chandrakasan, "A micro-power EEG acquisition SoC with integrated feature extraction processor for a chronic seizure detection system," *IEEE Journal of Solid-State Circuits*, vol. 45, no. 4, pp. 804–816, 2010.
- [126] L. Meng, M. G. Frei, I. Osorio, G. Strang, and T. Q. Nguyen, "Gaussian mixture models of ECoG signal features for improved detection of epileptic seizures," *Medical Engineering and Physics*, vol. 26, no. 5, pp. 379–93, 2004.
- [127] I. Osorio, M. G. Frei, S. Sunderam, J. Giftakis, N. C. Bhavaraju, S. F. Schaffner, and S. B. Wilkinson, "Automated seizure abatement in humans using electrical stimulation," *Annals of Neurology*, vol. 57, no. 2, pp. 258–68, 2005.
- [128] S. M. Haas, M. G. Frei, and I. Osorio, "Strategies for adapting automated seizure detection algorithms," *Medical Engineering and Physics*, vol. 29, no. 8, pp. 895–909, 2007.
- [129] I. Osorio and M. G. Frei, "Real-time detection, quantification, warning, and control of epileptic seizures: the foundations for a scientific epileptology," *Epilepsy and Behavior*, vol. 16, no. 3, pp. 391–6, 2009.
- [130] S. B. Wilson, "A neural network method for automatic and incremental learning applied to patient-dependent seizure detection," *Clinical Neurophysiology*, vol. 116, no. 8, pp. 1785–95, 2005.
- [131] S. B. Wilson, "Algorithm architectures for patient dependent seizure detection," *Clinical Neurophysiology*, vol. 117, no. 6, pp. 1204–16, 2006.

- [132] L. Shi, R. Agarwal, and M. N. S. Swamy, "Model-based seizure detection method using statistically optimal filters," *Proceedings of IEEE Engineering in Medicine and Biology Society Conference*, vol. 1, pp. 45–8, 2004.
- [133] M. T. Salam, M. Sawan, and D. K. Nguyen, "A novel low-power-implantable epileptic seizure-onset detector," *IEEE Transactions on Biomedical Circuits and Systems*, no. 99, 2011. Early Access.
- [134] R. Yadav, R. Agarwal, and M. N. S. Swamy, "A new improved model-based seizure detection using statistically optimal null filter," *Proceedings of IEEE Engineering in Medicine and Biology Society Conference*, pp. 1318–1322, 2009.
- [135] R. Yadav, R. Agarwal, and M. N. S. Swamy, "Model-based seizure detection for intracranial EEG recordings," *IEEE Transactions on Biomedical Engineering*, vol. 59, p. 10 pages, 2012 (accepted).
- [136] R. Yadav, M. N. S. Swamy, and R. Agarwal, "Evolution-based automatic seizure detection for intracranial EEG recordings," *IEEE Transactions on Biomedical Engineering*, 2011 (to be submitted).
- [137] R. L. Kutsy, D. F. Farrell, and G. A. Ojemann, "Ictal patterns of neocortical seizures monitored with intracranial electrodes: correlation with surgical outcome," *Epilepsia*, vol. 40, no. 3, pp. 257–66, 1999.
- [138] C. Amo, C. Saldana, M. G. Hidalgo, F. Maestu, A. Fernandez, J. Arrazola, and T. Ortiz, "Magnetoencephalographic localization of peritumoral temporal epileptic focus previous surgical resection," *Seizure*, vol. 12, no. 1, pp. 19–22, 2003.
- [139] G. Di Gennaro, P. P. Quarato, F. Sebastiano, V. Esposito, P. Onorati, A. Mascia, P. Romanelli, L. G. Grammaldo, C. Falco, C. Scoppetta, F. Eusebi, M. Manfredi,

- and G. Cantore, “Postoperative EEG and seizure outcome in temporal lobe epilepsy surgery,” *Clinical Neurophysiology*, vol. 115, no. 5, pp. 1212–9, 2004.
- [140] C. Barba, F. Doglietto, L. De Luca, G. Faraca, C. Marra, M. Meglio, G. F. Rossi, and G. Colicchio, “Retrospective analysis of variables favouring good surgical outcome in posterior epilepsies,” *Journal of Neurology*, vol. 252, no. 4, pp. 465–72, 2005.
- [141] E. Ben-Jacob, S. Boccaletti, A. Pomyalov, I. Procaccia, and V. L. Towle, “Detecting and localizing the foci in human epileptic seizures,” *Chaos*, vol. 17, no. 4, p. 043113, 2007.
- [142] L. Ding, C. Wilke, B. Xu, X. Xu, W. van Drongelen, M. Kohrman, and B. He, “EEG source imaging: correlating source locations and extents with electrocorticography and surgical resections in epilepsy patients,” *Journal of Clinical Neurophysiology*, vol. 24, no. 2, pp. 130–6, 2007.
- [143] C. E. Stafstrom, “Sites of interictal spike generation in neocortex,” *Epilepsy Currents / American Epilepsy Society*, vol. 4, no. 3, pp. 96–7, 2004.
- [144] I. Ulbert, G. Heit, J. Madsen, G. Karmos, and E. Halgren, “Laminar analysis of human neocortical interictal spike generation and propagation: current source density and multiunit analysis in vivo,” *Epilepsia*, vol. 45 Suppl 4, pp. 48–56, 2004.
- [145] D. Fabo, Z. Magloczky, L. Wittner, A. Pek, L. Eross, S. Czirjak, J. Vajda, A. Solyom, G. Rasonyi, A. Szucs, A. Kelemen, V. Juhos, L. Grand, B. Dombovari, P. Halasz, T. F. Freund, E. Halgren, G. Karmos, and I. Ulbert, “Properties of in vivo interictal spike generation in the human subiculum,” *Brain*, vol. 131, no. Pt 2, pp. 485–99, 2008.

- [146] K. G. Oweiss, *Statistical Signal Processing for Neuroscience and Neurotechnology*. Academic Press, 2010.
- [147] E. N. Brown, R. E. Kass, and P. P. Mitra, “Multiple neural spike train data analysis: state-of-the-art and future challenges,” *Nature Neuroscience*, vol. 7, no. 5, pp. 456–61, 2004.
- [148] M. Aghagolzadeh and K. Oweiss, “Compressed and distributed sensing of neuronal activity for real time spike train decoding,” *IEEE Transactions on Neural Systems and Rehabilitation Engineering*, vol. 17, pp. 116–127, Apr 2009.
- [149] D. A. Willming and B. C. Wheeler, “Real-time multichannel neural spike recognition with DSPs,” *IEEE Engineering in Medicine and Biology Magazine*, vol. 9, no. 1, pp. 37–9, 1990.
- [150] R. Chandra and L. M. Optican, “Detection, classification, and superposition resolution of action potentials in multiunit single-channel recordings by an on-line real-time neural network,” *IEEE Transactions on Biomedical Engineering*, vol. 44, pp. 403–412, May 1997.
- [151] R. Q. Quiroga, Z. Nadasdy, and Y. Ben-Shaul, “Unsupervised spike detection and sorting with wavelets and superparamagnetic clustering,” *Neural Computation*, vol. 16, pp. 1661–87, Aug 2004.
- [152] F. Wood, M. J. Black, C. Vargas-Irwin, M. Fellows, and J. P. Donoghue, “On the variability of manual spike sorting,” *IEEE Transactions on Biomedical Engineering*, vol. 51, pp. 912–918, Jun 2004.
- [153] H. Kaneko, H. Tamura, and S. S. Suzuki, “Tracking spike-amplitude changes to improve the quality of multineuronal data analysis,” *IEEE Transactions on Biomedical Engineering*, vol. 54, no. 2, pp. 262–272, 2007.

- [154] M. T. Wolf and J. W. Burdick, “A Bayesian clustering method for tracking neural signals over successive intervals,” *IEEE Transactions on Biomedical Engineering*, vol. 56, no. 11, pp. 2649–2659, 2009.
- [155] H.-L. Chan, T. Wu, S.-T. Lee, M.-A. Lin, S.-M. He, P.-K. Chao, and Y.-T. Tsai, “Unsupervised wavelet-based spike sorting with dynamic codebook searching and replenishment,” *Neurocomputing*, vol. 73, no. 7-9, pp. 1513–1527, 2010.
- [156] D. Velis, P. Plouin, J. Gotman, F. L. da Silva, and I. L. A. E. D. S. on Neurophysiology, “Recommendations regarding the requirements and applications for long-term recordings in epilepsy,” *Epilepsia*, vol. 48, pp. 379–384, Feb 2007.
- [157] A. Schad, K. Schindler, B. Schelter, T. Maiwald, A. Brandt, J. Timmer, and A. Schulze-Bonhage, “Application of a multivariate seizure detection and prediction method to non-invasive and intracranial long-term EEG recordings,” *Clinical Neurophysiology*, vol. 119, no. 1, pp. 197–211, 2008.
- [158] A. Schlogl and C. Brunner, “BioSig: A free and open source software library for BCI research,” *IEEE Computers*, 2008.
- [159] J. Gotman and L. Y. Wang, “State-dependent spike detection: concepts and preliminary results,” *Electroencephalography and Clinical Neurophysiology*, vol. 79, pp. 11–19, Jul 1991.
- [160] T. Pietila, S. Vapaakoski, U. Nousiainen, A. Varri, H. Frey, V. Hakkinen, and Y. Neuvo, “Evaluation of a computerized system for recognition of epileptic activity during long-term EEG recording,” *Electroencephalography and Clinical Neurophysiology*, vol. 90, no. 6, pp. 438–43, 1994.
- [161] A. Temko, E. Thomas, W. Marnane, G. Lightbody, and G. B. Boylan, “Performance assessment for EEG-based neonatal seizure detectors,” *Clinical Neurophysiology*, vol. 122, no. 3, pp. 474–82, 2011.

- [162] J. K. Peat and B. Barton, *Medical Statistics : a guide to data analysis and critical appraisal*. Blackwell Pub., 2005.
- [163] B. W. McMenamin, A. J. Shackman, L. L. Greischar, and R. J. Davidson, “Electromyogenic artifacts and electroencephalographic inferences revisited.,” *Neuroimage*, vol. 54, pp. 4–9, Aug 2010.
- [164] A. Antoniou, *Digital Signal Processing : signals systems and filters*. McGraw-Hill, 2006.
- [165] M. Akay, *Handbook of Neural Engineering*. Wiley, 2007.
- [166] M. Zijlmans, J. Jacobs, R. Zelmann, F. Dubeau, and J. Gotman, “High frequency oscillations and seizure frequency in patients with focal epilepsy,” *Epilepsy Research*, vol. 85, no. 2-3, pp. 287–92, 2009.
- [167] R. Agarwal and J. Gotman, “Adaptive segmentation of electroencephalographic data using a nonlinear energy operator,” *Proceedings of IEEE International Symposium on Circuits and Systems*, vol. 4, pp. 199–202, 1999.
- [168] J. F. Kaiser, “Some useful properties of Teager’s energy operators,” *Proceedings of IEEE International Conference on Acoustics, Speech, and Signal Processing*, vol. 3, pp. 149–152, 1993.
- [169] R. Agarwal and J. Gotman, “Long-term EEG compression for intensive-care settings,” *IEEE Engineering in Medicine and Biology Magazine*, vol. 20, pp. 23–9, Sep-Oct 2001.
- [170] E. I. Plotkin and M. N. S. Swamy, “Multistage implementation of parameter-invariant null filter and its application to discrimination of closely spaced sinusoids,” *Proceedings of IEEE International Symposium on Circuits and Systems*, pp. 767–770 vol.1, 1988.

- [171] E. I. Plotkin and M. N. S. Swamy, "Parameter-free structural modeling: A contribution to the solution of the separation of highly correlated AR-signals," *Proceedings of IEEE International Symposium on Circuits and Systems*, pp. D1–D4 3596, 1998.
- [172] E. I. Plotkin and M. N. S. Swamy, "Signal processing based on parameter structural modeling and separation of highly correlated signals of known structure," *Circuits Systems and Signal Processing*, vol. 17, pp. 51–68, 1998.
- [173] W. S. Steven, *The Scientist and Engineer's Guide to Digital Signal Processing*. California Technical Publishing, 2002.
- [174] P. Y. Ktonas, W. M. Luoh, M. L. Kejariwal, E. L. Reilly, and M. A. Seward, "Computer-aided quantification of EEG spike and sharp wave characteristics," *Electroencephalography and Clinical Neurophysiology*, vol. 51, no. 3, pp. 237–43, 1981.
- [175] N. B. Karayiannis, A. Mukherjee, J. R. Glover, P. Y. Ktonas, J. D. Frost, R. A. Hrachovy, and E. A. Mizrahi, "Detection of pseudo sinusoidal epileptic seizure segments in the neonatal EEG by cascading a rule-based algorithm with a neural network," *IEEE Transactions on Biomedical Engineering*, vol. 53, no. 4, pp. 633–641, 2006.
- [176] B. L. Davey, W. R. Fright, G. J. Carroll, and R. D. Jones, "Expert system approach to detection of epileptiform activity in the EEG," *Medical and Biological Engineering and Computing*, vol. 27, no. 4, pp. 365–70, 1989.
- [177] R. Bracewell, *The Fourier Transform and Its Applications*. McGraw-Hill, June 1999.

- [178] A. Burian and P. Kuosmanen, "Tuning the smoothness of the recursive median filter," *IEEE Transactions on Signal Processing*, vol. 50, no. 7, pp. 1631–1639, 2002.
- [179] J. J. Niederhauser, R. Esteller, J. Echauz, G. Vachtsevanos, and B. Litt, "Detection of seizure precursors from depth-EEG using a sign periodogram transform," *IEEE Transactions on Biomedical Engineering*, vol. 50, no. 4, pp. 449–58, 2003.
- [180] Y. Lee and S. Kassam, "Generalized median filtering and related nonlinear filtering techniques," *IEEE Transactions on Acoustics, Speech and Signal Processing*, vol. 33, no. 3, pp. 672–683, 1985.
- [181] T. Nodes and J. Gallagher, N., "Median filters: Some modifications and their properties," *IEEE Transactions on Acoustics, Speech and Signal Processing*, vol. 30, no. 5, pp. 739–746, 1982.
- [182] R. Yadav, R. Agarwal, and M. N. S. Swamy, "Computer-aided rapid review of depth EEG in epilepsy," *Proceedings of Insititute of Mental Health Research (IMHR) Annual Young Researchers' Conference*, p. 20, 2011.
- [183] E. Asano, K. Benedek, A. Shah, C. Juhasz, J. Shah, D. C. Chugani, O. Muzik, S. Sood, and H. T. Chugani, "Is intraoperative electrocorticography reliable in children with intractable neocortical epilepsy?," *Epilepsia*, vol. 45, no. 9, pp. 1091–9, 2004.
- [184] H. Stroink, R.-J. Schimsheimer, A. W. de Weerd, A. T. Geerts, W. F. Arts, E. A. Peeters, O. F. Brouwer, A. B. Peters, and C. A. van Donselaar, "Interobserver reliability of visual interpretation of electroencephalograms in children with newly diagnosed seizures.," *Developmental Medicine and Child Neurology*, vol. 48, pp. 374–377, May 2006.

- [185] S. B. Wilson, M. L. Scheuer, C. Plummer, B. Young, and S. Pacia, "Seizure detection: correlation of human experts," *Clinical Neurophysiology*, vol. 114, no. 11, pp. 2156–64, 2003.
- [186] A. Hufnagel, M. Dumpelmann, J. Zentner, O. Schijns, and C. E. Elger, "Clinical relevance of quantified intracranial interictal spike activity in presurgical evaluation of epilepsy," *Epilepsia*, vol. 41, no. 4, pp. 467–78, 2000.
- [187] J. M. Paolicchi, P. Jayakar, P. Dean, I. Yaylali, G. Morrison, A. Prats, T. Resnik, L. Alvarez, and M. Duchowny, "Predictors of outcome in pediatric epilepsy surgery.," *Neurology*, vol. 54, pp. 642–647, Feb 2000.
- [188] P. Krsek, B. Maton, P. Jayakar, P. Dean, B. Korman, G. Rey, C. Dunoyer, E. Pacheco-Jacome, G. Morrison, J. Ragheb, H. V. Vinters, T. Resnick, and M. Duchowny, "Incomplete resection of focal cortical dysplasia is the main predictor of poor postsurgical outcome.," *Neurology*, vol. 72, pp. 217–223, Jan 2009.
- [189] D. L. Gilbert, "Interobserver reliability of visual interpretation of electroencephalograms in children with newly diagnosed seizures.," *Developmental Medicine and Child Neurology*, vol. 48, pp. 1009–10, Dec 2006.
- [190] P. W. Kaplan and F. W. Drislane, *Nonconvulsive Status Epilepticus*. Demos Medical Publishing, New York, USA, 2008.
- [191] J. Mitra, J. R. Glover, P. Y. Ktonas, A. Thitai Kumar, A. Mukherjee, N. B. Karayiannis, J. Frost, J. D., R. A. Hrachovy, and E. M. Mizrahi, "A multistage system for the automated detection of epileptic seizures in neonatal electroencephalography," *Journal of Clinical Neurophysiology*, vol. 26, no. 4, pp. 218–26, 2009.

- [192] C. Borel and D. Hanley, "Neurologic intensive care unit monitoring," *Critical Care Clinics*, vol. 1, pp. 223–39, Jul 1985.
- [193] T. Madan, "Compression of long-term EEG using power spectral density," Master's thesis, Dept. of Electrical and Computer Engineering, Concordia University, 2005.
- [194] R. Yadav, R. Agarwal, and M. N. S. Swamy, "Smart monitoring and therapeutic application of the self-adapting seizure detection system," *IEEE Workshop on Adverse Response Monitoring (WARM)*, 2010.
- [195] R. Agarwal, E. I. Plotkin, and M. N. S. Swamy, "Statistically optimal null filters: Kalman equivalence," *Proceedings of IEEE International Conference on Acoustics, Speech, and Signal Processing*, vol. 1, pp. 173–176 vol.1, 2000.
- [196] R. Agarwal, E. I. Plotkin, and M. N. S. Swamy, "Statistically optimal null filters for processing short record length signals," *Proceedings of IEEE International Symposium on Circuits and Systems*, vol. 3, pp. 2277–2280 vol.3, 1995.
- [197] R. Agarwal, *Enhancement techniques of short-duration narrowband signals with application to ABR audiometry*. PhD thesis, Dept. of Electrical and Computer Engineering, Concordia University, 1995.
- [198] R. Agarwal, E. I. Plotkin, and M. N. S. Swamy, "Recursive implementation of statistically-optimal null filters," *Proceedings of IEEE International Symposium on Circuits and Systems*, vol. 2, pp. 245–248 vol.2, 1996.
- [199] R. Agarwal, E. I. Plotkin, and M. N. S. Swamy, "Statistically optimal null filter based on instantaneous matched processing," *Circuits Systems and Signal Processing*, vol. 20, pp. 37–61, 2001.

- [200] B. G. Amidan, T. A. Ferryman, and S. K. Cooley, "Data outlier detection using the Chebyshev theorem," *IEEE Aerospace Conference*, pp. 3814–3819 4555, 2005.
- [201] S. N. Rakhade and J. A. Loeb, "Focal reduction of neuronal glutamate transporters in human neocortical epilepsy," *Epilepsia*, vol. 49, no. 2, pp. 226–236, 2008.
- [202] M. Curtis and G. Avanzini, "Interictal spikes in focal epileptogenesis," *Progress in Neurobiology*, vol. 63, no. 5, pp. 541–67, 2001.
- [203] S. Demont-Guignard, P. Benquet, U. Gerber, and F. Wendling, "Analysis of intracerebral EEG recordings of epileptic spikes: Insights from a neural network model," *IEEE Transactions on Biomedical Engineering*, vol. 56, no. 12, pp. 2782–2795, 2009.
- [204] R. Yadav, A. K. Shah, J. A. Loeb, M. N. S. Swamy, and R. Agarwal, "A novel unsupervised spike sorting algorithm for intracranial EEG recordings," *Proceedings of IEEE Engineering in Medicine and Biology Society Conference*, pp. 7545–7548, 2011.
- [205] R. Yadav, A. K. Shah, J. A. Loeb, M. N. S. Swamy, and R. Agarwal, "Automatic spike sorting with dynamic codebook for intracranial EEG," *IEEE Transactions on Biomedical Engineering*, 2011 (to be submitted).
- [206] H. Kaneko, S. S. Suzuki, J. Okada, and M. Akamatsu, "Multineuronal spike classification based on multisite electrode recording, whole-waveform analysis, and hierarchical clustering," *IEEE Transactions on Biomedical Engineering*, vol. 46, no. 3, pp. 280–90, 1999.
- [207] P. Zhang, "Spike sorting based on automatic template reconstruction with a partial solution to the overlapping problem," *Journal of Neuroscience Methods*, vol. 135, no. 1-2, pp. 55–65, 2004.

- [208] R. Vollgraf and K. Obermayer, “Improved optimal linear filters for the discrimination of multichannel waveform templates for spike-sorting applications,” *IEEE Signal Processing Letters*, vol. 13, no. 3, pp. 121–124, 2006.
- [209] Y. Ghanbari, P. Papamichalis, and L. Spence, “Graph-Laplacian features for neural waveform classification,” *IEEE Transactions on Biomedical Engineering*, Nov 1 2010.
- [210] D. Ge, E. Le Carpentier, J. Idier, and D. Farina, “Spike sorting by stochastic simulation,” *IEEE Transactions on Neural Systems and Rehabilitation Engineering*, vol. 19, no. 3, pp. 249–259, 2011.
- [211] T. Takekawa, Y. Isomura, and T. Fukai, “Accurate spike sorting for multi-unit recordings,” *European Journal of Neuroscience*, vol. 31, pp. 263–272, Jan 2010.
- [212] M. Halkidi, Y. Batistakis, and M. Vazirgiannis, “On clustering validation techniques,” *Journal of Intelligent Information Systems*, vol. 17, no. 2, pp. 107–145, 2001.
- [213] G. Zhang, Y. H. Raol, F. C. Hsu, D. A. Coulter, and A. R. Brooks-Kayal, “Effects of status epilepticus on hippocampal GABAA receptors are age-dependent,” *Neuroscience*, vol. 125, no. 2, pp. 299–303, 2004.
- [214] H. K. Jung, J. H. Choi, and T. Kim, “Solving alignment problems in neural spike sorting using frequency domain PCA,” *Neurocomputing*, vol. 69, pp. 975–978, Mar 2006.
- [215] K. Balasubramanian and I. Obeid, “Fuzzy logic-based spike sorting system,” *Journal of Neuroscience Methods*, vol. 198, pp. 125–34, May 15 2011.
- [216] K. Younis, M. Karim, R. Hardie, J. Loomis, S. Rogers, and M. DeSimio, “Cluster merging based on weighted Mahalanobis distance with application in

- digital mammograph,” *Proceedings of IEEE National Aerospace and Electronics Conference*, pp. 525–530, 1998.
- [217] T. Schreck, J. Bernard, T. von Landesberger, and J. Kohlhammer, “Visual cluster analysis of trajectory data with interactive Kohonen maps,” *Information Visualization*, vol. 8, pp. 14–29–, 2009.
- [218] K. B. Zhang, M. A. Orgun, and K. Zhang, “HOV3: An approach to visual cluster analysis,” *Proceedings of Advanced Data Mining and Applications Conference*, vol. 4093, pp. 316–327–, 2006.
- [219] H.-P. Kriegel, P. Kroger, and A. Zimek, “Clustering high-dimensional data: A survey on subspace clustering, pattern-based clustering, and correlation clustering,” *ACM Transactions on Knowledge Discovery from Data*, vol. 3, pp. 1:1–1:58, March 2009.
- [220] H. Bergman and M. R. Delong, “A personal computer-based spike detector and sorter - implementation and evaluation,” *Journal of Neuroscience Methods*, vol. 41, pp. 187–197, Mar 1992.
- [221] H. S. Cho, D. Corina, J. F. Brinkley, G. A. Ojemann, and L. G. Shapiro, “A new template matching method using variance estimation for spike sorting,” *IEEE Engineering in Medicine and Biology Conference on Neural Engineering*, pp. 225–228 693, 2005.
- [222] T. Sato, T. Suzuki, and K. Mabuchi, “Fast template matching for spike sorting,” *Electronics and Communications in Japan*, vol. 92, pp. 57–63, Nov 2009.
- [223] A. Bragin, C. L. Wilson, J. Almajano, I. Mody, and J. Engel, “High-frequency oscillations after status epilepticus: epileptogenesis and seizure genesis,” *Epilepsia*, vol. 45, pp. 1017–23, Sep 2004.

- [224] A. B. Gardner, G. A. Worrell, E. Marsh, D. Dlugos, and B. Litt, “Human and automated detection of high-frequency oscillations in clinical intracranial EEG recordings,” *Clinical Neurophysiology*, vol. 118, no. 5, pp. 1134–1143, 2007.
- [225] M. Brazdil, J. Halamek, P. Jurak, P. Daniel, R. Kuba, J. Chrastina, Z. Novak, and I. Rektor, “Interictal high-frequency oscillations indicate seizure onset zone in patients with focal cortical dysplasia,” *Epilepsy Research*, vol. 90, no. 1-2, pp. 28–32, 2010.
- [226] J. Jacobs, P. Levan, C. E. Chatillon, A. Olivier, F. Dubeau, and J. Gotman, “High frequency oscillations in intracranial EEGs mark epileptogenicity rather than lesion type,” *Brain*, vol. 132, no. Pt 4, pp. 1022–37, 2009.
- [227] T. Akiyama, D. W. Chan, C. Y. Go, A. Ochi, I. M. Elliott, E. J. Donner, S. K. Weiss, O. C. Snead, J. T. Rutka, J. M. Drake, and H. Otsubo, “Topographic movie of intracranial ictal high-frequency oscillations with seizure semiology: epileptic network in Jacksonian seizures,” *Epilepsia*, vol. 52, no. 1, pp. 75–83, 2011.
- [228] F. Wendling, K. Ansari-Asl, F. Bartolomei, and L. Senhadji, “From EEG signals to brain connectivity: a model-based evaluation of interdependence measures,” *Journal of Neuroscience Methods*, vol. 183, pp. 9–18, Sep 2009.
- [229] P. LeVan, E. Urrestarazu, and J. Gotman, “A system for automatic artifact removal in ictal scalp EEG based on independent component analysis and bayesian classification,” *Clinical Neurophysiology*, vol. 117, no. 4, pp. 912–27, 2006.
- [230] S. Gibson, J. W. Judy, and M. D., “Spike sorting: The first step in decoding the brain,” *IEEE Signal Processing Magazine*, vol. 29, no. 1, pp. 124–145, 2012.